VOL. 590 NO. 1 JANUARY 24, 1992

Period.

8th Int. Symp. on Preparative Chromatography
Arlington, VA, May 13–15, 1991

JOURNAL OF

CHROMATOGRAPHY

INCLUDING ELECTROPHORESIS AND OTHER SEPARATION METHODS

SYMPOSIUM VOLUMES

ELSEVIER

JOURNAL OF CHROMATOGRAPHY

INCLUDING ELECTROPHORESIS AND OTHER SEPARATION METHODS

Scope. The *Journal of Chromatography* publishes papers on all aspects of chromatography, electrophoresis and related methods. Contributions consist mainly of research papers dealing with chromatographic theory, instrumental development and their applications. The section *Biomedical Applications*, which is under separate editorship, deals with the following aspects: developments in and applications of chromatographic and electrophoretic techniques related to clinical diagnosis or alterations during medical treatment; screening and profiling of body fluids or tissues with special reference to metabolic disorders; results from basic medical research with direct consequences in clinical practice; drug level monitoring and pharmacokinetic studies; clinical toxicology; analytical studies in occupational medicine.

Submission of Papers. Manuscripts (in English; *four* copies are required) should be submitted to: Editorial Office of *Journal of Chromatography*, P.O. Box 681, 1000 AR Amsterdam, Netherlands, Telefax (+31-20) 5862 304, or to: The Editor of *Journal of Chromatography, Biomedical Applications*, P.O. Box 681, 1000 AR Amsterdam, Netherlands. Review articles are invited or proposed by letter to the Editors. An outline of the proposed review should first be forwarded to the Editors for preliminary discussion prior to preparation. Submission of an article is understood to imply that the article is original and unpublished and is not being considered for publication elsewhere. For copyright regulations, see below.

Publication. The *Journal of Chromatography* (incl. *Biomedical Applications*) has 39 volumes in 1992. The subscription prices for 1992 are:

J. Chromatogr. (incl. *Cum. Indexes, Vols. 551–600*) + *Biomed. Appl.* (Vols. 573–611):
Dfl. 7722.00 plus Dfl. 1209.00 (p.p.h.) (total *ca.* US$ 4880.25)

J. Chromatogr. (incl. *Cum. Indexes, Vols. 551–600*) only (Vols. 585–611):
Dfl. 6210.00 plus Dfl. 837.00 (p.p.h.) (total *ca.* US$ 3850.75)

Biomed. Appl. only (Vols. 573–584):
Dfl. 2760.00 plus Dfl. 372.00 (p.p.h.) (total *ca.* US$ 1711.50).

Subscription Orders. The Dutch guilder price is definitive. The US$ price is subject to exchange-rate fluctuations and is given as a guide. Subscriptions are accepted on a prepaid basis only, unless different terms have been previously agreed upon. Subscriptions orders can be entered only by calender year (Jan.–Dec.) and should be sent to Elsevier Science Publishers, Journal Department, P.O. Box 211, 1000 AE Amsterdam, Netherlands, Tel. (+31-20) 5803 642, Telefax (+31-20) 5803 598, or to your usual subscription agent. Postage and handling charges include surface delivery except to the following countries where air delivery via SAL (Surface Air Lift) mail is ensured: Argentina, Australia, Brazil, Canada, China, Hong Kong, India, Israel, Japan*, Malaysia, Mexico, New Zealand, Pakistan, Singapore, South Africa, South Korea, Taiwan, Thailand, USA. *For Japan air delivery (SAL) requires 25% additional charge of the normal postage and handling charge. For all other countries airmail rates are available upon request. Claims for missing issues must be made within three months of our publication (mailing) date, otherwise such claims cannot be honoured free of charge. Back volumes of the *Journal of Chromatography* (Vols. 1–572) are available at Dfl. 217.00 (plus postage). Customers in the USA and Canada wishing information on this and other Elsevier journals, please contact Journal Information Center, Elsevier Science Publishing Co. Inc., 655 Avenue of the Americas, New York, NY 10010, USA, Tel. (+1-212) 633 3750, Telefax (+1-212) 633 3990.

Abstracts/Contents Lists published in Analytical Abstracts, Biochemical Abstracts, Biological Abstracts, Chemical Abstracts, Chemical Titles, Chromatography Abstracts, Clinical Chemistry Lookout, Current Contents/Life Sciences, Current Contents/Physical, Chemical & Earth Sciences, Deep-Sea Research/Part B: Oceanographic Literature Review, Excerpta Medica, Index Medicus, Mass Spectrometry Bulletin, PASCAL-CNRS, Pharmaceutical Abstracts, Referativnyi Zhurnal, Research Alert, Science Citation Index and Trends in Biotechnology.

See inside back cover for Publication Schedule, Information for Authors and information on Advertisements.

0021-9673/92/$05.00

This issue is printed on acid-free paper.

Printed in the Netherlands

JOURNAL OF CHROMATOGRAPHY

VOL. 590 (1992)

JOURNAL of CHROMATOGRAPHY

INCLUDING ELECTROPHORESIS AND OTHER SEPARATION METHODS

SYMPOSIUM VOLUMES

ELSEVIER

AMSTERDAM — LONDON — NEW YORK — TOKYO

View of Washington, DC, across the Potomac River with the Key Bridge and the symposium hotel in the foreground.

0021-9673/92/$05.00

Printed in the Netherlands

SYMPOSIUM ISSUE

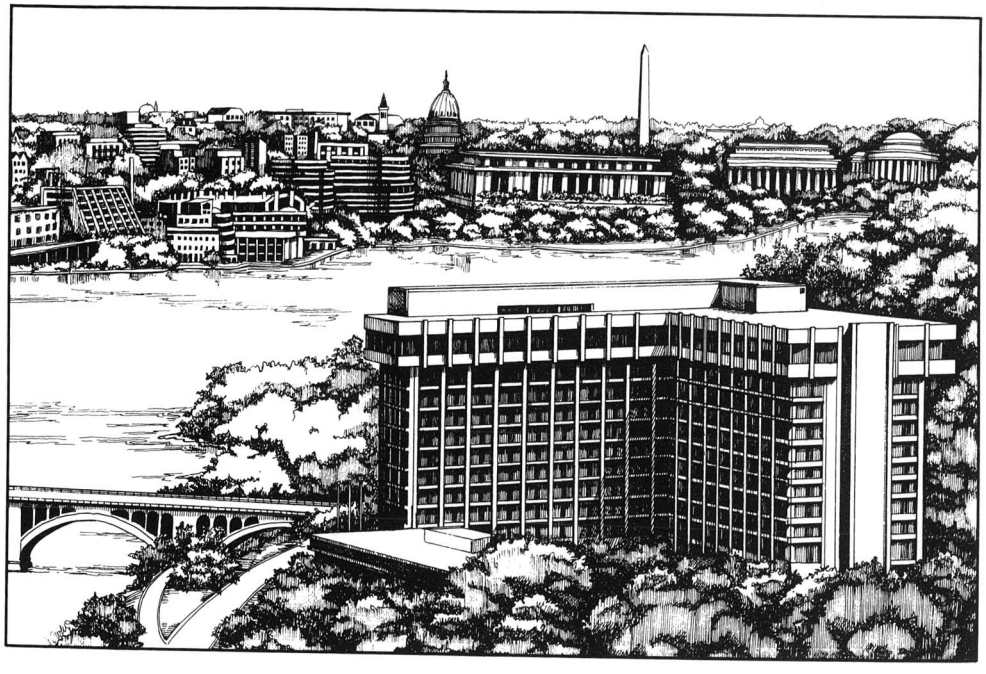

EIGHTH INTERNATIONAL SYMPOSIUM ON PREPARATIVE CHROMATOGRAPHY

Arlington, VA (USA), May 13–15, 1991

Guest Editor

G. GUIOCHON
(Knoxville and Oak Ridge, TN)

VOL. 590, NO. 1 JOURNAL OF CHROMATOGRAPHY JANUARY 24, 1992

CONTENTS

8TH INTERNATIONAL SYMPOSIUM ON PREPARATIVE CHROMATOGRAPHY, ARLINGTON, VA, MAY 13–15, 1991

In articles with more than one author, the name of the author to whom correspondence should be addressed is indicated in the article heading by a 6-pointed asterisk (*).

Journal of Chromatography, 590 (1992) 1
Elsevier Science Publishers B.V., Amsterdam

CHROMSYMP. 2468

Foreword

The *Eighth International Symposium on Preparative Chromatography (PREP'91)* took place in Arlington, VA, May 13–15, 1991, at the Washington Key Bridge Marriott Hotel. Like the previous meetings in this series, it was attended by slightly more than 250 participants. Thirty oral communications were presented and 43 poster contributions were exhibited and discussed. Two discussion sessions led to active exchanges of ideas on laboratory- and industrial-scale preparative chromatography.

All the organizers of a meeting can offer is an opportunity. The success of a scientific meeting depends on the quality of the scientific program and on the enthusiasm of the participants, providing for active public and private discussions. Nothing can replace a series of good contributions and a receptive audience. In this regard, the present meeting was highly successful. The quality of the presentations demonstrates the vigor of the research efforts being undertaken in both Academia and Industry in this important area of chromatography and also the importance of the separation problems encountered in various applications. The help of the members of the scientific committee in reviewing the abstracts submitted and in the organization of the program was greatly appreciated. The sponsorship of the Washington Chromatography Discussion Group is gratefully acknowledged. It is a pleasure to thank Drs. M. Diack, M. Z. El Fallah and S. Golshan-Shirazi who contributed actively to the smooth running of the meeting, and Mrs. Janet Cunningham, Symposium Manager, whose organizational skills allowed its successful operation.

This issue of the *Journal of Chromatography* includes some of the papers that were presented during the symposium. Although incomplete, this sample is representative of the nature and intensity of the research carried out in preparative chromatography. We hope that this volume will prove useful to those involved in this field. We are grateful to the Editor of the Symposium Volumes and to the editorial staff of the *Journal of Chromatography* for their professionalism and dedication in producing this volume.

Georges Guiochon

Journal of Chromatography, 590 (1992) 3–15
Elsevier Science Publishers B.V., Amsterdam

CHROMSYMP. 2385

Theory of optimization of ideal displacement chromatography of binary mixtures

S. C. David Jen and Neville G. Pinto*

Department of Chemical Engineering, University of Cincinnati, Cincinnati, OH 45221-0171 (USA)

ABSTRACT

The optimization of the displacement chromatographic separation of binary mixtures for maximizing the column throughput was investigated. The theory of coherence, based on the compound Langmuir model, was used to establish the general behavior of displacement chromatography through the use of distance–time diagrams. It is shown that columns should be operated at their resolution point for maximum throughput, and this is applicable to non-ideal displacement chromatography. Concentration of the feed sample to an optimum value is necessary to maximize the column throughput. The effects of the separation factor, capacity factors and resin saturation capacity with respect to throughput were also investigated. An analysis of the displacer affinity showed that low-affinity displacers are generally desirable in terms of development, regeneration and solubility requirements. A simple method is proposed for determining the optimum column loading for a given separation, and the extension of this approach to multi-component mixtures is discussed. This method can be used for the optimization of displacement separations of systems approximated by the compound Langmuir model.

INTRODUCTION

As the commercialization of biotechnology progresses, the need to develop cost-effective downstream processing strategies is becoming more intense [1]. Chromatographic purification steps, normally the most expensive steps, are therefore prime targets for reducing costs. Most current applications of preparative chromatography have used overloaded elution chromatography. It is known that preparative elution chromatography suffers from several drawbacks, including peak tailing, diluted product and low column loading [2]. In contrast, displacement chromatography provides several advantages, such as concentrated products, high column loading and low solvent consumption. Recently, progress in displacement chromatography for preparative applications, especially bioseparations, has been notable [2,3]. However, displacement chromatography is not yet widely accepted in downstream processing. There are several obstacles that hamper the application of this technique: lengthy regeneration, toxic displacers [4], low operational flow-rates [5] and complex method development and optimization [6]. Problems of regeneration and toxic displacers were recently addressed for ion-exchange displacement chromatography for protein purifications [7,8]. Novel support materials that enhance mass transfer through convective flow in the pores [9] may provide a solution to low operational flow-rates.

Method development and optimization of displacement chromatography are complicated by operation in the non-linear region of the isotherm and the use of displacers for achieving the separation. For chromatographic separations in elution mode, the fundamental resolution equation,

$$R_s = \frac{\sqrt{N}}{4} \cdot \frac{\alpha - 1}{\alpha} \cdot \frac{k_i' + 1}{k_i'} \quad (1)$$

has been used to establish guidelines for optimizing the resolution and the throughput in both the analytical and preparative modes [10,11]. However, eqn. 1 is not applicable to the optimization of displacement chromatography. Further, the most important parameter in preparative-scale separations, the column loading, can only be optimized

with a non-linear theory of chromatography. Previous approaches to optimizing displacement chromatography have used non-ideal chromatographic models to simulate specific separations [6,12,13]. Although these approaches predict the effects of axial dispersion and mass transfer rates, they cannot provide an overall picture of the dynamics of the displacement development process in a concise form, an essential component for a simple optimization technique. Distance–time diagrams [14] based on the theory of multi-component chromatography can provide such a tool for the efficient description of the chromatographic processes and at the same time be applicable to the cases where axial dispersion and mass transfer rates are important [15].

In this study, an optimization method based on the coherence theory of multi-component chromatography [14] was developed. The coherence theory assumes ideal chromatographic behavior, and uses the compound Langmuir model for representing multi-component equilibrium behavior. A key feature of this model is that it provides a mathematical transformation, the *h*-transformation, for depicting the dynamics of propagating systems, such as displacement development, in simple terms. The coherence theory has already been applied to displacement chromatography [2,14,16], and equations in terms of *h* compositions for calculating various resolution points are available for both systems involving stoichiometric [14] and non-stoichiometric adsorption behavior [2]. However, these equations have not been exploited for optimizing the displacement process. In this work, a framework has been developed for optimizing ideal displacement chromatography of binary mixtures. Analytical expressions in terms of mobile phase concentrations for displacement chromatography have been developed for the general case of non-stoichiometric adsorption, and effects of operating and thermodynamic parameters have been evaluated. Further, it has been shown that finite mass transfer rates do not alter optimal operating conditions identified with the coherence model.

The coherence approach to modeling displacement chromatography has been successful in several cases. For example, concentration profiles for the displacement chromatography of a fifteen-component rare earth mixture have been correctly calculated using the *h*-transformation [17], and the coherence model has been demonstrated to describe adequately displacement development in a high-performance liquid chromatographic system [18]. It has also been shown that a semi-ideal model [19] based on the compound Langmuir isotherm model predicted well the band profiles obtained earlier for the formation of the isotachic train. Further, for overloaded elution chromatography it has been demonstrated that optimum conditions identified with an ideal model are applicable to non-ideal cases, with minor modifications [15]. These results indicate that the development of an optimization model based on the compound Langmuir isotherm and ideal chromatographic behavior is likely to be practically useful. However, it must be emphasized that for systems that cannot be approximated by the compound Langmuir isotherm, such as systems that show selectivity reversal [20,21], the optimization method will have limited utility.

As the method developed is restricted to systems obeying the compound Langmuir isotherm, caution has to be exercised in using the coefficients of this isotherm. It has been shown that the use of single-component Langmuir coefficients in the compound Langmuir isotherm violates the Gibbs–Duhem relationship, unless the column saturation capacities are equal for all components [22,23]. For the chromatography of molecules of widely different size, such an assumption is unrealistic. Cox and Snyder [24] have reported significant effects of different column saturation capacities on overloaded elution chromatography. Nevertheless, if the compound Langmuir model is considered as a mathematical rather than a physical model, the use of different column saturation capacities becomes acceptable [25]. Further, the compound Langmuir model, based only on simple kinetic considerations, accounts only for competitive adsorption behavior. Hence, the use of single-component coefficients, although widely practised, is not recommended. Multi-component Langmuir coefficients can be conveniently measured with chromatographic methods [26,27], and these are recommended for use with the optimization procedure.

THEORY AND METHOD

Coherence theory

The coherence theory of chromatography [14] is based on the multi-component Langmuir isotherm. In terms of the elution capacity factor, k'_i, this isotherm takes the form

$$Q_i^* = \frac{k'_i c_i}{1 + \sum_{j=1}^{n} b_j c_j} \qquad i = 1, \ldots, n \tag{2}$$

When used with the coherence theory, the species in eqn. 2 are numbered according to their affinity for the stationary phase, with component i having a stronger affinity than component $i + 1$. Hence for displacement the displacer is component 1.

The coherence theory is most useful when compositions are expressed in an orthogonalized composition space called the h space [14]. The transformation from the c composition space to the h space involves the calculation of the roots of the equation

$$\sum_{i=1}^{n} \frac{b_i c_i}{h \cdot \frac{k'_i}{k'_1} - 1} = 1 \tag{3}$$

For systems involving trivial roots, these roots are obtained from

$$h_{j-1} = \frac{k'_1}{k'_j} \text{ or } h_j = \frac{k'_1}{k'_j} \text{ if } c_j = 0 \ (1 < j \leqslant n) \tag{4}$$

$$h_1 = 1 \quad \text{if} \quad c_1 = 0$$

In the h space, the adjusted composition velocity for a boundary with the jth root as the variable root is

$$U_j = h_j \prod_{i=1}^{n} h_i \prod_{i=1}^{n} \alpha_{i1} \tag{5}$$

where

$$\alpha_{i1} = k'_i / k'_1 \tag{6}$$

Real velocities can be calculated from adjusted velocities as follows

$$u_j = \frac{u_0}{1 + \frac{k'_{n+1}}{U_j}} \tag{7}$$

Column throughput: equation derivation

A distance–time diagram for displacement chromatography of a binary mixture can be generated from wave velocities (eqn. 5) calculated from the h compositions of the presaturant, feed and displacer solutions [14]. For a binary separation of components 2 and 3 using a displacer 1, a simplified distance–time diagram is shown in Fig. 1. Nine waves are generated and all these waves are sharp if

$$h'_3 < 1 + b_1 c_1^f \tag{8}$$

The adjusted time, τ, in Fig. 1 is defined as [14]

$$\tau = \frac{t}{k'_4} \cdot u_0 \tag{9}$$

Adjusted velocities for each wave can be obtained from eqn. 5 as

$$U_1 = \alpha_{42} (1 + b_2 c_2^f + b_3 c_3^f) \tag{10}$$

$$U_2 = \alpha_{41} h'_3 \tag{11}$$

$$U_3 = \alpha_{41} (1 + b_1 c_1^f) = U_8 = U_9 \tag{12}$$

$$U_4 = \alpha_{41} h'_2 \alpha_{21} (1 + b_1 c_1^f) \tag{13}$$

$$U_5 = \alpha_{41} (1 + b_1 c_1^f)(1 + b_2 c_2^f + b_3 c_3^f) \tag{14}$$

$$U_6 = \alpha_{41} h'_2 \alpha_{31} (1 + b_1 c_1^f) \tag{15}$$

$$U_7 = \alpha_{41} h'_3 \alpha_{31} (1 + b_1 c_1^f) \tag{16}$$

The h-roots in eqns. 11, 13, 15 and 16 can be related to the equilibrium data and the feed composition

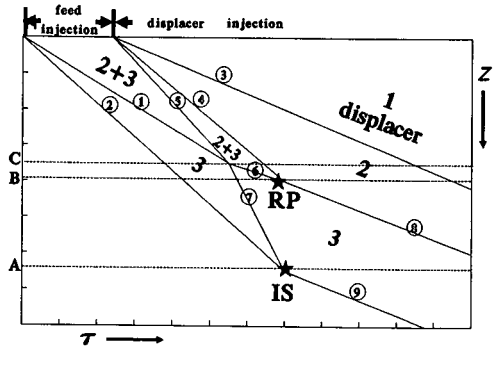

Fig. 1. Simplified distance–time diagram for the displacement chromatography of binary separations. The numbers in the circles represent the wave number.

$$h'_2 = \tfrac{1}{2}\left(\alpha_{13}(1 + b_3c_3^f) + \alpha_{12}(1 + b_2c_2^f) - \{[\alpha_{13}(1 + b_3c_3^f) - \alpha_{12}(1 + b_2c_2^f)]^2 + 4\alpha_{12}\alpha_{13}b_2c_2^fb_3c_3^f\}^{\frac{1}{2}}\right) \quad (17)$$

$$h'_3 = \tfrac{1}{2}\left(\alpha_{13}(1 + b_3c_3^f) + \alpha_{12}(1 + b_2c_2^f) + \{[\alpha_{13}(1 + b_3c_3^f) - \alpha_{12}(1 + b_2c_2^f)]^2 + 4\alpha_{12}\alpha_{13}b_2c_2^fb_3c_3^f\}^{\frac{1}{2}}\right) \quad (18)$$

Eqns. 10 and 14 can be used to calculate the coordinates of the first interference point, where wave 5 catches wave 1:

$$\tau_{15} = \frac{U_5}{U_5 - U_1} \cdot \tau_{feed} \quad (19)$$

and

$$z_{15} = \tau_{15}\, U_1 = \frac{U_1\, U_5}{U_5 - U_1} \cdot \tau_{feed} \quad (20)$$

Similarly, eqns. 13, 15, 19 and 20 give the second interference point, where wave 4 catches wave 6:

$$\tau_{46} = \frac{\dfrac{U_5\,(U_6 - U_1)}{U_5 - U_1} - U_4}{U_6 - U_4} \cdot \tau_{feed} = \tau^{RP} \quad (21)$$

and

$$z_{46} = U_4\left[\frac{\dfrac{U_5(U_6 - U_1)}{U_5 - U_1} - U_4}{U_6 - U_4} - 1\right]\tau_{feed} = z^{RP} \quad (22)$$

At this point the complete separation of components 2 and 3 is first achieved. This is defined as the resolution point (RP point in Fig. 1), and is indicated with the coordinates τ^{RP} and z^{RP} in eqns. 21 and 22. Note that the resolution point occurs whether or not eqn. 8 is satisfied.

Define a dimensionless time, θ, as:

$$\theta = \frac{t}{L} \cdot u_0 = \frac{t}{t_0} \quad (23)$$

In terms of θ, a resolution capacity θ^{RP}_{feed} is defined as the maximum feed time for which the resolution of the binary mixture can be achieved within a column length L. The resolution capacity can be calculated by substituting eqns. 9–16 and 23 into eqn. 22 and letting $L = z_{RP}$:

$$\theta^{RP}_{feed} = \frac{1 - \alpha_{32}}{1 + b_2c_2^f + b_3c_3^f - \alpha_{31}h'_2}(k'_2 - K'_1) \quad (24)$$

where $\alpha_{31}h'_2$ is only a function of properties of components 2 and 3. Therefore, the term outside the parentheses on the right-hand side of eqn. 24 is only a function of the properties and compositions of components 2 and 3. K'_1 is the frontal capacity factor of pure displacer, and can be directly measured experimentally from frontal chromatography of the displacer by

$$K'_1 = \frac{k'_1}{1 + b_1c_1^f} = \frac{T_1 - T_0}{T_0} \quad (25)$$

where T_1 is the breakthrough time of the displacer. In order to locate the isotachic point, the point beyond which all wave velocities are equal, it is necessary to locate the third interference point, where wave 7 catches wave 2 (Fig. 1). If eqn. 8 is satisfied, it can be shown from eqns. 11, 16 and 19–22 that

$$\tau_{27} = \frac{U_7 - U_1}{U_7 - U_2} \cdot \frac{U_5}{U_5 - U_1} \cdot \tau_{feed} = \tau^{IS} \quad (26)$$

and

$$z_{27} = \frac{U_7 - U_1}{U_7 - U_2} \cdot \frac{U_2\, U_5}{U_5 - U_1} \cdot \tau_{feed} = z^{IS} \quad (27)$$

If eqn. 8 is not satisfied, explicit equations cannot be derived for the isotachic coordinates. Analogous to the resolution capacity, an isotachic capacity, θ^{IS}_{feed}, can be defined as the maximum feed time for which the isotachic condition can be achieved within a column length L. The isotachic capacity can be calculated from eqn. 27 as

$$\theta^{IS}_{feed} = \frac{\left(1 - \dfrac{K'_1}{k'_2}\right)\left(1 - \dfrac{k'_3}{K'_1}\right)}{\dfrac{1 + b_2c_2^f + b_3c_3^f}{k'_2} - \dfrac{\alpha_{31}h'_3}{K'_1}} \quad (28)$$

It can also be shown from eqn. 12 that once the isotachic point is reached, the concentrations of components 2 and 3 are

$$c_2^{IS} = \frac{\alpha_{21}(1 + b_1c_1^f) - 1}{b_2} = \frac{\dfrac{k'_2}{K'_1} - 1}{b_2} \quad (29)$$

and

$$c_3^{IS} = \frac{\alpha_{31}(1 + b_1 c_1^f) - 1}{b_3} = \frac{\frac{k'_3}{K'_1} - 1}{b_3} \quad (29)$$

The band width for the zone of pure component 2, $\Delta\tau_{34}$, for the case when the resolution point is not attained in the column, $\theta_{feed} > \theta_{feed}^{RP}$, is given by

$$\Delta\tau_{34} = (\tau - \tau_{feed})\left(1 - \frac{U_3}{U_4}\right) \quad (30)$$

or, in terms of dimensionless time,

$$\Delta\theta_{34} = K_1\left(1 - \frac{\alpha_{12}}{h'_2}\right) \quad (31)$$

For the case when the resolution point is reached within the column, $\theta_{feed} < \theta_{feed}^{RP}$, the band width is

$$\Delta\tau_{38} = \frac{z_{RP}}{U_3} - \tau_{RP} + \tau_{feed} \quad (32)$$

In terms of dimensionless time,

$$\Delta\theta_{38} = \frac{(1 + b_2 c_2^f + b_3 c_3^f - \alpha_{31} h'_2)\left(1 - \frac{\alpha_{12}}{h'_2}\right)}{(k'_2 - k'_3)\left(\frac{1}{K'_1} - \frac{1}{k'_2}\right)} \cdot \theta_{feed} \quad (33)$$

It is convenient to define displacement time, θ_{disp}, as the time for the displacer front to exit the column. It can be shown from eqns. 9, 23 and 12 that

$$\theta_{disp} = 1 + K'_1 \quad (34)$$

Column regeneration is an important consideration in the optimization of the displacement process. In this study, it has been assumed that the carrier is used as the regenerant. The wave generated in this process is diffuse [14] with boundary velocities

$$U_{slow} = \alpha_{41} \quad (35)$$

and

$$U_{fast} = (1 + b_1 c_1^f)^2 \alpha_{41} \quad (36)$$

The time required to complete the regeneration step, θ_{reg}, can be calculated, using eqn. 35, to be

$$\theta_{reg} = k'_1 \quad (37)$$

Note that the time required for regeneration is directly proportional to the elution capacity factor of the displacer.

The column throughput for product 2, that is, the amount of pure component 2 produced per unit time, is

$$TH = \frac{\Delta\theta c_2^{IS}}{\theta_{feed} + \theta_{disp} + \theta_{reg}} \quad (38)$$

This equation can now be used in combination with eqns. 29, 31 and 33 to optimize the operating parameters with respect to the throughput of component 2.

RESULTS AND DISCUSSION

For the purpose of studying the importance of various operating parameters on column throughput, the system shown in Table I was used, unless stated otherwise. It was assumed that component 2 is the desired product, but the approach is also applicable if both 2 and 3 are desired products. Further, for simplicity, the concentrations of 2 and 3 in the feed were assumed to be equal. The optimizations are based on a fixed column length, but an equivalent optimization based on a fixed feed time can also be performed.

Optimization of column loading

Effects of feed time. Feed time significantly influences the column response and separation performance. For displacement chromatography, when the feed time is small, a constant pattern or the isotachic condition is reached within the column, and the fully developed displacement train travels with no further separation, resulting in an inefficient use of the column and the displacer. Therefore, to

TABLE I

LANGMUIR COEFFICIENTS AND OPERATING PARAMETERS USED IN THIS STUDY

Parameter	Component		
	1 (displacer)	2	3
Langmuir coefficients			
k'	15	10	5
b (ml/mg)	0.1875	0.125	0.0625
Feed concentration, C (mg/ml)	15	2	2

increase the column utilization without increasing the displacer consumption, the feed time can be further increased such that the isotachic condition is just reached at the column exit. This is the case shown by the line A in Fig. 1, and corresponds to a feed time given by θ^{IS}_{feed}. Most displacement chromatographic separations have been operated below θ^{IS}_{feed}.

An increase in the feed time beyond θ^{IS}_{feed} results in non-attainment of the isotachic condition. This is represented by the region above line A in Fig. 1. However, although the isotachic condition is not reached, there is clearly a zone, between lines A and B, where complete separation is achieved. Hence a feed time greater than θ^{IS}_{feed} can be used for complete separation, further extending the utilization of the column.

If the feed time is increased beyond θ^{RP}_{feed}, incomplete separation of components 2 and 3 results. This corresponds to the region above line B in Fig. 1. The incomplete separation results in a lower recovery of pure component 2, and hence the throughput can be expected to decrease.

This dependence of column throughput on feed time was verified with the system of Table I using eqn. 38 in combination with eqns. 29, 31, 33, 34 and 37, and is shown in Fig. 2. For feed times less than θ^{RP}_{feed} a linear dependence between throughput and feed time was obtained. The throughput was maximum for $\theta_{feed} = \theta^{RP}_{feed}$, and decreased for larger feed times because of decreased recovery. The maximum throughput is, from eqn. 38,

$$TH_{max} = \frac{\theta^{RP}_{feed}\, c_2^f}{\theta^{RP}_{feed} + \theta_{disp} + \theta_{reg}} \qquad (39)$$

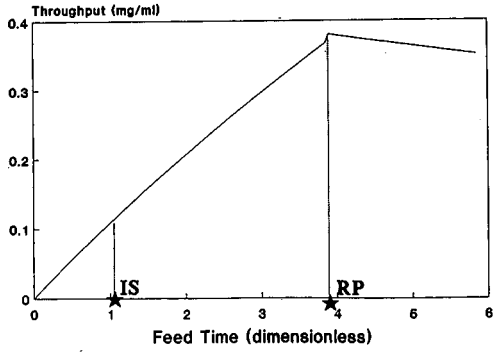

Fig. 2. Effects of feed time on throughput of component 2.

From Fig. 2 it can be seen that for a column loaded to θ^{RP}_{feed} the throughput of component 2 is close to four times larger than a column loaded to θ^{IS}_{feed}. Also, for feed times greater than θ^{RP}_{feed} the column is "overloaded". It should be noted that in all instances pure component 2 will be recovered at its isotachic concentration. However, total recovery of pure component 3 at its isotachic concentration can only be achieved if $\theta_{feed} \leqslant \theta^{IS}_{feed}$.

Optimum loading with non-ideal chromatographic behavior. The identification of θ^{RP}_{feed} as the optimum feed loading time was based on the assumption of ideal chromatography. In real systems, mass transfer resistances cannot be ignored. Mass transfer resistances will broaden boundaries, resulting in mixing between zones and, hence, lowered recoveries. As throughput will be affected, it is necessary to establish if the optimum feed loading criterion developed for ideal chromatography is valid in the non-ideal case.

In order to achieve this, displacement development was simulated for the system in Table I using an axial dispersion, linear driving force model [12]. The simulations were performed for a Peclet number of $1 \cdot 10^5$ and a range of Stanton numbers. Figs. 3–5 show chromatograms obtained for three feed times using a Stanton number of 200 in all instances. Fig. 3 is for a feed time of 1.05, θ^{IS}_{feed} for the ideal model, Fig. 4 is for a feed time of 3.89, θ^{RP}_{feed} for the ideal model, and Fig. 5 is for a feed time of 5.0. These and other simulations were used to calculate the throughput for component 2 of 98% purity, and the results are plotted in Fig. 6. It is clear that the dependence of throughput on feed time is very similar to the ideal

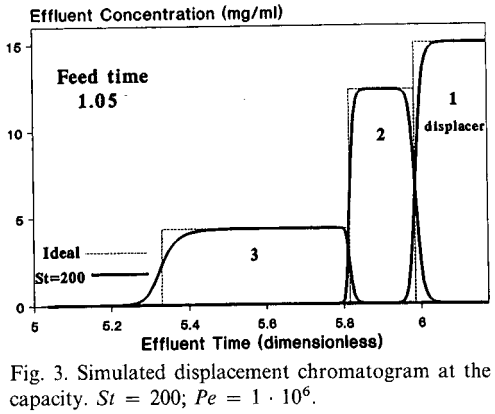

Fig. 3. Simulated displacement chromatogram at the isotachic capacity. $St = 200$; $Pe = 1 \cdot 10^6$.

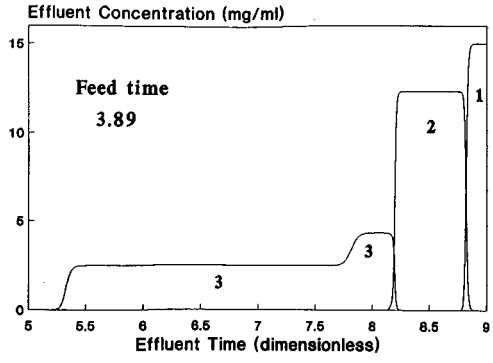

Fig. 4. Displacement chromatogram at the resolution capacity.

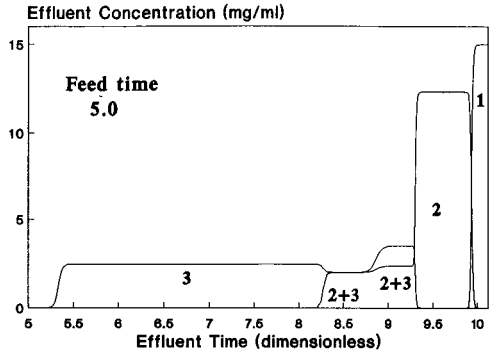

Fig. 5. Displacement chromatogram for column loading larger than its resolution capacity.

case. Although throughput decreases as the Stanton number increases, as is expected, in every instance θ_{feed}^{RP} obtained from the ideal case identifies the maximum throughput. This indicates that θ_{feed}^{RP} calculated from eqn. 24 can be used to optimize the column loading even when significant mass transfer resistances are present.

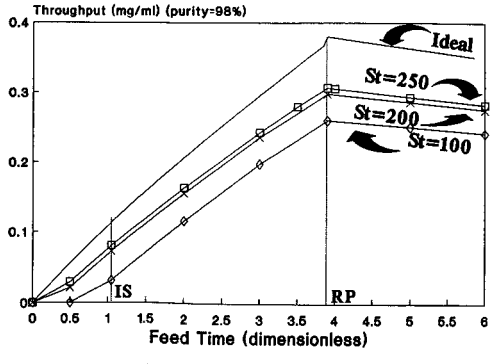

Fig. 6. Effect of non-ideality on column throughput.

In cases where mass transfer resistances or dispersion lead to significant overlap between adjacent zones in the displacement train, it is particularly important to optimize the feed loading. In Fig. 7 the recovery of component 2 (98% purity) is plotted as a function of feed time. It is clear that the θ_{feed}^{RP} provides the highest recovery. This can be easily understood from Figs. 3–5. For $\theta_{feed} < \theta_{feed}^{RP}$, as θ_{feed} increases the band width of the zones increases, and loss of useful products due to zone overlaps becomes less significant. Therefore, for example, operation at θ_{feed}^{IS} (Fig. 3) results in a lower recovery than operation at θ_{feed}^{RP} (Fig. 4). For $\theta_{feed} > \theta_{feed}^{RP}$ (Fig. 5), the separation of components 2 and 3 is not complete, which results in a lower recovery.

Also plotted in Fig. 7 is the total amount of product recovered as a function of feed time. Below θ_{feed}^{RP}, as the column is under-utilized, the amount recovered increases with increasing feed time. At and above θ_{feed}^{RP} the column is fully loaded, and the amount recovered remains constant. However, as θ_{feed}^{RP} represents the shortest feed time to attain the fully loaded condition, it gives the highest throughput.

Effects of feed concentration on throughput

It is well recognized that feed concentration has an important impact on the separation cost. For displacement chromatography, it is believed that the feed concentration should be as high as possible in order to load the sample at the top of the column. The effect of feed concentration on resolution capacity was investigated for the system in Table I. The effect of the total concentration of 2 and 3 was

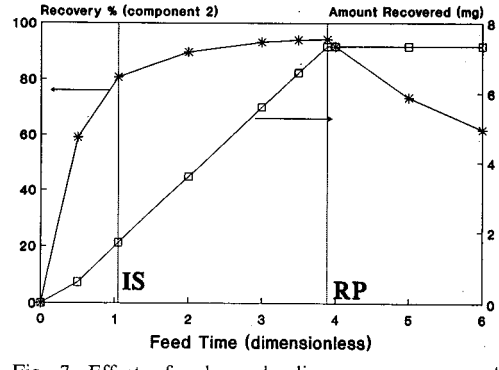

Fig. 7. Effect of column loading on recovery and amount recovered in non-ideal displacement chromatography. $St = 200$; $Pe = 1 \cdot 10^6$.

determined, keeping the displacer concentration constant. In all instances the concentrations of 2 and 3 were identical. The results of this study are shown in Fig. 8. The resolution capacity was initially found to decrease rapidly with increasing feed concentration. However, simultaneously, the maximum amount separated increased rapidly. Fig. 9 shows the cumulative effect on throughput. Throughput increases because for equal loadings the feed time decreases at higher feed concentrations.

An important feature of the dependence of throughput on feed concentration is the asymptotic approach to a maximum throughput. This has important implications in downstream processing. For dilute fermentation broths it is advantageous to concentrate the feed prior to a displacement separation. However, concentration beyond an optimum, determined by the economics of the displacement and concentration processes, may be counter-productive, as the gain in throughput will be insignificant.

Effects of properties of binary mixture on throughput

In this section only the effects of properties of the binary mixture will be considered, keeping the properties of the displacer constant. The effects of displacer properties will be discussed in the next section.

Separation factor. To study the effect of separation factor, α_{23}, on maximum column throughput, eqn. 24 was substituted into eqn. 39. Keeping all saturation capacities and k'_2 constant, the effect of α_{23} was obtained and is plotted in Fig. 10. At low values of the separation factor, the maximum

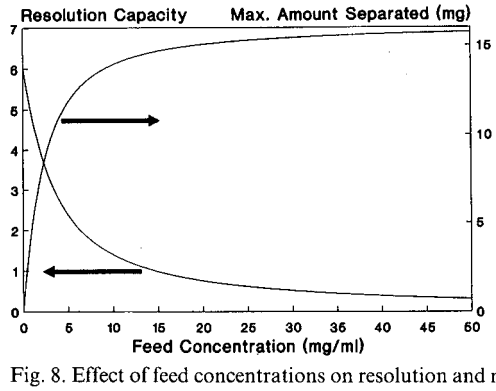

Fig. 8. Effect of feed concentrations on resolution and maximum amount separated.

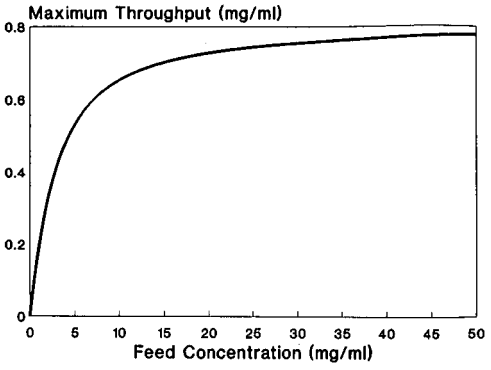

Fig. 9. Effect of feed concentrations on maximum column throughput.

throughput increases rapidly with increasing α_{23}. At high values of α_{23}, the behavior is asymptotic to an upper limit of the maximum throughput. Therefore, significant increases in separation factor will not in general translate into significant increases in throughput. Also, at low values of α_{23}, the throughput is proportional to $\alpha_{23} - 1$. This is in contrast to overloaded elution chromatography, where the throughput is proportional to $(\alpha_{23} - 1)^2$ [15]. Further, in the asymptotic region the throughput is approximately proportional to $(\alpha_{23} - 1)/\alpha_{23}$, which is similar to the dependence predicted by the resolution equation, eqn. 1, for elution chromatography. However, it should be noted that the relationship obtained is valid within the ideal model. For real columns, with limited efficiencies, the dependence of the throughput on the separation factor should be stronger [28].

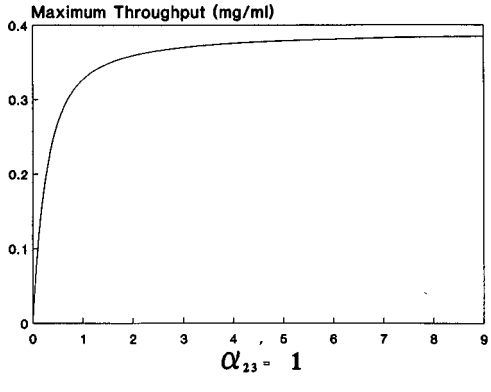

Fig. 10. Effect of separation factor on maximum column throughput.

Capacity factor. The effect of capacity factor on maximum throughput was also obtained by combining eqns. 24 and 39. In this instance, saturation capacities and separation factors were kept constant and both k'_2 and k'_3 were increased. The result is shown in Fig. 11. The maximum throughput was found to increase almost proportionally to k'_2, owing to the attainment of higher column loadings at higher capacity factors. This result is in contrast to elution chromatography, where optimum capacity factors are considered to be between 1.5 and 5. In elution chromatography, higher capacity factors result in longer separation times and hence lower throughputs. In displacement chromatography, however, the displacer velocity, not the capacity factors of the feed components, is the prime determinant of the separation time. Therefore, capacity factors should be as large as possible in order to maximize the throughput, within the limitation that these capacity factors are less than the capacity factor of the displacer.

Saturation capacity. The effect of saturation capacities on the maximum throughput was also studied by substituting eqn. 24 into eqn. 39. As the saturation capacities are $k'_i/\phi b_i$, the b_i values were systematically varied keeping all other parameters constant. Identical saturation capacities were used for components 2 and 3. The effect observed (Fig. 12) is similar to the effect of feed concentration and separation factor, with a strong dependence at low saturation capacities and asymptotic behavior at high saturation capacities. At low values the maximum throughput is small owing to the limited loading capacity, although the displacement effect is

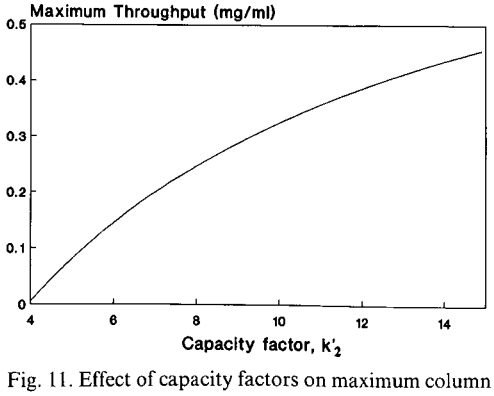

Fig. 11. Effect of capacity factors on maximum column throughput.

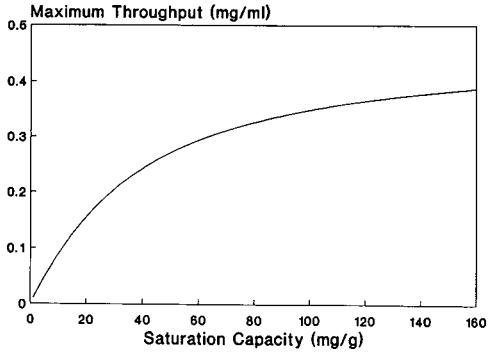

Fig. 12. Effect of saturation capacity on maximum column throughput.

pronounced [29]. This result indicates that nonporous supports, normally of low saturation capacity, are not suitable for displacement chromatography, although they may have more favorable mass transfer characteristics. Also, as low saturation capacities may result from a high modulator concentration, it is important to optimize the type and concentration of modulator used.

Effects of displacer on column throughput

Minimum displacer concentration. With reference to Fig. 1, the first requirement for a successful displacement separation of components 2 and 3 is that U_5 should be larger than U_1. From eqns. 10 and 14, this requires a minimum displacer concentration such that

$$K'_1 < k'_2 \tag{40}$$

This condition is consistent with the requirement that θ^{RP}_{feed} should be positive (eqn. 24). Attainment of the isotachic condition further requires that U_7 must be larger than U_2 (Fig. 1). This requires that

$$K'_1 < k'_3 \tag{41}$$

When only eqn. 40 is satisfied, component 3 is eluted and component 2 is displaced. The conditions given by eqns. 40 and 41 are represented in Fig. 13. Note that these conditions require that the slope of the operating line be less than the slope at infinite dilution of the isotherms of the mixture components, a well known condition for displacement chromatography [2].

Effects of displacer concentration on throughput. The effect of displacer concentration on throughput

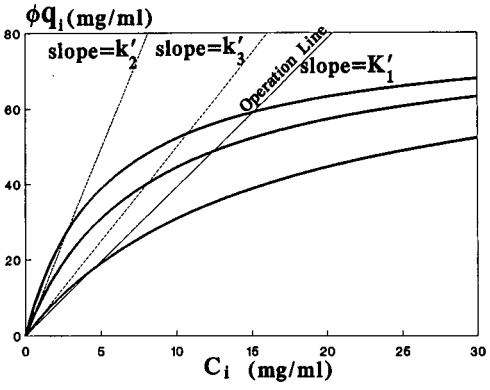

Fig. 13. Displacer and feed adsorption isotherms and operation line.

was determined from eqns. 25, 34 and 39, and is shown in Fig. 14. At low concentrations, significant gains can be made with regard to the throughput by increasing displacer concentration. However, at higher concentrations the dependence of throughput on displacer concentration is weak. This weak dependence is due to small frontal capacity factors at high concentrations (eqn. 25), which makes θ_{disp} almost independent of concentration (eqn. 34). Hence the maximum throughput (eqn. 39) is only weakly influenced. The weak influence at high concentrations indicates that a higher displacer concentration may not always be economically favored. Also, it should be noted that the highest displacer concentration that can be used in practice may be limited by solubility and mass transfer considerations [12,30].

Displacer optimization. A requirement in the selection of a displacer is that the displacer affinity be higher than that of any of the components in the mixture. However, displacer affinity also influences the column regeneration (eqn. 37) and, hence, column throughput. As displacers with the same value of K'_1 will give the same displacement separation for a given mixture, it is possible to reduce θ_{reg} without affecting the displacement separation. From eqn. 25, a reduction in k'_1 can be compensated for by a change in the feed concentration c_1^f. This is illustrated on the operating diagram in Fig. 15 for three displacers 1, 1′ and 1″. As an example, displacers 1 and 1″ would give the same separation if displacer concentrations of c'_1 and c''_1 were used, respectively. However, as 1″ has a lower k'_1 value, the regeneration would be quicker with this displacer. This analysis indicates that a displacer with b_1 values as small as possible and with k'_1 values close to the affinities of the desired components should be selected for maximum throughput.

The importance of optimizing displacer affinity with respect to both column development and regeneration has recently been demonstrated for the ion-exchange displacement chromatography of proteins [7,8]. It has been shown that lower affinity polyelectrolyte displacers can be used effectively for displacement development, and they are more efficiently removed from the column during regeneration than analogous higher affinity displacers. This is consistent with the conclusions reached above.

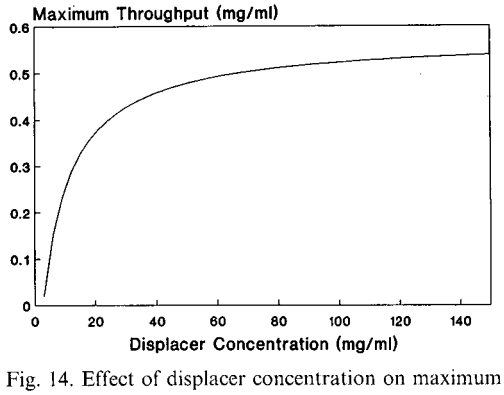

Fig. 14. Effect of displacer concentration on maximum column throughput.

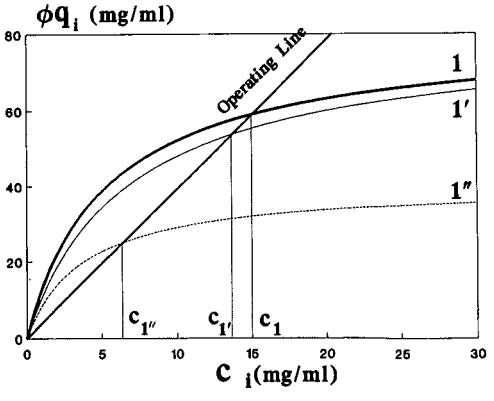

Fig. 15. Effects of concentration and affinity on displacer frontal capacity.

Simple method for determination of maximum column loading

For practical applications, it is very useful to establish a simple procedure for determining θ^{RP}_{feed} and θ^{IS}_{feed}. This can be done with two sets of experiments. An elution chromatographic separation should be performed with a sample concentration low enough to ensure no interference between components. From these data, the elution capacity factors can be calculated

$$k'_i = \frac{t_i - t_0}{t_0} \tag{42}$$

The frontal capacity factor, K'_{im}, defined as

$$K'_{im} = \frac{T_{im} - T_0}{T_0} \tag{43}$$

is obtained from a frontal injection of the sample at its feed concentration.

These capacity factors can be used to calculate required h compositions [27]. For binary mixtures,

$$\alpha_{31} h'_2 = \frac{K'_{3m}}{K'_{2m}} \quad \text{and} \quad \alpha_{31} h'_3 = \frac{k'_3}{K'_{3m}} \tag{44}$$

Also, it has been shown [27] that

$$K'_{2m} = \frac{k'_2}{1 + b_2 c_2^f + b_3 c_3^f} \tag{45}$$

Substituting eqns. 44 and 45 into eqns. 24 and 28, θ^{RP}_{feed} and θ^{IS}_{feed} are obtained in terms of the measured parameters:

$$\theta^{RP}_{feed} = \frac{1 - \dfrac{k'_3}{k'_2}}{\dfrac{k'_2}{K'_{2m}} - \dfrac{K'_{3m}}{K'_{2m}}} (k'_2 - K'_1) \tag{46}$$

and

$$\theta^{IS}_{feed} = \frac{\left(1 - \dfrac{K'_1}{k'_2}\right)\left(\dfrac{k'_3}{K'_1} - 1\right)}{\dfrac{k'_3}{K'_{3m} K'_1} - \dfrac{1}{K'_{2m}}} \tag{47}$$

It is interesting that with very dilute feed samples K'_{im} approaches k'_i, and eqns. 46 and 47 reduce to

$$\theta^{RP}_{feed} = k'_2 - K'_1 \quad \text{and} \quad \theta^{IS}_{feed} = k'_3 - K'_1 \quad \text{as} \quad c_i^f \to 0 \tag{48}$$

These correspond to the maximum feed times for the resolution and isotachic conditions, respectively. For complete resolution, the maximum feed time is simply the difference between the infinite dilution slope of the isotherm of the more retained component and the slope of the operating line for the displacement process (Fig. 13). Similarly, for the isotachic condition, the maximum feed time is given by the difference between the infinite dilution slope of the less retained component and the slope of the operating line.

Extension to multi-component mixtures

The procedure developed here for a binary mixture can be extended to multi-component systems in most instances. Fig. 16 shows the distance–time diagram for displacement chromatography of a ternary mixture. For this case, there are two resolution points and one isotachic point. Similarly, for an n-component mixture, there are $n - 1$ resolution points and one isotachic point. The optimum loading will depend on the desired component. For an n-component system with the displacer as the highest affinity component, the maximum throughput occurs at the ith resolution point if the desired product is the ith component.

If $h'_{n+1} < 1 + b_1 c_1^f$, then all the waves generated are sharp, and all the resolution and isotachic points can be calculated as a function of separation factors and the h-root compositions of the feed. Further, these h-roots can be expressed in terms of the frontal and elution capacity factors [27]. The capacity factors can be calculated from eqns. 42 and 43. In cases where diffuse waves are generated in an n-component displacement, this method is still ap-

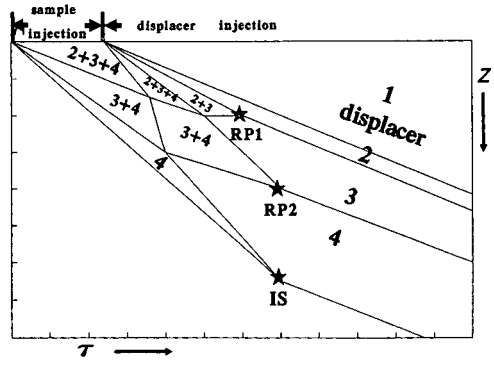

Fig. 16. Simplified distance–time diagram for the displacement chromatography of ternary separations.

plicable for the calculation of the resolution points, but not for the isotachic point. The generation of diffuse waves can be predicted from

$$K'_{n+1,m} > K'_1 \tag{49}$$

Finally, a similar methodology can be applied to the determination of the maximum feed time in overloaded elution chromatography.

CONCLUSIONS

The coherence theory provides a general and convenient framework for the optimization of displacement chromatography. Using this framework, it has been shown that throughput for a binary separation is maximized when the column is operated at the resolution point. Further, the result appears to be valid when mass transfer and/or axial dispersion effects are significant. Therefore, the optimum column loading is almost independent of the column efficiency, and the recovery and column efficiency will be traded in a compromise maximizing the throughput.

The effects of feed concentration, separation factor, saturation capacities and displacer concentration on the throughput have also been determined. Larger values of all these parameters give higher throughputs. However, in each instance the optimum value will not, in general, be the highest value of the parameters, because of an asymptotic dependence of throughput on these parameters. With regard to the capacity factor of the desired component, k'_2, and the displacer, k'_1, a high value of k'_2 and a low value of k'_1 are desired. A high value of k'_2 enhances column loading, and a low value of k'_1 is advantageous with respect to column development, regeneration and displacer solubility. However, the lowest value of k'_1 is limited by the affinity of the most strongly retained component in the mixture.

This optimization method, developed here for a binary mixture, can be extended to multi-component systems. In this instance, if the ith component is the desired product, the maximum throughput will be established by the ith resolution point, that is, the point on the distance–time diagram where the ith component is completely separated from the remainder of the mixture.

Finally, the use of the compound Langmuir model in this study places restrictions on its applications to the systems deviating markedly from Langmuir behavior.

ACKNOWLEDGEMENT

This work was supported in part by Grant No. CTS-8909742 from the National Science Foundation. This support is gratefully acknowledged.

SYMBOLS

a_i	affinity constant, Langmuir parameter of adsorbate i
b_i	Langmuir parameter of adsorbate i
c_i	mobile phase concentration of adsorbate i
c_i^f	feed concentration of adsorbate i
c'_1	required concentration of the displacer, 1′, in Fig. 15
c''_1	required concentration of the displacer, 1″, in Fig. 15
h	h-root
h'_i	h-root of frontal injection of the binary mixtures
k'_i	elution capacity factor of adsorbate i at the infinite dilution, $k'_i = \phi a_i$
k'_4	elution capacity factor of the dummy species
K'_1	frontal capacity factor of the displacer
K'_{im}	frontal capacity factor of ith component in frontal chromatography of the binary mixture
L	column length
n	number of adsorbates
N	number of theoretical plates
Pe	Peclet number, product of interstitial velocity and column length divided by effective axial dispersion coefficient
q_i	average stationary phase concentration of adsorbate i
q_i^*	equilibrium stationary phase concentration of adsorbate i
Q_i	$Q_i = \phi q_i$
Q_i^*	$Q_i^* = \phi q_i^*$
St	Stanton number, product of mass transfer rate and column length divided by interstitial velocity
t	real time
t_0	column hold-up time in elution chromatography

t_i retention time of adsorbate i in linear isocratic elution chromatography
T_0 column hold-up time in frontal chromatography
T_1 breakthrough time in frontal or displacement chromatography of the displacer
T_{im} retention time of the ith component in frontal chromatography of the binary mixture
TH throughput (amount of product produced per unit of time) divided by the column flow-rate
TH_{max} maximum value of TH, occurring at the resolution point
u_0 interstitial bulk phase velocity
u_i true velocity of adsorbate i
U_i adjusted velocity of adsorbate i
z column distance

Greek letters

α separation factor
ϕ column phase ratio
θ dimensionless time (t/t_0)
θ_{feed} dimensionless feed time (or column loading) for injection of the binary mixture
θ_{feed}^{IS} maximum dimensionless feed time with which the isotachic condition can be achieved
θ_{feed}^{RP} maximum dimensionless feed time with which the complete separation is possible
τ adjusted time (unit of length)

REFERENCES

1 B. J. Spalding, *Bio/Technology*, 9 (1991) 229–233.
2 J. Frenz and Cs. Horváth, in Cs. Horváth (Editor), *High-Performance Liquid Chromatography —Advances and Perspectives*, Vol. 5, Academic Press, New York, 1988, pp. 211–314.
3 S. M. Cramer and G. Subramanian, *Sep. Purif. Methods*, 19 (1990) 31–91.
4 H. Colin, in P. R. Brown and R. A. Hartwick (Editors), *High-Performance Liquid Chromatography*, Wiley, New York, 1989, p. 415.
5 G. Subramanian and S. M. Cramer, *Biotechnol. Prog.*, 5 (1989) 92.
6 A. M. Katti, E. V. Dose and G. Guiochon, *J. Chromatogr.*, 540 (1990) 1–20.
7 S.-C. D. Jen and N. G. Pinto, *J. Chromatogr. Sci.*, 27 (1991) in press.
8 S.-C. D. Jen and N. G. Pinto, *J. Chromatogr.*, 519 (1990) 87–98.
9 N. B. Afeyan, N. F. Gordon, I. Mazsaroff, L. Varady, S. P. Fulton, Y. B. Yang and F. E. Regnier, *J. Chromatogr.*, 519 (1990) 1–29.
10 J. M. Miller, *Chromatography: Concepts and Contrasts*, Wiley, New York, 1988.
11 G. K. Sofer and L. E. Nyström (Editors), *Process Chromatography: a Practical Guide*, Academic Press, San Diego, 1989.
12 M. W. Phillips, G. Subramanian and S. M. Cramer, *J. Chromatogr.*, 454 (1988) 1–21.
13 T. Gu, G.-J. Tsai and G. T. Tsao, *Biotechnol. Bioeng.*, 37 (1991) 65–70.
14 F. Helfferich and G. Klein, *Multicomponent Chromatography: Theory of Interference*, Marcel Dekker, New York, 1970.
15 S. Golshan-Shirazi and G. Guiochon, *Anal. Chem.*, 61 (1989) 1276.
16 H.-K. Rhee and N. R. Amundson, *AIChE J.*, 28 (1982) 423–433.
17 F. Helfferich and D. B. James, *J. Chromatogr.*, 46 (1970) 1–28.
18 J. Frenz and Cs. Horváth, *AIChE J.*, 31 (1985) 400–409.
19 A. M. Katti and G. Guiochon, *J. Chromatogr.*, 449 (1988) 25–40.
20 S. Golshan-Shirazi and G. Guiochon, *J. Chromatogr.*, 545 (1991) 1–26.
21 F. Antia and Cs. Horváth, paper presented at the *8th International Symposium on Preparative Chromatography, PREP '91*, Washington, DC, May, 1991.
22 D. B. Broughton, *Ind. Eng. Chem.*, 40 (1948) 1506.
23 C. Kemball, E. K. Rideal and E. A. Guggehnheim, *Trans. Faraday Soc.*, 44 (1948) 952.
24 G. B. Cox and L. R. Snyder, *J. Chromatogr.*, 483 (1989) 95–110.
25 E. C. Markham and A. F. Benton, *J. Am. Chem. Soc.*, 53 (1931) 497.
26 J. M. Jacobson and J. Frenz, *J. Chromatogr.*, 499 (1990) 5–19.
27 S.-C. D. Jen and N. G. Pinto, presented at the *8th International Symposium on Preparative Chromatography, PREP '91*, Arlington, VA, May, 1991.
28 G. B. Cox and L. R. Snyder, *J. Chromatogr.*, 483 (1988) 95–110.
29 T. Gu, G. T. Tsao, G.-J. Tsai and M. R. Ladisch, *AIChE J.*, 36 (1990) 1156–1162.
30 J. Frenz, P. van der Schriek and Cs. Horváth, *J. Chromatogr.*, 330 (1985) 1–17.

Journal of Chromatography, 590 (1992) 17–33
Elsevier Science Publishers B.V., Amsterdam

CHROMSYMP. 2421

Displacement effects in preparative gradient high-performance liquid chromatographic separations

G. B. Cox*

Prochrom Inc., 5622 W 73rd Street, Indianapolis, IN 46278 (USA)

L. R. Snyder☆

LC Resources, 3182C Old Tunnel Road, Lafayette, CA 94549 (USA)

ABSTRACT

Experiments were carried out which were designed to elucidate the influence of gradient parameters on the strong displacement effects which have been observed in the preparative chromatography of proteins. Unexpected loading phenomena were observed in which a proportion of the model protein load was not taken up by the column, even though the saturation capacity of the column was not exceeded. This proportion was a function of the mobile phase composition at which the protein was loaded. Low solvent strengths were seen to be essential to allow high preparative sample loads. It was shown that the saturation capacity of the column changed little with gradient parameters and also that the saturation capacities calculated on the assumption of approximate Langmuir isotherm behaviour were in error. Mass overloaded separations of binary mixtures of proteins all demonstrated the existence of displacements between the solutes, even when a substantial amount of the second-eluting protein was not adsorbed on initial loading. It was demonstrated that the gradient slope had little effect on the separation because of the very sharp displacement zones observed. Steeper gradients allowed a higher production rate without incurring a decrease in purity or recovery. Guidelines for the design of reversed-phase gradients for the purification of proteins are given with a view to maximising solute–solute displacements. Such gradients will allow the maximum production rates of purified product.

INTRODUCTION

Displacement effects between solutes in isocratic mass overloaded chromatography are now well documented [1–4]. Much of this work has been carried out by computer simulation [1,2], although some experimental work which supports these results has been published [1,3,4]. The interactions between the solutes which give rise to these displacements in preparative chromatography are controlled by their adsorption isotherms. Although some conclusions can be drawn from a study of the individual isotherms of the solutes, the interactions can only be correctly predicted if the competitive isotherm between them is known [5].

The determination of these competitive isotherms is at the least both tedious and difficult. Further, it is usually impossible to determine the isotherms where the solutes are not available in a pure form and in reasonable amounts. Predictions can be made if a model based on the competitive Langmuir isotherm is assumed and this has been the basis of much of the computer simulation work. Unfortunately, although a good qualitative understanding may be gained from these results, the competitive Langmuir model is not valid for all cases [6]. This means that the isotherms have to be determined experimentally in order to obtain good predictions of the experimental results. In many practical cases, this requirement renders modelling impractical and only the qualitative results from the simulations are useful.

We have reported experimental results for isocratic separations [3] where the simple simulations based on the competitive Langmuir model do not give valid predictions. These are cases in which the

☆ Present address: LC Resources, 2930 Camino Diablo, Walnut Creek, CA 94596, USA.

0021-9673/92/$05.00

saturation capacities of the column for the two solutes of interest are markedly dissimilar. Where the saturation capacity for the first-eluting solute is significantly greater than that for the second (*i.e.*, the isotherms cross), the bands merge. Conversely, the second component may displace the first when it has the greater saturation capacity [$w_{s(2)} > w_{s(1)}$]. It is probable that as the saturation capacities for the two components become closer in value their behaviour will move from the extreme case to one intermediate between this and a case at least qualitatively similar to that predicted by the competitive Langmuir model.

We have also reported [7,8] the modeling of gradient elution separations under conditions of mass overload. The parallels between preparative isocratic and gradient elution separations are many [7]; thus, one would expect to see some of the different types of solute interactions which are observed in isocratic separations carried over into the corresponding gradient chromatograms. The peak shape distortions predicted from Craig counter-current simulations of overloaded gradient separations are similar in nature to those found in the simulations of isocratic separations. We have also shown [8] that in the gradient separations of peptides and proteins there are additional factors influencing the separation, related to the different S values (the slope of a plot of log k' against solvent strength modifier concentration) for the solute molecules.

Both modelling and experimental data indicate that even stronger displacement effects may be seen under gradient elution conditions for large molecules than for small solutes. Evidence for this exists both in our own preliminary results and in the work of Mant *et al.* [9]. In the latter instance, it has been demonstrated that extremely strong displacements can occur between peptide molecules. These purifications were carried out under conditions of strong retention and it was seen that separations of these compounds could be effected under isocratic conditions appropriate for the loading of the sample on to the column rather than elution. This sample displacement could explain the sharp boundaries between the components which we observed in our preparative gradient separations of proteins [8], as these gradients began at low concentrations of organic modifier (*i.e.*, conditions of strong retention).

The purposes of the experimental work reported in this paper were threefold: to extend our initial data, which showed very significant displacement effects occurring in the preparative gradient elution chromatography of protein standards, to verify the parallels between gradient and isocratic separations and to observe the effects on the displacements of the slope and the range of compositional change in the gradient.

EXPERIMENTAL

Equipment

LC system. An HP 1090 M liquid chromatograph (Hewlett Packard, Avondale, PA, USA) fitted with a preparative autoinjector was used for part of this work. The remainder was carried out using an HP 1090 L liquid chromatograph fitted with a diode-array detector. A second system (HP 1090 L) was used for the analysis of fractions taken during preparative experiments.

Data system. Initial work was done using a Nelson Analytical Data System, based on an HP 200 computer (Nelson Analytical, Cupertino, CA, USA) for data collection and storage in addition to the system built into the HP 1090 M chromatograph. The Nelson software was modified in-house to incorporate the calculation of the capacity factors, efficiencies and skews of detected peaks. In later work an HP 3365 Chem Station was used.

Chromatography

Columns. All columns were constructed from stainless steel and were packed by a downward slurry technique. Separations of proteins were carried out using either an experimental Zorbax PSM 1000 C_8 packing (particle size 7 μm, pore size 1000 Å) (DuPont, Wilmington, DE, USA) packed into 15 cm × 4.6 mm I.D. columns or Zorbax PRO-10 Protein Plus (10 μm, pore size 300 Å) packed into 25 cm × 4.6 mm I.D. columns. Small molecule separations were performed using Zorbax ODS (5 μm, pore size 70 Å) packed into a 15 cm × 4.6 mm I.D. column.

Chemicals and mobile phases. Methanol and acetonitrile were obtained as high-performance liquid chromatographic (HPLC)-grade solvents from J. T. Baker (Phillipsburg, NJ, USA). Trifluoroacetic acid (TFA) was obtained from J. T. Baker, protein

standards from Sigma (St. Louis, MO, USA) and phenol, benzyl alcohol, cresol and 2-phenylethanol from Aldrich (Milwaukee, WI, USA).

Chromatography of proteins was performed using gradients made from mixtures of 0.1% aqueous trifluoroacetic acid and 0.1% trifluoroacetic acid in acetonitrile. Gradients for the other separations were formed from methanol and water.

RESULTS AND DISCUSSION

Small molecules

Our earlier discussion of the effects of elution gradients on separations [8] did not address the situation where the saturation capacities of the column for the components of interest differ. This is inherent in the simulation model in that the equations based on the Langmuir model assume equal w_s values. This and the effects of deviations from Langmuir behaviour are discussed in more detail in the Appendix. In order to investigate this aspect, gradient separations were carried out for compounds which had been shown earlier to have different saturation capacities under isocratic elution conditions. It was assumed for this part of the study that although the isotherms would clearly change with the eluent composition owing to the changes in the distribution coefficients, the saturation capacities would remain constant. Other studies [10] have shown that the saturation capacity for benzyl alcohol remains constant over a moderate range of solvent composition.

Our previous work [3], which reported the effects of unequal saturation capacities in isocratic mass overloaded separations, used mixtures of either phenol and benzyl alcohol or of *p*-cresol and 2-phenylethanol as solutes. It was found that the saturation capacities of the aromatic alcohols were approximately double those of the phenols. The same solute pairs were chosen for the gradient elution studies. Table I shows the separation conditions for these experiments together with the S values for the components, determined from the gradients reported here and from others with 2.5 times the gradient run time.

It may be noted that the S value for benzyl alcohol is larger than that of phenol, whereas those of *p*-cresol and 2-phenylethanol are equal under the separation conditions chosen. From our earlier discussion of the effect of S values on gradient separations [8], the phenol–benzyl alcohol separation should be characterised by an increase in selectivity as the load increases. The other separation should show a constant selectivity with load. In the isocratic experiments, benzyl alcohol was shown to displace the earlier eluting phenol very strongly, whereas *p*-cresol merged with the earlier eluting 2-phenylethanol. Following the principle that for corresponding separations the data from isocratic and gradient elution experiments are related, then the former pair of solutes should show displacement and the latter pair should merge in the gradient experiments.

The result of loading a mixture of 3 mg of phenol and 1 mg of benzyl alcohol is shown in Fig. 1a. As would be predicted from the isocratic experiment, there is a pronounced displacement of phenol by benzyl alcohol. This is demonstrated by the rapid

TABLE I

OPERATING CONDITIONS FOR SMALL-MOLECULE GRADIENT SEPARATIONS

Flow-rate: 1.0 ml/min. Detector: UV, wavelengths 254 and 280 nm.

Solute	Column	Gradient		S
		Range	Time (min)	
Phenol	Zorbax ODS	0–40%	20	2.69
Benzyl alcohol	(15 cm × 4.6 mm I.D.)	CH_3OH–H_2O		2.99
2-Phenylethanol	Zorbax ODS	10–70%	17	2.27
p-Cresol	(15 cm × 4.6 mm I.D.)	CH_3OH–H_2O		2.27

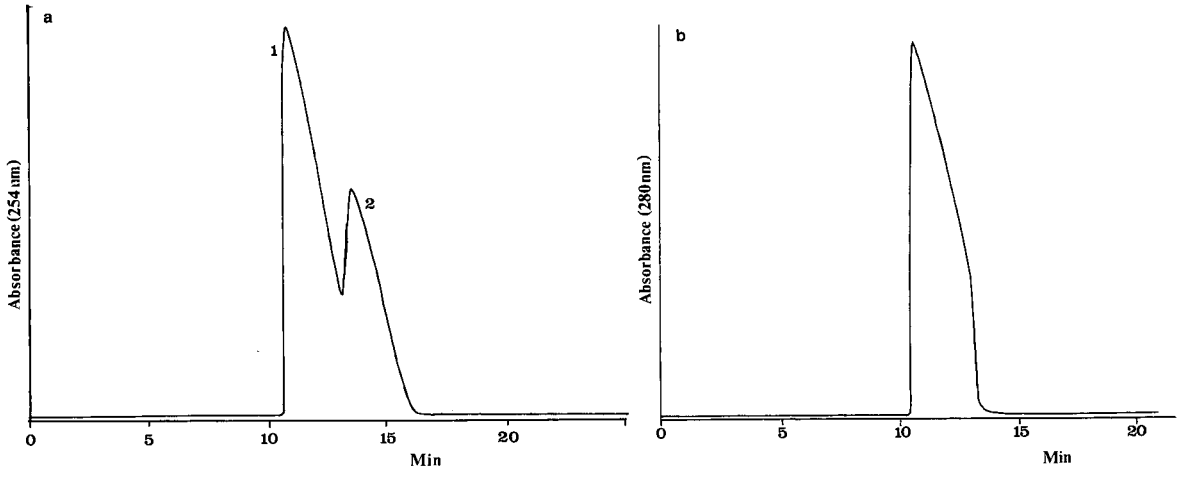

Fig. 1. (a) Gradient elution preparative chromatograms of 3 mg each of phenol and benzyl alcohol. Flow-rate, 1 ml/min; detection, UV, 254 nm. For other conditions, see Table I. Peaks: 1 = phenol; 2 = benzyl alcohol. (b) As for (a), with UV detection at 280 nm.

drop of the trailing edge of the peak envelope of phenol (monitored at 280 nm, where benzyl alcohol has a very small UV absorption) to the baseline (Fig. 1b). It is also of interest that the resolution between the peaks for the given sample load is slightly larger for the gradient separation as compared with the isocratic chromatogram [3]. From the relationship between selectivity and solvent composition derived in the Appendix, this difference is not surprising, as the solutes will certainly be eluting at a mobile phase concentration different from that used isocratically.

With the other solute pair studied, *p*-cresol and 2-phenylethanol have equal S values and hence no such increase in selectivity should be noted. In fact, the two peak maxima move closer as the sample load is increased. The separation, in this instance with the injection of 3 mg of *p*-cresol and 1 mg of benzyl alcohol, is shown in Fig. 2a. Because of the difficulty in deconvolution of the chromatograms taken at the two wavelengths, the separation was repeated, collecting fractions through the peaks at 5-s intervals. The reconstructed chromatogram (Fig. 2b) shows

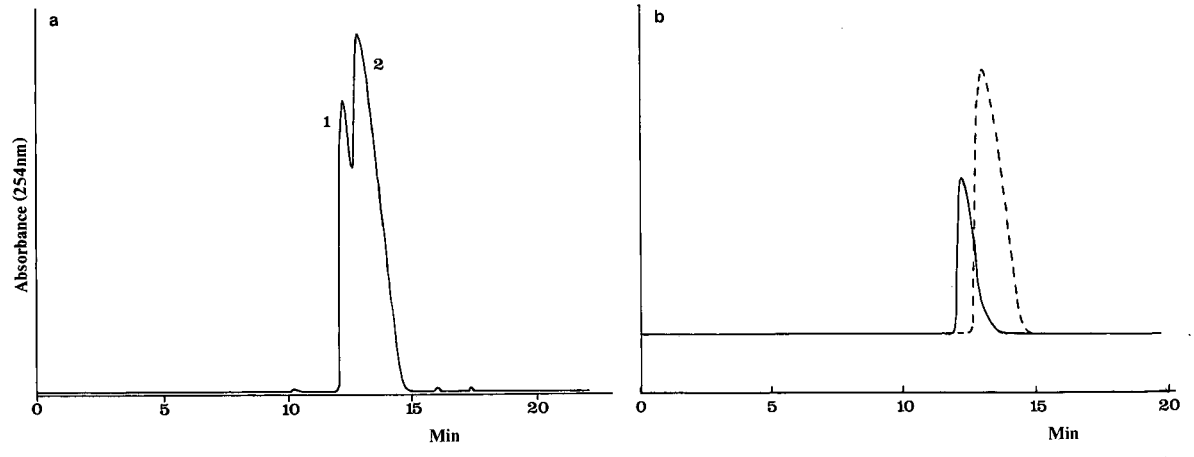

Fig. 2. (a) Gradient elution preparative chromatograms of 3 mg each of *p*-cresol and 2-phenylethanol. Flow-rate, 1 ml/min; detection, UV, 254 nm. For other conditions, see Table I. Peaks: 1 = 2-phenylethanol; 2 = *p*-cresol. (b) As for (a), chromatogram reconstructed from fraction analysis. Solid line, 2-phenylethanol; dashed line, *p*-cresol.

clearly that no displacement effects are present and the peaks merge, just as was seen for the previously reported isocratic separation. Again, the degree of overlap of the peaks was less under the gradient conditions when compared with isocratic chromatograms using the same sample load, where the two components were completely merged. It would be expected from eqn. 11 in the Appendix that the selectivity might decrease for these solutes. This result may reflect the conclusions drawn elsewhere [11] that the required resolution in gradients for optimum separations in preparative chromatography were seen to be less than for the corresponding isocratic case.

Hence the preparative isocratic and gradient separations follow similar courses as predicted by the original modelling, even in cases where the displacements and "tag-alongs" are much greater than predicted from the models [6].

It should be pointed out that there is no advantage in the use of gradient elution for the purification of these small molecules by preparative liquid chromatography. The isocratic separation will always give the higher production rate, if only because of the time necessary for re-equilibration of the column. This is not necessarily the case with larger molecules, such as proteins, where elution gradients have an important rôle to play in their purification.

Protein samples

We have earlier reported that the gradient elution mass overloaded separations of proteins on a 1000 Å pore size C_8 packing result in dramatically large displacement effects [8]. These data were obtained for the solute pairs of lysozyme and cytochrome *c* and of ribonuclease A and cytochrome *c*. In both experiments the first component was strongly displaced from the packing by the second-eluted peak. The latter peak was very little distorted by the presence of the first, moving only slightly to shorter retention time. The boundary between the peaks was very sharp, allowing high recoveries of the pure components.

The displacements observed were significantly greater than are predicted by the Craig modelling and are probably related to differences between the approximate Langmuir behaviour assumed in that model and the real isotherms. Large molecules such as proteins cannot follow a true Langmuir isotherm, as their size dictates that more than one solvent molecule is displaced per molecule adsorbed on the packing material surface [12]. Consideration of some of the effects of this phenomenon have shown [10] that although the saturation capacities determined from the experimental data are lower than those expected from consideration of the surface area of the packing material, the course of the separation should be as predicted by the calculations based on the Langmuir isotherm. It is known, however, that proteins undergo a number of configuration changes during chromatography, and it is not surprising that their behaviour deviates from that expected.

This initial work was carried out using only one gradient profile, of 20 min duration and encompassing a wide range of solvent compositions. In optimising gradients for preparative separations we have previously suggested [13] that a small solvent compositional range should be employed together with a short gradient run time (t_G). The purpose of this is to reduce the overall run time and thus to increase the production rate of the purification. In order to calculate the effects of changes in the gradient profile on the separation, it is necessary to determine the values of S, the slope of the plot of log k' *versus* solvent composition, and of k'_w, the capacity factor at zero percentage of the organic modifier. These can be determined [14] from two gradient experiments carried out at analytical loads. Experiments to determine the gradient parameters for cytochrome *c* and lysozyme were carried out using a 300 Å pore size packing. Under these conditions, the S values for the two proteins were approximately equal, with values close to 20.

Gradient experiments at elevated loadings were carried out using the 300 Å pore diameter packing material. The conditions are shown in Table II. A 20-mg amount of each solute was loaded. This is higher than was used in our earlier study, because the 300 Å packing had a higher surface area (by a factor of *ca.* 10) than the 1000 Å pore packing used then. The chromatograms are shown in Fig. 3. Fig. 3a shows the chromatogram, monitored at 290 and 480 nm (dashed line), for the 20-min run. The sample concentrations in this run were too high to maintain a linear detector response at the peak maxima where typical detector overload response is seen. Fortunately, the area of overlap between the peaks occurs

TABLE II

GRADIENT CONDITIONS FOR PROTEIN SEPARATIONS

Column: Zorbax Pro-10 Protein Plus (25 cm × 4.6 mm I.D.)	
Gradient:	
Solvent A:	0.1% aqueous trifluoroacetic acid
Solvent B:	0.1% trifluoroacetic acid in acetonitrile
Range:	5 to 70% B
Gradient time:	(a) 20 min
	(b) 50 min
Flow-rate: 1 ml/min	
Detection: UV, wavelengths 290 and 480 nm	

at absorbances where the detector response is reliable. Fig. 3b shows the chromatograms (290 and 480 nm) from the 50-min gradient.

These chromatograms show the same very strong displacement effects as were seen in our earlier experiments. The maxima of the two peaks in the 50-min gradient are better separated than those in the 20-min run, as would be expected from the use of the shallower gradient. Interestingly, because of the displacement, there is little difference in the purity or recovery of the two components between the two experiments. Hence, there is no reason not to use the steeper gradient, as this has a direct influence on the production rate possible from the system. The major difference between the two gradients lay in the cytochrome *c* peak. In both gradients a small tail may be observed which runs into the lysozyme peak. With a gradient time (for a range of 5–70% acetonitrile) of 20 min, the tail consisted of 0.3% of the cytochrome *c* peak area. In the experiment with a

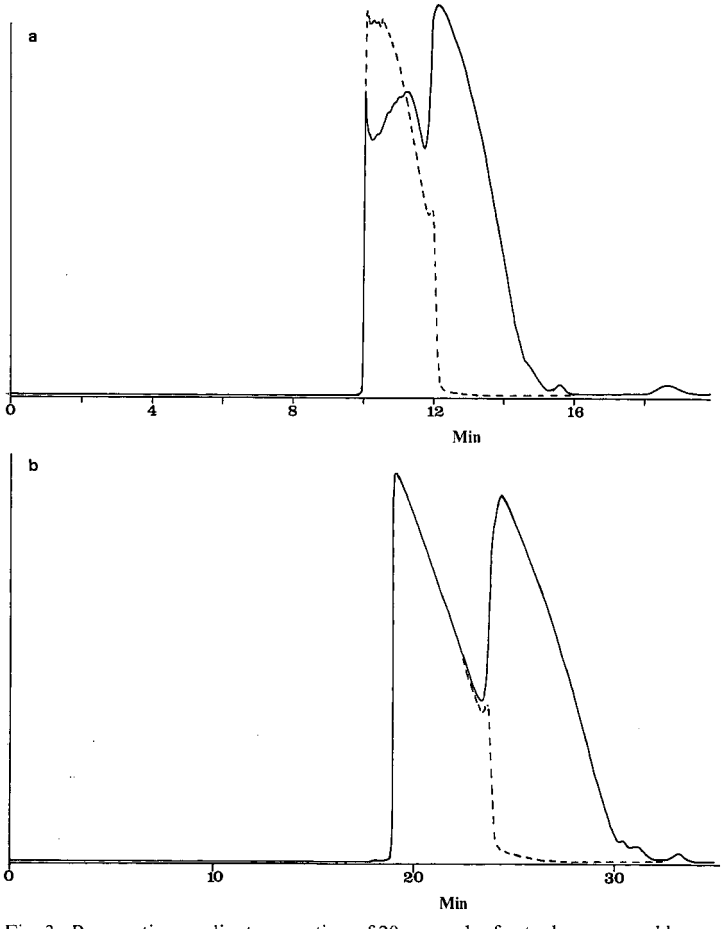

Fig. 3. Preparative gradient separation of 20 mg each of cytochrome *c* and lysozyme. Conditions as in Table II. (a) 20-min run time; (b) 50-min run time. Solid line, 290 nm; dashed line, 480 nm.

shallower gradient, this tail increased to 1.2% of the peak area.

In order to study this further, a number of gradients of different slopes were run under mass overload. Table III summarises the conditions used in the experiments. Columns 15 cm rather than 25 cm in length were used. This reduction in length was not expected to affect the results significantly.

The chromatograms were monitored at wavelengths of 295 and 480 nm in order to prevent overload of the detector electronics. The chromatograms of two of the overloaded runs are shown in Fig. 4. Fig. 4a shows the chromatograms (290 and 480 nm) from the 15-min gradient and Fig. 4b those for the 60-min gradient. Subtraction of the normalised 480-nm chromatogram from the 290-nm chromatogram in Fig. 4b results in a difference chromatogram with the response from the cytochrome *c* eliminated. This difference chromatogram (Fig. 4c) indicates that the lysozyme peak is not distorted by the displacement, but appears totally unaffected. The difference chromatogram also shows the presence of a minor component displaced by the cytochrome *c* peak. This material is probably a component of the lysozyme sample used.

In order to quantify the degree of overlap between the two main peaks, a goal purity of 99.5% cytochrome *c* was chosen. Ignoring the minor impurity for the moment, the recovery of cytochrome *c* at cut points appropriate for the collection of 99.5% pure material was calculated from the chromatograms. The results are shown in Table IV. There is very little

TABLE III

GRADIENT CONDITIONS FOR STUDY OF THE EFFECT OF GRADIENT PARAMETERS ON THE MASS-OVERLOADED SEPARATION OF PROTEINS

Column: Zorbax Pro-10 Protein Plus (15 cm × 4.6 mm I.D.)
Gradient:
Solvent A: 0.1% aqueous trifluoroacetic acid
Solvent B: 0.1% trifluoroacetic acid in acetonitrile
Range: 5–70% B
Gradient time: (a) 15 min
(b) 30 min
(c) 45 min
(d) 60 min
Flow-rate: 1 ml/min
Detection: UV, wavelengths 295 and 480 nm
Sample: cytochrome *c*, 3 mg; lysozyme, 10 mg.

TABLE IV

PURITY AND RECOVERY OF CYTOCHROME *c*

Gradient time (min)	Purity (%)	Recovery (%)
15	99.46	93.1
30	99.47	93.7
45	99.50	91.3
60	99.50	95.9

difference between the different gradients in terms of the purity and recovery and any variation in these parameters with gradient slope presumably results from experimental error. In contrast to the earlier experimental data, no differences in the tailing of the cytochrome *c* peak arising from changes in the gradient time could be seen in these experiments.

In addition to the gradient slope, the range of the gradient can also be an important factor in the purification of proteins. As the protein molecules are effectively completely retained for much of the gradient (when the solvent strength is low), the production rate can in theory be increased by elimination of this early part of the gradient [14]. This is a standard technique in analytical protein separations where the analysis time can be appreciably shortened by using only that part of the gradient in which the proteins elute. A study was carried out to investigate how the protein separations and solute–solute interactions were affected by such a reduction in the gradient range.

Single solutes. A set of experiments in which the components were introduced singly was first carried out. Details of the gradients used are given in Table V. Analytical (0.01 mg) and preparative (3 and 10 mg) loads of each component were used.

From the S and k_w values for the proteins studied, it was possible to calculate the values of k' (k'_0) for the solutes in the starting mobile phase composition of the gradients. These are shown in Table VI and range from 11 for cytochrome *c* at the highest initial composition to over $2 \cdot 10^6$ for lysozyme at the lowest.

Gradients starting at 24 or 31% acetonitrile resulted in incomplete uptake of the solutes. Fig. 5a shows a composite chromatogram assembled from an analytical-scale (0.05 mg) run with a mixture of the two components (dotted line), a chromatogram

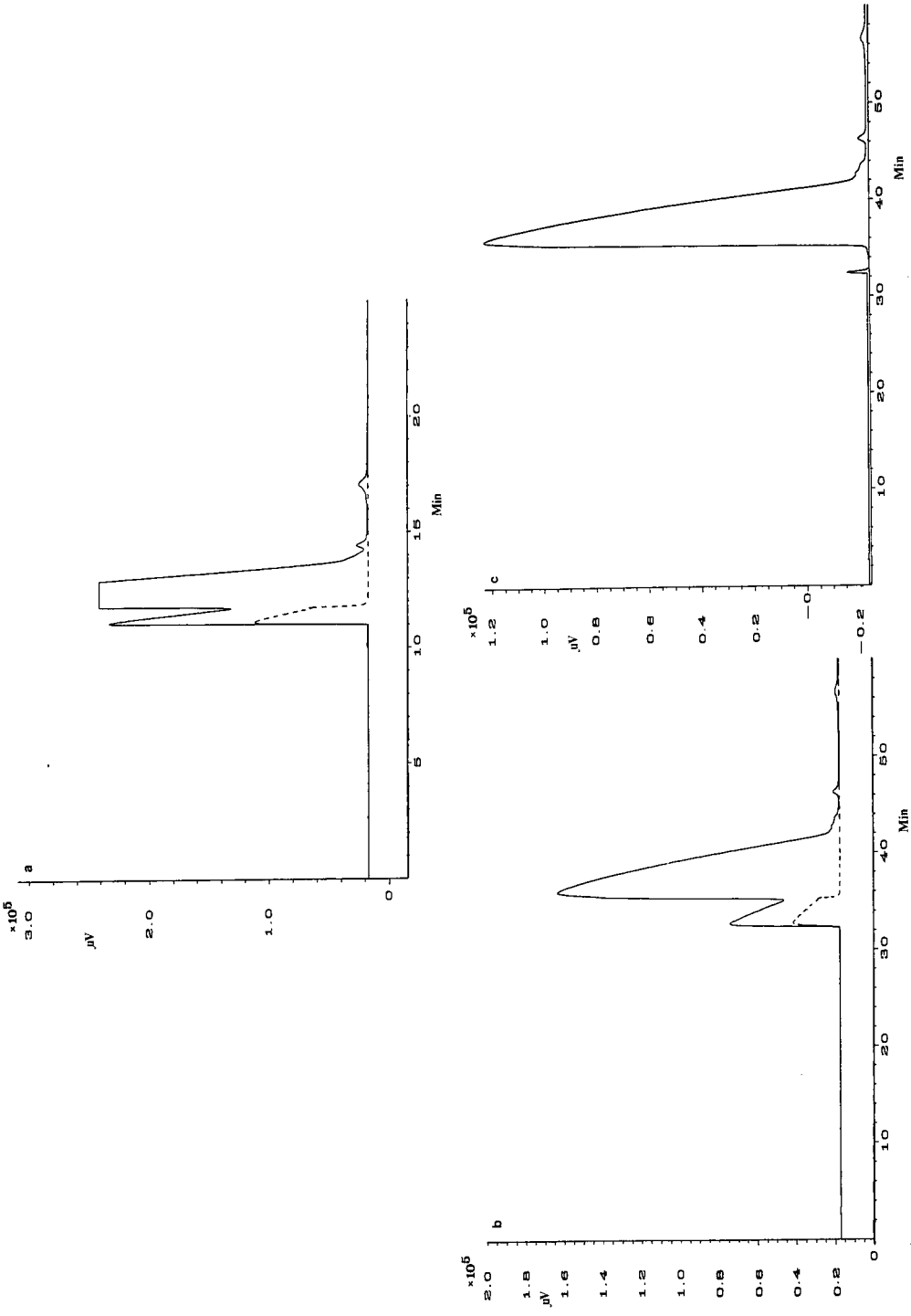

Fig. 4. Chromatograms obtained using two different gradient slopes for cytochrome *c* and lysozyme. (a) Conditions in Table III(a); (b) conditions as in Table III(d); (c) difference chromatogram (normalized 280 nm–475 nm) showing lysozyme peak and impurity.

TABLE V

GRADIENT CONDITIONS: STUDY OF GRADIENT RANGE

Other conditions as Table III.

Slope (%/min)	Start %B	End %B	Duration (min)
2.8	31	45	5
1.4	31	45	10
0.93	31	45	15
0.7	31	45	20
2.8	24	52	10
2.8	17	59	15
2.8	10	66	20

TABLE VI

INITIAL CAPACITY FACTORS IN GRADIENTS

Initial %B	k_0	
	Cytochrome *c*	Lysozyme
10	216 000	2 660 000
17	7800	77 300
24	287	2249
31	11	65

from injection of 10 mg of cytochrome *c* (dashed line) and a chromatogram from injection of 10 mg of lysozyme (solid line). These were all run using a

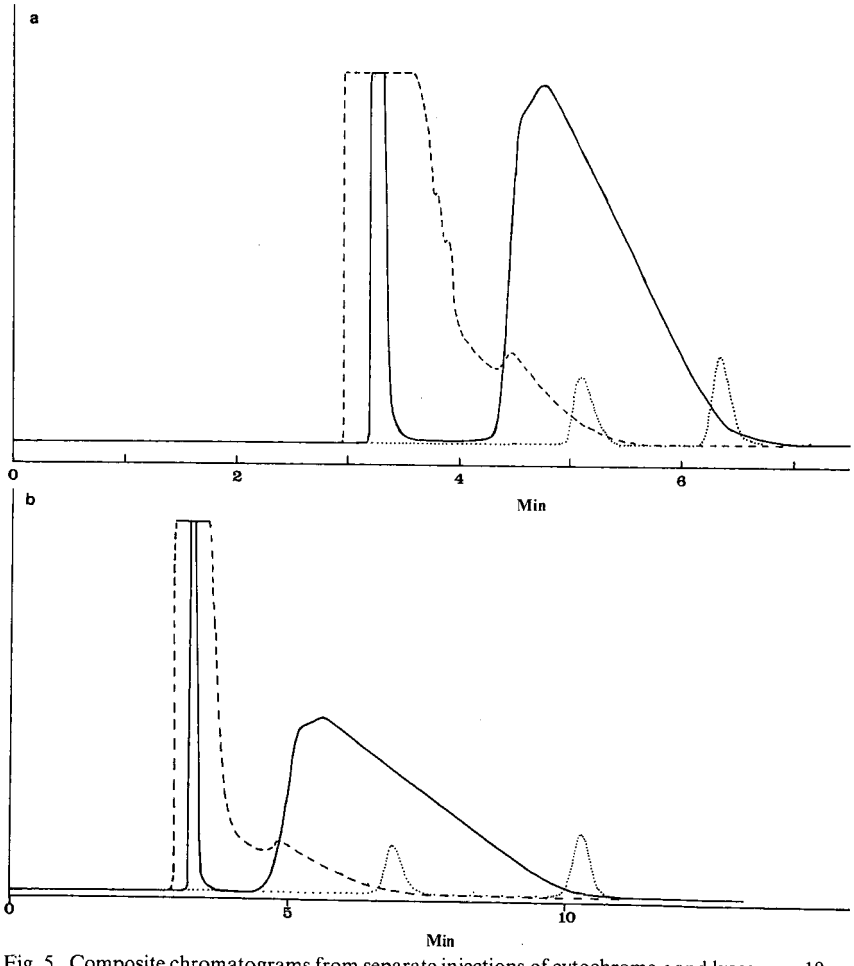

Fig. 5. Composite chromatograms from separate injections of cytochrome *c* and lysozyme. 10 mg of each compound, gradients from 31 to 45% acetonitrile in 0.1% TFA in (a) 5 min and (b) 15 min. Dashed lines, cytochrome *c*; solid lines, lysozyme; dotted lines, analytical (0.05 mg) injection of a mixture under the same conditions. Other conditions as Table III.

starting concentration of 31% acetonitrile and a gradient slope of 2.8%/min. It should be noted that the analytical chromatograms shown in all of the figures here are not on the same scale as the preparative chromatograms.

The cytochrome *c* peak begins elution at t_0 of the column and ends, as expected, at the retention time of the non-overloaded peak. The lysozyme peak is split. Only 8.6 mg of lysozyme, as estimated from peak-area data, were retained by the column regardless of the subsequent slope, the excess being eluted as a non-retained peak. A capacity even lower than this, estimated as slightly over 1.5 mg, was seen for cytochrome *c*. Fig. 5b shows similar chromatograms with a gradient slope of 0.93%/min. Other than the longer time scale, the two sets of chromatograms are essentially identical in all important respects.

With an initial acetonitrile concentration of 24% and the same gradient slope as for Fig. 5a, higher capacities for cytochrome *c* and lysozyme (7 and 9.4 mg, respectively) were seen. For gradients, still with the same slope as in Fig. 5a but commencing at 17% and 10% initial concentration of acetonitrile, all the material injected was retained.

From the known loads and the band widths of the peaks in the analytical and preparative runs, it was possible to calculate the saturation capacities of the columns by the procedure described elsewhere [15]. In addition, the apparent saturation capacity for each solute was determined by calculation of the mass retained by the column. This was done by taking the ratio of areas of the non-retained and the retained peaks and distributing the known mass injected between them. The calculated (band-width data) and apparent (peak-area ratio) saturation capacities for the two solutes under the different gradient conditions are shown in Table VII.

The values of the saturation capacity calculated from the band width for lysozyme range between 12.5 and 19 mg. If these values were accurate, then a significant amount of unretained protein should have been eluted in those earlier experiments where 20-mg loads of each protein were used. This is also true for the data for cytochrome *c*, where the saturation capacity is calculated to be less than 10 mg under all conditions. As suggested in an earlier paper [15], these saturation capacity values represent a minimum value rather than a true figure owing, perhaps, to the non-Langmuir adsorption of the proteins. The calculated saturation capacities should be approximately doubled to reach a more appropriate value. More importantly, the band-width data suggest that the actual column saturation capacity does not significantly change with the initial solvent composition. This is in contrast to the "apparent" values of saturation capacity (determined from the ratio of retained and non-retained solutes) which show a strong dependence on the initial solvent composition in the opposite direction from the much smaller trend in the values calculated from band width. It follows that the change in protein uptake with initial solvent strength is not a

TABLE VII

COMPARISON OF SATURATION CAPACITIES: CALCULATED *VS.* APPARENT

Gradient		w_s (mg)			
Start	Slope	Calculated		Apparent	
		Cytochrome *c*	Lysozyme	Cytochrome *c*	Lysozyme
31	2.8	–	18.5	2[a]	8.6
31	1.4	–	18.9	2[a]	8.6
31	0.9	–	18.6	2[a]	8.6
24	2.8	8.2	15.7	7	9.4
17	2.8	9.1	12.9	10+	10+
10	2.8	8.4	12.6	10+	10+

[a] This value was obtained from the chromatography by assuming a likely shape for the retained cytochrome *c* peak and subtracting it from the overall peak envelope. The associated error is less than 0.5 mg.

phenomenon due to changes in the saturation capacity of the solutes in the column.

The observed relationship between the calculated saturation capacity of the proteins and the solvent strength at the beginning of the gradient may well be due to changes in the isotherms caused by changes in the interaction of the proteins with the surface of the packing material. At lower solvent strengths this interaction would be expected to be stronger and the protein conformation on the surface would be likely to change, bringing more of the hydrophobic groups within it into contact with the surface of the stationary phase. This probably would have the effect of making a larger "footprint", which in turn would result in the displacement of more solvent molecules per protein. According to our understanding of the changes in isotherm thus expected, this would result in a lower measured saturation capacity.

The foregoing implies that the lack of take-up of the proteins by the column on loading at relatively high solvent strength is due to reasons other than a decreased saturation capacity. One problem which has been seen in the past is that too high a water concentration in the mobile phase can lead to poor wetting of the packing, leading to only partial uptake of the solute. This is clearly not the case here; increasing the water concentration leads to a better uptake. From Table VI, at 24% acetonitrile the k' of lysozyme is over 2000. Hence the equilibrium in the column is expected to favour uptake of the solute rather than its exclusion. Nevertheless, a small amount of material is not retained on introduction of the sample. One possibility [16] is that the adsorption of the large amount of protein on the surface of the packing displaces acetonitrile. The local increase in acetonitrile concentration may well be sufficient to desorb a certain amount of the protein, which is then swept down the column in the acetonitrile-rich band. Adsorption of the protein at low initial solvent strengths would not create a high enough local acetonitrile concentration to cause this desorption. The effect would be expected to increase as the initial acetonitrile concentration in the gradient increases. Experiments to verify this possibility are in progress.

Mixed solutes. Similar experiments to those above were carried out with samples consisting of mixtures of the proteins using the same packing material and gradients. Chromatograms from a mixture of 3 mg of cytochrome *c* and 10 mg of lysozyme are shown in Figs. 6–8 as overlays of analytical and preparative chromatograms. Again, the analytical chromatograms are displayed on a greatly increased scale.

The cytochrome *c* peak in the 31–45% gradient (Fig. 6) is displaced by the front of the lysozyme envelope. This is seen by the tail of the peak, which now ends considerably earlier than the elution time

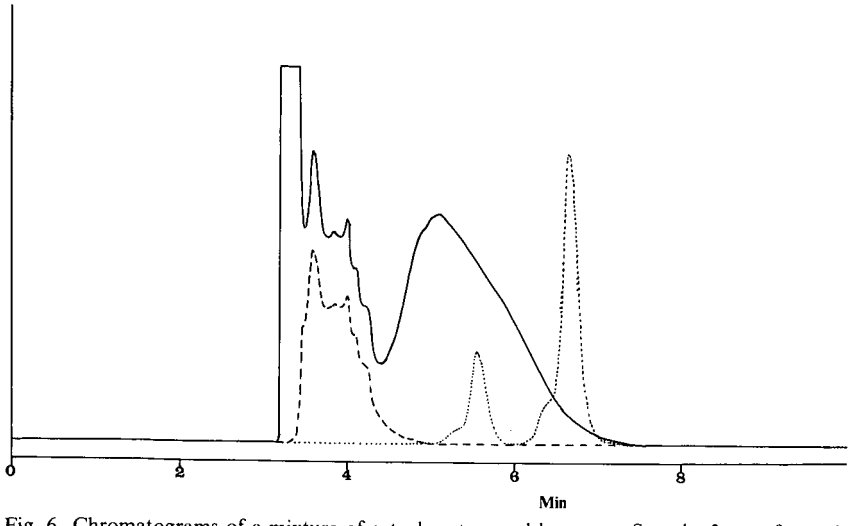

Fig. 6. Chromatograms of a mixture of cytochrome *c* and lysozyme. Sample, 3 mg of cytochrome *c* and 10 mg of lysozyme. Other conditions as in Fig. 5. Solid line, 290 nm; dashed line, 480 nm; dotted line, mixture of cytochrome *c* and lysozyme, 0.05 mg each.

of the same component under analytical load. There is a noticeable tail to the peak, which corresponds to the relatively slow increase in concentration of lysozyme as it begins to elute. As seen in later chromatograms, as the peak front of lysozyme becomes closer to the vertical, the tail of the cytochrome *c* peak diminishes.

Strangely, it appears that the non-retained lysozyme peak may be displaced from the column by the cytochrome *c* at the same time; certainly the non-retained lysozyme elutes earlier than the cytochrome *c* peak envelope, unlike the situation seen in Fig. 5 where the unretained lysozyme elutes at the same retention time as the unretained cytochrome *c* when injected separately. This could be ascribed to the initial uptake of protein being at the surface of the particle, thus blocking the pores and preventing their penetration by the unsorbed lysozyme molecules. These molecules, in being excluded from the pore volume within the particle, would then elute earlier than adsorbed or permeating species. Such a mechanism does not explain why cytochrome *c* is apparently not excluded from the packing. If the process is purely one of building a crust of adsorbed protein at the surface of the particle, then a proportion of cytochrome *c* should also be excluded by the same mechanism. In addition, it would be expected that the formation of such a crust would be favoured by increased energy of interaction of the solutes with the packing (the molecules would "stick" faster and then be less likely to move) and that there would be less protein (rather than more) adsorbed at lower solvent strengths.

Similar displacement effects, coupled with the non-adsorption of a proportion of the injected lysozyme, are seen in gradients with the same range of solvent composition but longer duration (lower slope). Although the separation between the peak maxima increases as expected, the band widths also increase, giving qualitatively very similar separations at the different slopes. The actual separation between the bands is controlled more by the displacement between them than by the gradient profile, just as was seen in the initial experiments (Fig. 3). As the initial acetonitrile concentration is decreased to 24 and 10%, but with constant gradient slope (Figs. 7 and 8), the peaks maintain approximately a constant width but move to longer retention time. At the same time, the amount of non-retained material decreases, as expected from the saturation capacities measured for single solutes.

Optimization of the gradient

Although the band-width data suggest that the true column capacity does not change with the gradient, in practice the load which may be applied to the column depends on the initial solvent composition. In order to make maximum use of the column

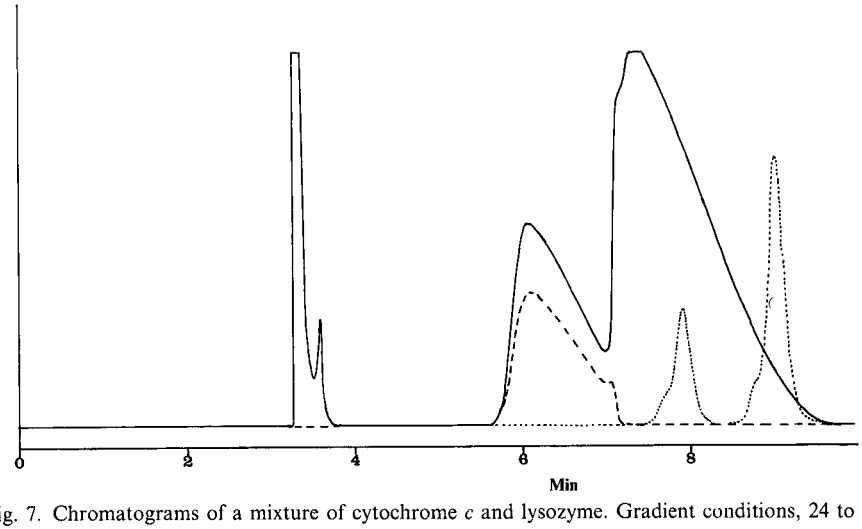

Fig. 7. Chromatograms of a mixture of cytochrome *c* and lysozyme. Gradient conditions, 24 to 52% acetonitrile in 10 min. Other conditions as in Fig. 6.

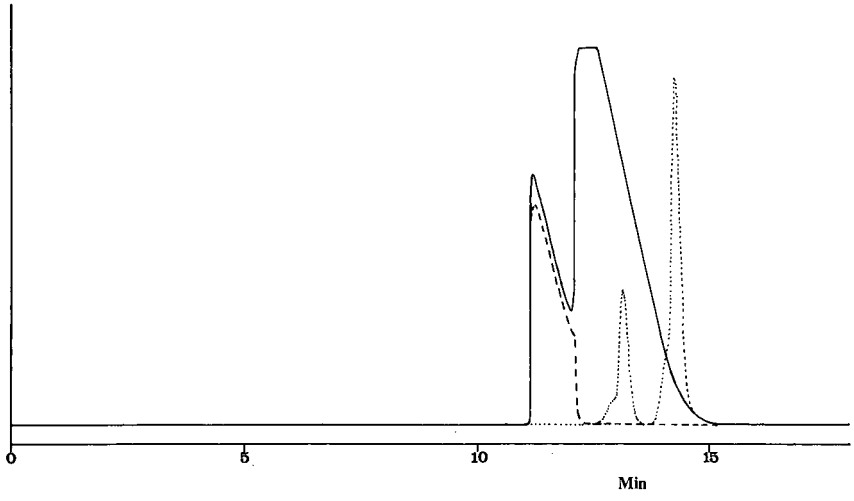

Fig. 8. Chromatograms of a mixture of cytochrome *c* and lysozyme. Gradient conditions, 10 to 66% acetonitrile in 20 min. Other conditions as in Fig. 6.

capacity, it is necessary to begin the gradient under conditions of very strong retention. This means that, even with a steep gradient, the retention time of the solute will be long. This will impact on the production rate of the separation. If the non-retention of the solutes by the column is a loading phenomenon, then it should be possible to load the column under strong retention conditions, quickly change the solvent strength to a high value and elute the components rapidly. If the effect is due in some way to a change in the dynamic capacity of the column, then it would be expected that the "excess" protein would be rapidly eluted from the column as the solvent composition was changed from the loading to the starting composition.

An experiment was performed to investigate this by loading the column at 10% acetonitrile, holding the acetonitrile concentration at 10% for 5 min and then rapidly changing the mobile phase (over 1 min) to 31% acetonitrile and subsequently running an elution gradient from 31 to 45% acetonitrile over 5 min (Fig. 9). No protein eluted during the period of rapid change, and the chromatogram shows no non-retained peaks, but is closely similar to the others which started at low solvent strength and maintained a constant gradient slope. The cytochrome *c* peak is clearly displaced by the lysozyme, as seen from comparison with the analytical chromatogram obtained under identical conditions.

In order to maximise the production rate for the preparative HPLC purification of proteins, it appears that a number of aspects need to be addressed. The sample must be loaded on the column under strongly retaining conditions. It should be noted that often a small concentration of organic component must be present in the mobile phase to ensure wetting of the packing material, such that the solutes will be able to interact with its surface. Where the solutes are hydrophilic and elute at low concentrations of organic component, this starting concentration will have to be determined with care.

Once the sample has been introduced, the mobile phase solvent strength is increased in a rapid gradient. This allows the displacements to occur. It is not yet known if there is an optimum for this gradient slope to maximise the displacements. This short gradient is intended to bring the mobile phase to the correct solvent strength for the beginning of a second, shallower gradient during which the components are eluted. The slope and range of this gradient are chosen to allow an adequate analytical resolution between the components, but should be as steep as possible. As it is highly probable that the actual gradients needed for the solution of any one problem will be separation dependent, the actual values of the parameters for both gradients will need to be determined experimentally on a case by case basis.

The displacements are maximised by the opera-

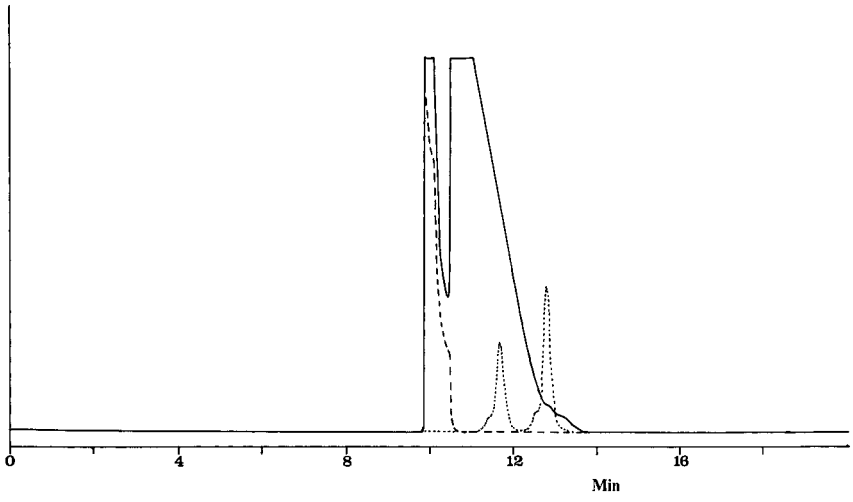

Fig. 9. Chromatogram of a mixture of cytochrome *c* (3 mg) and lysozyme (10 mg). Gradient, 5 min at 10%, from 10 to 31% in 1 min, from 31 to 45% acetonitrile in 5 min. Other conditions as in Fig. 6.

tion of the column such that the elution front of the displacing peak has a sharp increase in solute concentration. The column must therefore be operated under conditions of high efficiency. Not surprisingly, this is the same conclusion as has been reached for isocratic chromatography of small molecules where the column efficiency controls the width of the overlap zones of the displacing solute bands. Work designed to investigate the effects of column efficiency on solute–solute displacements in preparative elution chromatography is ongoing.

CONCLUSIONS

The mass overloaded gradient elution separation of small molecules is closely similar to the corresponding isocratic separation. This extends to the displacement effects observed between mass-overloaded components. Where the second-eluted component has the higher saturation capacity, displacement effects are observed, just as in the isocratic case. Where the first component has the higher saturation capacity, the peaks merge.

The previous report that equations for the relationship between band width and sample load yield low values of saturation capacity for proteins has been confirmed. This is probably due to the assumption of Langmuir isotherm behaviour. Proteins cannot follow this precisely; even in the most favourable case their size dictates multiple displacement of solvent molecules on adsorption.

Displacement effects within preparative elution gradients occur between protein solutes under a wide range of conditions. The initial solvent strength affects the practical loadability greatly; at (relatively) high initial solvent strength the loadability is severely compromised by the inability of the column to retain samples injected at loads well below the saturation capacity. Samples should therefore be introduced at low solvent strength.

The slope of the latter part of the gradient was demonstrated to have little influence on the overlap of well separated bands. The gradient profile adopted for heavily overloaded preparative gradient separations of proteins must be carefully designed to allow high loading, solute–solute displacement effects and a rapid elution of the peaks of interest to maximise the production rate of the purification.

APPENDIX

Non-Langmuir adsorption: consequences for solute interactions

Langmuir retention is represented in Fig. A1. Initially a solute molecule X (cross-hatched cube) is in the mobile phase, and a solvent molecule M (white cube) is in the stationary phase. The retention of X requires a displacement of M. The area required for

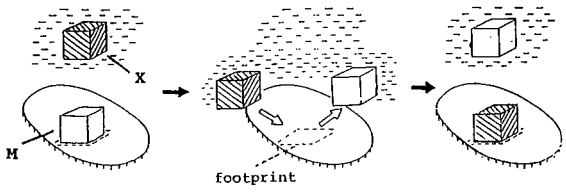

Fig. A1. Representation of sample retention in HPLC by a displacement process. Sample (X) and mobile phase (M) molecules of equal size.

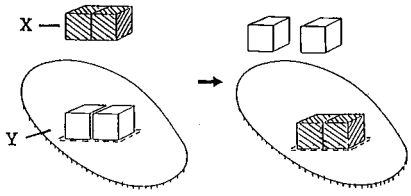

Fig. A3. Representation of sample retention in HPLC by a displacement process. Sample molecules (X and Y) of different sizes, equal saturation capacities but unequal footprints.

the retention of either X or M (known as the "footprint") is the same and the thickness of a monolayer of X or M is also the same. From this it follows that the column saturation capacities for X and M are the same, assuming equal densities.

A similar retention process involving a second solute molecule Y can be visualised, wherein the white cube in Fig. A1 might now represent Y instead of M. Again, there is a one-for-one displacement process, so that the w_s values for X and Y are the same. This is essentially the model which has been assumed in most computer simulations of preparative LC. This model gives rise to the Langmuir isotherm.

If the footprints of the two solutes are the same, it can be seen (Fig. A2) that even if one of the solutes is twice the size of the other, the Langmuir equations will still hold. In this instance, the saturation capacity (w_s) values of the two solutes taken on a weight basis will differ, although the saturation capacities determined on a molar basis will be equal.

Fig. A3 shows the case where the molecule of X has twice the footprint of solute Y. For adsorption of X to occur (assuming that the surface of the packing is uniformly filled with the two solutes) two molecules of solute Y must be displaced. Equally, for each molecule of X to be displaced, two molecules of Y may be adsorbed. Thus, on a molar basis, the saturation capacity of Y will be double that of X. If solutes X and Y are of equal molecular weight, then the weight-based saturation capacities will also be unequal. In the situation where X has twice the molecular weight of Y, the weight-based saturation capacities will again be equal. It follows that conclusions as to the likelihood of displacement or peak merging should be made based on molar saturation capacities rather than weight-based saturation capacities.

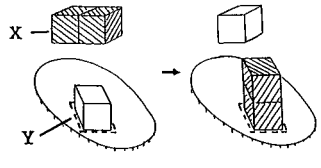

Fig. A2. Representation of sample retention in HPLC by a displacement process. Sample molecules (X and Y) of different sizes (and w_s values), but equal footprints.

The two solutes, X and Y, each displace a certain number of solute molecules. These numbers are represented by n and p respectively. If X and Y have different footprints, then n and p are not equal and n/p molecules of Y will displace one molecule of X. Assuming that the activity coefficients are constant, the equilibria occurring at this point on the surface can be represented by

$$X_m + nM_a \rightleftharpoons X_a + nM_m \quad (1)$$

$$Y_m + pM_a \rightleftharpoons Y_a + pM_m \quad (2)$$

$$X_a + (n/p)Y_m \rightleftharpoons X_m + (n/p)Y_a \quad (3)$$

$$K_X = \Theta_X C_m^n / \Theta_m C_X^n \quad (4)$$

$$K_Y = \Theta_Y C_m^p / \Theta_m C_Y^p \quad (5)$$

$$\Theta_X = w_{Xs}/w_s \quad (6)$$

$$\Theta_Y = w_{Ys}/w_s \quad (7)$$

where, K_X and K_Y are equilibrium constants for eqns. 1 and 2, Θ_i refers to the fraction of stationary phase sites occupied by molecular species i, C_i is the mobile phase concentration of i (g/ml), w_{is} is the weight of i in the stationary phase (g/ml) and w_s is the weight of the adsorbed monolayer.

If we first assume that $n = p = 1$, that C_X and $C_Y \ll C_m$, V_m is the volume of mobile phase in the column and that all activity coefficients remain constant, the selectivity is given by

$$\alpha = \frac{[(\text{weight of Y in stationary phase}) \cdot (\text{weight of X in mobile phase})]}{[(\text{weight of X in stationary phase}) \cdot (\text{weight of Y in mobile phase})]}$$

$$= w_{Ys} C_X V_m / w_{Xs} C_Y V_m = K_Y / K_X \quad (8)$$

In this situation, the selectivity does not change with load.

When $n \neq p$, the mobile phase modifier concentration becomes important. We assume that in a binary mobile phase mixture the concentration of the stronger solvent does not change in the mobile phase with sample load and that the stationary phase contains only molecules of the solutes and the strong mobile phase component, *i.e.*,

$$\Theta_X + \Theta_Y + \Theta_b \approx 1 \quad (9)$$

where Θ_b is the fraction of stationary phase sites occupied by the strong mobile phase component.

Calculation of α in the same fashion as earlier results in a changed relationship:

$$\alpha = (K_Y / K_X)(\Theta_b / C_b)^{p-n} \quad (10)$$

Combination of eqns. 11 and 12 results in

$$\alpha = [(K_Y / K_X)(C_b^{n-p})](1 - \Theta_X - \Theta_Y)^{p-n} \quad (11)$$

This equation shows that α will change with sample size, in that the term $(1 - \Theta_X - \Theta_Y)$ will decrease with increasing sample size. This term is less than unity. If $p > n$, the selectivity will decrease with increasing sample size, *i.e.*, at some point the peak maxima will merge and change elution order. Because $p > n$, the individual solute isotherms (measured on a molar basis) will cross. Conversely, selectivity will increase with sample size if $n > p$ and the isotherms will diverge. These two cases correspond to the situations in Fig. A3 where the second-eluting component has respectively a smaller and a larger saturation capacity.

If we now assume that the solute concentrations are very high and the entire surface of the packing is covered with solute molecules, then eqn. 3 is particularly relevant to the discussion. The equilibrium constant for this process is

$$K = [X_m][Y_s]^{n/p} / [X_a][Y_m]^{n/p} \quad (12)$$

Comparing the cases for $n = p$ and $n > p$, it is clear that (at our given k' value) the concentration of Y in the stationary phase will have a much greater influence in the latter situation and, in comparison with the former instance, the concentration of X in the stationary phase will be much reduced. If X is the earlier eluted species, the peak will be much more displaced than when $n = p$ (equal molar saturation capacity values) and the recovery of X and Y will be higher. If X is the later eluted species, its displacement from the surface by Y means that it will elute earlier. The extent of the interaction will determine if the solutes will simply show a strong tag-along, if they will merge or if the second-eluted component will be displaced to the front of the first-eluting peak.

In practice, the entire surface of the packing is not filled only with solute molecules. As a significant proportion is taken up by solute molecules in strongly overloaded separations, the phenomena predicted will be observed to an extent less than may be assumed from the above equilibria. This will be determined by the relative surface area occupied by the solvent molecules.

REFERENCES

1 J. E. Eble, R. L. Grob, P. E. Antle, G. B. Cox and L. R. Snyder, *J. Chromatogr.*, 405 (1987) 31.
2 G. Guiochon and S. Ghodbane, *J. Phys. Chem.*, 92 (1988) 3682.
3 G. B. Cox and L. R. Snyder, *J. Chromatogr.*, 483 (1989) 95.
4 J. Newburger and G. Guiochon, *J. Chromatogr.*, 484 (1989) 153.
5 S. Golshan-Shirazi, M. Z. El Fallah and G. Guiochon, *J. Chromatogr.*, 541 (1991) 195.
6 M. Czok, S. Golshan-Shirazi, G. Guiochon, A. M. Katti and Z. Ma, presented at the *7th International Symposium on Preparative Chromatography, Ghent, April, 1990.*
7 J. E. Eble, R. L. Grob, P. E. Antle and L. R. Snyder, *J. Chromatogr.*, 405 (1987) 51.
8 L. R. Snyder, J. W. Dolan and G. B. Cox, *J. Chromatogr.*, 484 (1989) 437.
9 C. T. Mant, T. W. Lorne Burke and R. S. Hodges, *Chromatographia*, 24 (1987) 565.
10 J. E. Eble, R. L. Grob, P. E. Antle and L. R. Snyder, *J. Chromatogr.*, 384 (1987) 45.
11 L. R. Snyder, J. W. Dolan and G. B. Cox, *J. Chromatogr.*, 540 (1991) 21.

12 X. Geng and F. E. Regnier, *J. Chromatogr.*, 296 (1984) 15.
13 L. R. Snyder, J. W. Dolan, D. C. Lommen and G. B. Cox, *J. Chromatogr.*, 484 (1989) 425.
14 M. A. Quarry, R. L. Grob and L. R. Snyder, *Anal. Chem.*, 58 (1986) 907.
15 G. B. Cox, L. R. Snyder and J. W. Dolan, *J. Chromatogr.*, 484 (1989) 409.
16 A. Lee, personal communication.

Journal of Chromatography, 590 (1992) 35–47
Elsevier Science Publishers B.V., Amsterdam

CHROMSYMP. 2465

Factors affecting the separation and loading capacity of proteins in preparative gradient elution high-performance liquid chromatography

Yan-Bo Yang, Kervin Harrison and David Carr

Vydac/The Separations Group, 17434 Mojave Street, Hesperia, CA 92345 (USA)

Georges Guiochon*

**Department of Chemistry, University of Tennessee, Knoxville, TN 37996-1501 and Division of Analytical Chemistry, Oak Ridge National Laboratory, Oak Ridge, TN 37831-6120 (USA)*

ABSTRACT

The optimum conditions for the purification of proteins by gradient elution in reversed-phase liquid chromatography were studied, with emphasis on the column length. Because of the strong dependence of the retention of proteins on the mobile phase composition, very short columns can be used successfully to perform analytical separations. A similar conclusion is extended to preparative separations. Columns with different lengths and diameters were used. The dependence of the loading capacity for touching band separation on the column length, diameter and volume was studied, in addition to the regeneration time between successive runs, the starting mobile phase composition and the necessary column efficiency.

INTRODUCTION

The preparative purification of proteins by gradient elution raises problems which are different from those found in the separation of low-molecular-weight compounds in gradient elution or in isocratic purifications. Under isocratic conditions, the mechanism of band broadening in preparative chromatography is fairly well understood [1] and it is experimentally easy, if tedious, to determine the equilibrium isotherms necessary for the calculation of band profiles [2]. Then, agreement between calculated and experimental band profiles is excellent [3,4]. Modeling gradient elution separations is more difficult [5,6]. This is possible, however, if one can measure the equilibrium isotherms over the whole useful range of mobile phase compositions [6]. This has been done for small molecules, for which this range is wide, and excellent agreement has been reported between experimental and calculated profiles for single-component band profiles for 3-phenylpropanol [7].

The modeling of protein separations in gradient elution is much more complex. Under isocratic conditions, the protein isotherms in reversed-phase chromatography tend to be rectangular [8]. The useful range of concentrations is very narrow and the reproducibility of the measurements is questionable [9]. Serious experimental problems are also found. Until these problems have been solved, this method cannot provide much help and an empirical approach becomes necessary.

The conclusions of theoretical studies of isocratic separations is that concentration overload is necessary to achieve high production rates and to reduce the cost of recovery of the purified product from the mobile phase, and that the most important factor limiting the production rate is related to the minimum column efficiency necessary to achieve a sufficient degree of separation between the bands of the

0021-9673/92/$05.00

main component and of the closest impurities [10–14]. However, these conclusions do not extend simply to the separation of proteins in gradient elution. In this instance, proteins seem to be released from the column very rapidly, as if a trap door were open when the mobile phase reaches a certain composition [15].

Hence the column length has little effect on the separation between proteins under analytical conditions [15–18]. The classical equations relating the number of theoretical plates of the column, the resolution between two components, their separation and retention factors do not apply in this instance. It is difficult to derive an alternative relationship involving these parameters and the gradient rate for the separation of small molecules [19]. This does not seem to be either possible or useful with proteins.

The major factors that control the separation of proteins in gradient elution seem to be the gradient rate and the dependence of the retention factor of the two components on the mobile phase composition [15–20]. This dependence is usually logarithmic, but the slope of dlog k'/dC, where k' is the retention factor of the component of interest and C the concentration of the strong solvent in the mobile phase, depends considerably on the molecular weight of the solute considered. It is gradual for small molecules, intermediate for peptides and very steep for proteins [15].

It has been reported that, in gradient elution, the dependence of the resolution between two compounds of similar molecular weight on the column efficiency decreases steadily with increasing molecular weight [15–20]. It is considered that, for most proteins, only a thin layer at the top of the column contributes effectively to the separation. This is so because a very small change in the mobile phase composition is sufficient to shift the adsorption behavior of the protein molecule from totally adsorbed to almost not adsorbed. Hence, once a molecule has been released from its original adsorption site, it undergoes almost no adsorption again. The remainder of the column contributes to band broadening but not to retention. Therefore, the extent of the influence of the column efficiency on the resolution depends on the fractional length of the column at which the retention factor becomes lower than about 0.5. Beyond that position, the molecule is essentially unretained. The influence of the column efficiency is stronger for shallow gradients, but it is impractical to set the gradient rate below a certain limit [19]. In the literature, there are examples of gradient separations performed on 1- and 25-cm columns [17,18] and showing the same resolution. In general, however, the poorer separation is achieved on the shorter column for small molecules (*e.g.*, small peptides) [20].

Although there have been applications of this phenomenon for the rapid analytical separations of proteins with very short columns [15–18], its consequences in the preparation of purified proteins by preparative chromatography have not yet been investigated in detail. A separation strategy based on the use of very short columns would be of great value, however. The industrial separation of proteins is an important application of preparative chromatography. It is very costly, requiring large volumes of solvents which are more difficult to recycle in gradient elution than under isocratic conditions. The use of a column longer than necessary results in excessive expense, the need for too high an inlet pressure and the processing of undue solvent volumes, all contributing to increase production costs.

At this stage, however, there is little theoretical background available for the optimization of the experimental conditions of a separation based on gradient elution. The models available in analytical chromatography for the optimization of the gradient slope are too limited in their range of applicability [19,21,22]. They either borrow or adapt equations and concepts from isocratic chromatography. Their validity is questionable. Their extension to overloaded elution chromatography is impractical. Therefore, experiments are necessary to develop an understanding of the separation process and assist in the development of the proper models.

This work was undertaken to elucidate the influence of the column length and efficiency on the separation of proteins in gradient elution. As a first step, we investigated the experimental conditions resulting in touching band separation, as it is a situation where the competitive interactions of the two proteins with the stationary phase still contribute moderately to the separation. The displacement effect remains moderate and the influence of column efficiency is relatively more important than under overlapping band conditions. We also studied

the dependence of the column saturation capacity on the cross-sectional area and the influence of the initial solvent composition. The time needed to regenerate the column between two successive runs was also determined.

EXPERIMENTAL

Apparatus

The separations were studied using two liquid chromatographs. The first was assembled from two ConstaMetrics-III metering pump (LDC/Milton Roy, Riviera Beach, FL, USA), a dynamic on-line solvent mixer of volume 2.4 ml (Beckman, Fullerton, CA, USA), a Model 7125 syringe-loading sample injector (Rheodyne, Cotati, CA, USA), a SpectroMonitor D variable-wavelength UV detector (LDC/Milton Roy), an IBM-compatible PC computer (Equus/Systems, Hesperia, CA, USA) with an OkiData printer (Oki America, Mount Laurel, NJ, USA) and a strip-chart recorder (Kipp & Zonen, Veendam, Netherlands). The system was operated with a program developed in-house.

The second system was assembled from a Model 2360 gradient programmer (Isco, Lincoln, NE, USA), an IsoChrom LC pump (Spectra-Physics, San Jose, CA, USA), a Model 7126 injector with different-sized loops (Rheodyne), an L-3000 photodiode-array detector (Hitachi, Tokyo, Japan), an IBM-compatible PC (Equus/Systems), an IBM PC graphic printer (IBM, Valhalla, NY, USA) and a 900 Series intelligent interface (Nelson Analytical, Cupertino, CA, USA), which connects the detector to the computer integrator with dual channels converting analog to digital data.

Products and chemicals

Two lots of Vydac 218TP silica C_{18} (The Separations Group, Hesperia, CA, USA) packing materials with different particle sizes were used: the 5-μm particle size lot is typical of the materials used in the analysis of proteins and the 10-μm particle size lot is typical of those used in preparative applications. The influence of the particle size in the separation of proteins in reversed-phase chromatography has been discussed in detail in ref. 18.

Lysozyme (molecular weight, MW = 14 307, grade I from chicken egg white) and cytochrome *c* (MW 12 300, type III from horse heart) were purchased from Sigma (St. Louis, MO, USA), trifluoroacetic acid (TFA) from Pierce (Rockford, IL, USA) and HPLC-grade acetonitrile (ACN) from J. T. Baker (Phillipsburg, NJ, USA). All chemicals were used as received.

Chromatographic conditions and procedures

The 5-and 10-μm Vydac 218TP silica C_{18} packing materials were slurry packed into stainless-steel columns of different lengths and diameters, as needed.

The mobile phases were prepared from 0.1% (v/v) TFA in water as solvent A and 0.1% TFA in pure ACN as solvent B. Prior to use, all solvents were degassed by sonication under vacuum. The gradients were run at a flow-rate of 1 ml/min and at a rate of 2%B/min, unless indicated otherwise. The initial gradient composition was variable.

Lysozyme and cytochrome *c* were dissolved in solvent A at concentrations of 10 and 5 mg/ml, respectively. Different loading amounts were achieved by adjusting the sample volume, except for one series of experiments in which the concentration was adjusted.

For most of the single-component experiments, the elution profiles were monitored with the SpectroMonitor D variable-wavelength UV detector at 300 nm, where the response is lower than at 254 or 280 nm. Experiments with binary mixtures were monitored at 300 and 320 nm with the L-3000 photodiode-array detector. Both proteins were detected at the former wavelength, but only cytochrome *c* at the latter. The detector sensitivity was adjusted depending on the sample size.

Retention volumes and band widths were measured from the recorded chromatogram. The band width is the width of the recorded profile at half-height. The detector gave a linear response in the sample size range used. The column efficiency was measured with biphenyl, using ACN–water (60:40) as the mobile phase, at a flow-rate of 1 ml/min, unless indicated otherwise. The retention factor is 2.0.

RESULTS AND DISCUSSION

Band width in gradient elution and column efficiency

Although the column length has little influence on the band width of proteins in gradient elution, this does not necessarily mean that the column effi-

TABLE I

INFLUENCE OF COLUMN PLATE NUMBER ON PEAK WIDTH OF PROTEIN

Column No.	Column length (cm)[a]	V_R (ml)	$W_{1/2}$[b] (ml)	N[c]	h
1	5	16.05	0.18	2459	4.0
2	15	18.17	0.20	9157	3.3
3	25	19.81	0.22	14198	3.5

[a] All columns 0.46 cm I.D.

[b] Peak width at half-height. Lysozyme injected, 50 μg/ml column volume. Other conditions as in Fig. 2.

[c] Column plate number was determined using ACN–water (60:40) as the mobile phase (1.0 ml/min; $k' = 2$) and biphenyl as the solute.

ciency is without effect. The column efficiency depends also on the quality of the packing and on the mobile phase velocity. We performed two series of experiments to clarify some issues related to the influence of the column efficiency on the band width.

The influence of the total column efficiency was studied by making three columns of different lengths (Table I) with Vydac 218TP C_{18} silica (5 μm, 300 Å), using the same packing method. The efficiencies of the three columns are proportional to the column length, with an average reduced plate height of 3.5. Sample sizes proportional to the column volume (50 μl of the lysozyme solution per ml of column volume) were injected. The band widths measured are reported in Table I. The band width varies in the same order as the column efficiency, the more efficient column, which is also the longer column, giving the wider band. The same relationship is observed under isocratic conditions, as the HETP of the three columns is the same. However, whereas under isocratic conditions the distance between two bands increases in proportion to the column length, we see in Table I that this is no longer true under the conditions of gradient elution. The retention volumes, and hence the distance between two bands, increase only slightly with increasing column length, less than 25% for a fivefold increase in the column length. The ratio $w_{1/2}/t_R$ is constant within the precision of the measurements (the values are 0.0112, 0.0110 and 0.0111 for the 5-, 15- and 25-cm columns, respectively). Hence we cannot expect an improvement in performance with increasing column length.

Fig. 1 compares the chromatograms obtained with two columns of the same length, but packed differently with the same material and having different reduced plate heights (3.0 and 5.6) for the same mobile phase velocity. The band width of the two proteins are 0.21 and 0.23 ml on the first column and 0.23 and 0.26 ml on the second column, *i.e.*, 10 and 13% larger on the less efficient column, respectively. The distances between the two bands are the same on the two chromatograms. Hence the resolution between the two proteins is better on the more efficient column. This is also demonstrated by the band of the lysozyme impurity (Fig. 1), which is well resolved on the first chromatogram but appears as a shoulder on the second. Although the

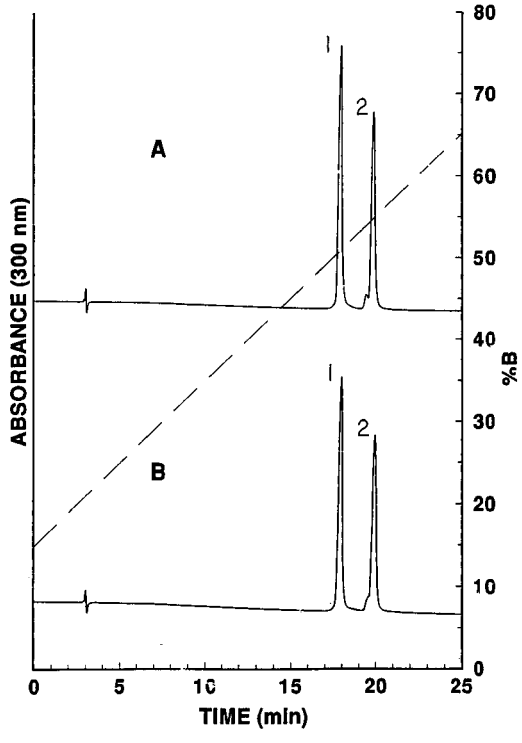

Fig. 1. Comparison of protein separations on columns of different efficiencies. Experimental conditions: 25 × 0.46 cm I.D. columns packed with Vydac 218TP, 5 μm, 300 Å (lot number 900201-25RE); flow-rate, 1.0 ml/min; gradient from 15 to 65% B in 25 min; UV detection at 300 nM; sample size, 20 μl of a mixture of cytochrome *c* (peak 1) and lysozyme (peak 2); column efficiency: (A) 65 208 plates/m (or $h = 3$) and (B) 35 900 plates/m (or $h = 5.6$).

gain in resolution is certain, however, it is not proportional to the square root of the plate number (*i.e.*, 1.37), as would happen under isocratic conditions.

In summary, the column HETP has an influence on the resolution achieved in gradient elution and the column should certainly be as well packed as possible, but the effect is not important. It seems probable that this effect would decrease to the point of being negligible under overlapping band conditions, when the band broadening due to the axial dispersion and mass-transfer resistance becomes negligible compared with the thermodynamic band broadening due to the non-linear behavior of the isotherm. The effect of the column length at a constant value of the plate height is also small. We now consider this effect in more detail.

Loading amount and column length

The elution band width under gradient conditions for the three columns in Table I is plotted in Fig. 2 *versus* the amount of lysozyme injected (gradient from 15 to 65% B in 25 min) for large sample sizes and in Fig. 3 for very small loadings. For a very small sample size (less than *ca.* 20 μg), the bands have nearly the same widths on all three columns (see also Table I). When the sample size increases, all three curves rise and tend to become linear at high loadings. For a given sample size, the longer column gives the smaller band width, but the effect is due to the larger loading factor of the shorter column at constant sample amount, obviously causing more band broadening of thermodynamic origin.

This effect is apparent on comparing Fig. 2 and Fig. 4, in which the band width is now plotted *versus* the loading ratio (in μg/ml column volume). For a given loading ratio, the band width is larger for the longer column. The ratio of the band widths for the 25- and 5-cm columns also increases with increasing loading factor. This suggests that the separation performance should be better with the shorter column.

Fig. 5 shows the plot of the resolution between lysozyme and cytochrome *c* as a function of the loading ratio. There is not much difference between the results obtained with the three columns. However, for a given loading ratio and a given column

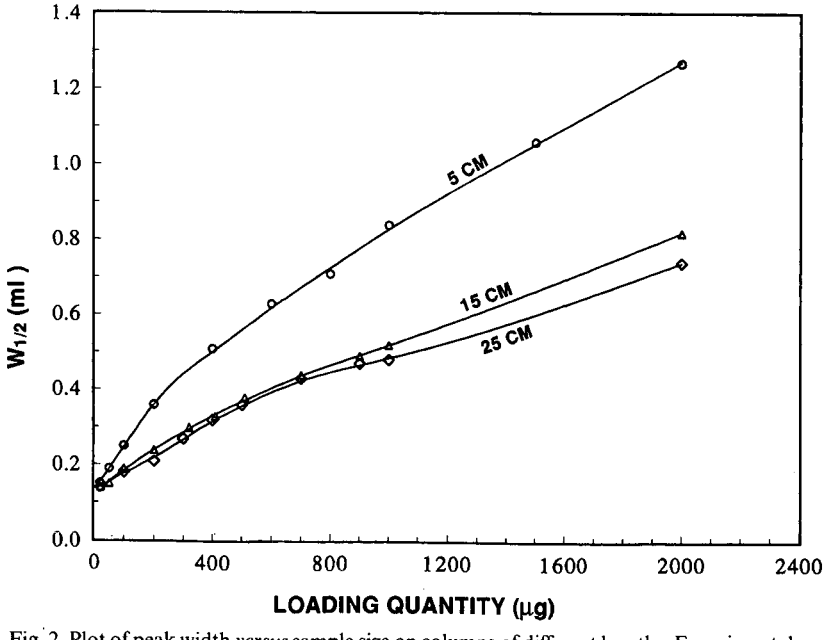

Fig. 2. Plot of peak width *versus* sample size on columns of different lengths. Experimental conditions: three columns, 5, 15 and 25 cm × 0.46 cm I.D., were packed with Vydac 218TP, 5 μm, 300 Å (lot number 890706-14); flow-rate, 1.0 ml/min; gradient, 15 to 65% B in 25 min; detection, UV at 300 nm; sample, lysozyme, 1% in 0.1% TFA–water, injected by varying the sample volume.

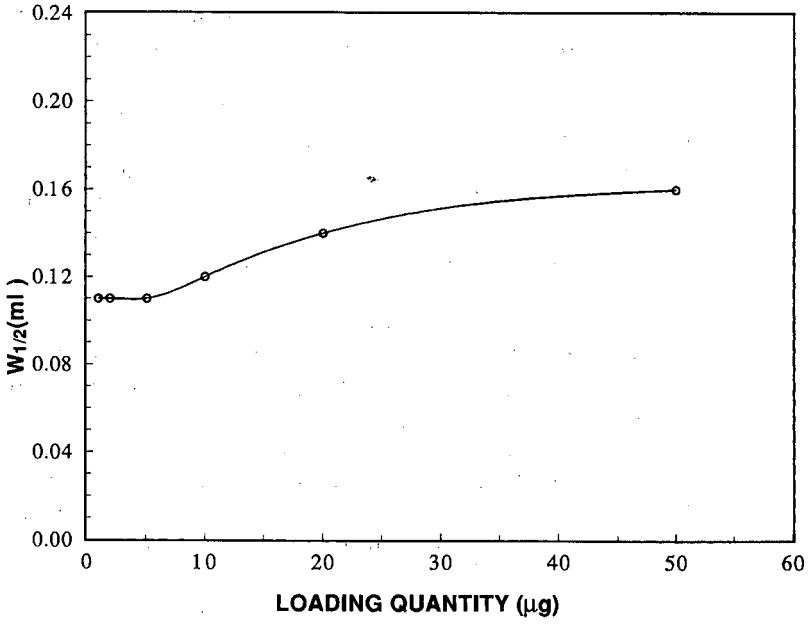

Fig. 3. Plot of peak width *versus* sample size at low loadings on the 15-cm column. Experimental conditions as in Fig. 2.

diameter, the resolution obtained with the shorter column is slightly better. The performance seems to be best with the 12.5-cm column. All the results tend towards the same limit at large loading ratios.

Column regeneration time

It is particularly critical in the gradient elution chromatography of proteins, whether analytical or preparative, to achieve reproducible results. One

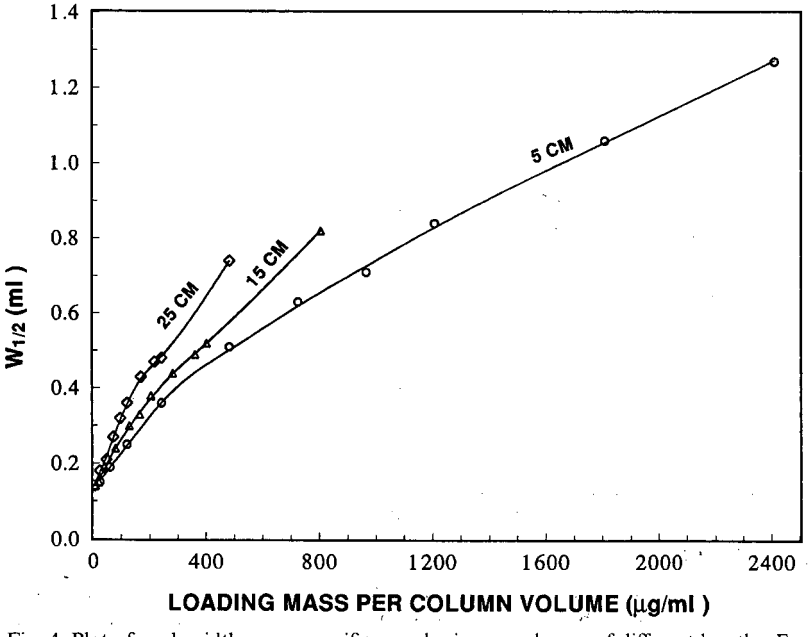

Fig. 4. Plot of peak width *versus* specific sample size on columns of different lengths. Experimental conditions as in Fig. 2.

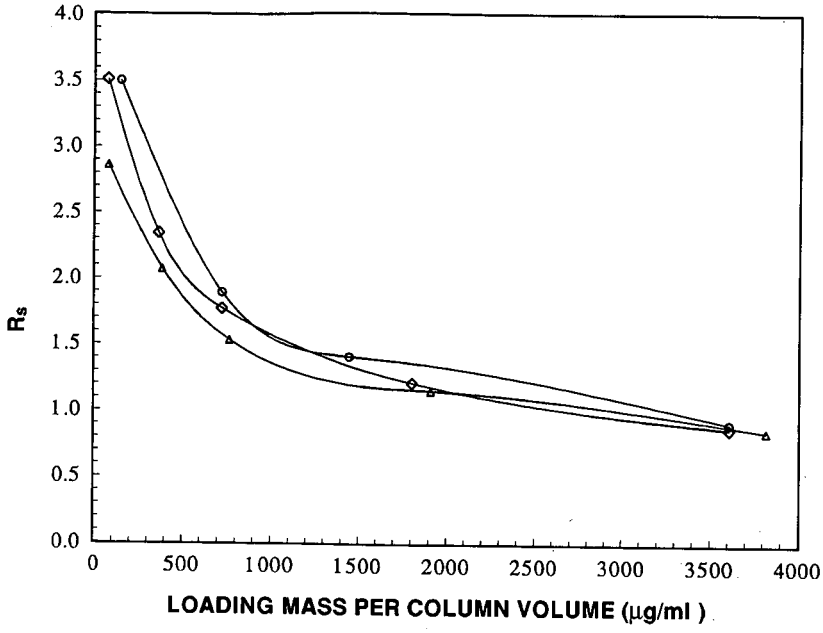

Fig. 5. Plot of resolution between cytochrome *c* and lysozyme *versus* sample size. Experimental conditions: (◇) 25 × 0.46 cm, (○) 12.5 × 0.46 cm and (△)5 × 1.0 cm I.D. columns packed with Vydac 218TP, 10 µm, 300 Å (lot number 891208-21); flow-rate, 1.0 ml/min; gradient, 15 to 65% B in 25 min; detection, UV at 300 nm; sample, cytochrome *c* (0.5%) and lysozyme (1%) in solvent A.

important factor in this respect is the re-equilibration of the column between successive runs. All the components of the feed sample must be eluted from the column. This may require that the column be washed with a suitable solution, and then that the initial solvent be pumped through the column for a period. Conventionally, analysts pump about 15–20 column volumes of the initial eluent before making a new injection [21]. This is a very costly proposition in preparative chromatography as much time is wasted waiting for the column to be operational again, and the solvent cannot be recycled, otherwise the impurities extracted from the column would be returned to it. It is useful to determine in various instances what amount of solvent must be pumped through the column to achieve reproducible results.

In Fig. 6, the band width and the retention volume of lysozyme on the three columns are plotted *versus* the time during which the initial solvent is pumped into the column before a second run is started again. The volume needed to return to a constant chromatogram is only 5 min, a value which is surprisingly independent of the column volume. This time is twice that needed to flush the mixer, which may explain the result. Then, the regeneration time needed could be made still shorter by emptying the mixer and filling it between each run.

This result is independent of the composition of the initial solvent, up to 25% B. When the initial solvent composition is 35% B, the results are no longer reproducible, although we have never observed any split peak. This is related to the fact that the isocratic elution of lysozyme with a finite, reasonable retention time can be achieved in the concentration range of 34–40% B. We have also observed that when the column is flushed with pure solvent B for a long time, reconditioning takes longer.

Band width and initial solvent composition

The higher the initial solvent composition, the shorter is the cycle and the higher is the production rate, as long as the feed components are eluted under gradient conditions. With proteins, it is easier to define an optimum upper concentration of the

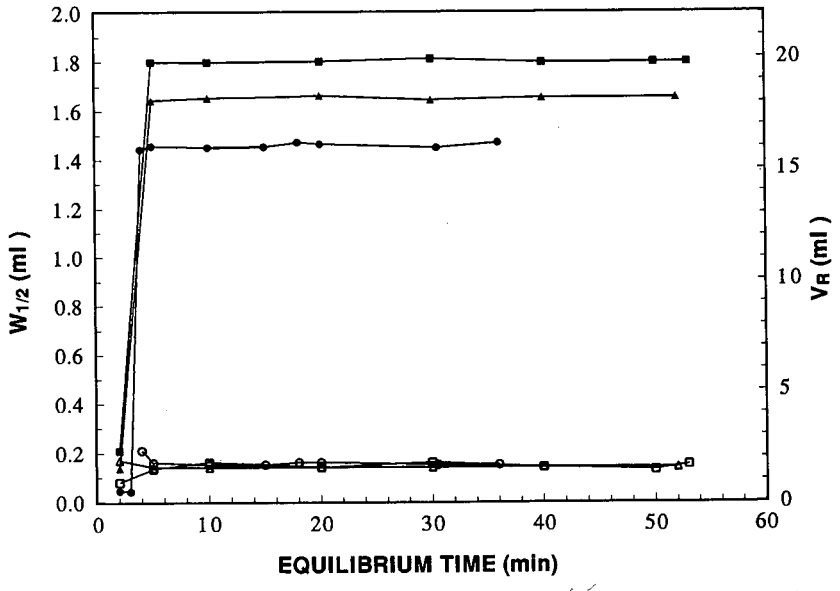

Fig. 6. Influence of regeneration time on the retention time (V_R) and peak width ($W_{1/2}$) of lysozyme. Experimental conditions as in Fig. 2, except sample volume (2 μl). V_R: ● = 5; ▲ = 15; ■ = 25 cm. $W_{1/2}$: ○ = 5; △ = 15; □ = 25 cm.

strong solvent in the initial mobile phase, as the retention of proteins is very high until it falls abruptly to low values.

Fig. 7 shows a plot of the band width *versus* the loading factor for the 25-cm column for different initial compositions. There is little difference between the results obtained with initial concentrations between 0 and 25% B. The best results seem to

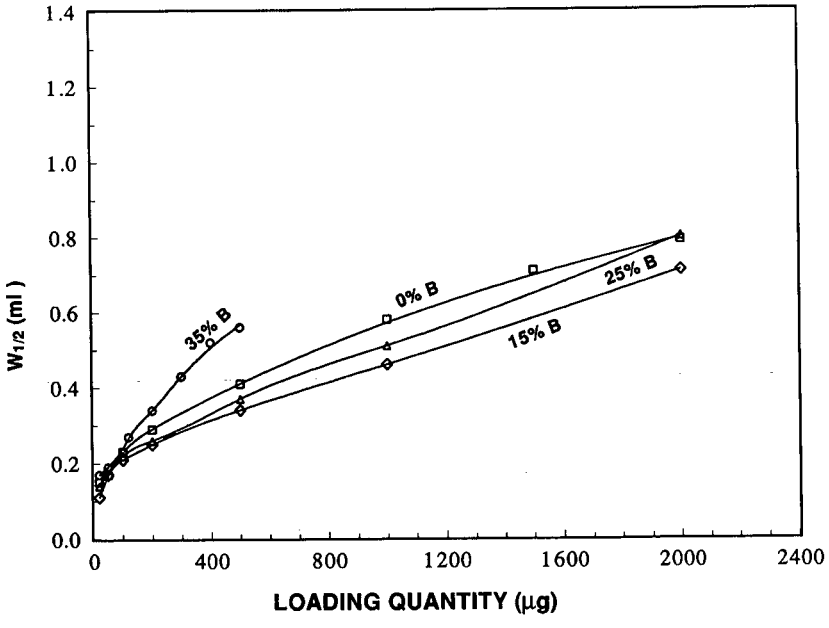

Fig. 7. Plot of peak width *versus* sample size for different initial gradient solvent compositions. Experimental conditions as in Fig. 2, except 25 × 0.46 cm I.D. column, packed with Vydac 218TP, 5 μm, 300 Å (lot number 890706-17A).

have been obtained with 15% B, but this optimum is barely significant. Given the reduction in cycle time achieved by starting with 25% B, this is probably the most economical condition.

The result becomes very different, however, if the initial concentration is 35%. Although the elution of a single-mode band is always observed, this elution is carried out through a mixed process, which is no longer pure gradient elution but involves a significant migration rate as soon as the sample is injected. The characteristics of the chromatogram are close to those observed under isocratic conditions.

Volume and concentration loading

The amount of feed injected into the column is given by the product of the sample volume and its concentration. It is still not entirely clear whether there is any good reason to prefer the injection of large volumes of a dilute solution or of small volumes of a concentrated solution, and also it seems that an intermediate combination can be optimum [23]. However, the result does not need to be the same in gradient elution and under isocratic conditions.

Fig. 8 compares the dependence of the band width and the retention volume of lysozyme on the loading amount for two sets of different, fairly extreme conditions. In the first instance volumes increasing from 2.2 to 200 μl of a 1% solution were injected into the column, and in the second, a constant volume (200 μl) of solutions with concentrations increasing from 0.001 to 1% was injected.

There is very little difference between the two sets of results obtained. This conclusion is in agreement with the assumptions of our model of gradient elution chromatography. The sample is strongly adsorbed in a thin slice at the top of the column. This slice is nearly saturated, in agreement with a rectangular isotherm. When the sample size increases, the thickness of the slice also increases, but the stationary phase concentration and the thickness of the saturated slice do not depend on the concentration of the sample used, only on its total amount.

As a consequence, gradient elution could be used to concentrate dilute solutions. A 0.001% solution can be introduced in the column. With a very steep gradient a strong concentration of the band takes place and the eluate solution may reach a concentration of *ca.* 10%. In fact, the solubility limit and the increase in the band viscosity beyond 2–3 cP

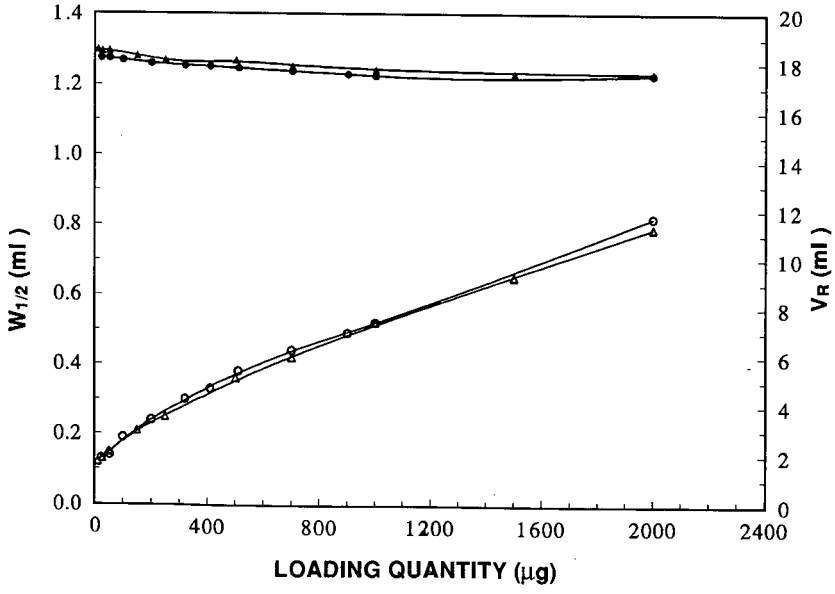

Fig. 8. Plots of retention volume and peak width *versus* sample size when the sample amount is adjusted at constant volume or constant concentration. Experimental conditions as in Fig. 2, except 15 × 0.46 cm I.D. column; sample, lysozyme; volume change by injecting 1% solution, concentration change by injecting 200 μl of different concentrations. V_R: ▲ = constant volume (200 μl); ● = constant concentration (1%). $W_{1/2}$: △ = constant volume (200 μl); ○ = constant concentration (1%).

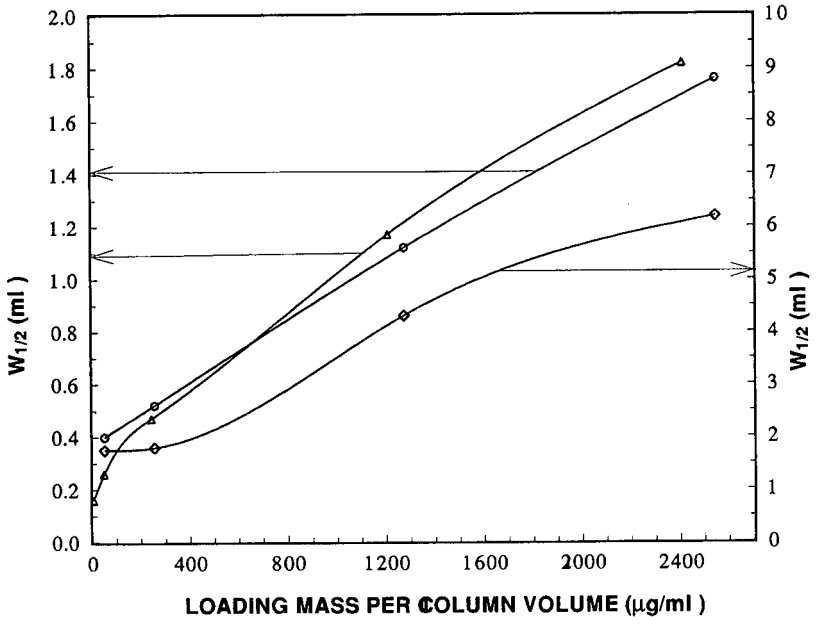

Fig. 9. Plot of peak width *versus* sample size for columns of similar volume and different length and diameter. Columns: (△) 25 × 0.46 cm I.D. (volume 4.15 ml, N = 8200 plates, h = 3.05 at 1 ml/min, with biphenyl) and (○,◇) 5 × 1.0 cm I.D. [volume 3.93 ml, N = 1600 plates, h = 3.1 at (○) 1 ml/min and N = 1400 plates, h = 3.6 at (◇) 4.73 ml/min, with biphenyl] packed with Vydac 10 μm, 300 Å (lot number 891208-21); flow-rate, 1.0 and 4.73 ml/min; gradient, 15 to 65% B in 25 min; detection, UV at 300 nm; chart speed, 1.0 cm/min; sample, lysozyme injected by varying the volume.

and the fingering effects which could arise as a consequence of this viscosity difference [24] constitute the only practical limits to the sample concentration.

Influence of column diameter and volume on the band width

Two columns having nearly the same volume (4 ml) were packed with 10-μm Vydac 218TP silica C_{18}, one 25 cm × 0.46 cm I.D. and the other 5 cm × 1.0 cm I.D. with volumes of 4.15 and 3.93 ml, respectively. The former column was operated at 1 ml/min and the latter successively at 1 ml/min (constant flow-rate) and 4.73 ml/min (constant flow velocity). When the volume flow-rate was increased, the gradient slope (in % ACN/min) was kept constant. The band width of lysozyme on these two columns were measured for increasing sample amounts. The results are shown in Fig. 9.

Similar results were obtained with the two columns at constant volume flow-rate (1.0 ml/min). This is consistent with the fact that the reduced plate heights (h) of the two columns are about the same (3.1) at 1.0 ml/min. The short, wide column, however, is operated at a much lower velocity than the longer column. The wide column shows an increased performance with increasing loading amount. At sample loadings above 0.66 mg/ml, narrower peaks are obtained on the 1 cm than on the 0.46 cm I.D. column. When the sample loading drops below 0.66 mg/ml, broader peaks are obtained, particularly at very low sample sizes. This indicates that the small diameter column is more advantageous than the large diameter column in the analytical range (small sample sizes), and *vice versa* in high loading applications.

At constant flow velocity, much broader volumetric peak widths (see the right-hand ordinate in Fig. 9) are obtained on the wide column, which is operated at a higher volume flow-rate. However, the comparison must take into account the change in retention volume. In gradient elution, a higher flow-rate results in an earlier elution of the band, and hence in its elution at a lower solvent strength. This means that the elution volume will be higher and so will be the volume band width. For example,

when comparing the chromatograms on the two columns at the same mobile phase velocity, with a 1270 mg/ml loading, there is a 2.9-fold increase in the retention volume and a 3.5-fold increase in the volumetric band width for the wider column. This performance decrease seems to be a consequence of the larger reduced plate height (3.6 instead of 3.1 at 1 ml/min). In addition, when the flow-rate is increased, the gradient delay due to the system dead volume changes, although the gradient slope (in % ACN/min) was kept constant [19,21,22].

Assuming that the separation peformances of the two columns of equal volume are comparable, the advantages of the short, wide column can be summarized as follows. First, even if we keep the mobile phase velocity constant, the inlet pressure is considerably decreased, in proportion to the ratio of the column lengths. Second, the cycle time can be dramatically reduced, as it is possible to use a very high flow-rate during the column regeneration (see Fig. 6), the flow-rate resistance of a short column being so low. The production rate increases in proportion to the reverse of the cycle time. Third, the band width is slightly narrower with the shorter, wider column at high sample loadings, which may permit the use of a still shorter column, thus decreasing the expense and the amount of solvent consumed and increasing further the production rate.

It was not possible to detect the bands obtained on the wider column with a sample of less than 20 μg, showing a significantly higher degree of dilution in the mobile phase. The phenomenon was observed at both flow-rates, 1.0 and 4.73 ml/min. If we operate the columns at constant velocity, the dilution of the product and the volume of solvent needed increase. If we operate the column at constant flow-rate, the production rate, the amount of solvent needed and the degree of dilution remain nearly constant. These results suggest that the flow velocity may not necessarily be kept constant when a separation procedure using gradient elution is scaled-up by increasing the column diameter.

Elution profiles

Fig. 10 compares the elution profiles obtained on the two columns of constant volume, with the same sample amounts. These profiles are nearly identical at high loadings. At low loadings, the profile obtained on the wider column is much worse, which

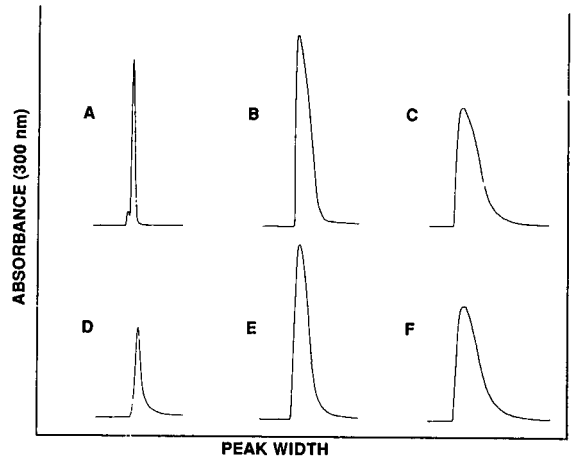

Fig. 10. Comparison of chromatograms obtained with lysozyme on columns of the same volume and different diameter. Columns and experimental conditions as in Fig. 9, except all chromatograms with a flow-rate of 1 ml/min. Peaks A, B and C (20-, 500- and 1000-μl injection, respectively) were obtained with the 25 × 0.46 cm I.D. column and D, E and F (20-, 500- and 1000-μl injection, respectively) with the 5 × 1.0 cm I.D. column.

explains the justified favor that narrow columns enjoy among analysts. There is no reason for prejudices justified in the analytical applications of chromatography to be extended to its preparative applications, where they are unwarranted.

Whereas analytical columns for the fast analysis of proteins by gradient elution should be narrow, preparative columns should be wide and shorter than analytical columns.

Touching band separations

Band profiles and band widths are useful characteristics of separations and their study has permitted a detailed analysis of the band broadening mechanism observed when a column is overloaded with proteins under gradient elution conditions. Another approach for this study is the comparison of chromatograms obtained under touching band conditions, a simple and moderate degree of column overloading.

Fig. 11 compares the chromatograms obtained on three columns, the two columns studied in the previous section (25 × 0.46 cm I.D. and 5 × 1 cm I.D.) and a 12.5 x 0.46 cm I.D. column. The same chromatogram, corresponding to touching band conditions, is eventually obtained with the three

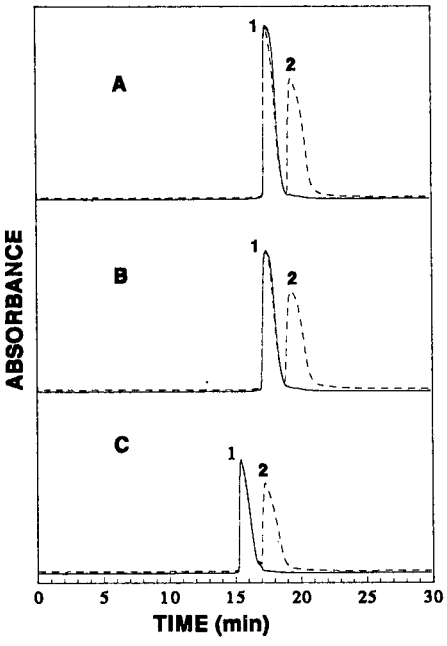

Fig. 11. Comparison of the touching band chromatograms obtained on columns of different dimensions. Columns and experimental conditions as in Fig. 5. Chromatograms A, B and C were obtained with the 25 × 0.46 cm, 5 × 1.0 cm and 12.5 × 0.46 cm I.D. columns, respectively. Injection volumes: (A and B) 500 μl; (C) 250 μl. Dashed lines, detection at 300 nm; solid lines, detection at 320 nm. 1, cytochrome *c*; 2, lysozyme.

columns when the sample amount injected is progressively increased. The sample amount corresponding to touching band conditions is identical for the two columns which have the same volume (5 mg of lysozyme and 2.5 mg of cytochrome *c*), and it is twice as small for the column which has half the volume of the other two columns.

CONCLUSIONS

We have shown that the loading capacity of a chromatographic column in gradient elution is proportional to its volume. Under isocratic conditions, there is a plate number threshold below which the separation is impossible. As the column length has little influence on the resolution, there is no such threshold in gradient elution. Within a wide range of combinations, short, wide columns give nearly the same production rate as long, narrow columns of the same volume.

The packing quality of the column, *i.e.*, its reduced plate height under analytical conditions, remains important and efforts should be made to pack preparative columns at least as carefully as analytical columns and to select high-quality packing materials.

It remains unclear, at this stage, how thin a column operated under gradient elution can be. There is a lower limit set by the homogeneity of the hydrodynamic performance. The flow velocity should be the same all over the column cross-section. This can probably be achieved with fairly thin columns. Specifications regarding column homogeneity and also the semantic problem of deciding when a thin column becomes a membrane may decide. A more practical limitation results from the extra-column sources of band broadening.

Finally, preparative chromatography does not deal with single-component profiles or with the resolution between independent bands. It deals with the production of pure components and their extraction from complex feeds. At high concentrations displacement effects take place in gradient elution as under isocratic conditions. These effects increase considerably the production rate above that which could be suggested by chromatograms. The investigation of their influence on the production rate under gradient elution conditions is in progress and the results will be reported later [25].

ACKNOWLEDGEMENTS

We thank Bernard Newman, John Kindsvater, Carol MacHarg and Angela Burnell for their comments.

REFERENCES

1 G. Guiochon, S. Golshan-Shirazi and A. Jaulmes, *Anal. Chem.*, 60 (1988) 1856.
2 J. Zhu, A. M. Katti and G. Guiochon, *J. Chromatogr.*, 552 (1991) 71.
3 S. Golshan-Shirazi and G. Guiochon, *Anal. Chem.*, 60 (1988) 2634.
4 S. Jacobson, S. Golshan-Shirazi and G. Guiochon, *AIChE J.*, 37 (1991) 836.
5 F. D. Antia and C. Horvath, *J. Chromatogr.*, 484 (1989) 1.
6 M. Z. El Fallah and G. Guiochon, *Anal. Chem.*, 63 (1991) 859.
7 M. Z. El Fallah and G. Guiochon, *Anal. Chem.*, 63 (1991) 2244.

8 A. Velayuhdan and C. Horvath, *J. Chromatogr.*, 435 (1988) 221.
9 M. Z. El Fallah and G. Guiochon, *Biotechnol. Bioeng.*, in press.
10 J. H. Knox and H. M. Pyper, *J. Chromatogr.*, 363 (1986) 1.
11 L. R. Snyder, G. B. Cox and P. E. Antle, *Chromatographia*, 24 (1987) 82.
12 G. Guiochon, S. Ghodbane, S. Golshan-Shirazi, J.-X. Huang, A. Katti, B.-C. Lin and Z. Ma, *Talanta*, 36 (1989) 19.
13 S. Golshan-Shirazi and G. Guiochon, *Anal. Chem.*, 61 (1989) 1276.
14 S. Golshan-Shirazi and G. Guiochon, *Anal. Chem.*, 61 (1989) 1368.
15 F. E. Regnier, *Science*, 222 (1983) 245.
16 H. Englehardt and H. Mueller, *Chromatographia*, 19 (1984) 77.
17 R. M. Moore and R. R. Walters, *J. Chromatogr.*, 317 (1984) 119.
18 M. Verzele, Y.-B. Yang, C. Dewaele and V. Berry, *Anal. Chem.*, 60 (1988) 1329.
19 P. Jandera and J. Churáček, *Gradient Elution in Column Liquid Chromatography —Theory and Practice*, Elsevier, Amsterdam, 1985.
20 K. Stone and K. Williams, presented at the *2nd Symposium of the Protein Society, 1988*, abstract T911.
21 L. R. Snyder, J. L. Glajch and J. J. Kirkland, *Practical HPLC Method Development*, Wiley, New York, 1988, p. 153.
22 D. W. Armstrong and R. E. Boehm, *J. Chromatogr. Sci.*, 22 (1984) 378.
23 A. M. Katti and G. Guiochon, *Anal. Chem.*, 61 (1989) 982.
24 M. Czok, A. M. Katti and G. Guiochon, *J. Chromatogr.*, 550 (1991) 705.
25 Y.-B. Yang, K. Harrison and G. Guiochon, in preparation.

Journal of Chromatography, 590 (1992) 49–58
Elsevier Science Publishers B.V., Amsterdam

CHROMSYMP. 2428

Economic considerations important in the scale-up of an ovalbumin separation from hen egg-white on the anion-exchange cellulose DE92

Peter R. Levison*, Stephen E. Badger and David W. Toome

Whatman Specialty Products Division, Springfield Mill, Maidstone, Kent ME14 2LE (UK)

Mark L. Koscielny, Linda Lane and Edward T. Butts

Whatman Specialty Products Division, 6 Just Road, Fairfield, NJ 07004 (USA)

ABSTRACT

The scale-up of the separation of hen egg-white proteins has been investigated using Whatman DE92 anion-exchange cellulose. Having developed suitable chromatographic conditions, a maximum binding capacity of 100 mg protein/ml packed DE92 was determined in a 25-ml column. The process was scaled up 1000-fold and the influence of batch and column techniques on the chromatographic step assessed. Data indicate column processes to be more efficient than batch in the adsorptive stage.

INTRODUCTION

Ion-exchange chromatography is a major tool in the downstream processing of commercially important biopolymers. Being an adsorptive process relying on the electrical charge of the feedstock components, ion-exchange is a highly versatile and selective technique, often giving rise to a high degree of purification in a single step. Low-pressure ion-exchange media are traditionally based on polysaccharide supports including cellulose, agarose and dextran [1,2].

In order to make a process economically attractive and in many instances commercially viable, it is important to optimise throughput without adversely compromising product purity. There are several factors which directly influence throughput and these include capacity, kinetics and flow-rate. Cellulose is a macroporous sorbent and thus offers a very high protein binding capacity [3,4] and fast kinetics of adsorption/desorption [5,6] factors which influence both binding efficiency during the adsorptive process and chromatographic resolution in the desorptive process. In many instances process-time *i.e.* flow-rate becomes an influencing factor, and it is generally perceived that non-fibrous celluloses *i.e.* microgranular products are unable to support high flow-rates. We have confirmed this perception in studies where axial flow columns containing Whatman DE52 and QA52 were evaluated [4,7].

It has been reported that cellulose-based media exhibit fast flow performance in radial flow columns [8,9] and we have demonstrated that DE52 and QA52 support flow-rates up to 6-fold faster than in an axial flow column of identical volume whilst maintaining good chromatographic resolution [10,11].

We have previously investigated a number of parameters which affect the economics of process-scale column chromatography using Whatman QA52. These include studies on capacity and kinetics [5], feedstock composition [12], process optimisation [13] and scale-up [14,15].

In the present study we have extended these investigations to DE92, a recently developed fast-flowing anion-exchange cellulose, and have exam-

0021-9673/92/$05.00

ined various scale-up parameters, in the separation of hen egg-white proteins in a three phase investigation. Firstly, the chromatographic conditions were developed at laboratory scale and shown to scale-up at least 1000-fold. Secondly, the maximum binding capacity of DE92 was determined using a suitable hen egg-white feedstock. Thirdly, the influence of batch *versus* column techniques were examined for the process-scale separation of hen egg-white proteins. This latter stage is complementary to a previously reported study using DE52 [3,16].

Hen egg-white is a natural protein-rich feedstock used commercially in the food processing and enzyme manufacturing industry. It is an ideal feedstock for process-scale ion-exchange studies since it is a freely available, multicomponent system which requires dilution and clarification in order for it to be effective for chromatography without fouling either the column components or chromatographic medium.

In food processing industries, for example, the feedstock volume is typically large. The key to economic success in these processes is optimal throughput. A means of improving throughput is reducing the process time and this can be achieved by increasing flow-rate in a column process or reduced handling/wash times in a batch process. In order to facilitate these improvements Whatman developed a range of anion- and cation-exchange media during 1990 based on fibrous cellulose, *i.e.* DE92, QA92, CM92 and SE92. These products may be operated at flow-rates 2-3-fold faster than the microgranular cellulosic media. In the present study we demonstrate that DE92 can be operated at high flow-rates in a process-scale system without loss of capacity or binding efficiency for the target proteins.

EXPERIMENTAL

Materials

Cell debris remover (CDR), DE52, DE92 and a PREP-25 column were obtained from Whatman Specialty Products (Maidstone, UK). Ovalbumin was obtained from Sigma (Poole, UK) Tris(hydroxymethyl)aminomethane (Tris) was obtained from Merck (Dagenham, UK). Sephadex G-25 medium was obtained from Pharmacia (Milton Keynes, UK). All other chemicals were of reagent grade. Fresh size 2 hen eggs were obtained from Barradale Farms (Headcorn, UK).

Feedstock preparation

Egg-whites were separated from 600 fresh hen eggs and diluted to 14% (v/v) with 0.025 *M* Tris–HCl buffer, pH 7.5 [17]. The egg-white suspensions were clarified using a total of 22 kg pre-equilibrated CDR in a batch mode. Spent CDR was removed by centrifugation through a 1.6 × 0.06 mm slotted screen (EHR 500 basket centrifuge, Robatel and Mulatier, Lyons, France) and the sample clarified by filtration through a grade 541 filter paper (Whatman Scientific, Maidstone, UK). The clear solution (200 l) containing *ca.* 10 mg total protein per ml was used for chromatography.

Chromatographic studies

Chromatographic development

Egg-white feedstock (7 ml) was applied to a DE92 column (15.5 cm × 1.5 cm I.D.) pre-equilibrated with 0.025 *M* Tris–HCl buffer, pH 7.5 [18], and non-bound material removed by washing with 0.025 *M* Tris–HCl buffer, pH 7.5 (50 ml). Bound material was eluted using a linear gradient of 0–0.5 *M* NaCl in 0.025 *M* Tris–HCl buffer, pH 7.5 (200 ml). The chromatography was carried out at a flow-rate of 2 ml/min.

A parallel experiment was carried out using DE92 packed in a PREP-25 column (16 cm × 45 cm I.D.) at a flow-rate of 2 l/min with a 1000-fold scale-up throughout.

Capacity determination

Egg-white feedstock was applied to a column of DE92 (15.5 cm × 1.5 cm I.D.) previously equilibrated with 0.025 *M* Tris–HCl buffer, pH 7.5 at a flow-rate of 2 ml/min over a period of 300 min by which time the absorbance of the eluate at 280 nm was similar to that of the feedstock. Non-bound material was removed by washing with 0.025 *M* Tris–HCl buffer, pH 7.5 (50 ml). Bound material was eluted with 0.025 *M* Tris–HCl buffer, pH 7.5 containing 0.5 *M* NaCl (100 ml). The flow-rate was maintained at 2 ml/min throughout.

Process-scale chromatography

DE92 (25 kg) was equilibrated with 0.025 *M* Tris–HCl buffer, pH 7.5. The ion exchanger was used with the egg-white feedstock (200 l) accordingly: (i) batch adsorption/batch desorption; (ii) batch adsorption/column desorption; (iii) column adsorption/column desorption. All procedures were carried out at room temperature (15–20°C).

(i) Batch adsorption/batch desorption. DE92 (25 kg) was stirred with the CDR-treated feedstock (200 l). The DE92 was collected by centrifugation and washed with 0.025 *M* Tris–HCl buffer, pH 7.5 (200 l). Bound material was eluted using 0.025 *M* Tris–HCl buffer, pH 7.5 containing 0.5 *M* NaCl (200 l). In this study elution was carried out on the centrifuge wall for half of the DE92 and in a stirred tank for the remainder of the DE92.

(ii) Batch adsorption/column desorption. DE92 (25 kg) was stirred with the CDR-treated feedstock (200 l). The slurry (8%, w/v) was pump-packed into a PREP-25 column (16 cm × 45 cm I.D.) at a pressure of *ca.* 10 p.s.i.

The bed was washed with 0.025 *M* Tris–HCl buffer, pH 7.5 (100 l) and bound material eluted using a linear gradient of 0–0.5 *M* NaCl in 0.025 *M* Tris–HCl buffer, pH 7.5 (200 l) at a flow-rate of 2.0 l/min.

(iii) Column adsorption/column desorption. DE92 (25 kg) was slurried to 14% (w/v) in 0.025 *M* Tris–HCl buffer, pH 7.5 and pump-packed into a PREP-25 column at a pressure of *ca.* 10 p.s.i. The egg-white feedstock (200 l) was loaded onto the column and non-bound material removed by washing with 0.025 *M* Tris–HCl buffer, pH 7.5 (100 l). Bound material was eluted using a linear gradient of 0–0.5 *M* NaCl in 0.025 *M* Tris–HCl buffer, pH 7.5 (200 l). A flow-rate of 2.0 l/min was maintained throughout.

Assays

Pooled fractions obtained at various stages of the chromatography were assayed for protein content using A_{280} measurement against standard solutions of ovalbumin.

Throughout the column procedures the effluent was monitored for absorbance at 280 nm and by conductivity.

Rechromatography of fractions

For each process-scale study samples of (a) egg-white feedstock, (b) non-bound material and (c) salt-eluted material were rechromatographed using DE52.

The salt-eluted material (c) was desalted by gel filtration through a column (12.5 cm × 1.0 cm I.D.) containing Sephadex G-25 medium, previously equilibrated with 0.025 *M* Tris–HCl buffer, pH 7.5.

The fractions were rechromatographed on a column (15 cm × 1.0 cm I.D.) containing DE52, previously equilibrated with 0.025 *M* Tris–HCl buffer, pH 7.5. Non-bound material was removed by washing with 0.025 *M* Tris–HCl buffer, pH 7.5 (25 ml) and bound material eluted using a linear gradient of 0–0.5 *M* NaCl in 0.025 *M* Tris–HCl buffer, pH 7.5 (100 ml). Flow-rate was maintained at 2 ml/min, and the absorbance at 280 nm and the conductivity of the eluent were continuously monitored.

RESULTS AND DISCUSSIONS

In our earlier studies on egg-white chromatography using DE52 we used a feedstock containing *ca.* 10 mg/ml total protein [3,16], as we considered this to be a typical and suitable working concentration of proteins. In the present study we used a similar feedstock for the evaluations of DE92. Under analytical loadings *i.e.* total protein loaded is < 5% of total capacity, a typical separation of egg-white proteins was seen for DE92 (Fig. 1a). The non-bound fraction consisted of two components, the basic protein lysozyme and the acidic protein conalbumin (mol. wt. 77 000 dalton). The adsorbed material contained low levels of conalbumin with the major component being ovalbumin (mol. wt. 45 000 dalton). The fibrous nature of the cellulose matrix in DE92 gives rise to significant size exclusion of larger molecules and this is evident by the very low levels of conalbumin which adsorb to the medium. Under identical conditions the conalbumin component is retained by both DE52 [3] and QA52 [7], which based on microgranular cellulose do not exhibit similar size-exclusion properties. Having developed a suitable chromatographic system using a laboratory column the separation was scaled-up

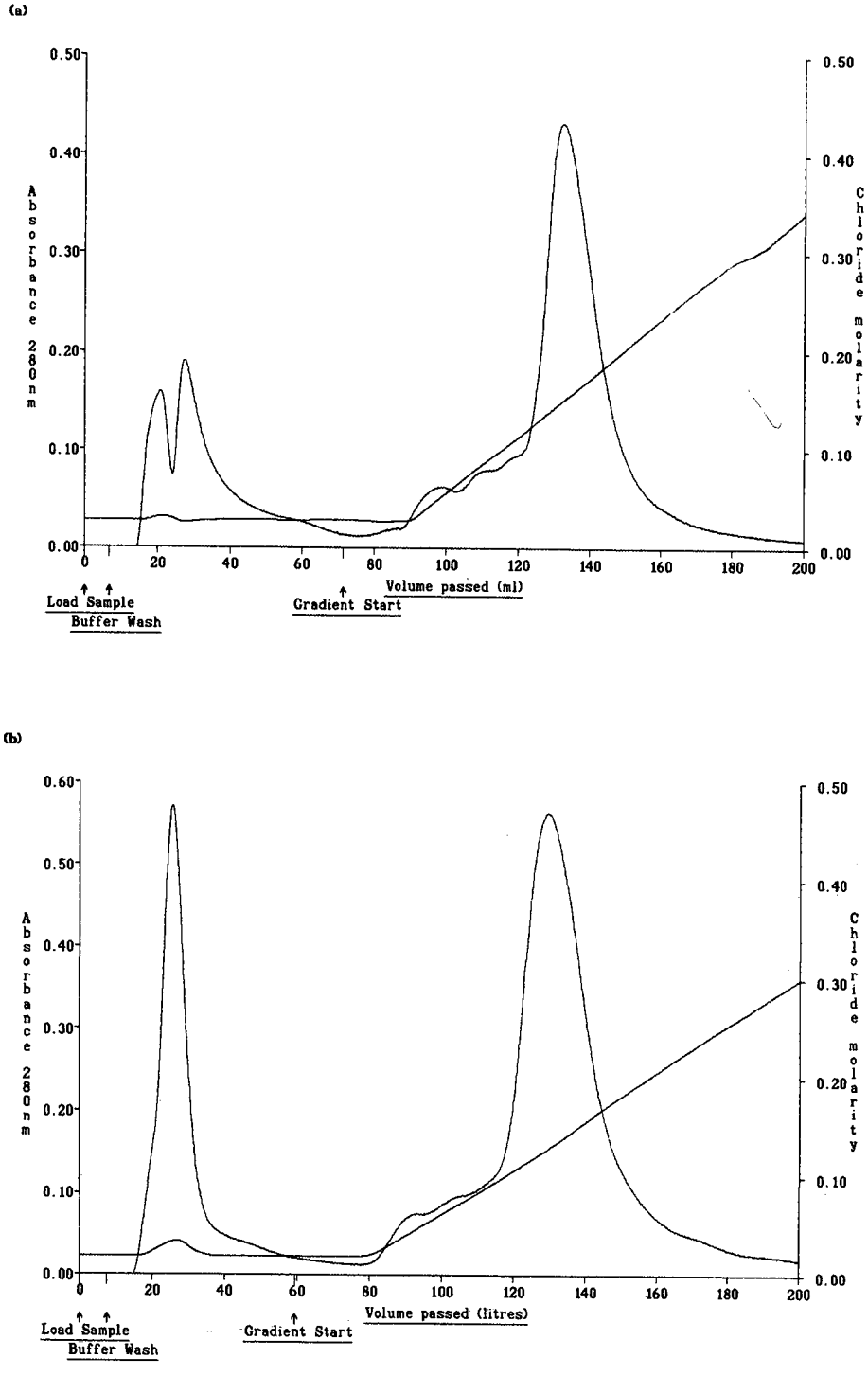

Fig. 1. Column chromatography of hen egg-white proteins on DE92 using 0.025 *M* Tris–HCl buffer, pH 7.5 at (a) laboratory-scale (15.5 cm × 1.5 cm I.D.) and (b) process-scale (16 cm × 45 cm I.D.).

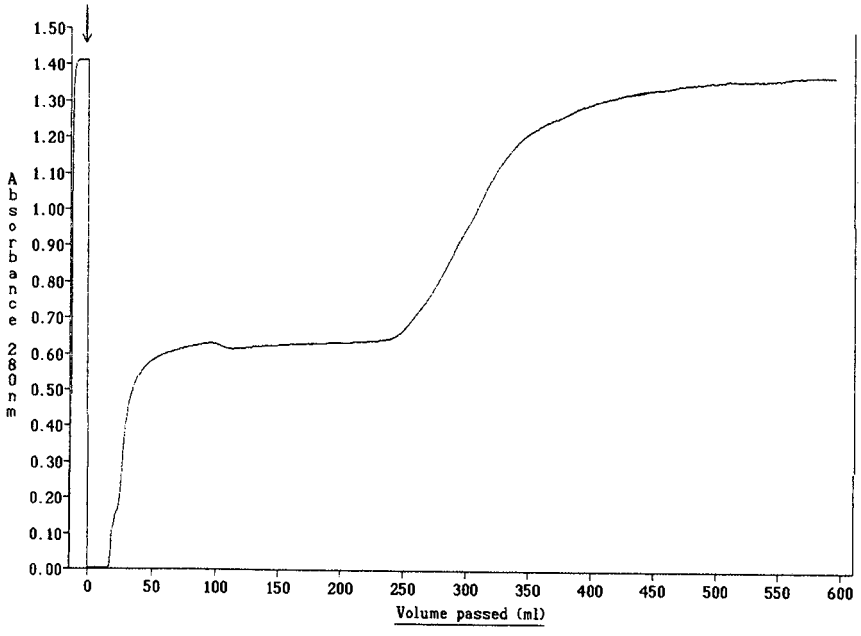

Fig. 2. Absorbance profile of column eluate during a saturation loading of DE92 with 10 mg/ml hen egg-white proteins using 0.025 *M* Tris–HCl buffer, pH 7.5. Absorbance of the feedstock is identified by the arrow.

1000-fold by increasing bed diameter 30-fold whilst maintaining column bed height and linear flow-rate (*ca.* 75 cm/h). This separation is represented in Fig. 1b and clearly the DE-92 process has scaled-up satisfactorily.

In order to determine the maximum capacity of the column for egg-white proteins, the feedstock (10.4 mg/ml) was applied to a laboratory column of DE92. Following a 610-ml loading of the column, the absorbance of the eluate at 280 nm was similar to the absorbance of the feedstock, indicating that a saturation loading had been achieved. The absorbance profile of the column eluate during this study is represented in Fig. 2. During the adsorption stage a non-linear stepped absorbance was observed. The shape can be attributed to components of the egg-white eluting from the column in order of ascending acidity due to protein–protein displacement etc., resulting in the ovalbumin component only being retained. Similar observations were reported for the treatment of goat serum with CDR [15]. Following the column loading and buffer wash, a total of 2.688 g protein were bound to the DE92 which reflects a capacity of 98 mg protein/ml packed column volume. Elution of bound protein with NaCl resulted in recovery of 89%. In a similar experiment using DE52 a capacity of 158 mg protein/ml packed column volume was obtained with 98% recovery of bound protein [19].

In a process-scale separation, throughput is very critical and although it may be possible to operate a column of DE92 at a capacity of 98 mg/ml packed column volume, this is clearly an inefficient adsorptive process since only 66% of the total ovalbumin present in the feedstock bound to the DE92, based on an average ovalbumin content of 63.8% (w/w) of total egg-white protein [20]. In separations where the feedstock is freely available in excess then inefficient adsorption may be acceptable, but in many instances the value of the feedstock and/or target, coupled with increased process times and added effluent treatment outweigh any potential benefits of such a step. It would therefore be desirable to carry out the process under conditions where as close to 100% of the target binds to the medium during a single contacting operation.

In order to scale-up the chromatography while maintaining an efficient binding process, 200 l of egg-white feedstock was applied to 25 kg DE92, *i.e.* a loading of *ca.* 75 mg protein/ml packed column

TABLE I

PROTEIN CAPACITIES DURING PROCESS-SCALE CHROMATOGRAPHY OF EGG-WHITE PROTEINS

Run	Adsorption mode	Desorption mode	Feedstock total protein (g)	Stage of chromatography	Total protein (g)		Binding efficiency (%)
					In mobile phase	Adsorbed to DE92	
1	Batch	Batch centrifuge wall	1846[a]	Loading	256	667	69.1
				Wash	29	638	
				Elution	572	66	
2	Batch	Batch stirred tank		Loading	256	658	68.4
				Wash	27	631	
				Elution	609	22	
3	Batch	Column	1965	Loading	571	1394	66.0
				Wash	98	1296	
				Elution	1097	199	
4	Column	Column	1945	Loading	426	1519	72.3
				Wash	113	1406	
				Elution	1421	–	

[a] Split into 2 lots after loading.

volume, which is submaximal loading as determined previously (Fig. 2). In this study we have compared batch and column techniques under similar process-chromatography conditions. The loading capacity data for these studies are summarised in Table I. In order to determine the efficiency of the adsorptive process with respect to total feedstock proteins a binding efficiency is calculated according to eqn. 1:

$$\text{Binding efficiency (\%)} = \frac{\text{mass of protein adsorbed}}{\text{mass of protein loaded}} \cdot 100 \quad (1)$$

The batch loading data indicate that *ca.* 68% of applied protein is adsorbed to the DE92 and this compares to a binding efficiency of *ca.* 72% for column loading. These observations are consistent with those obtained using DE52 [3,16] and are expected since a batch step is in fact a simple equilibrium process and can be regarded as having a theoretical plate count of one. On the other hand, a column has a higher plate count and consequently will be more efficient during the loading procedure.

The elution stages were efficient in all cases and are consistent with our previous studies on DE52 [3,16].

The data indicate that *ca.* 55 mg protein bound per ml (g) of DE92 from a loading of *ca.* 75 mg total proteins/ml. Based on an ovalbumin content of 63.8% (w/w) of total egg-white protein [20] then assuming 100% adsorption of the ovalbumin (*ca.* 48 mg/ml), only small amounts of other proteins would be expected to have bound to the DE92. This is confirmed in the rechromatography of various fractions obtained during the process. The egg-white feedstock gives a typical chromatogram on DE52 (Figs. 3a, 4a, 5a and 6a). The lysozyme component does not bind to the column and the two adsorbed components elute in the order conalbumin followed by ovalbumin. In each adsorption-process the lysozyme and conalbumin constituents did not bind to the DE92 whereas the ovalbumin was totally bound (Figs. 3b, 4b, 5b and 6b). Chromatograms of the pooled-bound material, following desalting, are represented in Figs. 3c, 4c, 5c and 6c. In each case the proteins bound to the DE92 appear not to be significantly different and as suggested above are predominantly ovalbumin.

In any chromatographic process there are two key factors which affect the success and economics of the separation. Firstly the binding efficiency of the medium for the target during a single adsorptive cycle and secondly the purity of the product. Bind-

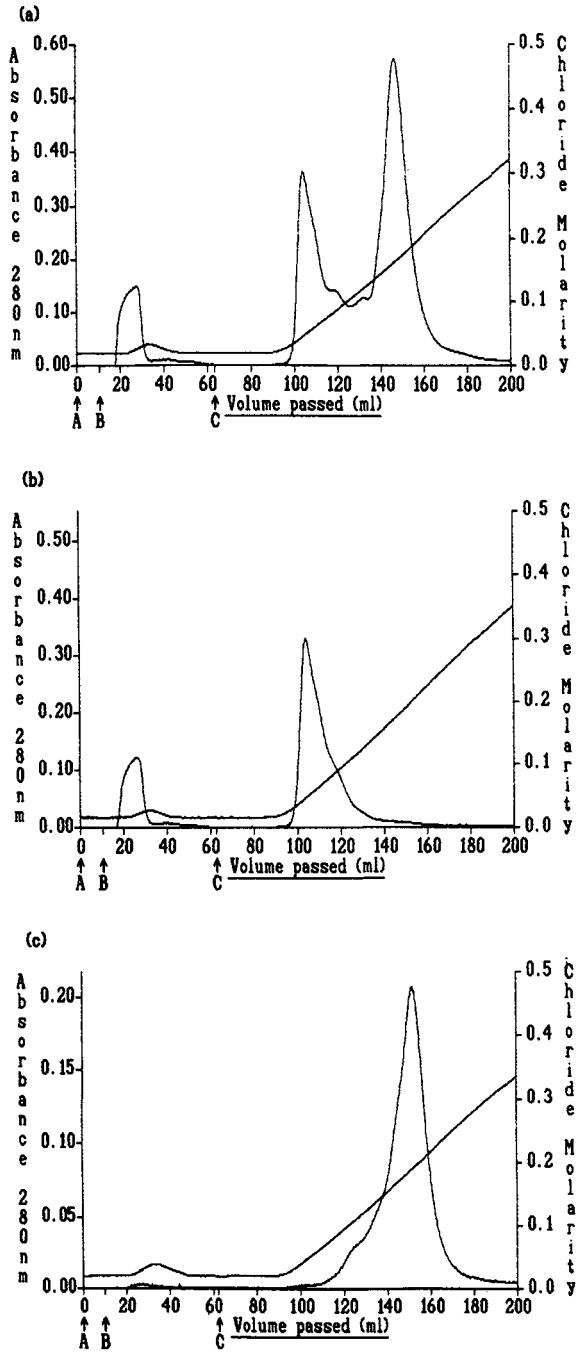

Fig. 3. Rechromatography using DE52 of individual fractions eluted during chromatography of hen egg-white proteins on DE92 following batch adsorption/batch centrifuge wall desorption using 0.025 *M* Tris–HCl buffer, pH 7.5. (a) Egg-white feedstock, (b) non-bound material, (c) salt-eluted material. A = Load sample; B = buffer wash; C = gradient start.

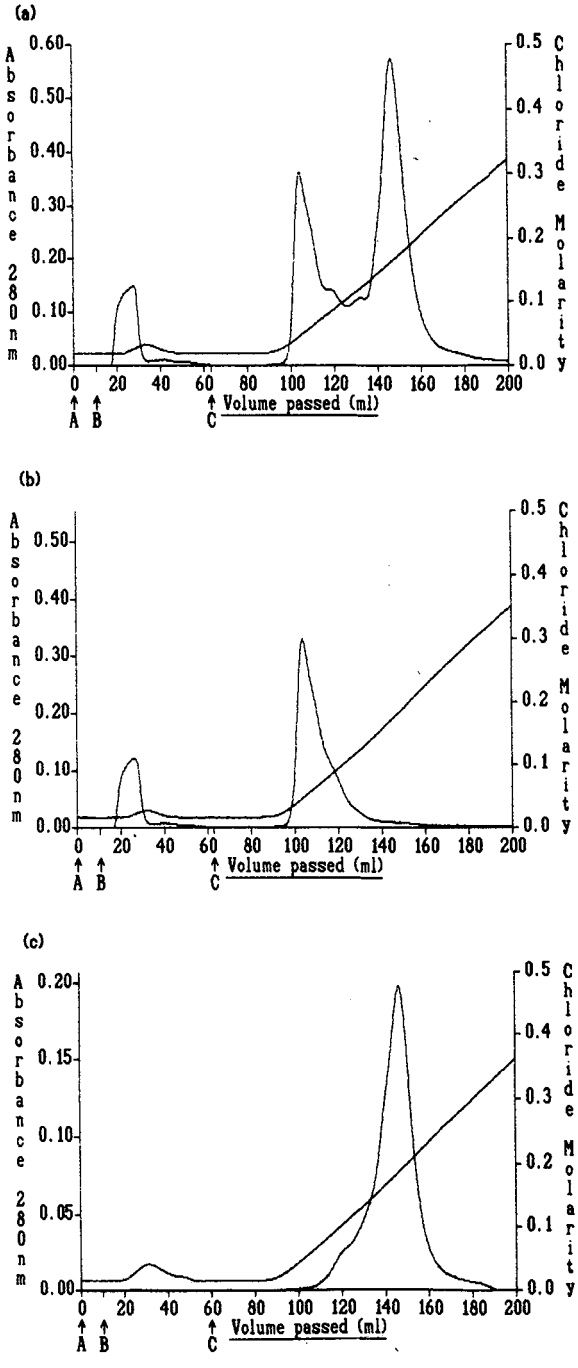

Fig. 4. Rechromatography using DE52 of individual fractions eluted during chromatography of hen egg-white proteins on DE92 following batch adsorption/batch stirred tank desorption using 0.025 *M* Tris–HCl buffer, pH 7.5. (a) Egg-white feedstock, (b) non-bound material, (c) salt-eluted material. A = Load sample; B = buffer wash; C = gradient start.

ing efficiency is dependent on the contact time between the target and ion-exchange medium and this is affected by flow-rate and the kinetics of adsorption. Product purity is generally dependent on the elution conditions and desorption kinetics of the medium. Since the DE92 was overloaded with protein such that the ovalbumin component displaced conalbumin and other weakly acidic components, the requirements for highly controlled elution and fast kinetics are reduced. This is confirmed in Figs. 3c and 4c where the step eluted bound material appeared to be very similar to the gradient eluted material Figs. 5c and 6c. Had the DE92 not been overloaded with egg-white feedstock *e.g.* reducing the feedstock volume to *ca.* 50 l then all acidic components would have been expected to adsorb to the medium. Consequently the gradient eluted material would give a significantly greater purity fraction than the bulk step eluted material.

Whatman ion-exchange celluloses exhibit fast kinetics of adsorption [5,6] but as discussed above are often used at low flow-rates. A typical linear flow-rate for DE52 would be *ca.* 30 cm/h using a process-scale axial column [3]. In the present study DE92 was used at a linear flow-rate of *ca.* 75 cm/h, the fibrous nature of the medium facilitating its fast flow properties. We have demonstrated that a protein separation using a natural feedstock can be effected using DE92 and this can be scaled-up from the laboratory to process-scale. Using *ca.* 56% of the total egg-white protein binding capacity of the DE92, the separation could be carried out at process-scale using either batch or column adsorption/desorption techniques with a very high binding efficiency. It is evident that column loading is more efficient than batch although the latter is potentially more time efficient especially in separations where large volumes of dilute feedstock may be involved.

In many production separations the requirement is for 100% recovery of a high value target protein with less regard for capacity of the medium. Consequently slow adsorption kinetics may be tolerated since binding efficiency is of low importance. When binding efficiency does become important, for example, where a competitor product may be available at a comparable cost, then throughput optimisation becomes a key factor. In these separations adsorption/desorption kinetics and flow-rate become determinants in media selection. Whatman

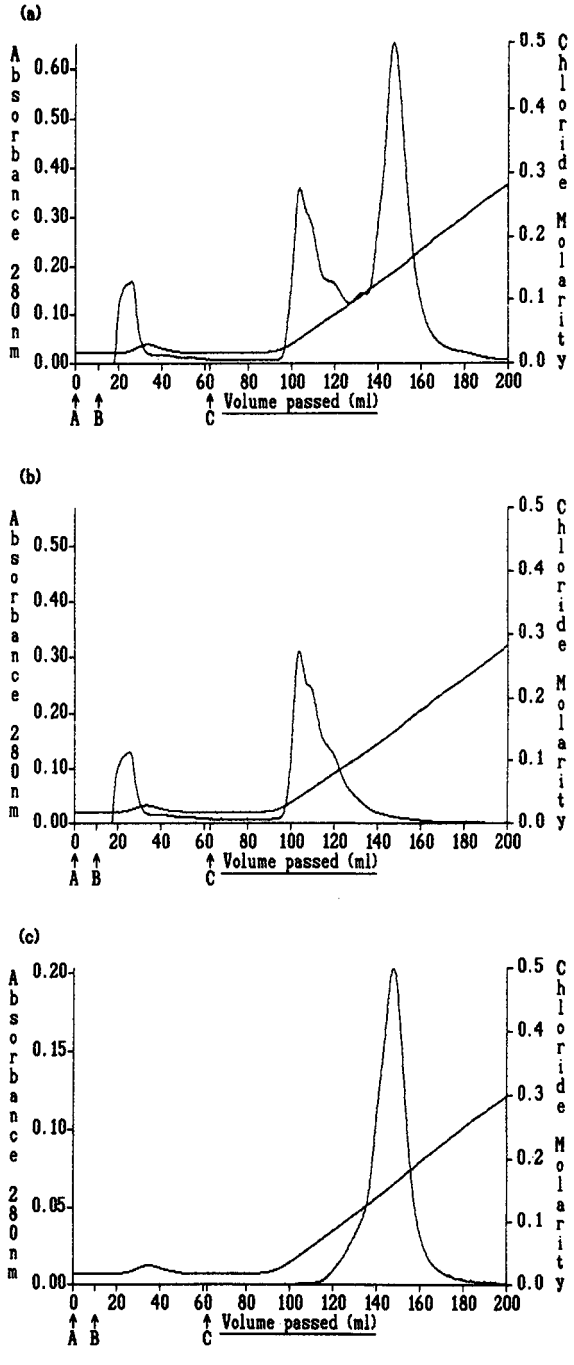

Fig. 5. Rechromatography using DE52 of individual fractions eluted during chromatography of hen egg-white proteins on DE92 following batch adsorption/column desorption using 0.025 *M* Tris–HCl buffer, pH 7.5. (a) Egg-white feedstock, (b) non-bound material, (c) salt-eluted material. A = Load sample; B = buffer wash; C = gradient start.

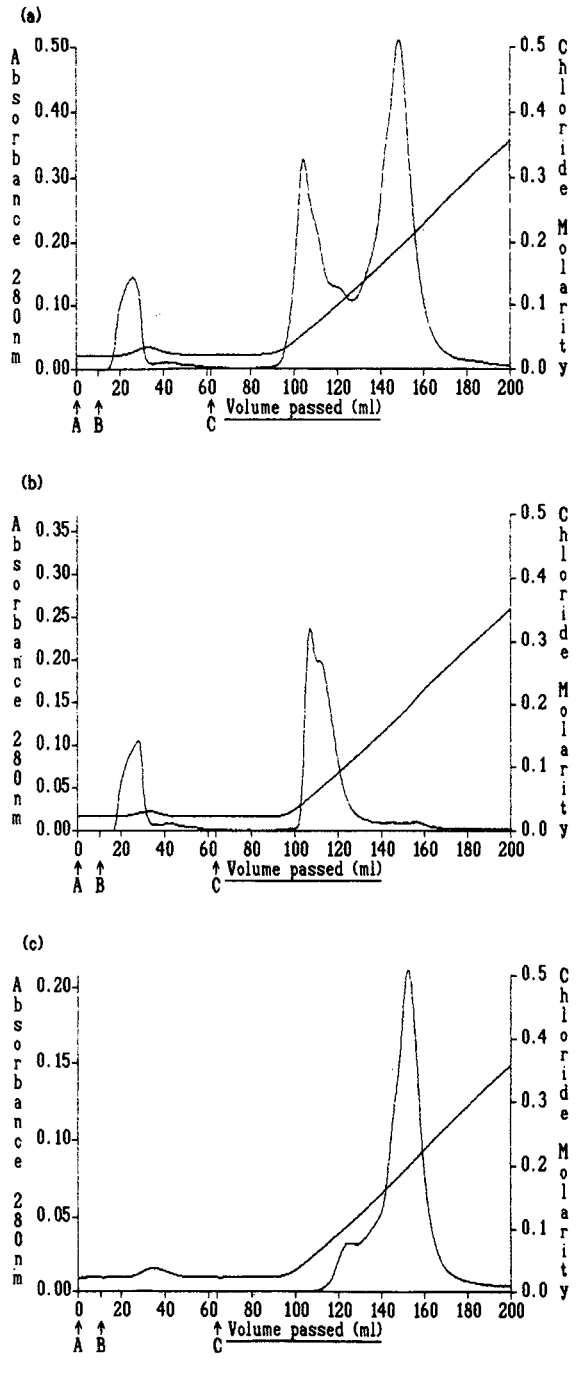

Fig. 6. Rechromatography using DE52 of individual fractions eluted during chromatography of hen egg-white proteins on DE92 following column adsorption/column desorption using 0.025 *M* Tris–HCl buffer, pH 7.5. (a) Egg-white feedstock, (b) non-bound material, (c) salt-eluted material. A = Load sample; B = buffer wash; C = gradient start.

ion-exchange celluloses offer fast binding kinetics and consequently are effective in providing high binding capacity and efficiency while ensuring good product purity. Dependent on the process requirements then either microgranular products, *i.e.* DE52, CM52, etc, or fibrous products, DE92, CM92, etc, may be applicable. The selection of either of these media types will depend on the nature of the target molecule, *i.e.* molecular weight or feedstock volume which could influence flow-rate, process time etc. The data in this study taken with our previous evaluations of DE52 [16] and QA52 [15] demonstrate that Whatman ion-exchange celluloses are suitable for process-scale protein separations in a range of manufacturing industries, where product yield and purity are key economic considerations.

REFERENCES

1 D. Friefelder, *Physical Biochemistry*, W. H. Freeman & Co., San Francisco, CA, 2nd ed., 1982, p. 249.
2 E. F. Rossomando, *Methods Enzymol.*, 182 (1990) 309.
3 P. R. Levison, S. E. Badger, D. W. Toome, D. Carcary and E. T. Butts, in D. L. Pyle (Editor), *Separations for Biotechnology 2*, Elsevier Applied Sci. Publ., London, 1990, p. 381.
4 P. R. Levison and F. M. Clark, *Pittsburgh Conference 1989, Atlanta, 1989*, Abstracts, p. 752.
5 P. R. Levison, D. W. Toome, S. E. Badger, D. Carcary and E. T. Butts, *Pittsburgh Conference 1990, New York, 1990*, Abstracts, p. 1079.
6 G. Leaver, J. R. Conder and J. A. Howell, *Advances in Separation Processes*, (*Symposium Series*, No. 118) Institute of Chemical Engineers, London, 1990, p. 1.1.
7 L. Lane, M. L. Koscielny, P. R. Levison, D. W. Toome and E. T. Butts, *Bioseparation*, 1 (1990) 141.
8 V. Sazena and M. Dunn, *Bio/Technology*, 7 (1989) 255.
9 V. Saxena, K. Subramanian, S. Saxena and M. Dunn, *BioPharm*, March (1989) 46.
10 P. R. Levison, E. T. Butts, M. L. Koscielny and L. Lane, in Y. Briand, C. Doinel and A. Faure (Editors), *Proteins Purification Technologies*, Vol. 4, G.R.B.P., Clermont-Ferrand, 1990, p. 137.
11 L. Lane, M. L. Koscielny, E. T. Butts and P. R. Levison, *Pittsburgh Conference 1990, New York, 1990*, Abstracts, p. 1078.
12 P. R. Levison, D. W. Toome, S. E. Badger, B. N. Brook and D. Carcary, *Chromatographia*, 28 (1989) 170.
13 W. E. Schwartz, F. M. Clark and I. B. Sabran, *LC · GC*, , 4 (1986) 442.
14 W. E. Schwartz, F. M. Clark, M. L. Koscielny, S. J. Powell, P. R. Levison and C. Ralston in C. Doinel, A. Faure and O. Robert (Editors), *Proteins Purification Technologies*, Vol. 3, G.R.B.P., Villebon-Yvettes, 1988, p. 448.

15 P. R. Levison, M. L. Koscielny and E. T. Butts, *Bioseparation*, 1 (1990) 59.
16 P. R. Levison, S. E. Badger, D. W. Toome, D. Carcary and E. T. Butts, *Advances in Separation Processes* (*Symposium Series*, No. 118) Institute of Chemical Engineers, London, 1990, p. 6.1.
17 D. D. Perrin and B. Dempsey, *Buffers for pH and Metal Ion Control*, Chapman & Hall, London, 1979, p. 143.
18 Whatman Specialty Products Division, *Use of Whatman 90 Series Ion Exchange Celluloses; Leaflet IL 11*, Whatman Paper, Maidstone, 1991.
19 P. R. Levinson, in G. Subramanian (Editor), *Preparative and Process-Scale Liquid Chromatography*, Ellis Horwood, Chichester, in press.
20 W. Bolton, in C. Long, E. J. King and W. M. Sperry (Editors), *Biochemist's Handbook*, E. & F. N. Spoon, London, 1971, p. 764.

Journal of Chromatography, 590 (1992) 59–76
Elsevier Science Publishers B.V., Amsterdam

CHROMSYMP. 2379

High-performance membrane chromatography of serum and plasma membrane proteins

Djuro Josić* and Joachim Reusch

Säulentechnik Dr. Ing. Herbert Knauer GmbH, Am Schlangengraben 16, W-1000 Berlin 20 (Germany)

Klemens Löster, Oliver Baum and Werner Reutter

Institut für Molekularbiologie und Biochemie, Freie Universität Berlin, Arnimallee 22, W-1000 Berlin 33 (Dahlem) (Germany)

ABSTRACT

Porous discs made of poly(glycidyl methacrylate) were used for high-performance membrane chromatography (HPMC) of proteins. In model experiments, separations of standard proteins by anion-exchange HPMC using a DEAE disc were carried out. The influences of sample distribution and disc diameter and thickness on separation performance were studied. The separation disc allowed a scaling-up from analytical (diameter 10 mm) to semi-preparative (diameter 50 mm) dimensions. In an application study, separations with anion-exchange and affinity HPMC were carried out using different complex samples such as rat serum and plasma membrane proteins. In all experiments the results on poly(glycidyl methacrylate) discs were comparable to those achieved on adequate high-performance liquid chromatographic (HPLC) columns. However, the separations on HPMC discs could be carried out faster than corresponding separations on HPLC columns. The pressure drop on the discs was low even at high flow-rates. The experiments show that the poly(glycidyl methacrylate) discs used are especially suitable for the isolation of proteins and other biopolymers which occur in a diluted state in complex mixtures.

INTRODUCTION

High-performance membrane chromatography (HPMC) was introduced several years ago, chiefly for biopolymer separation. Initial investigations revealed that HPMC can be used in affinity chromatography with results similar to those achieved with high-performance liquid chromatographic (HPLC) columns [1–4]. Several techniques of membrane construction exist. One strategy consists in bundling several thin membranes made of synthetic hollow fibres or cellulose, another involves compact, porous, disc-shaped membranes, made of silica gel or polymer supports, and a third option is a combination of these two strategies. The beads, which are non-porous in most instances, are polymerized between the fibres. Remarkable results in biopolymer separations have been achieved especially with separation devices that consist of several bundled membranes and with compact discs [1–4]. The membranes with beads polymerized into hollow-fibre matrices have a low capacity for larger molecules. However, they can be used for sample preparation, *e.g.*, desalting of sugar mixtures before HPLC analysis [5].

Apart from analytical and preparative separations of biopolymers, membranes can be used for the immobilization of enzymes. With such a reactor, containing the immobilized enzyme carbonic anhydrase, synthetic substrates could be converted successfully in a very rapid manner [4].

Membranes have several important advantages over HPLC columns. The chromatographic separation is carried out on a wide, thin disc, so that there is only a pressure drop even at high flow-rates. The fact that separations on membranes can be carried out very quickly is due to the fast reaction kinetics in these systems [6]. Improved reaction kinetics in a disc also explain a phenomenon that occurs in membrane reactors with immobilized carbonic an-

hydrase, which may appear puzzling at first, namely increased enzymatic activity at higher flow-rates [4]. Technical problems have hampered further increases in the use of HPMC. The bundling of thin membranes often leads to leakages in the system, which in turn causes the mobile phase (and the sample) to flow beyond the edges and therefore past the membranes. Another equally important problem is the distribution of the sample or the mobile phase, coming out of a narrow capillary, on the wide disc surface. If the dead volume is large enough, distribution is ensured before and after the disc, but the separation performance is impaired owing to peak broadening.

This paper deals with the HPMC of standard proteins and serum and membrane proteins with diethylaminoethyl (DEAE) groups, heparin and collagen as ligands. Compact discs were used, made of poly(glycidyl methacrylate). Through the introduction of distribution discs, the problems of sample distribution have been solved to a great extent. The identical chemical and mechanical properties of the separation disc allowed a scaling-up from analytical to (for the time being) semi-preparative dimensions.

EXPERIMENTAL

Animals and chemicals

Male or female Wistar or Buffalo rats (Institut für Molekularbiologie und Biochemie, Berlin, Germany), weighing about 160–180 g each were fed on a commercial diet containing 18–20% (w/w) of protein (Altromin R, Altromin, Lage/Lippe, Germany). Chemicals of analytical-reagent grade were purchased from Merck (Darmstadt, Germany), Serva (Heidelberg, Germany) or Sigma (Munich, Germany). All detergents were purchased from Sigma.

The following standard proteins were used: ferritin, immunoglobulin G, transferrin, bovine serum albumin (BSA), ovalbumin, conalbumin and soybean trypsin inhibitor (STI). Other samples containing protein were rat serum and rat kidney, liver and Morris hepatoma plasma membranes. Plasma membranes were isolated by zonal centrifugation using a Kontron centrifuge (Kontron Analytik, Munich, Germany) as described elsewhere [3,7]. Membrane purity was routinely checked by electron microscopy and by assaying of marker enzymes as described by Tauber and Reutter [7]. Protein in membrane and serum samples was determined according to the procedure of Lowry *et al.* [8] or in the presence of detergent according to Smith *et al.* [9], using a protein determination kit (Pearce, Rodgau, Germany).

Enzyme assays

Enzyme units are given as micromoles per minute. Nucleotide pyrophosphatase (NPPase) was routinely assayed according to a modified method of Elovson [10]. An amount of 100 μl of substrate solution, containing thymidine 5′-monophosphate *p*-nitrophenyl ester was added to 290 μl of 100 m*M* Tris–HCl (pH 8.9) and 10 μl of sample. The mixture was incubated at 37°C for 30 min. Enzymatic reaction was stopped by adding 600 μl of 0.1 *M* NaOH, and the absorbance at 405 nm was measured using a Eppendorf (Hamburg, Germany) spectrophotometer. Dipeptidyl peptidase IV (DPP IV) activity was determined according to the method of Nagatsu *et al.* [11], using tosylglycineproline *p*-nitroanilide (Bachem, Bubendorf, Switzerland) as substrate. Between 10 and 100 μl of sample were added to 90–180 μl of 0.1 *M* Tris–HCl buffer (pH 8.0) and 10 μl of substrate, and incubated at 37°C for 30 min. The reaction was stopped by adding 800 μl of 1 *M* sodium acetate (pH 4.5) and the absorbance was measured at 405 nm using an Eppendorf spectrophotometer.

HPLC

The HPLC system consisted of two pumps, a programmer, a spectrophotometer with a deuterium lamp and a Knauer loop injection valve (all from Knauer, Berlin, Germany) and a fraction collector (Bio-Rad, Munich, Germany). In ion-exchange chromatography the salt gradient was controlled by measuring the osmotic pressure (Halbmikro-Osmometer, Type Dig. L; Knauer).

Columns and membranes (discs)

The membranes and the poly(glycidyl methacrylate) discs that were used for separation were produced using the method of Tennikova *et al.* [1]. The thickness of the membrane layers was 1, 2, 3 and 7 mm. They were cut out in a disc shape of 10, 20, 25, 40 and 50 mm diameter using moulds of high-grade

steel and then installed in the corresponding cartridges. When the separation discs were used for ion-exchange or hydrophobic-interaction HPMC, the chosen ligands were previously bound synthetically [1,12,13]. In affinity chromatography the ligand was positioned on the membrane in epoxy form *in situ*, according to the following procedure (this applies to the 25 mm diameter disc): after installing the disc in the appropriate cartridge, any remaining non-polymerized components were washed out with 20 ml of methanol. The disc was then rinsed with 40 ml of doubly distilled water and 40 ml of 0.1 *M* sodium phosphate buffer (pH 8.0) containing 0.5 *M* NaCl. The ligand, *e.g.*, heparin, was added in amounts of 50 mg per gram of support. For a 25 mm diameter disc of thickness 2 mm (about 0.5 g of support), 25 mg of heparin in 25 ml of 0.1 *M* sodium phosphate buffer (pH 8.0) (binding buffer) were mixed with 0.5 *M* NaCl and pumped at a flow-rate of 1 ml/min. This solution was left to circulate on the disc for at least 2 h. Subsequently the disc was rinsed with 50 ml of binding buffer. Any remaining free epoxy groups were blocked with 0.2 *M* Tris–HCl buffer (pH 8.0). The disc was then rinsed with phosphate-buffered saline (PBS) (pH 7.4) and stored at 4°C after further use. The immobilization of collagen has been described elsewhere [3].

Other anion-exchange membranes were Mem Sep DEAE (Millipore, Eschborn, Germany), 20 mm in diameter and *ca.* 10 mm thick, Zeta Prep DEAE (Atlanta, Heidelberg), 50 mm in diameter and *ca.* 10 mm thick and Acti Disc DEAE (FMC, Rockland, ME, USA), 40 mm in diameter and 2 mm thick. Membranes from the above producers with different active groups were also used for immobilization of heparin or collagen.

For HPMC experiments with porous discs, a disc cartridge developed in our laboratory was used (see below). For some experiments an Amicon (Danvers, MA, USA) ultrafiltration cell of 40 mm diameter and 50 ml volume was used [4].

For comparison, HPLC columns packed with silica gel or polymer beads were used. These were TSK DEAE 5 PW, 10 μm particle size, 1000 Å pore size, column dimensions 75 × 7.5 mm I.D. (Tosohaas, Yamaguchi, Japan) and Euramid WAEX, 7 μm particle size, 300 Å pore size, column dimensions 60 × 8.0 mm I.D. (Säulentechnik Knauer, Berlin, Germany). Eupergit C30N polymethacrylamide beads, particle size 30 μm, pore size *ca.* 500 Å, with active epoxy groups for ligand immobilization (Röhm Pharma, Weiterstadt, Germany) were used as the support for affinity chromatography. The immobilization of the ligands on Eupergit C30N beads has been described elsewhere [12].

Buffers

The buffers used for anion-exchange HPMC and HPLC were (A) 10 m*M* Tris–HCl (pH 7.6) and (B) was buffer A containing 1 *M* sodium chloride. In some experiments 0.1–0.25% (v/v) of Triton X-100 (reduced) was added to both buffers.

Buffer A for heparin and collagen HPMAC was 5 m*M* Tris–HCl (pH 8.0) and buffer B was buffer A containing 500 m*M* sodium chloride. In some experiments 0.25% (v/v) of Triton X-100 (reduced) or another detergent was added to both buffers.

Sodium dodecyl sulphate–polyacrylamide gel electrophoresis (SDS-PAGE)

The dialysed and freeze-dried samples were dissolved in 62.5 m*M* Tris–HCl buffer (pH 6.8) containing 3% (w/v) of SDS, 5% (v/v) of mercaptoethanol, 10% (v/v) of glycerol and 0.001% (w/v) of bromophenol blue. In other experiments, 10–30 μl of sample were taken from the collected fractions after HPMC or HPLC separation and mixed with buffer containing five times higher concentrations of the above-mentioned substances. The amount of the buffer taken for the experiments was measured in such a way as to yield the original concentration after dilution with the sample. SDS-PAGE was carried out by the Laemmli method [14], using a mini system (Protean; Bio-Rad). The amount of applied protein was between 5 and 20 μg per line.

RESULTS AND DISCUSSION

Construction of the separation unit

Sample distribution is one of the main problems when wide but thin discs are used for separation. Tennikova *et al.* [1] overcame these difficulties by installing the chromatographic unit, that is, the disc, at the bottom of a filtration device. The sample or, during rinsing and elution, the mobile phase, is added and pumped through the porous disc. A disadvantage of this method is the very high dead volume accumulating before the separation unit, the

disc or the membrane. If the sample is applied by an HPLC pump, its dilution through the following mobile phase is inevitable. The use of an Amicon filtration device for concentration of protein solutions avoids these consequences [4]. The chromatographic disc is installed instead of an inert, porous membrane at the bottom of the filtration device. The sample is transported through the porous disc by means of compressed air. The container is subsequently connected with the HPLC pump and filled with buffer A. In the next step the elution buffer is pumped into the container and stirred. This results in a buffer gradient with an exponential slope. A chromatogram obtained through this method, using a DEAE disc, is shown in Fig. 1.

The disadvantage of this method lies in the complicated sample application. When rinsing the disc and during subsequent elution, the container has to be switched from the compressed air pipe to a chromatographic pump. During this procedure it is also difficult to reproduce the gradient. It is therefore advisable to control the salt concentration, *e.g.*, by measuring the osmotic pressure in the collected fractions (see Fig. 1).

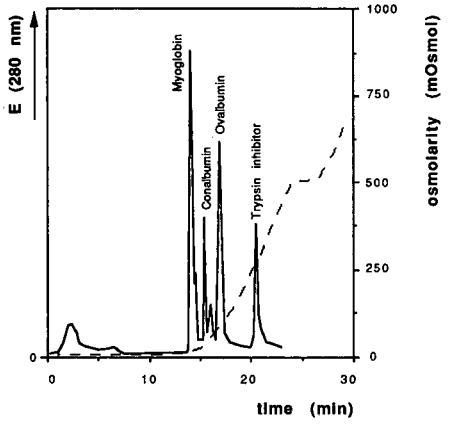

Fig. 1. Anion-exchange HPMC of standard proteins. The chromatographic unit, with a DEAE poly(glycidyl methacrylate) disc was installed at the bottom of an Amicon filtration device. The sample was applied by means of compressed air. The container was subsequently filled with buffer A and proteins were eluted by an exponential salt gradient (see also text and ref. 2). Chromatographic conditions: separation unit, DEAE poly(glycidyl methacrylate) disc, diameter $d = 40$ mm, thickness $h = 2$ mm; buffer A, 10 m*M* Tris–HCl (pH 7.6); buffer B, buffer A containing 1 *M* NaCl; flow-rate 1.5 ml/min; pressure, 1–2 bar; room temperature. The slope of the exponential gradient was controlled by measuring the osmotic pressure (dashed line).

The advantage of this method is that it allows fairly large amounts of diluted sample to be applied. Only one pump is required for gradient elution. Continuous stirring, which takes place before the separation unit, provides good sample distribution, thereby making use of the entire disc surface. This kind of sample application is therefore recommended in preparative chromatography with its large sample volumes. It is also useful in affinity chromatography, where elution is usually carried out by a step gradient. When discs are used for enzyme immobilization, this strategy is the method of choice for the enzymatic conversion of the substrate [4].

Another option for solving the sample distribution problem is the construction of holders with large dead volumes before the separation membrane or disc. Such systems have fairly large capacities. However, their use in high-performance chromatographic separations is limited, as peak broadening is considerable, as shown in Fig. 2. The application of such units for the concentration of certain components in the sample preparation procedure, or for the removal of components, has proved very effective.

With the MemSep cartridges, and partly with the ZetaPrep and FMC systems, the ratio between the width of the disc and its thickness is much more favourable, owing to bundling of single membranes. This eases the problem of sample distribution, but leads to difficulties through leakages. The

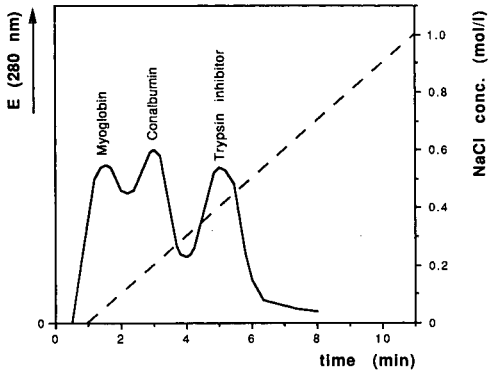

Fig. 2. Anion-exchange HPMC of standard proteins by using the chromatographic disc embedded in a filtration unit. Chromatographic conditions: separation unit, Acti-Disk (FMC), $d = 40$ mm, $h = 2$ mm; separation buffers as in Fig. 1; flow-rate, 5 ml/min; pressure, 1 bar; room temperature. The gradient is shown (dashed line).

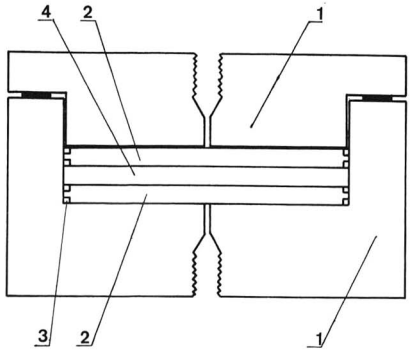

Fig. 3. Construction scheme of the disc cartridge for HPMC. The diameters of the discs used in the experiments were 10, 25 and 50 mm. 1 = Holder; 2 = distribution plates; 3 = O-rings; 4 = disc made of poly(glycidyl methacrylate).

seals have to be installed in such a way that the sample is pumped through the membrane and not through the hollow space between the membrane and the cartridge. After initial difficulties, the problem was solved for MemSep cartridges, for instance, by positioning appropriate seals between single membranes. The problem of inadequate pressure resistance of such discs has not yet been solved satisfactorily. So far the cartridges can only be operated at pressures up to about 10 bar.

When compact discs made of porous, synthetic materials are used, bundling is not so favourable. Polymerization allows the direct production of thicker layers. Leakage problems are easily avoided through O-rings. The construction scheme of the type of disc cartridge used in the experiments is shown in Fig. 3. As mentioned before, the problem of sample distribution is most acute when relatively thin but wide discs are used. Experiments have shown that only a small portion of the disc, usually in its centre, is used for the binding or separation of the sample, when distribution plates are taken, which are in common use for HPLC columns. The jet of liquid coming out of a capillary with a maximum diameter of 1 mm could not be distributed adequately on a surface of 25 mm diameter. Apart from poor distribution, another problem arose. The extreme pressure building up in the centre of the disc shortened the life of the separation device considerably. Therefore, appropriate distribution plates had to be installed before and behind the separation device. The patterns in Fig. 4. give an idea of the construction of the distribution plates.

In Fig. 4 the sample distribution using different types of plates is shown. By using a disc with active epoxy groups, the distribution of a sample could be monitored by injecting a ferritin solution. The protein ferritin with its iron content and reddish colour reacts on reaching the disc with its reactive epoxy groups and is immobilized. This results in an illustration of the distribution pattern of the sample. In all twenty plates were investigated, and only a few typical patterns are shown in Fig. 4. As can be seen, the best distribution is achieved with plate 3. With

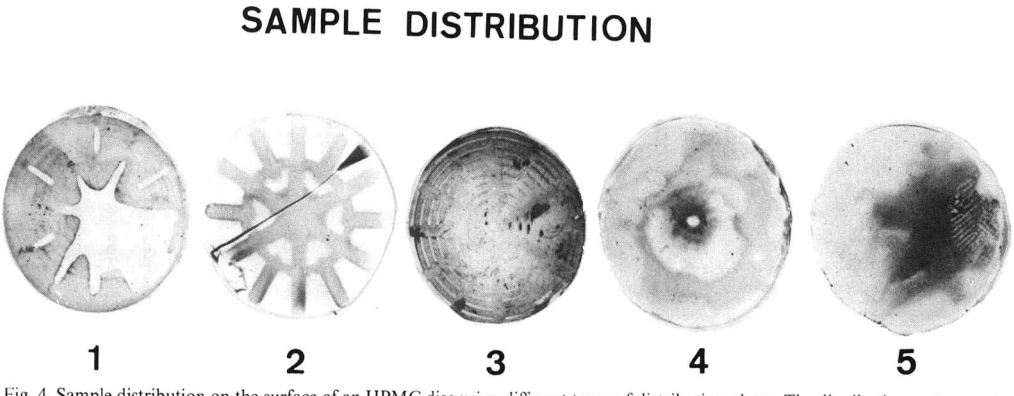

Fig. 4. Sample distribution on the surface of an HPMC disc using different types of distribution plates. The distribution patterns were made by immobilization of ferritin on an epoxy-activated poly(glycidyl methacrylate) disc of 25 mm diameter and 2 mm thickness. For more details see text.

plate 1, for example, only about 60% of the available disc surface was used owing to poor sample distribution. With chromatographic columns, and even with those separation devices which contain bundled membranes, the ratio between layer thickness and diameter is much better. Poor distribution on the surface is compensated for through subsequent spreading in the first few millimetres of the separation layer. Such compensation is impossible when the layer of a disc with a large diameter is very thin, invariably resulting in lower capacity and poor separation. Fig. 5. shows the chromatograms on a DEAE disc of 25 mm diameter and 2 mm thickness. A comparison was made between a separation carried out with an optimized distributor and one carried out without such optimization. Fig. 5 also shows a MemSep disc chromatogram. This disc consists of a large number of bundled membranes. Finally, a chromatogram is shown (Fig. 5D) which was obtained on an HPLC column using the same standard proteins.

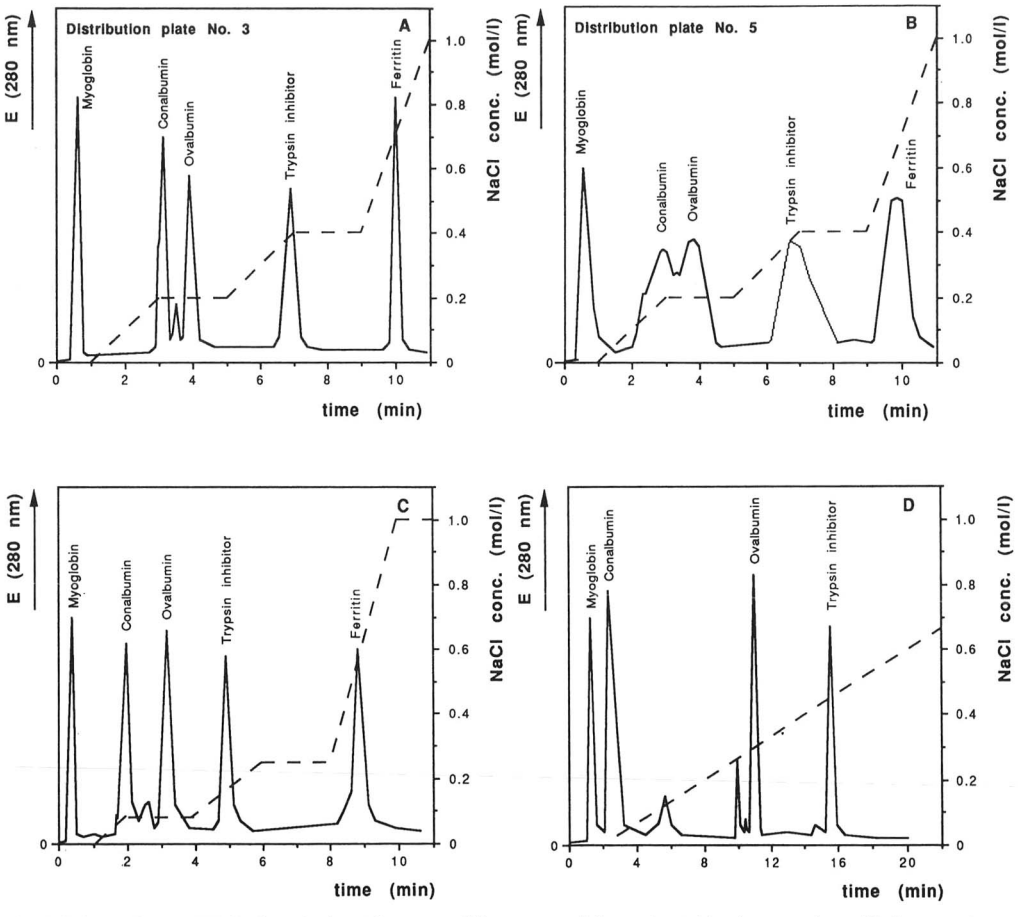

Fig. 5. Anion-exchange HPMC of standard proteins on two different types of discs and cartridges in comparison with the separation on a HPLC column. (A and B) a DEAE poly(glycidyl methacrylate) disc, $d = 25$ mm, $h = 2$ mm, was used, (A) with optimized distribution; (C) separation performed on a MemSep disc consisting of a large number of bundled membranes; (D) separation with a WEAX HPLC column (see also Experimental). Chromatographic conditions: flow-rates on discs, 3 ml/min; pressure, 1–4 bar; the flow-rate on HPLC column, 1 ml/min; pressure, 10–12 bar. Buffers and other conditions as in Figs. 1 and 2.

Optimization of separation

According to investigations by Unarska *et al.* [6], reaction rates in membranes made of nylon fibres are several hundred times faster than those in the corresponding low-pressure columns with agarose beads. In the experiments a system with protein A as ligand and IgG as ligate was used. The much improved reaction kinetics with a disc made of porous poly(glycidyl methacrylate) with the immobilized enzyme carbonic anhydrase also explain the at first puzzling phenomenon of increased enzymatic activity at higher flow-rates [4]. We therefore decided to investigate the influence of the flow-rate on chromatographic separations with poly(glycidyl methacrylate) discs. The results of such an experiment are shown in Fig. 6. It can be seen that a separation of three standard proteins can be achieved within 10 min or less. The optimal flow-rate for discs of 25 mm diameter and 2 mm height is between 3 and 5 ml/min.

In Fig. 7, the influence of disc thickness on separation performance is shown. With increasing thickness better separation is achieved. At present the maximum thickness that is technically possible is 10 mm. However, thicker layers may lead to further improvements in performance, once they can be produced and installed in holders through appropriate technology. Similar results were achieved

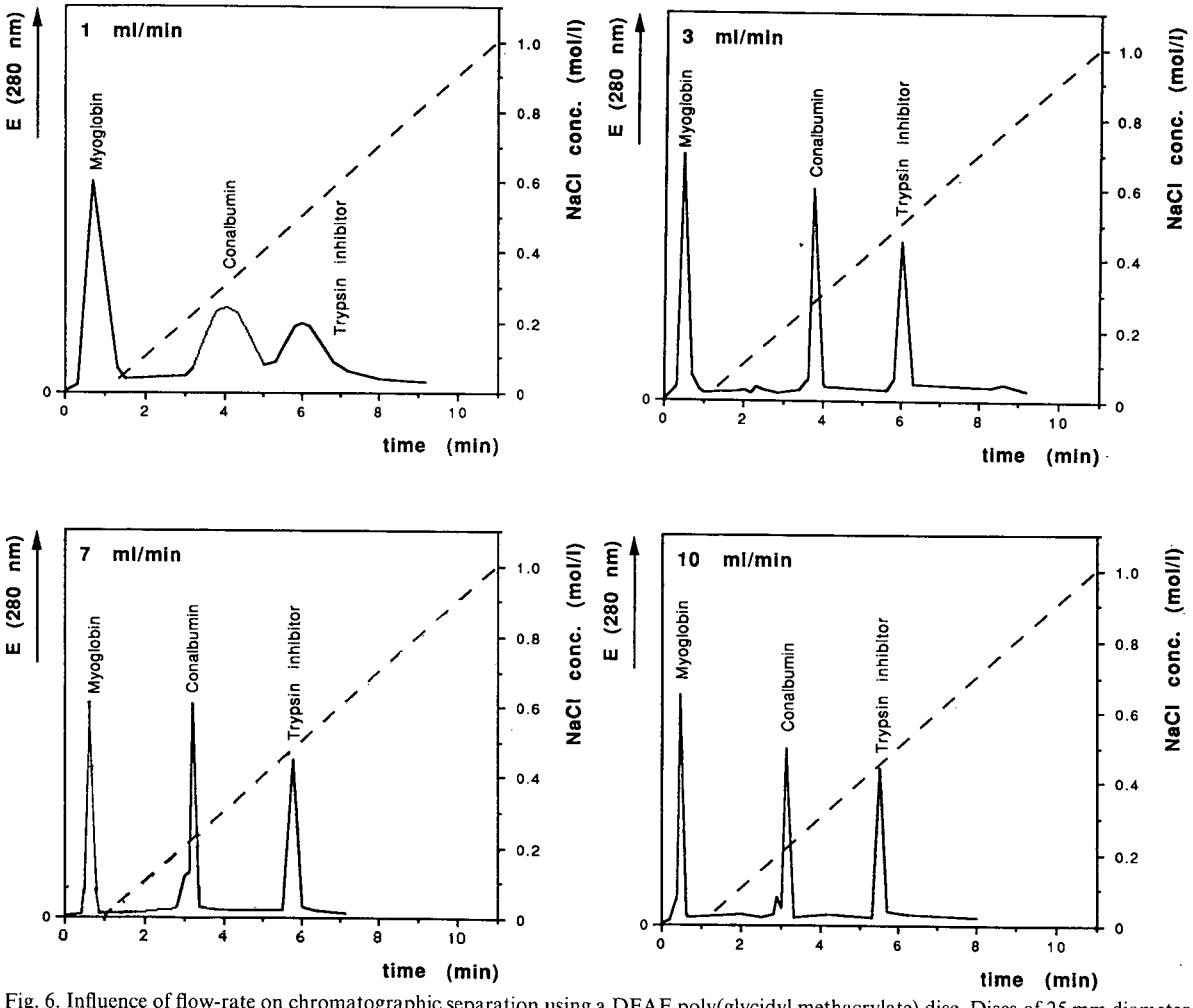

Fig. 6. Influence of flow-rate on chromatographic separation using a DEAE poly(glycidyl methacrylate) disc. Discs of 25 mm diameter and 2 mm thickness were used. Other chromatographic conditions as in Figs. 1 and 2.

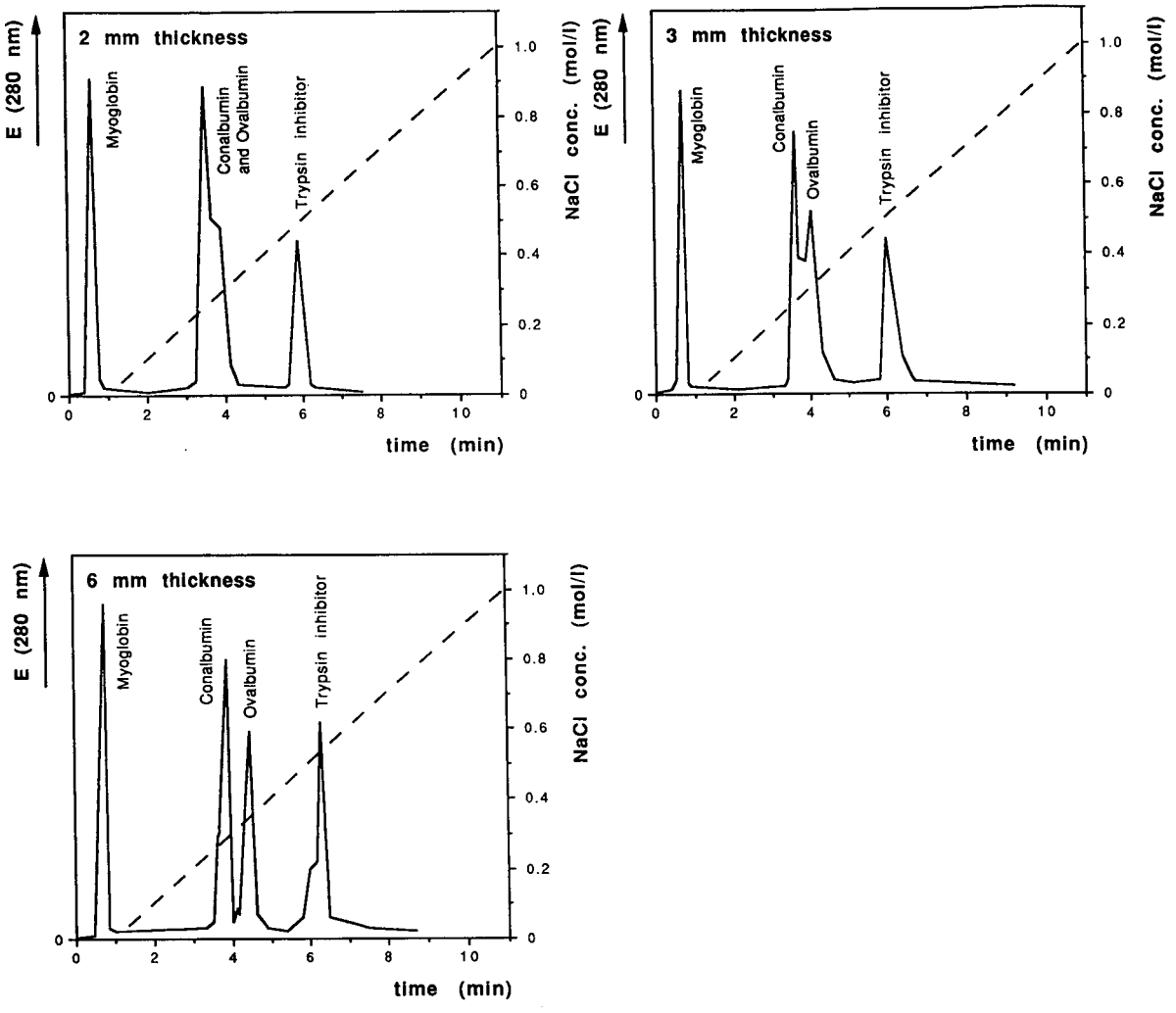

Fig. 7. Influence of disc thickness on separation performance. Several DEAE poly(glycidyl methacrylate) discs of 25 mm diameter but different thicknesses were used. Chromatographic conditions as in Fig. 2.

with discs of 10 mm diameter (not shown here). Apart from the direct production of discs with different thicknesses, higher capacity and improved separation performance can be achieved through the bundling of thin discs. The MemSep and ZetaPrep discs, among others, adopt this approach. However, in these two instances very thin, elastic membranes made of hollow fibres are bundled. When porous poly(glycidyl methacrylate) discs are used instead, the options of bundling are limited. The compact disc is thicker and less flexible than fibre membranes. In such systems it is therefore more difficult to avoid leakages. Only when the disc diameter did not exceed 10 mm, could bundling be carried out without further complications. Separations with such a system are shown in Fig. 8. Here the difficulties can be overcome simply by producing thicker discs, so far up to 10 mm (see above). The results shown here are in some contrast to those obtained by Tennikova *et al.* [1], who did not observe any improvement in the separation performance when the flow-rate was increased or thicker discs were used. They carried out their experiments with discs whose chemical composition was identi-

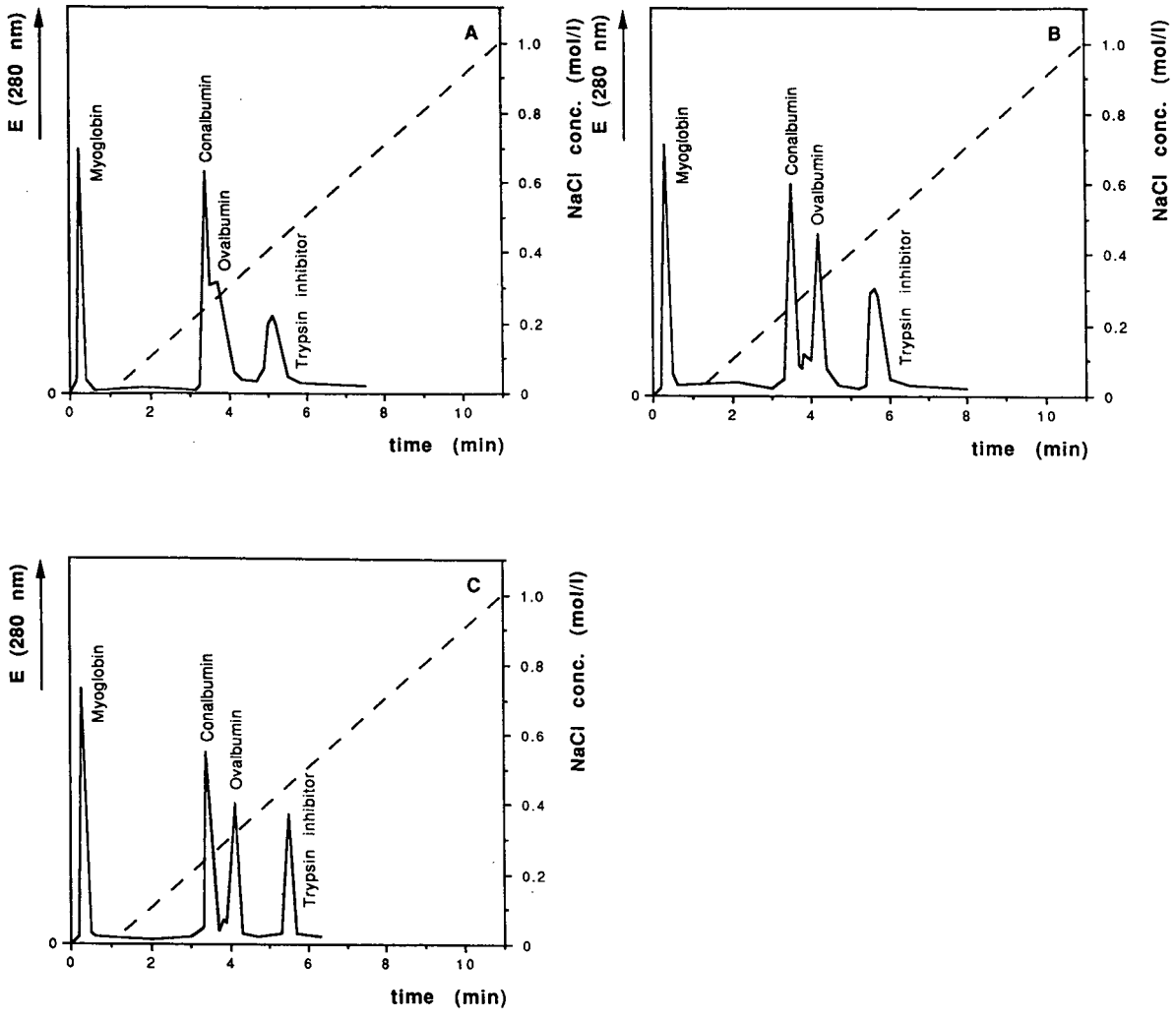

Fig. 8. Influence of disc thickness on separation performance. Comparison between separation with a compact disc and a separation unit constructed of several thin discs piled up. DEAE poly(glycidyl methacrylate) discs of 10 mm diameter were used. (A) Disc thickness 2 mm; (B) three discs were piled up, total thickness 6 mm; (C) separation on a compact disc of 6 mm thickness. Chromatographic conditions as in Fig. 2.

cal with those used here. However, the mechanical structure of their separation device was fundamentally different from the construction of the cartridge shown above.

Influence of detergents on separations

When poly(glycidyl methacrylate) discs are used for the separation of hydrophobic proteins, for their purification and possibly virus inactivation in the sample, it is important to check the influence of detergents on the separation and on the stability of the equipment. We investigated the non-ionic detergents Triton X-100 (reduced), Triton X-114 (reduced), octyl glucoside and decanoyl- and octanoyl-N-methylglucamide (MEGA-10 and MEGA-8), and also the zwitterionic detergent 3-[(3-chloro)dimethylammonio]-1-propane sulphonate (CHAPS) and the anionic detergent SDS.

As the support is strongly hydrophilic, one would expect that the use of non-ionic detergents would

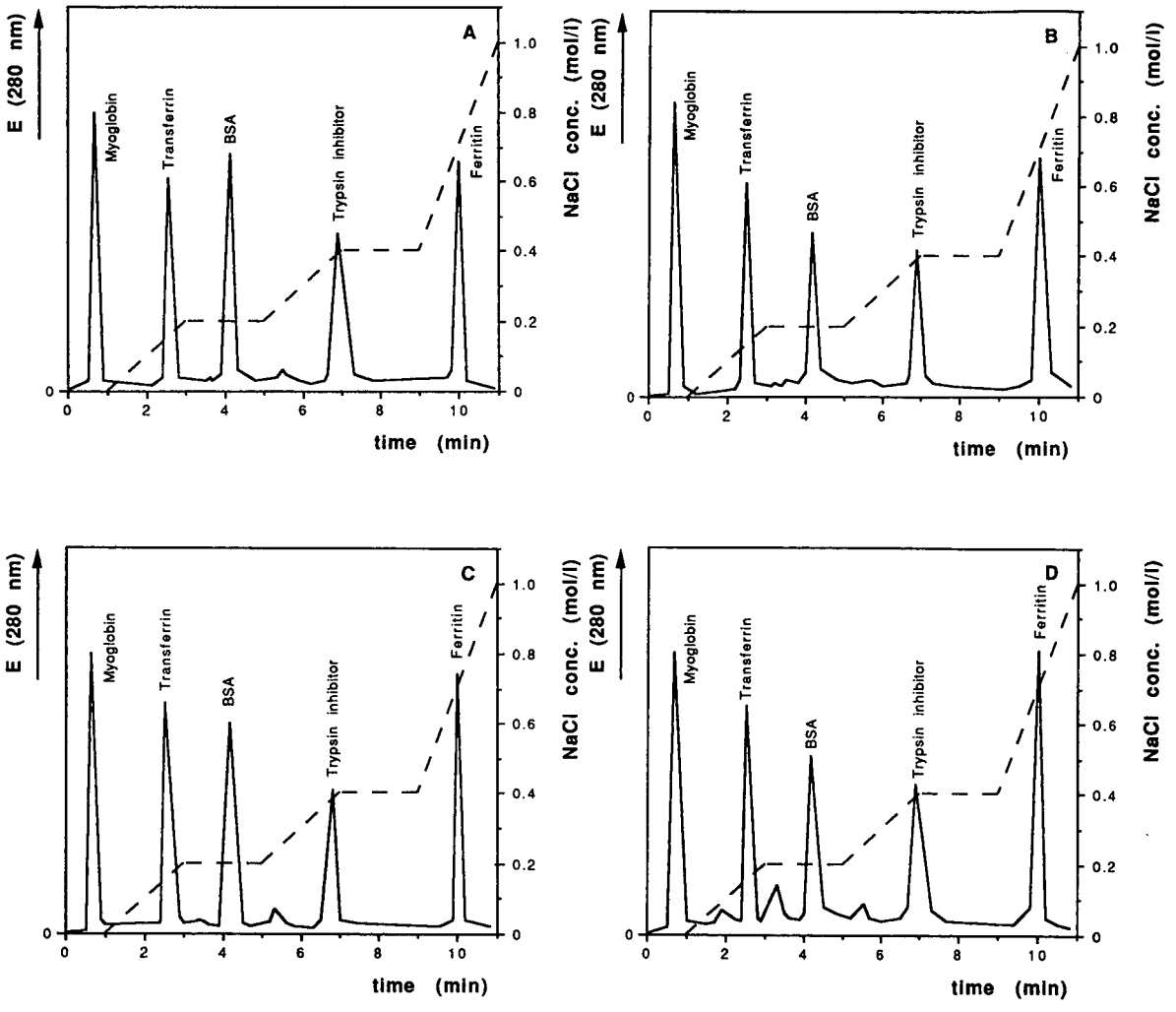

Fig. 9. Influence of non-ionic and zwitterionic detergents on anion-exchange HPMC. Detergents added to both buffers: (A) Triton X-100 (reduced), 0.25% (v/v); (B) octyl glucoside, 0.25% (w/v); (C) CHAPS, 0.25% (w/v). (D) Separation of standard proteins without addition of detergent, after more than 100 runs. In some of the previous runs ionic or non-ionic detergents were used. Chromatographic conditions as in Fig. 2.

have no negative influence on the separation [1,13]. Fig. 9 shows separations of standard proteins without and with detergent, here the non-ionic detergent Triton X-100 (reduced), the non-ionic detergent octyl glucoside and the zwitterionic detergent CHAPS. The separation can be carried out with 0.25% Triton X-100 (reduced). At concentrations of Triton X-100 (reduced) higher than 0.25%, several technical problems arise. For instance, increased amounts of foam impaired optical detection. Also, the solubility of the detergent is poor at high salt concentrations, which can lead to the clouding of buffer B. With the use of Triton X-114 (reduced), the solubility problems in buffer B are even more acute. For example, in affinity chromatography, where the salt concentrations in the buffers are lower and where the separation is monitored by SDS-PAGE instead of optical detection, higher concentrations of Triton detergents can be used [4]. Other detergents, such as octyl glucoside,

MEGA-10 and CHAPS, can be used in higher concentrations, up to about 1%, without adversely affecting the separation. Octyl glucoside was tested up to a concentration of 2%.

Although some detergents were used at concentrations that exceeded their respective critical micelle concentrations, no difficulties were observed in the experiments. With Triton X-100 and especially Triton X-114, high salt concentrations of 1 *M* NaCl in buffer B together with a detergent concentration of 0.25% (v/v) or more, clouding can occur. However, this impaired the optical detection only and left the chromatographic separation unaffected. Consequently, a concentration of about 0.25% (v/v) of Triton X-100 (reduced) and 0.1% (v/v) of Triton X-114 (reduced) have to be considered as the maxima for optical detection. As had to be expected, no separation was achieved when SDS was added. This detergent binds to the proteins and consequently they all have uniform negative charges, so they can no longer be separated through different charges on the molecule surfaces (the chromatogram is not shown). Treatment of the discs with SDS can be essential for removing hydrophobic substances during the purification procedures. The experiments with this detergent were carried out in order to verify the possibility of removing hydrophobic substances and reusing the disc after its purification.

All the detergents, including SDS, could be washed out successfully after application. Separation without detergents was possible even after SDS had been used in previous separations and washed out. Neither the quality of the separation nor the recovery suffered any decline (Fig. 9D). For purification of the discs the use of SDS or the other ionic or non-ionic detergents that we investigated can be recommended. The separation performance is not impaired after rinsing the disc. Before the separation shown in the lower half of Fig. 9 was carried out, different detergents had been applied and washed out several times, using the same disc, namely SDS, Triton X-100 (reduced), octyl glucoside and CHAPS. The disc showed the same separation performance after this treatment and after more than 100 separations.

TABLE I

CAPACITY OF DEAE POLY(GLYCIDYL METHACRYLATE) DISCS FOR BSA IN RELATION TO DISC DIAMETER AND LAYER THICKNESS

Layer thickness (mm)	Diameter (mm)	Capacity (mg BSA)
2	10	4
	25	25
	50	150
4	10	10
	25	60
	50	300

Scaling up

The poly(glycidyl methacrylate) discs used in the experiments had diameters between 10 and 50 mm. The results of separations using DEAE discs with diameters of 10, 25 and 50 mm are shown in Fig. 10. It can be seen that the results obtained with a 10 mm diameter disc can also be achieved with a 50 mm diameter disc. The DEAE disc of 50 mm diameter and 4 mm thickness had a capacity of as much as 300 mg of serum albumin. A further improvement in capacity and separation performance is possible through a larger surface and thicker layers (see Table I and Figs. 7 and 8).

Separation experiments with membrane and serum proteins

In order to test the discs in experiments with biological samples, serum and membrane proteins with different hydrophobic properties were chosen. The separations were carried out in anion-exchange and affinity modes. Apart from separation performance, protein recovery and of enzymatic activity were determined.

Anion-exchange HPMC. Fig. 11 shows the separation of serum proteins by anion-exchange HPMC. A compact disc made of poly(glycidyl methacrylate) and a MemSep disc consisting of several bundled membranes (see above) were used. Although a direct comparison of the separation results is not possible owing to the different geometries of the separation devices [the MemSep disc has a diameter of 20 mm and is 10 mm thick, whereas the poly(glycidyl methacrylate) disc has dimensions of 25 × 2 mm], it can be said that the results are fundamentally the same. With the DEAE poly(glycidyl methacrylate) disc, elution is carried out at

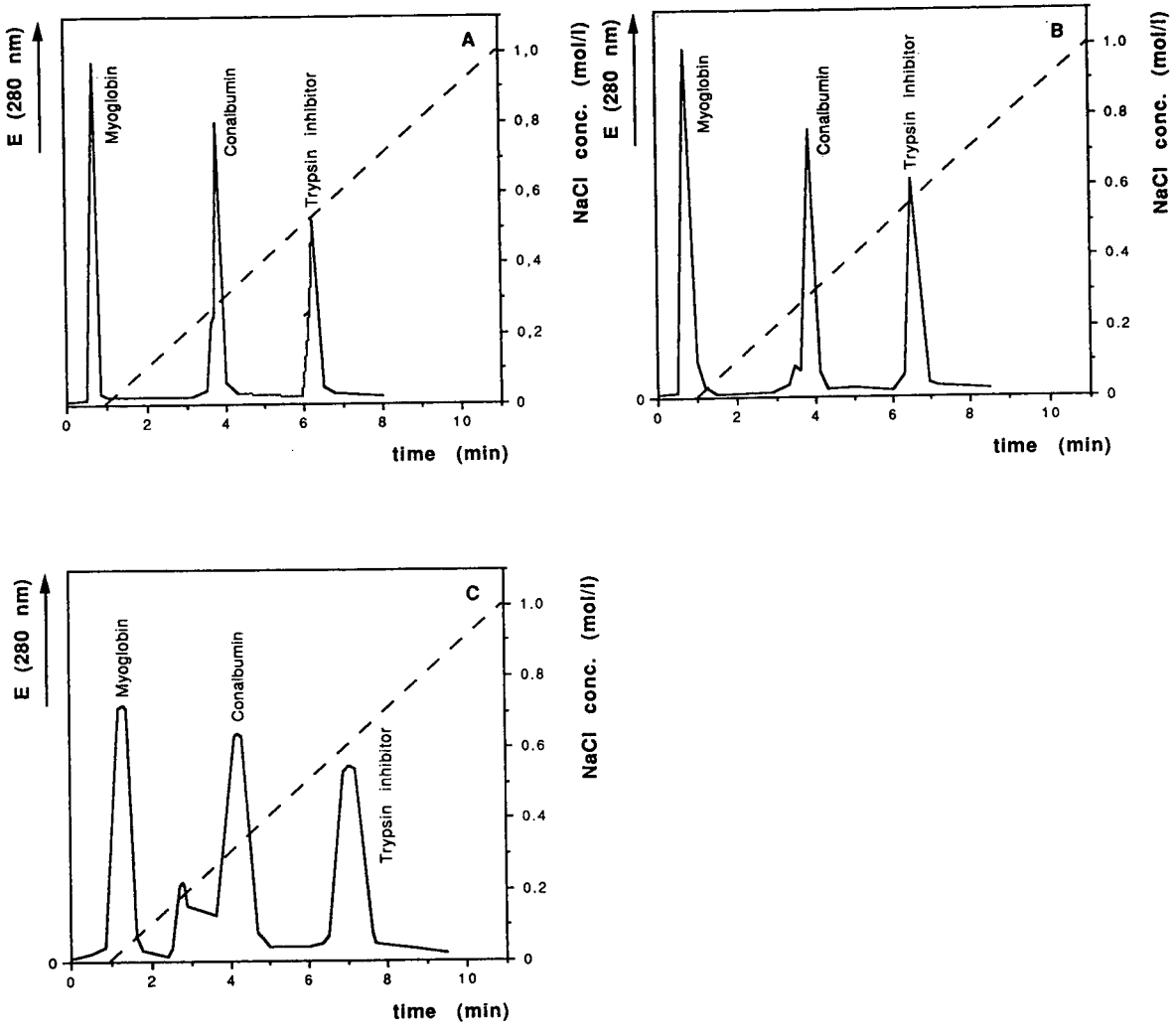

Fig. 10. Scaling-up of separation using DEAE poly(glycidyl methacrylate) discs with diameters between 10 and 50 mm. (A) A disc of diameter 10 mm and 4 mm thickness was used and 200 μg of myoglobin, 300 μg of conalbumin and soybean trypsin inhibitor were applied to the disc. (B) A disc of diameter 25 mm and 4 mm thickness was used and 1 mg of myoglobin, 2 mg of conalbumin and soybean trypsin inhibitor were applied to the disc. (C) A disc of diameter 50 mm and 4 mm thickness was used and 5 mg of myoglobin, 10 mg of conalbumin and soybean trypsin inhibitor were applied to the disc. The pressure on the discs was between 3 and 5 bar; other chromatographic conditions as in Fig. 2.

higher salt concentrations than with the MemSep disc. Consequently, the poly(glycidyl methacrylate) disc can be defined as a stronger anion exchanger than the MemSep disc. Addition of 0.25% of the non-ionic detergent Triton X-100 (reduced) was helpful in the separations with either device (see the lower part of Fig. 11). This agrees with the results obtained in previous separation experiments involving serum proteins, where it was shown that serum albumin, which constitutes a large portion of the proteins contained in the sample, has a strong tendency to aggregate with other serum proteins [15]. This is prevented by Triton X-100, and consequently the contamination of other proteins with serum albumin is much lower when the detergent was added (*cf.*, SDS-PAGE in Fig. 11). The protein recovery was above 85% in all the experiments.

In Fig. 12 the separation of membrane proteins

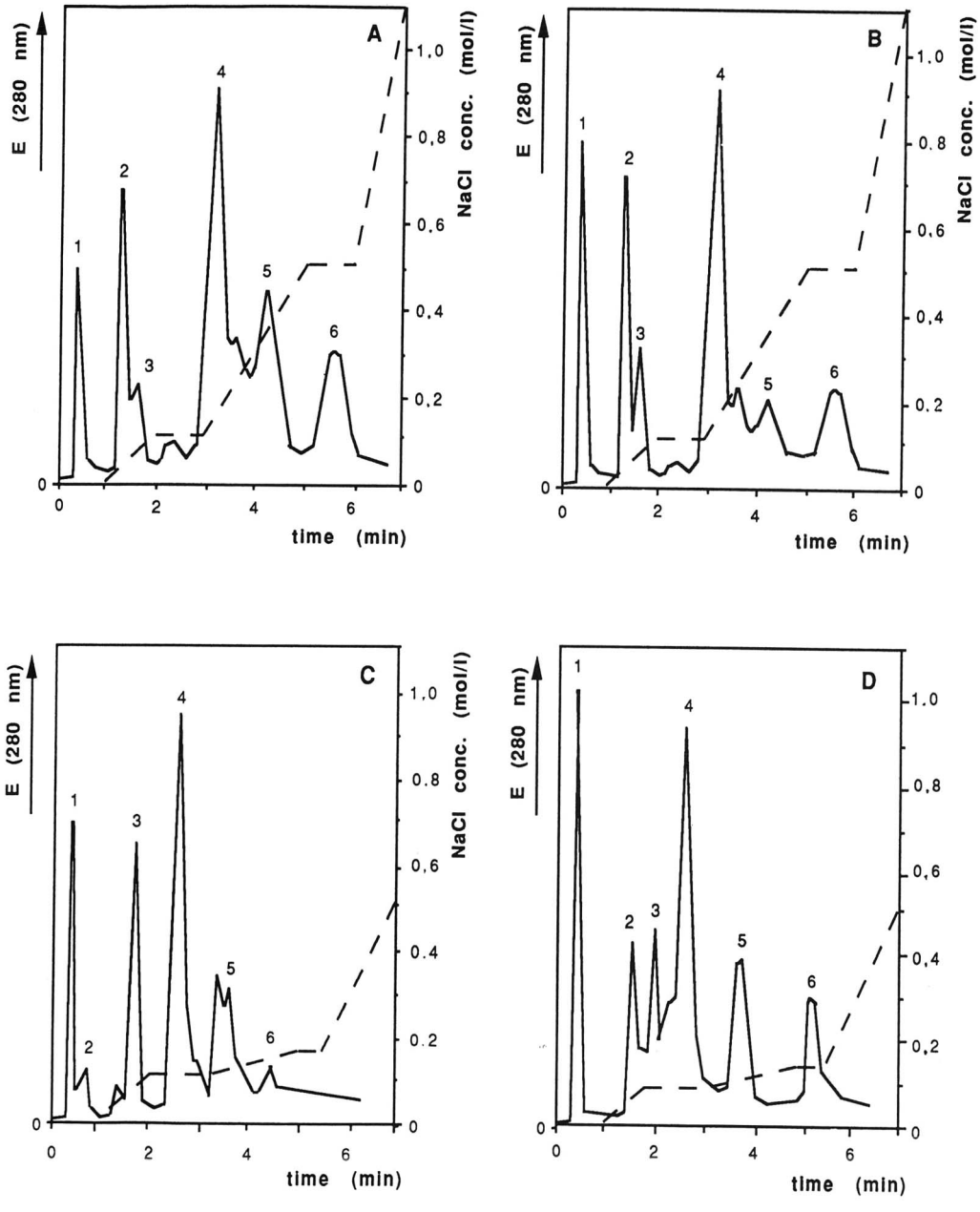

Fig. 11.

(Continued on p. 72)

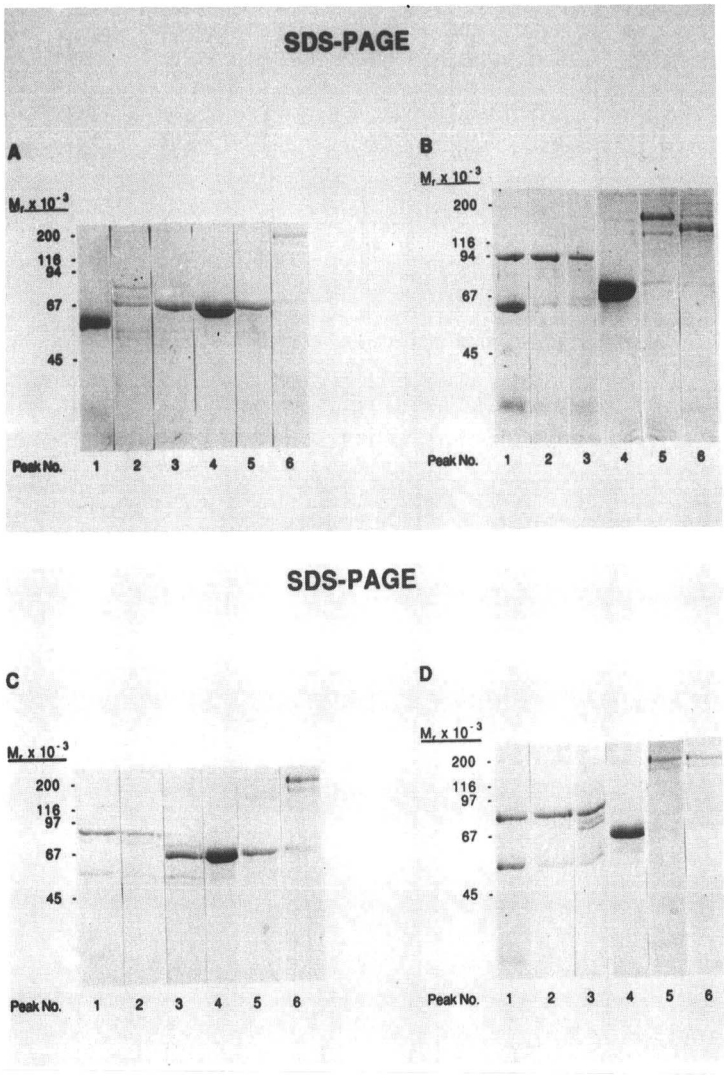

Fig. 11. Separation of rat serum proteins by anion-exchange HPMC. The DEAE poly(glycidyl methacrylate) disc had a diameter of 25 mm and a thickness of 2 mm. The chromatograms are shown on the previous page. The separations were performed (A) in the absence and (B) in the presence of 0.25% (v/v) of the detergent Triton X-100 (reduced). Separations of the same samples on a MemSep disc (C) in the absence and (D) in the presence of 0.25% (v/v) of reduced Triton X-100 (reduced) are also shown. In each experiment 100 μl serum of 8.2 mg of protein were applied. The separations were controlled by SDS-PAGE and the recovery by measuring the protein concentration in collected fractions. The recovery of proteins from the DEAE poly(glycidyl methacrylate) disc was 87% with no detergent and 93% when Triton X-100 (reduced) was used. For separation on the MemSep disc the recovery was 86% without the use of the detergent and 95% when detergent was used. Corresponding SDS-PAGE results are shown, other chromatographic conditions as in Figs. 2 and 5.

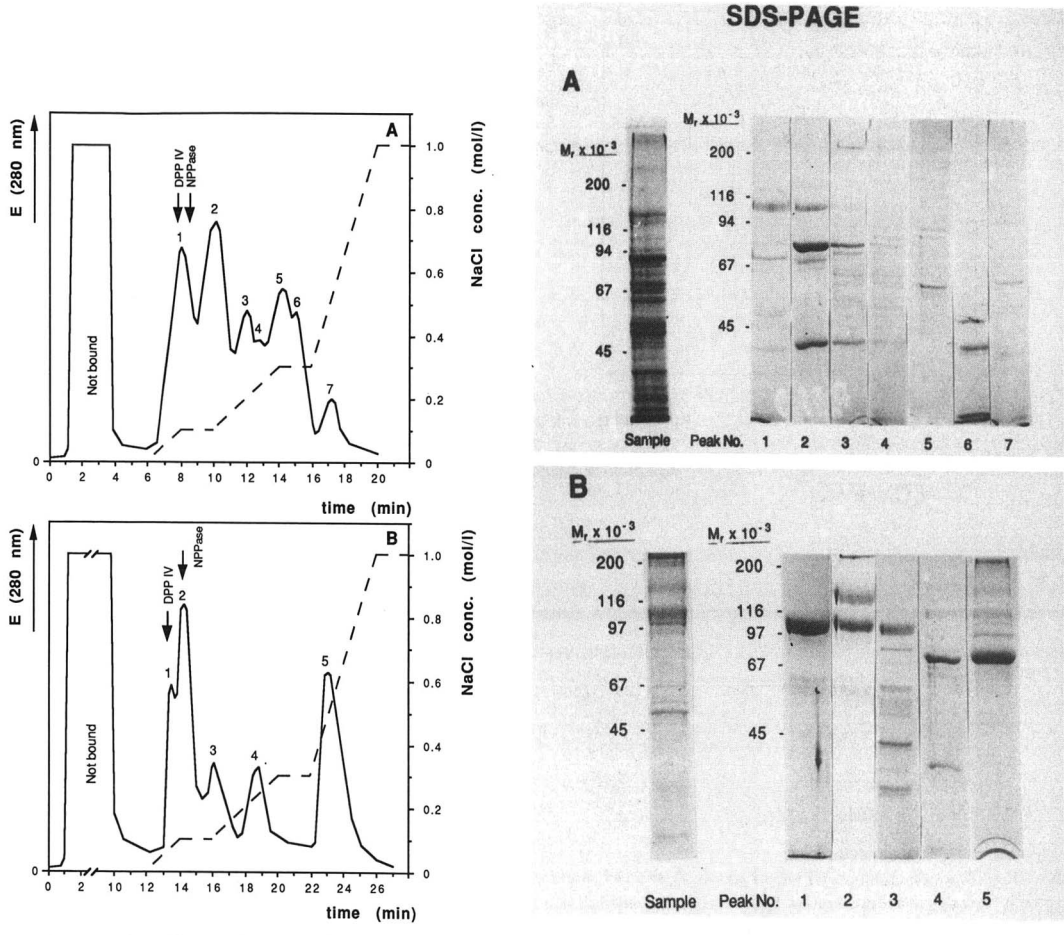

Fig. 12. Separation of kidney plasma membrane proteins with different degrees of hydrophobicity on a DEAE poly(glycidyl methacrylate) disc. (A) Extract after freezing and thawing with less hydrophobic proteins. About 7 mg of protein were used. The recovery of protein was 89% and the recovery of enzymatic activity for DPP IV was 78% and for NPPase 87%. (B) Extract after solubilization of plasma membranes with 1% (v/v) of detergent Triton X-100 (reduced). About 7 mg of protein were used. The recovery of protein was 91% and the recovery of enzymatic activity for DPP IV was 81% and for NPPase 84%. The separations were controlled by SDS-PAGE and the recovery by measuring the protein concentration and enzymatic activity of DPP IV and NPPase in the collected fractions. Corresponding SDS-PAGE results are shown. Chromatographic conditions: DEAE poly(glycidyl methacrylate) disc, 25 mm diameter, 3 mm thickness; buffer A, 10 m*M* Tris–HCl (pH 7.6); buffer B, buffer A containing 1 *M* NaCl; 0.25% (v/v) of Triton X-100 (reduced) was added to both buffers; flow-rate, 3 ml/min; pressure, 1–3 bar; temperature, 0°C (ice cooled); the gradient is shown (dashed lines).

with different degrees of hydrophobicity is shown. The separation, recovery of protein and enzymatic activity were good. The separation of less hydrophobic proteins from the extract of plasma membranes after freezing–thawing [16] required less time when HPMC was used (15 min) instead of an HPLC column (45 min) [17]. Fig. 13 shows the anion-exchange HPMC of the annexin CBP 65/67 on a DEAE poly(glycidyl methacrylate) disc. Until now it was possible to separate this protein by hydroxyapatite HPLC and collagen HPAC and collagen HPMAC. The separation by reversed-phase

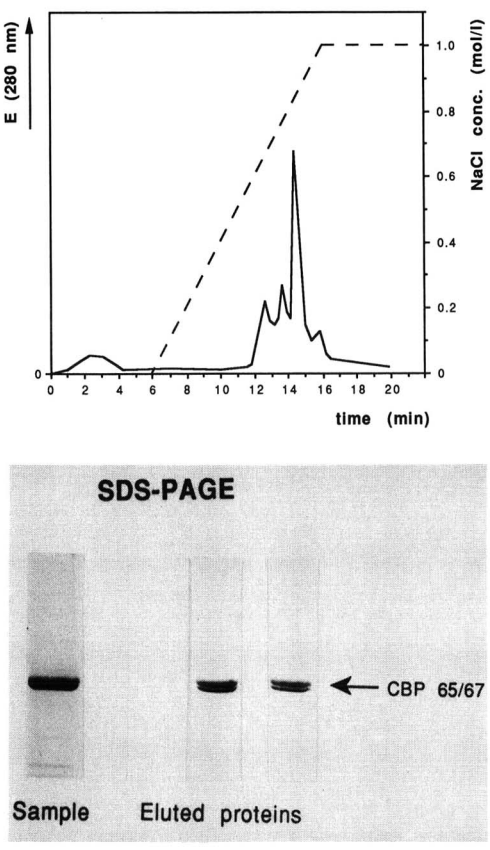

Fig. 13. Anion-exchange HPMC of annexin CBP 65/67 from rat liver plasma membranes on a DEAE poly(glycidyl methacrylate) disc. A 3-mg amount of protein was applied to the disc and 2.85 mg of protein (95%) were recovered by gradient elution. To ensure the solubility of the protein, 1 m*M* EDTA and 0.25% (w/v) of octyl glucoside were added to both buffers. Other chromatographic conditions as in Fig. 12. Eluted proteins in peaks correspond to the bands in SDS-PAGE.

HPLC required the addition of at least 50% formic acid to the eluent. Without formic acid the protein bound irreversibly to the support and could not be recovered [18]. Experiments with anion-exchange HPLC, with both silica gel-based and polymer-based supports, failed and the annexin could not be recovered from the column. The number of different peaks which can be observed in Fig. 13 is probably due to microheterogeneity of this protein [18].

Heparin and collagen HPMAC. In order to investigate the use of the separation devices for the immobilization of high-molecular-weight ligands and their chromatographic separation, heparin and collagen were immobilized on an epoxy-activated poly(glycidyl methacrylate) disc. The separation of very hydrophobic membrane proteins from plasma membranes of Morris hepatoma 7777 by heparin HPMAC is shown in Fig. 14. Although a linear gradient between 0 and 0.5 *M* NaCl was applied, all the bound proteins were eluted as one peak only. This agrees with the results obtained with plasma membrane and serum protein separations on columns with immobilized heparin [12]. Therefore, a mere step gradient is usually adequate in heparin HPAC and HPMAC for the elution of the bound proteins. In the experiment shown in Fig. 14, an important advantage of such discs for the isolation of certain substances from highly dilute solutions is shown. A disc 50 mm in diameter and 4 mm thick was used, and about 200 mg of heparin were immobilized. The membrane proteins are highly hydrophobic and easily aggregate and precipitate, even when 1% of Triton X-100 is added. It is therefore advisable to extract these proteins from dilute solutions. In this experiment 120 mg of protein were dissolved in 500 ml of buffer and applied to the disc at a flow-rate of 10 ml/min. The whole separation process (application of sample and elution) took less than 90 min. The application of 500 ml of sample on a heparin-HPAC column takes 5–10 times longer. Fig. 15 shows the separation of the annexins CBP 65/67, CBP 35 and CBP 33 on a collagen HPMAC disc. The annexins could be separated in a similar manner as on a column, but the separation time in this experiment was 12 min. An HPLC separation with immobilized collagen takes 40 min [18]. Collagen immobilization on a packed column with a support containing active groups is almost impossible and the viscous collagen solution can hardly be pumped through the column. However, the collagen could be applied without difficulty to an epoxy-activated disc because of the low pressure drop. After washing out the non-bound collagen, the pressure on the disc did not exceed 4 bar at a flow-rate of 3 ml/min.

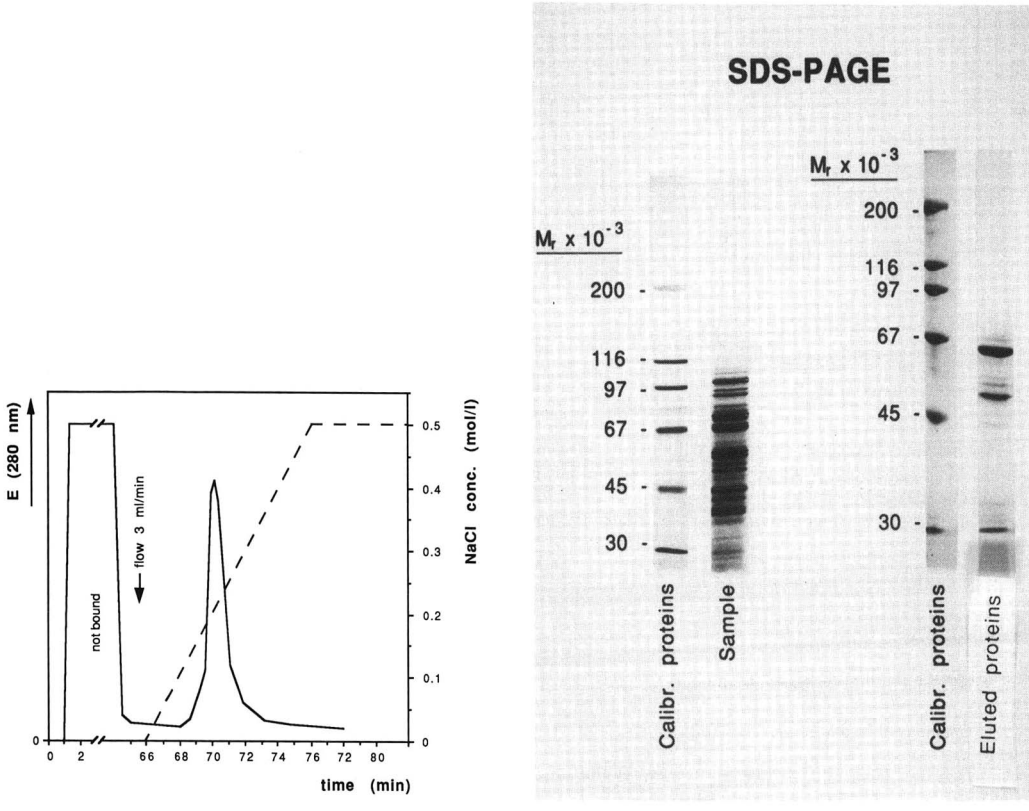

Fig. 14. Separation of hydrophobic proteins from Morris hepatoma 7777 plasma membranes by heparin HPMAC. A sample containing 120 mg of plasma proteins was extracted with 1% Triton X-100 (reduced), diluted to 500 ml with Tris-buffered saline (pH 8.0) and applied to a disc of 50 mm diameter and 4 mm thickness immobilized with 200 mg of heparin. The sample was applied at a flow-rate of 10 ml/min and the elution of bound proteins was performed at a flow-rate of 3 ml/min. An amount of 0.25% (v/v) of Triton X-100 (reduced) was added to both buffers. The pressure was 9 bar during sample application and 2–3 bar during elution. The separation was controlled by SDS-PAGE and the recovery by protein determination in the collected fractions. The recovery of proteins was 84%. The temperature was 0°C (ice cooled). The gradient is shown (broken line).

CONCLUSIONS

After solving the problems concerning sample distribution and cartridge construction, compact discs made of hydrophilic poly(glycidyl methacrylate) polymer yield results at least as good as those obtained with corresponding HPLC columns. When thicker layers are constructed, the use of poly (glycidyl methacrylate) discs does not depend on the bundling of single, thinner components. So far 10 mm thick layers have been produced through polymerization in a compact disc.

In separation systems made of compact discs, the reaction rate is better than in packed columns. Therefore, fast separations are possible at high flow-rates. The low pressure drop in these systems allows the use of low-pressure pumps. The hydrophilic support made of poly(glycidyl methacrylate) is chemically stable and heat resistant, and it can therefore be used at high pH and high temperatures. The use of detergents does not present any difficulties, allowing the separation of hydrophobic sample components. The system can be rinsed in an adequate way after each separation.

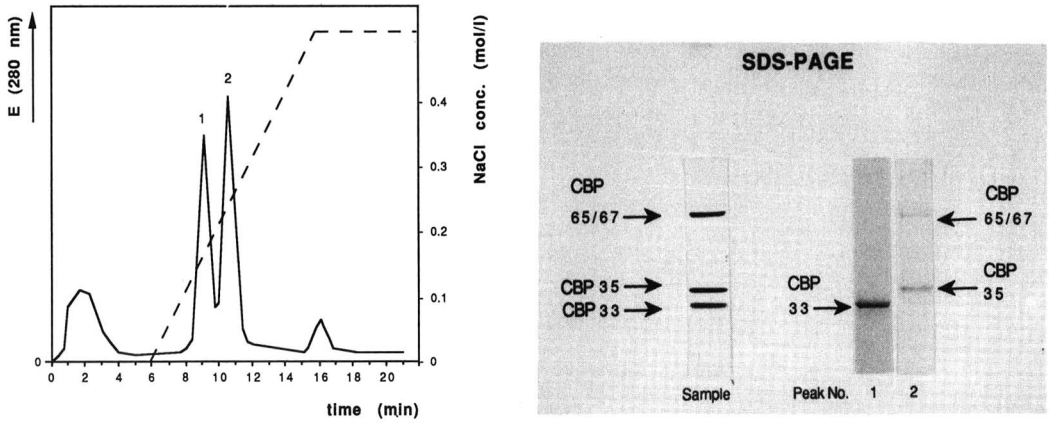

Fig. 15. HPMAC of annexins CBP 65/67, CBP 35 and CBP 33 on a poly(glycidyl methacrylate) disc with immobilized collagen. About 20 mg of collagen were immobilized on an epoxy-activated poly(glycidyl methacrylate) disc of 25 mm diameter and 2 mm thickness. The amount of protein applied to the disc was 4 mg and 3.7 mg of protein (93%) were recovered. SDS-PAGE of the collected fractions (1,2) is shown. Other chromatographic conditions: flow-rate, 2 ml/min; pressure, 2–3 bar; temperature, 0°C. The gradient is shown (dashed line).

REFERENCES

1 T. B. Tennikova, B. G. Belenkii and F. Svec, *J. Liq. Chromatogr.*, 13 (1990) 63.
2 B. Champluvier and M.-R. Kula, *J. Chromatogr.*, 539 (1991) 315.
3 Dj. Josić, K. Zeilinger, Y.-P. Lim, M. Raps, W. Hofman and W. Reutter, *J. Chromatogr.*, 484 (1989) 327.
4 H. Abou-Rebyeh, F. Körber, K. Schubert-Rehberg, J. Reusch and Dj. Josić, *J. Chromatogr.*, 566 (1991) 341.
5 L. J. Cummings, D. L. Hardy and A. Stevens, *Int. Lab.*, 9/10 (1990) 40.
6 M. Unarska, P. A. Davies, M. P. Esnouf and B. J. Bellhouse, *J. Chromatogr.*, 519 (1990) 53.
7 R. Tauber and W. Reutter, *Eur. J. Biochem.*, 83 (1978) 37.
8 D. H. Lowry, N. J. Rosenbrough, A. L. Farrand and R. J. Rendall, *J. Biol. Chem.*, 195 (1951) 265.
9 P. K. Smith, R. I. Krohn, G. T. Hermanson, A. K. Malla, F. H. Gartner, M. D. Provenzano, E. K. Fujimoto, N. M. Goeke, B. J. Olson and D. C. Klenk, *Anal. Biochem.*, 150 (1985) 76.
10 J. Elovson, *J. Biol. Chem.*, 255 (1980) 5807.
11 T. Nagatsu, M. Hino, H. Fuyamada, T. Hayakawa, S. Sakakibara, Y. Nakagawa and T. Takemoto, *Anal. Biochem.*, 74 (1976) 406.
12 Dj. Josić, W. Reutter and D. M. Krämer, *Angew. Makromol. Chemie*, 166/167 (1989) 249.
13 F. Švec, *US Pat.*, 4 923 610 (1990).
14 U. K. Laemmli, *Nature (London)*, 227 (1970) 680.
15 Dj. Josić, W. Reutter and J. Reusch, *J. Chromatogr.*, 476 (1989) 309.
16 Dj. Josić, W. Schütt, R. Neumeier and W. Reutter, *FEBS Lett.*, 185 (1985) 182.
17 Dj. Josić, W. Hofmann, B. Wieland, R. Nuck and W. Reutter, *J. Chromatogr.*, 359 (1986) 315.
18 Y.-P. Lim, *M.D. Thesis*, Freie Universität Berlin, Berlin, 1991.

Journal of Chromatography, 590 (1992) 77–82
Elsevier Science Publishers B.V., Amsterdam

CHROMSYMP. 2409

Utility of small-particle silica in preparative chromatography

J. Timothy Gotsick* and Donald E. Schmidt, Jr.

Rainin Instrument Company, 1780 Fourth Street, Berkeley, CA 94710 (USA)

ABSTRACT

Three columns filled with octadecylsilane-bonded spherical silica were studied to determine their behavior with different sample loads below and in the "overload" region. The stationary phases were as similar as possible, differing only in their particle sizes (8, 5 and 3 μm diameter). Optimum and non-optimum flow-rates, as determined by a plot of plate height *versus* flow-rate, were used with each particle size. Chromatograms were compared using peak width at half-height as a measure of preparative utility, after the method of Perry and Szczerba [*J. Chromatogr.*, 484 (1989) 267]. It was found that the three particle sizes became equivalent in peak width at a given sample load soon after entering the "overload" region. Although the larger particles gave a slightly wider range of linear peak width to sample load response, at no time did the larger particles offer a greater loading capacity than the smaller particles. Until overloaded, the larger particles gave less sample capacity than the smaller particles. The potential benefits of these findings as they influence throughput are discussed, and the terms "laboratory-scale" and "process-scale" preparative high-performance liquid chromatography are defined and discussed in the light of the results.

INTRODUCTION

In preparative high-performance liquid chromatography (HPLC), the desired purity is normally fixed; hence there is a minimum resolution which must be attained for the separation to be worthwhile. Once this needed resolution is attained, one must balance the sample capacity against the speed of the separation to maximize throughput within the limitations of the available hardware. Of course, the resolution is affected by both the speed and sample capacity of the separation, but purity is the one consideration which is set *a priori*, and also the prime factor when evaluating the utility of a separation.

The question of how best to achieve these goals is still subject to debate. In particular, the utility of small particle *versus* large particle stationary phases in preparative-HPLC remains a controversy. One school of thought holds that large (>20 μm) particles will give the most useful preparative separations owing to their low back-pressure, high capacity and low cost [1–3]. Implicit in this approach is the assumption that the separation is independent of the particle size if the column length is variable [4] over a wide range. Recently it has been shown theoretically that smaller particles allow higher production rates [5,6], even under conditions of column overload [7].

A method suggested by Perry and Szczerba [8] of comparing the preparative utility of small and large particle columns may shed more light on the advantages of small particles in preparative-HPLC. This method, termed the "equal-cut-point" approach, compared the peak widths at various loadings on columns of equal length containing C_{18} stationary phases of particle diameter 80, 40, 20 and 10 μm. For columns containing 20-, 40- and 80-μm materials there was a clear advantage for the column containing the smaller particles. Within the range of loadings studied, more sample could be loaded on the smaller particle column given equal peak widths.

Two findings of Perry and Szczerba's study are surprising: (1) although their results indicated a clear superiority for the smaller particle columns in

0021-9673/92/$05.00

the 20–80 μm range, here was no advantage of the 10- over the 20-μm material; no explanation was given for this finding; and (2) whereas theory predicts that peak width should be independent of stationary phase particle size for high (non-linear isotherm) loadings, this effect was not apparent in Perry and Szczerba's findings.

In this study we used the method of Perry and Szczerba to determine whether there is an advantage within packings based on particles of less than 10 μm diameter for use in preparative chromatography. Three 15-cm analytical columns were packed with reversed-phase material based on particles of 3, 5 and 8 μm diameter porous silica and peak widths were determined over a wide range of sample loads.

EXPERIMENTAL

Materials

Spherical silica used in the study was manufactured at Rainin Instrument (Berkeley, CA, USA) by a proprietary process. Physical data for the silicas are given in Table I. Particle sizes were determined using a Brinkmann (Westbury, NY, USA) Model 2010 particle size analyzer. Surface area and pore size were determined using the BET nitrogen sorption method on a Quantachrome (Syosset, NY, USA) Autosorb-1. Bonding of the C_{18} functionality was performed identically for the three silica sizes. Stainless-steel columns (150 × 4.6 mm I.D.) in the Dynamax format were packed using a high-pressure slurry packing apparatus.

Solvents were of HPLC grade from EM Science (Gibbstown, NJ, USA). Chromatography was isocratic and the mobile phase was methanol–water–acetic acid (80:20:1, v/v/v), degassed by sonication prior to use. Methyl salicylate was purchased from Humco Labs. (Texarkana, TX, USA) and used without further purification.

TABLE I

PHYSICAL CHARACTERISTICS OF BASE SILICAS

Nominal particle size (μm)	Actual median particle size (μm)	Surface area (m^2/g)	Pore diameter (Å)
3	4.32	176	120
5	5.66	195	108
8	8.68	175	112

Equipment

Unless indicated otherwise, all equipment was obtained from Rainin Instrument. HPLC was performed using a Rainin HPX pump, a Rheodyne Model 7125 injector and a 20-μl sample loop. A Humonics Optiflow 1000 liquid flow meter was employed to ensure that consistent flow-rates were maintained. A Rainin UV-1 variable-wavelength detector was used in the extended range mode. A cell ratio of 7.5 was employed for extended range measurements. HPLC runs were controlled and data collected by Rainin Method Manager software used on an Apple Macintosh SE computer. A Knauer Model 87 variable-wavelength detector (10 mm flow cell) was used in one set of experiments.

Procedure

To prevent saturation of the extended range of the UV-1 detector, a wavelength (340 nm) was chosen such that the peak at maximum loading remained on-scale. This allowed detection over more than five orders of magnitude concentration range (0.005–140 g/l). The solute was dissolved in the mobile phase at eleven different concentrations, and the samples were run at three flow-rates, 0.4, 0.7 and 1.0 ml/min, on each of the three columns. When peak volume is plotted against sample load beyond overload, the three flow-rates give equivalent peak volumes (data not shown). The peak width in minutes at half-height of each peak was determined using Method Manager data reprocessing software.

RESULTS AND DISCUSSION

Fig. 1. shows the plate height (*H*) *vs.* flow-rate plots obtained for columns packed with the three different particle sizes. The asymmetries on each column were between 1.00 and 1.25 for toluene with methanol–water (65:35) as the mobile phase. The flow-rates for minimum plate height in columns of 4.6 mm I.D. were determined from these data to be 0.4 ml/min for the 8-μm, 0.7 ml/min for the 5-μm and 1.0 ml/min for the 3-μm particle sizes. Table II gives the approximate back-pressure of the three columns at each different flow-rate with methanol–water–acetic acid (80:20:1) as the mobile phase.

Figs. 2–4 depict the peak widths at half-height *versus* the column loads at the three different flow-

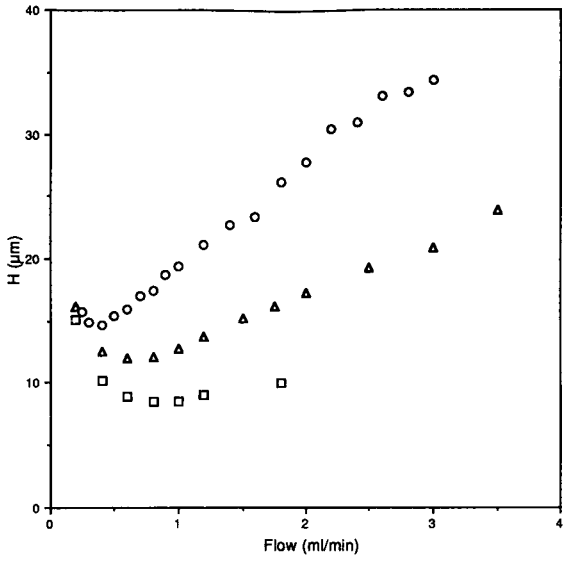

Fig. 1. Plot of plate height (H) *vs.* flow-rate for three particle sizes: ○ = 8; △ = 5; □ = 3 μm. All columns C_{18}, 150 × 4.6 mm I.D.; sample, toluene in methanol–water (65:35); mobile phase, methanol–water (65:35).

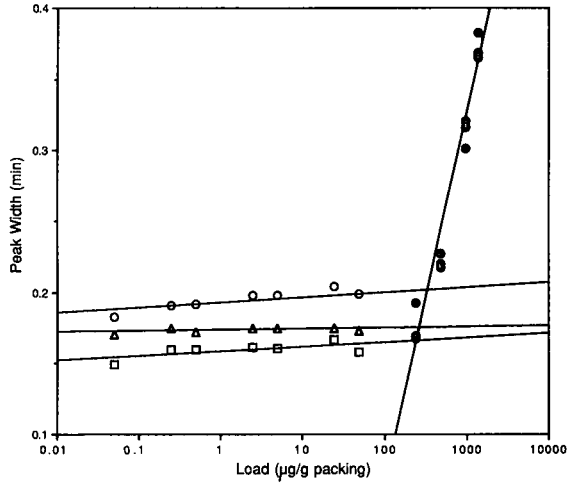

Fig. 2. Plot of peak width at half height *vs.* sample load at 0.4 ml/min flow-rate for three particle sizes: ○ = 8; △ = 5; □ = 3 μm; with (●) 3, 5 and 8 μm overloaded. All columns C_{18}, 150 × 4.6 mm I.D.; sample, methyl salicylate in methanol–water–acetic acid (80:20:1); mobile phase, methanol–water–acetic acid (80:20:1).

rates. The peak widths were determined using the Rainin UV-1 detector in the extended range mode of operation. This detector uses a unique flow cell which has a 9-mm flow path connected in series with a 1-mm flow path. In the analytical mode of operation the absorbance difference between the two flow paths is measured using dual-beam optics. The absorbance difference is equivalent to a flow path length of 8 mm. In the extended range mode of operation, when the absorbance limit is exceeded in the 9-mm flow path, the detector software automatically switches to single-beam operation and monitors the absorbance in the 1-mm flow path. The 1-mm absorbance response is scaled so that it becomes an extension of the 8-mm dual beam response. The result is an extension of the dynamic absorbance range of the detector by a factor of

TABLE II

BACK-PRESSURE FOR 150 × 4.6 mm I.D. C_{18} COLUMNS FOR DIFFERENT FLOW-RATES

Particle size (μm)	Back-pressure (p.s.i.)		
	0.4 ml/min	0.7 ml/min	1.0 ml/min
3	1250	2200	3100
5	650	1100	1600
8	250	450	650

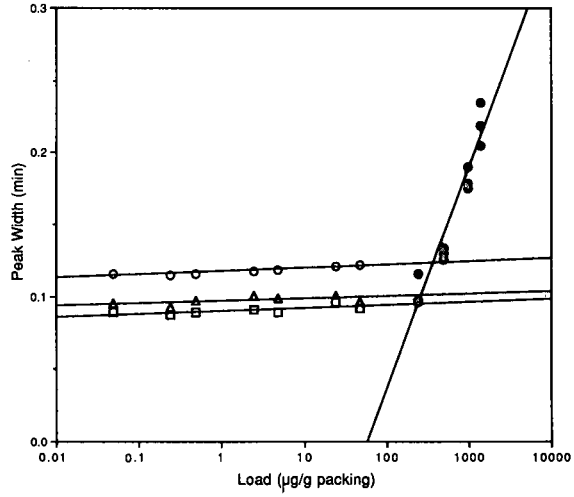

Fig. 3. Plot of peak width at half height *vs.* sample load at 0.7 ml/min flow-rate for three particle sizes: ○ = 8; △ = 5; □ = 3 μm; with (●) 3, 5 and 8 μm overloaded. All columns C_{18}, 150 × 4.6 mm I.D.; sample, methyl salicylate in methanol–water–acetic acid (80:20:1); mobile phase, methanol–water–acetic acid (80:20:1).

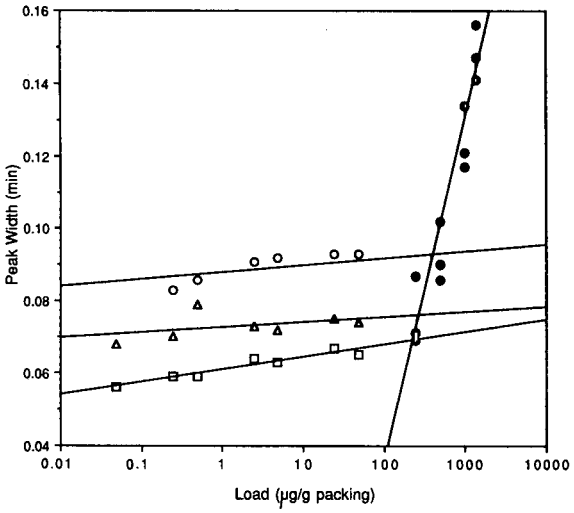

Fig. 4. Plot of peak width at half height *vs.* sample load at 1.0 ml/min flow-rate for three particle sizes: ○ = 8; △ = 5; □ = 3 µm; with (●) 3, 5 and 8 µm overloaded. All columns C_{18}, 150 × 4.6 mm I.D.; sample, methyl salicylate in methanol–water–acetic acid (80:20:1); mobile phase, methanol–water–acetic acid (80:20:1).

eight without having to alter manually the length of the flow cell.

To confirm the accuracy of the extended range mode of operation of the UV-1 instrument, the measurements in Fig. 2 were also determined using a Knauer multi-wavelength detector. Loadings from 0.1 to 50 µg were determined at a wavelength of 250 nm and loadings from 100 to 2800 µg were determined at 350 nm. Both the UV-1 and the Knauer instruments (data not shown) gave similar peak widths.

Note that these graphs are depicted as straight lines, one for each particle size at concentrations below the level where column overload is apparent, and one line which includes the points for all three particle sizes above the concentration at which overload is obvious, as evidenced by an increase in peak width. The use of straight lines to express the data instead of a curve seems justified in the light of the expected high degree of linearity ($r^2 \geqslant 0.94$) exhibited by the data in the pre- and post-overload conditions. Note, however, that the lines are only for visualization purposes, and the data are actually two straight lines with an abrupt joining transition, which is no doubt a curve.

These graphs support the conclusion that the column with larger particles has a wider linear range in which the column is not overloaded [9]. More important, however, is the fact that the smaller particle column gives a narrower peak width for a given sample under many conditions. Only above the sample overload point of the larger particle column do the differing particle size columns become equivalent. Prior to this point, the smaller particle size column gives a narrower peak width than the larger particle size column even though the smaller particle column may be overloaded. This equivalence of differing particle sizes under overload conditions has been noted by other workers [6]. The difference in the onset of overload between columns of two particle sizes is indeed small (of the order of 125 µg per gram of packing between 3 and 8 µm particles), but at no point does the larger particle column give narrower peak widths. This behavior held for all three flow-rates tested.

These experiments support the proposal of Perry and Szczerba [8], in which an "equal cut point" approach is proposed as a more useful means of evaluating particle size with regard to utility in preparative HPLC. Perry and Szczerba's study encompassed larger particle sizes (10–80 µm) than presented here, and they used irregular silica, whereas we evaluated spherical silica. In addition, Perry and Szczerba used an injection solvent stronger than their mobile phase to allow the investigation of extremely high loadings [10]. Other workers [11] have noted the band broadening that can result from this practice. This could add disproportionately to peak width at high sample concentrations.

The need for the use of injection solvents stronger than the mobile phase reveals a problem which many researchers have commented upon, that of solubility. Particularly in reversed-phase chromatography, the sample solubility in the mobile phase may not be high enough to achieve overload. The solute used in our study, methyl salicylate, is infinitely soluble in 100% methanol, but only soluble to *ca.* 150 g/l in methanol–water–acetic acid (80:20:1). In this mobile phase, the capacity factor (k') of methyl salicylate is *ca.* 1.0. If a larger k' is needed, the solubility of the solute would be reduced even further, and mass overload conditions might not be achievable without larger injection volumes. For instance, if the mobile phase were

methanol–water–acetic acid (70:30:1), the sample loop would have to be doubled in size. At a composition of 60:40:1, the sample loop would need to be more than six times larger in order to deliver the same amount of sample. Clearly, this would cause increased band broadening.

In contrast to the system studied by Perry and Szczerba [8], the system studied in this work shows that the peak width does become independent of the particle size at high column loadings. We are unable to explain definitively their results in comparison with ours, but two factors seem likely to have contributed to the difference. First, Perry and Szczerba used an irregular silica which may have had a surface area greater than the 190 m^2/g of the spherical silica tested here. This would probably have caused a difference in the loading at which overload would have been initially apparent. Second, the higher concentrations of dibutyl phthalate (DBP) which Perry and Szczerba loaded utilized 100% methanol instead of the mobile phase as the injection solvent [10]. Solubility problems may well account for the difference in results, as DBP has a significantly lower solubility than the methyl salicylate used here, and a vastly higher solubility in methanol than in the mobile phase used by Perry and Szczerba. Our work only involved loadings at which the sample was soluble in the mobile phase, thus avoiding solubility-induced problems.

Many discussions on preparative HPLC have overlooked the problem of sample solubility, but it is significant nonetheless and, as previously noted, it is especially troublesome in reversed-phase chromatography. Unlike analytical chromatography where the constraints on the mobile phase are limited only to maximizing resolution, preparative chromatography has the added complication of demanding maximum solubility of the sample in the mobile phase. When working under overload conditions, where the peak width is independent of particle size, the larger particle stationary phase would be the most suitable owing to its low back-pressure and consequent high flow-rates. However, when sample solubility makes overload impossible, the use of small particles will allow the use of mobile phases that maximize sample solubility. In reversed-phase chromatography, solubility is normally aided by increasing the proportion of organic solvent in the mobile phase. However, this will cause a decrease in k', which will decrease the resolution if all other factors are held equal. If a smaller particle stationary phase is used, this decrease can be compensated for by the higher plate count which smaller particles normally give:

$$R_s = 0.25N^{1/2}(\alpha - 1)/[k'/(k' + 1)] \quad (1)$$

where R_s is the resolution, N the plate number and α the separation factor. This has the added benefit of decreasing the run time per separation, thereby increasing the throughput. Halving the k' would require squaring the number of plates to maintain the same resolution, so there are practical limits to this approach.

Alternatively, if more than sufficient resolution can be attained at a given k', the flow-rate may be increased. Although a decrease in plate number will occur at any flow-rate greater than the optimum, the throughput will increase. The flexibility that small particle size preparative systems offer has already been utilized by some workers to effect difficult separations [12]. Hardware limitations impose the greatest restriction on the extent to which these techniques can be utilized.

Clearly, the use of small particles in preparative HPLC offers increased throughput under certain conditions. However, the conditions that warrant their use need to be defined more clearly. Although several workers have commented on the different types of preparative HPLC [4,13], there has been no standardized categorization of the conditions under which preparative chromatography is conducted. The needs and resources of industrical "process-scale" chromatography should be distinguished from those of "laboratory-scale" methods.

Process-scale chromatography involves situations where equipment is dedicated to a specific separation and the production rate (throughput/cost) is the dominant consideration. Normally the equipment is large, with columns ranging from 5 cm to hundreds of centimeters in diameter. Often the length of the column is tailored to the desired separation. Process chromatography usually also requires dedicated areas for the equipment and for solvent storage.

This is in contrast to laboratory-scale work, where the length of the column is limited to those which can be purchased, and the range of flow-rates and column diameters is constrained by the limita-

tions of available HPLC pumps. Perry and Szczerba [8] have previously set forth these conditions as those likely to confront the laboratory-scale preparative chromatographer. Usually these systems are not dedicated to a single separation in order to produce a single product but are used to prepare many different samples for other purposes such as spectroscopic analysis or field testing. A lengthy study to determine the ideal column type and solvent system to increase α values and maximize solubility may not be justified. Laboratory-scale work is often done on the standard laboratory bench and probably is limited to columns of 1–5 cm I.D. The versatility which small particles offer to the preparative chromatographer would seem to be most valuable for laboratory-scale preparative work.

There is definitely some overlap between these two types of preparative chromatography and, as hardware capabilities are improved, the division between the two will probably increase to larger column diameters. The availability of more powerful pumps would allow the use of larger diameter columns or standard size columns (25 cm or less in length) with smaller particles on the laboratory scale.

CONCLUSIONS

The use of small particles in laboratory-scale preparative chromatography is seen to be most advantageous on several grounds. A large number of plates makes a separation easier and allows the freedom to manipulate the mobile phase and flow-rate to obtain the highest throughput while guaranteeing purity for all but the most difficult separations. These advantages are most apparent in reversed-phase separations, where small particles give smaller peak widths than would larger particles at almost all loadings. When solubility considerations are also taken into account, it is clear that the use of small particles in laboratory-scale preparative HPLC has benefits that improvements in hardware capabilities will increase.

ACKNOWLEDGEMENTS

We thank Bruce Jones and Miguel Zuliani for obtaining the physical data on the silicas used in this study. We also thank Rainin Instrument for the facilities and time with which to conduct this research.

REFERENCES

1 B. A. Bidlingmeyer (Editor), *Preparative Liquid Chromatography (Journal of Chromatography Library*, Vol. 38), Elsevier, Amsterdam, 1987.
2 L. R. Snyder and G. B. Cox, *J. Chromatogr.*, 483 (1989) 85.
3 A. W. J. De Jong, H. Poppe and J. C. Kraak, *J. Chromatogr.*, 209 (1981) 432.
4 J. H. Knox and H. M. Pyper, *J. Chromatogr.*, 363 (1986) 1.
5 S. Golshan-Shirazi and G. Guichon, *Anal. Chem.*, 61 (1989) 1368.
6 H. Colin, *J. Sep. Sci. Technol.*, 22 (1987) 1851.
7 J. Newburger, L. Liebes, H. Colin and G. Guichon, *J. Sep. Sci. Technol.*, 22 (1987) 1933.
8 J. A. Perry and T. J. Szczerba, *J. Chromatogr.*, 484 (1989) 267.
9 P. D. McDonald and B. A. Bidlingmeyer, in B. A. Bidlingmeyer (Editor), *Preparative Liquid Chromatography (Journal of Chromatography Library*, Vol. 38), Elsevier, Amsterdam, 1987, p. 29.
10 J.A. Perry, 1990, personal communication.
11 H. T. Rasmussen and H. M. McNair, *J. Liq. Chromatogr.*, 13 (1990) 3079.
12 G. Franke and F. Verillon, *J. Chromatogr.*, 450 (1988) 81.
13 M. Verzele and C. Dewaele, *Preparative High Performance Liquid Chromatography: a Practical Guideline*, TEC, Ghent, 1985, pp. 62–74.

Journal of Chromatography, 590 (1992) 83–91
Elsevier Science Publishers B.V., Amsterdam

CHROMSYMP. 2407

Characterization of synthetic macroporous packing materials in low-pressure cartridges and columns

Kenneth W. Talmadge, Lee C. Dunn*, Mohamed Abouelezz, Harvard Morehead, Mohsen Navvab, Cheryl Ordunez, Theodore L. Tisch and Christopher J. Siebert

Bio-Rad Laboratories, Research and Development, Life Science Group, 3300 Regatta Blvd., Richmond, CA 94804 (USA)

ABSTRACT

Three ion-exchange packing materials, Macro-Prep 50 S, Macro-Prep 50 CM and Macro-Prep 50 Q (strong cation, weak cation and strong anion, respectively) were characterized with respect to dynamic protein-binding capacities and chemical stability and resolution following exposure to 0.1 and 1.0 *M* NaOH. The pore-size distribution in the hydrated state was determined by size-exclusion chromatography on a Macro-Prep *t*-Butyl hydrophobic interaction (HIC) sorbent. Isolation of anti-Klenow antibodies from goat serum was performed on a 1-l Macro-Prep 50 S column. Specific anti-Klenow antibodies were affinity purified on a semi-preparative scale using Klenow coupled to an Affi-Prep 10 (NHS activated) sorbent. Recombinant Klenow polymerase from *Escherichia coli* was purified in one chromatographic step on an Econo-Pac heparin 5-ml cartridge.

INTRODUCTION

The introduction of ion-exchange cellulose particles as a column packing material in the 1950s and 1960s was a significant event in the history of protein purification [1,2]. During that period, polysaccharide-based chromatographic packing materials [3] were introduced for use in a broad range of applications, including ion exchange [4]. Over the next three decades, improvements in the physical and chemical properties of ion-exchange sorbents led to the current, highly efficient materials suitable for the high-performance liquid chromatography (HPLC) of biopolymers [5].

Enhanced resolution was accomplished by going to smaller and smaller particle sizes. The use of particles with diameters $\leqslant 10$ μm as packing materials in HPLC required expensive high-pressure equipment, columns and hardware designed to withstand these pressures. These high-performance sorbents were primarily designed for analytical separations and not as sorbents in preparative chromatography. Hence there was a need for new packing materials. Reducing downstream-processing costs and increasing the scale of high-performance separations placed new demands on chromatographic materials. This necessitated a better understanding of the physical and chemical properties of sorbents used in process chromatography.

Pharmaceutical and biotechnology industries need chromatographic materials with sufficient chemical stability to withstand harsh sanitation conditions, good mechanical strength to hold up under the pressures and flow-rates required for large-scale separations, and high dynamic loading capacities, with high recoveries of biological activity. To meet these rigorous standards, a new macroporous methacrylate polymer, Macro-Prep 50 sorbent, was developed for process chromatography. The physical and chemical properties of these macroporous sorbents have been described [6], including pore structure, ionic capacities, static protein binding capacities and chemical and thermal stability. Some of the studies were performed on Econo-Pac cartridges (prepacked devices for low-pressure chromatography). These cartridges are easy to use and come in a convenient size before scale-up to larger preparative columns.

In continuation of this characterization, data are presented in this paper on the size-exclusion proper-

0021-9673/92/$05.00

ties, dynamic protein-binding capacities, chemical stabilities and resolution of Macro-Prep 50 sorbents. To explore the potential of the new Macro-Prep sorbents in biological applications, a Klenow/anti-Klenow antibody system has been studied. Klenow, which is the fragment representing the carboxyl-terminal two-thirds of the DNA polymerase 1 [7], has been cloned and overproduced in *Escherichia coli* [8]. Klenow is an important enzyme in molecular biology, and is used in dideoxy methods for DNA sequencing. The purification of anti-Klenow from goat serum on Macro-Prep 50 S sorbent has been demonstrated [6]. This application is expanded to include (a) preparative isolation of goat antibodies on a 1-l Macro-Prep 50 S column, (b) purification of the specific anti-Klenow antibodies on an Affi-Prep 10–Klenow affinity column and (c) semi-preparative purification of recombinant Klenow, from *E. coli*, using an Econo-Pac heparin cartridge.

EXPERIMENTAL

Materials

Goat serum (Bethyl Labs., Montgomery, TX, USA) was obtained from goats inoculated with Klenow DNA polymerase. Affi-Prep 10, Macro-Prep *t*-Butyl HIC, Macro-Prep 50 S sorbent, Econo-Pac S, CM, Q, and heparin cartridges, Coomassie Brilliant Blue R-250, MAPS binding buffer, protein assay standard I (bovine γ-globulin), protein dye reagent, protein cation and anion HPLC standards, sodium dodecyl sulfate (SDS), dithiothreitol (DTT), Tween 20, horseradish peroxidase-conjugated protein G, Klenow DNA polymerase and TMB substrate (3,3′,5,5′-tetramethylbenzidine) were obtained from Bio-Rad Labs. (Richmond, CA, USA). Bovine serum albumin (BSA), cytochrome *c*, blue dextran, ferritin, human immunoglobulin G (IgG), *Staphylococcus aureus*, thimerosal and thyroglobulin were obtained from Sigma (St. Louis, MO, USA). Ovalbumin was obtained from Calbiochem-Boehring (La Jolla, CA, USA). Glycine, ethanolamine and isopropanol were obtained from Aldrich (Milwaukee, WI, USA). All other chemicals were of analytical-reagent grade.

Chromatography

HPLC was performed with an HRLC Model 800 chromatography system (Bio-Rad Labs.). Low-pressure liquid chromatography was performed with an Econo System, consisting of a Model EP-1 Econo pump, Model EM-1 Econo UV monitor and a Model ES-1 Econo System controller (Bio-Rad Labs.). Fractions were collected with a Model 2110 fraction collector (Bio-Rad Labs.). All buffers were filtered through 0.2-μm membrane filters (Gelman Sciences, Ann Arbor, MI, USA).

Size exclusion

A column (30 × 1 cm I.D.) was packed under gravity with Macro-Prep *t*-Butyl HIC sorbent to a height of 16.7 cm. The column was equilibrated with phosphate-buffered saline (PBS: 20 m*M* phosphate + 140 m*M* NaCl, pH 7.2) and run at a linear velocity of 15.3 cm/h (0.2 ml/min). The calculated column volume was 13.1 ml. *Staphylococcus aureus* was used to determine the interstitial volume, V_o (5.6 ml), potassium chromate was used to determine the volume of solvent in the column, V_t (10.3 ml), and V_e were determined (in duplicate) for blue dextran ($2 \cdot 10^6$ dalton), thyroglobulin (670 000 dalton), ferritin (440 000 dalton), bovine serum albumin (BSA) (68 000 dalton), ovalbumin (44 000 dalton) and cytochrome *c* (12 000 dalton).

Chemical stability of Macro-Prep 50 ion exchangers

The chemical stability of Macro-Prep 50 CM, Q and S sorbents in 5-ml Econo-Pac cartridges was investigated using the following protocol. One hundred gradient cycles were run from 0 to 100% B in 10 min at a flow-rate of 1.0 ml/min on a Model 800 HRLC gradient system, equipped with a Bio-Rad Labs. Model AS-100 autosampler. The buffers used in the gradient cycles were buffer A, 20 m*M* phosphate (pH 6.9), and buffer B, A + 1.0 *M* NaCl. Each gradient cycle was followed by a 35-ml wash with 0.1 *M* NaOH (1.0 ml/min). Protein standards were injected onto the cartridges at the end of the wash cycle and the chromatograms were compared with those obtained for a cartridge not previously exposed to base.

The CM, Q and S sorbents were also tested by washing with 1 *M* NaOH at 1.0 ml/min using a peristaltic pump for periods of up to 72 h. The Econo-Pac cartridges were removed periodically, equilibrated in 25 m*M* phosphate buffer (pH 8.0) and connected to a Model 800 HRLC gradient system, equipped with a Bio-Rad Labs. Model AS-100 au-

tosampler. The protein cation standard was analyzed on the Econo-Pac 50 CM and S sorbents and the protein anion standard on the Q sorbent.

Dynamic protein-binding capacity

Protein samples were loaded onto Macro-Prep 50 sorbents packed in 5.0-ml Econo-Pac cartridges in the indicated buffers at flow-rates of 0.50, 1.0, 5.0 and 10.0 ml/min until the absorbance at 280 nm of the effluent reached 50% of the absorbance of the starting protein solution. The cartridge was washed free from unbound protein, at a flow rate no greater than that used for loading, until the absorbance of the effluent dropped to $\leqslant 2\%$ of the maximum absorbance of the starting protein solution. Bound protein was eluted using the buffers indicated below. BSA (3.0 mg/ml) was bound to the CM sorbent in 20 m*M* sodium acetate (pH 5.0) and eluted with this buffer containing 1.0 *M* NaCl. BSA (3.0 mg/ml) and ferritin (0.1 mg/ml) were bound to the Q sorbent in 50 m*M* Tris (pH 8.3) and eluted with this buffer containing 2.0 *M* NaCl. IgG (0.5 mg/ml) and cytochrome *c* (1.0 mg/ml) were bound to the S sorbent in 20 m*M* sodium acetate (pH 5.0) and eluted with this buffer containing 1.5 *M* NaCl. Protein concentrations were determined from absorbance values measured at 280 nm.

Isolation of the IgG fraction from goat serum

The IgG fraction containing the anti-Klenow antibodies was isolated from goat serum on the Macro-Prep 50 S sorbent packed in a column (23 × 7.5 cm I.D.). After equilibrating the column in buffer A [20 m*M* MOPS (4-morpholinepropanesulfonic acid), pH 6.8)], goat serum (1 l; 122 g of protein) dialyzed against buffer A was applied to the column at a flow-rate of 40 ml/min. Proteins were eluted using a linear salt gradient from 0 to 50% buffer B (buffer A + 1.0 *M* NaCl) in 100 min. Fractions were collected and analyzed for Klenow binding and protein.

Protein assay

Protein assays were generally performed in microtiter plates using the Bio-Rad Labs. protein assay [9]. Calibration graphs were prepared using bovine γ-globulin (standard 1). Typically, wells were filled with 5–40 μl of sample. The total volume in the wells was adjusted to 40 μl with sample buffer and 250 μl of fourfold diluted protein dye concentrate were added to each well. The plates were incubated at room temperature for 10 min and then read at 595 nm using a Model 3550 microplate reader (Bio-Rad Labs.).

SDS-polyacrylamide gel electrophoresis (SDS-PAGE)

Electrophoretic separations were performed under reducing conditions by the method of Laemmli [10] on 7.5% or 12% pre-cast Mini-PROTEAN II ready gels (Bio-Rad Labs.), using the Mini-PROTEAN II cell and a Model 500/200 power supply (Bio-Rad Labs.). Staining was done with Coomassie Brilliant Blue and quantification of the gels was performed using a Model 620 video densitometer (Bio-Rad Labs.).

Enzyme-linked immunosorbent assay (ELISA)

Antibody detection. Determination of specific antibody activity against Klenow was performed by coating wells of microtiter plates (Bio-Rad Labs.) overnight at 4°C with 50 μl of Klenow at a concentration of 1.0 μg/ml in 50 m*M* sodium carbonate buffer (pH 9.6). Plates were washed once with 200 μl of PTT [20 m*M* sodium phosphate (pH 7.2) containing 120 m*M* sodium chloride, 0.05% Tween 20 and 0.01% thimerosal]. Wells were incubated for 2 h at room temperature with PTT containing 0.5% BSA (referred to as PTTB) to block non-specific binding sites on the plates. The plates were then washed once with 200 μl of PTT, blotted dry and sealed with Parafilm before storing at 4°C. Samples were assayed for antibody-binding activity by adding duplicate 50-μl aliquots diluted in PTTB to the Klenow-coated plates for 1–3 h at room temperature. The plates were washed twice with PTT and incubated for 1 h at room temperature with 100 μl of horseradish peroxidase-conjugated protein G diluted 1/10 000 in PTTB. The plates were then washed three times with PTT and the enzyme activity was measured by adding 100 μl of the TMB substrate for 5–10 min at room temperature before stopping the reactions with 100 μl of 0.5 *M* sulfuric acid. The plates were read at 450 nm using a Model 3550 microplate reader.

Klenow detection. For the detection of Klenow, plates were coated overnight at 4°C with 50 μl of goat anti-Klenow antibodies at a concentration of

46 μg/ml in 50 m*M* sodium carbonate buffer (pH 9.6). The incubations and wash steps were similar to those described above for the antibody ELISA, except that the enzyme conjugate used was horseradish peroxidase conjugated to the goat anti-Klenow antibody. The conjugate was prepared according to the procedure of Wilson and Nakane [11].

Coupling of Klenow to Affi-Prep 10

Affi-Prep 10 is a N-hydroxysuccinimide (NHS)-activated macroporous polymeric sorbent [12] used for the covalent coupling of proteins via their free amino groups. Affi-Prep 10 (12 ml of a 50% suspension in isopropanol) was transferred to a 15-ml coarse sintered-glass funnel and rapidly washed with three 5-ml aliquots of cold deionized water, acidified with acetic acid to pH 4. Immediately following these washes, 4.0 ml (2.17 mg/ml) of purified Klenow (Bio-Rad Labs.) in 100 m*M* sodium carbonate (pH 8.3) were added carefully to the top of the 6-ml sorbent bed and allowed to drain through the bed over a 6-min period. The sorbent was washed with 8.0 ml of 100 m*M* sodium carbonate (pH 8.3) and the effluent collected and saved for protein assay. The sorbent was then washed with 8 ml of 1.0 *M* ethanolamine (pH 8.5) to block any unreacted NHS sites, and washed with 15 ml of deionized water, 15 ml of MAPS binding buffer, pH 9.0 (Bio-Rad Labs.), 15 ml of deionized water, 15 ml of 100 m*M* glycine (pH 2.5) and 15 ml of PBS. A total of 4.2 mg of Klenow was coupled to 5.9 ml of Affi-Prep 10, as determined by the difference between the total protein added and the unbound protein.

Affinity purification of anti-Klenow antibody

The IgG fraction from the Macro-Prep 50 S column (Fig. 3) containing anti-Klenow antibodies was dialyzed against PBS. An aliquot (4.0 ml) containing 36 mg of protein was injected onto 5.9 ml of Affi-Prep 10–Klenow affinity sorbent (7.5 × 1.0 cm I.D.) equilibrated in PBS and recycled over this column for at least 2 h at 0.5 ml/min. The column was then washed with PBS until the absorbance at 280 nm of the effluent was ≤ 0.05. The bound anti-Klenow antibody (4.2 mg) was eluted from the affinity sorbent at 0.5 ml/min using 100 m*M* glycine (pH 2.5). Immediately after elution, the pH of the antibody fraction was adjusted between 6 and 8 with 1.0 *M* Tris base (pH 10.6) and the sample was dialyzed against PBS.

Isolation of recombinant Klenow from E. coli

Recombinant Klenow was obtained from *E. coli* cells. The first steps of the purification were similar to those described by Joyce and Grindley [8]. Lysed cells were centrifuged at 10 000 *g* and the supernatant was treated with polyethyleneimine (0.2%) and sodium chloride (0.2 *M*) to precipitate nucleic acids and some proteins. The supernatant was adjusted to 60% ammonium sulfate, centrifuged and the supernatant dialyzed against 10 m*M* potassium phosphate (pH 7.0) containing 1 m*M* DTT. The Klenow was then purified on an Econo-Pac heparin 5-ml cartridge, which was equilibrated with buffer A [10 m*M* potassium phosphate (pH 7.0) + 1 m*M* DTT]. Samples of the supernatant were loaded onto the cartridge at a flow-rate of 2.0 ml/min. After washing with buffer A to remove unbound proteins, Klenow was eluted from the cartridge using a 30-min linear salt gradient from 0 to 100% B (A + 0.5 *M* NaCl). Fractions were assayed for protein and binding to anti-Klenow antibodies by ELISA.

RESULTS AND DISCUSSION

Physical properties and stability

In protein separations on macroporous sorbents, two important geometric parameters to consider are the mean pore size and pore-size distribution. These physical characteristics determine the accessibility of the internal pore surface of the bead to proteins. The surface and pore structure of the Macro-Prep beads have been characterized by mercury intrusion porosimetry [6]. These beads have a mean particle size of 50 μm, surface area 18–22 m^2/g, pore size 1200 Å and pore volume ≥ 0.5 ml/g. A unique feature of these sorbents is that most of the pore volume is found between 1000 and 1500 Å [6].

One of the limitations of mercury intrusion porosimetry is that the analysis must be done on a dry powder. As chromatography is done on a hydrated bead, the porosimetry results may not accurately reflect the microenvironment of the beads. To obtain a pore-size profile of the hydrated beads, size-exclusion chromatography [13] was performed on a Macro-Prep *t*-Butyl HIC packing material in PBS.

As this experiment was done under low salt conditions (140 m*M* NaCl), hydrophobic interaction effects, which are maximized at high salt concentrations, should be minimal. Hence, the relative elution order should not be influenced by the HIC functionality.

The average distribution coefficients, K_{ave}, can be calculated from $K_{ave} = (V_e - V_o)/(V_t - V_o)$, where V_o is the interstitial volume, V_t is the total volume of solvent in the column and V_e is the elution volume of the protein sample. *Staphylococcus aureus* was used to determine the interstitial volume (estimated molecular weight *ca.* 10^9 dalton). The volume of solvent within the sorbent is given by $V_i = V_t - V_o$. From these calculations, the working volume of the Macro-Prep sorbents is 36%. The plot of K_{ave} *versus* log (molecular weight) for a number of proteins is shown in Fig. 1. If the mid-point between blue dextran (10^6 dalton) and thyroglobulin ($6.7 \cdot 10^5$ dalton) represents the mean exclusion limit for the Macro-Prep sorbent, then proteins up to 10^6 dalton should be able to penetrate the pores. From the mercury porosimetry data, a mean pore size of 1200 Å was calculated for the Macro-Prep sorbent [6]. These experimental data are consistent with the prediction made by Vanecek and Regnier [14] that a 1000 Å pore should allow free access to proteins $> 10^5$ dalton. In addition, Unger *et al.* [15] predicted that the pore diameter must be at least five times the protein diameter to permit access of the protein to the internal surface. In order for thyroglobulin, which has a diameter of 172 Å [16], to permeate the sorbent, the minimum pore size must be 860 Å. Hence the size-exclusion data presented here are consistent with the earlier reported porosimetry results [6].

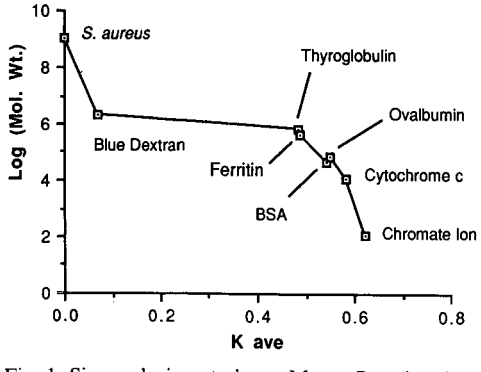

Fig. 1. Size-exclusion study on Macro-Prep butyl HIC sorbent packed in a Bio-Rex MP column (16.7 × 1.0 cm I.D.).

Mechanical strength is an important prerequisite for any cost-effective chromatographic matrix for downstream processing in the biotechnology industry. Mechanical strength of the Macro-Prep sorbents in aqueous solutions has been demonstrated by measuring back-pressures at increasing flow-rates. The maximum linear velocity that could be reached is 3800 cm/h for the CM, 5700 cm/h for the Q and 4560 cm/h for the S sorbents [6].

As reported previously [6], no changes in performance of Macro-Prep ion-exchange sorbent were observed during 100 gradient cycles in 10 × 1.0 cm I.D. columns. In addition, there was little or no decrease in ionic or protein binding capacity after prolonged treatment with acid, base or detergents. Stability to NaOH is particularly important because this reagent is commonly used to sanitize chromatographic materials. With this in mind, column lifetime and stability studies were performed by subjecting the Macro-Prep 50 CM, Q and S sorbents in Econo-Pac 5-ml cartridges to 100 gradient cycles, with each cycle containing a 35-min wash with 0.1 *M* NaOH at 1.0 ml/min. Protein standards were injected onto the columns every tenth cycle to evaluate performance parameters. For each of the three ion-exchange sorbents very similar profiles were obtained (data not shown), demonstrating the lifetime stability of these sorbents. To take this investigation one step further, the chemical stability was examined by comparing the separation of protein mixtures in 5-ml cartridges before and after exposure to 1.0 *M* NaOH. After 4, 24, 48 and 72 h, the sorbents were washed free of NaOH, equilibrated in buffer, and protein standards were injected to evaluate performance. Retention times and symmetry (B/A at 10% peak height) of the protein peaks for the initial injection and after 4, 48 or 72 h exposure were used to measure column performance. The results are shown in Table I. The symmetry factor, B/A, is used to measure peak fronting or tailing and is one criterion used to determine packing efficiency [13].

The values for the CM and S sorbents remained unchanged after 72 h of exposure. The Macro-Prep 50 Q sorbent underwent noticeable changes in retention time after 4 h, and these changes became even more pronounced after 48 h of exposure.

TABLE I

STABILITY OF MACRO-PREP 50 CM, Q AND S SORBENTS IN ECONO-PAC CARTRIDGES IN 1 *M* NaOH

Macro-Prep 50 CM, Q and S sorbents packed in Econo-Pac 5-ml cartridges were washed with 1.0 *M* NaOH. The indicated protein standards were injected before and after exposure for up to 72 h. as described under Experimental. The results are expressed as retention times (RT) and peak symmetry (Sym) (*B* and *A* are measured from the apex perpendicular to the curve at 10% above the baseline).

Protein	Time (h)	CM		Q		S	
		RT (min)	Sym (*B*/*A*)	RT (min)	Sym (*B*/*A*)	RT (min)	Sym (*B*/*A*)
Myoglobin	0	3.9	1.29	5.6	1.09	4.2	1.58
	4	–	–	5.3	1.02	–	–
	48	3.9	1.32	4.8	1.19	4.1	1.02
	72	3.9	1.31	–	–	4.3	0.86
Ribonuclease A	0	7.5	0.64	–	–	6.5	0.70
	3	7.4	0.57	–	–	6.5	0.52
	48	7.4	0.57			6.7	0.47
Cytochrome *c*	0	8.9	1.90	–	–	7.6	2.92
	48	8.7	2.22	–	–	7.5	3.40
	72	8.7	2.25			7.6	3.83
Conalbumin	0	–	–	8.2	0.93	–	–
	4	–	–	7.7	0.89	–	–
	48	–	–	7.4	1.07	–	–
Ovalbumin	0	–	–	10.7	1.11	–	–
	4	–	–	10.2	1.20	–	–
	48	–	–	9.6	1.13	–	
Trypsin inhibitor	0	–	–	15.2	1.21	–	–
	4	–	–	15.0	0.44	–	–
	48	–	–	14.1	1.05	–	

However, the data in Table I indicate that no significant decrease in resolution of the proteins on the Macro-Prep Q sorbent occurred with the decrease in retention time. The symmetry value of 0.44 for trypsin inhibitor cannot be readily explained, as the symmetry value increases to 1.05 after 48 h. The results of the chemical stability studies indicate that the Macro-Prep CM and S sorbents can be sanitized with 1.0 *M* NaOH and the Q sorbent can be safely sanitized with 0.1 *M* NaOH.

Dynamic protein-binding capacity

Static binding capacities of the three Macro-Prep ion-exchange sorbents have been reported [6]. A more meaningful measure of a packing material's performance is the dynamic binding capacity, which measures the capacity of a sorbent to bind proteins under solvent flow conditions. Dynamic protein-binding capacities of ion-exchange sorbents (Fig. 2) in 5-ml Econo-Pac cartridges were measured at flow-rates of 0.5, 1.0, 5.0 and 10.0 ml/min. When the flow-rate was increased from 0.5 to 10.0 ml/min, the BSA-binding capacity decreased by 29% for the CM sorbent. For the Q sorbent, the BSA binding decreased by 9.4% and the ferritin binding capacity decreased by 42%. For the S sorbent, the IgG capacity decreased by 55%, whereas the cytochrome *c* capacity increased slightly but was within experimental error. For the CM, Q and S ion-exchange sorbents, the protein-binding capacities of smaller proteins, such as cytochrome *c* (12 000 dalton) and BSA (68 000 dalton), were essentially unaffected by flow-rates as high as 10.0 ml/min. However, the binding capacities for larger proteins such as IgG (150 000 dalton) and ferritin (440 000 dalton) were substantially reduced as the flow-rate was increased.

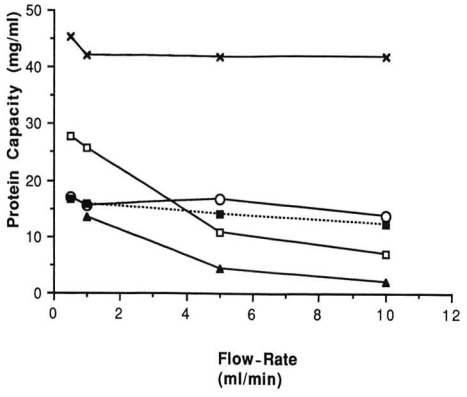

Fig. 2. Dynamic protein binding capacities of Macro-Prep 50 CM, Q and S sorbents *versus* flow-rate. The binding of BSA (■) to the Macro-Prep 50 CM sorbent, BSA (○) and ferritin (▲) to the Macro-Prep Q sorbent and cytochrome *c* (×) and IgG (□) to the Macro-Prep 50 S sorbent, were carried out in Econo-Pac cartridges at the indicated flow-rates as described under Experimental.

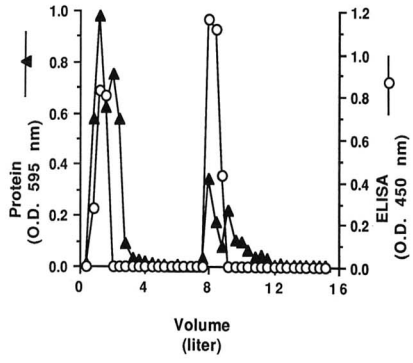

Fig. 3. Fractionation of goat serum on Macro-Prep 50 S sorbent. Goat serum (1.0 l), dialyzed against 20 m*M* MOPS buffer (pH 6.8), was applied at 40 ml/min to the column (23 × 7.5 cm I.D.) equilibrated in 20 m*M* MOPS buffer (pH 6.8). The proteins were eluted with a 0–50% gradient over 100 min, using 20 m*M* MOPS buffer (pH 6.8) containing 1.0 *M* NaCl. Fractions of 400 ml were collected and assayed for Klenow binding (○) and protein (▲) as described under Experimental.

Purification of antibodies against Klenow from goat serum

The isolation of an IgG fraction from goat serum using Macro-Prep 50 S sorbent in an Econo-Pac 5-ml cartridge described by Dunn *et al.* [6] was scaled up to a 1-l column (Fig. 3). This column was used to process 1 l of serum to yield 8.8 g of IgG which was >96% pure by SDS-PAGE (Fig. 5, lane 3). Hence this IgG purification demonstrated the scale-up capabilities from a 5-ml Econo-Pac cartridge to a 1-l column.

Specific anti-Klenow antibodies were purified on a Klenow affinity sorbent, prepared by coupling purified Klenow to Affi-Prep 10, a pressure-stable polymer derivatized with a N-hydroxysuccinimide (NHS) ester [12]. Binding of the specific anti-Klenow antibodies to the affinity matrix was achieved by recycling the IgG fraction or goat serum over the affinity sorbent. In one experiment, 4 ml (36 mg of total protein) of the purified IgG fraction from the Macro-Prep 50 S column were loaded onto the column and 100-μl aliquots were withdrawn from the recycling buffer at 0, 1.5, 3 and 16 h. These aliquots were analyzed for Klenow binding acitvities by ELISA. After 1.5 h, no activity was found in the recycled antibody solution, indicating that all of the anti-Klenow antibodies were bound to the sorbent. The bound Klenow antibodies (4.2 mg) were eluted from the column using 100 m*M* glycine (pH 2.5). Under conditions of antibody excess, the affinity column had a maximum capacity to bind 6.9 mg (46 nmol) of Klenow antibody. Based on the binding of one antibody molecule per Klenow molecule, this represents an 84% binding efficiency of the affinity sorbent. The purification of anti-Klenow on the affinity sorbent was confirmed in ELISA titrations (data not shown). In these experiments, serial three-fold dilutions of each of the three fractions (goat serum, IgG fraction from the Macro-Prep 50 S column and affinity-purified anti-Klenow antibodies) were assayed for Klenow-binding activity by ELISA. Based on the protein required to attain 50% of maximum activity, the affinity-purified anti-Klenow exhibited a three-fold higher specific activity than the IgG fraction, which in turn had a twelve-fold higher activity than the starting goat serum.

Purification of recombinant Klenow from E. coli

Recombinant Klenow was initially purified as described by Joyce and Grindley [8] to obtain a 60% ammonium sulfate supernatant and was further purified by passing 15 ml of the crude supernatant over an Econo-Pac heparin cartridge (Fig. 4). He-

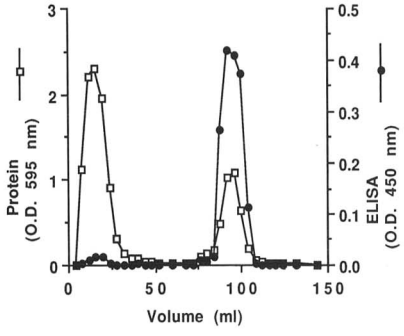

Fig. 4. Purification of Klenow on an Econo-Pac heparin cartridge. An aliquot of 15 ml of the ammonium sulfate supernatant (2.4 mg/ml) was applied to an Econo-Pac heparin 5-ml cartridge equilibrated in 10 m*M* potassium phosphate buffer (pH 7.0) containing 1 m*M* DTT (loading buffer). Bound proteins were eluted with a 30-min linear gradient of 0 to 0.5 *M* NaCl in 10 m*M* potassium phosphate buffer (pH 7.0) containing 1 m*M* DTT at 2.0 ml/min. Fractions of 4.0 ml were collected and assayed for binding to anti-Klenow using ELISA (●) and protein (□) as described under Experimental.

parin is a linear glycosamine–glycan composed of mostly sulfated 1,4-linked glycosamine and glucuronic acid residues. Proteins bind to heparin ionically or by more specific interactions. The capacity of the heparin cartridge was 1.3 mg/ml. The Klenow was assayed by ELISA using the affinity-purified anti-Klenow described above, conjugated to horseradish peroxidase. Most of the protein did not bind to the heparin sorbent, whereas all the Klenow was bound and eluted as a single peak in the salt gradient. The SDS-PAGE analysis (Fig. 5, lanes 5, 6 and 7) of the proteins in the crude cell extract fraction and the bound and unbound fractions indicated that the bound protein was a single band which migrated the same as the purified Klenow standard.

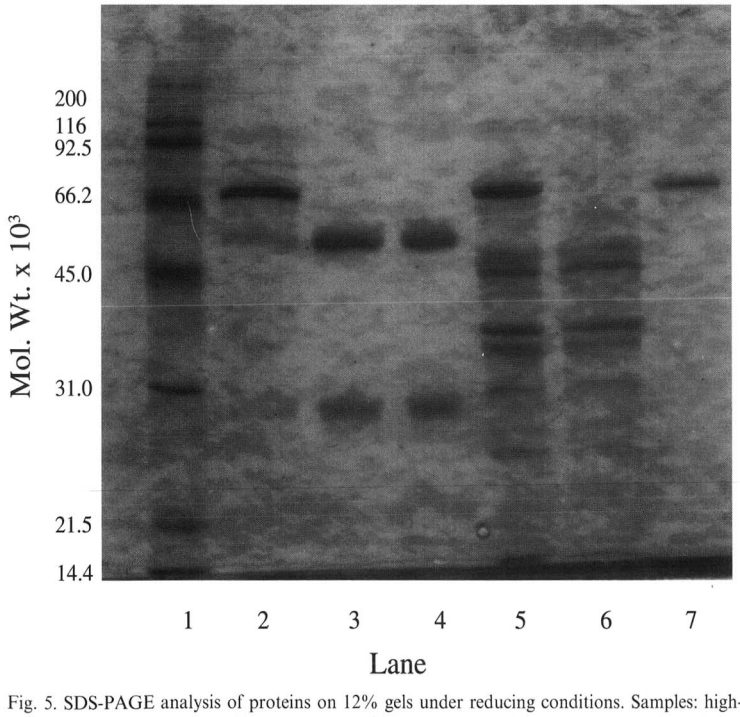

Fig. 5. SDS-PAGE analysis of proteins on 12% gels under reducing conditions. Samples: high- and low-molecular-weight Bio-Rad Labs. standards (lanes 1), dialyzed goat serum (lane 2), IgG pool from Macro-Prep 50 S column (lane 3), goat IgG standard (lane 4), crude cell extract containing Klenow (lane 5), unbound fraction from crude cell extract on Econo-Pac heparin cartridge (lane 6) and bound fraction (Klenow) from Econo-Pac heparin cartridge (lane 7).

REFERENCES

1 E. A. Peterson and H. A. Sober, *J. Am. Chem. Soc.*, 78 (1956) 751.
2 S. R. Himmelhoch and E. A. Peterson, *Anal. Biochem.*, 17 (1966) 383.
3 J. Porath and P. Flodin, *Nature (London)*, 183 (1959) 1657.
4 C. Male, *Methods Med. Res.*, 12 (1970) 221.
5 F. E. Regnier, *Anal. Biochem.*, 126 (1982) 1.
6 L. Dunn, M. Abouelezz, L. Cummings, M. Navvab, C. Ordunez, C. J. Siebert and K. W. Talmadge, *J. Chromatogr.*, 548 (1991) 165.
7 H. Klenow and I. Henningsen, *Proc. Natl. Acad. Sci. U.S.A.*, 65 (1970) 168.
8 C. M. Joyce and N. D. F. Grindley, *Proc. Natl. Acad. Sci. U.S.A.*, 80 (1983) 1830.
9 M. M. Bradford, *Anal. Biochem.*, 72 (1976) 248.
10 U. Laemmli, *Nature (London)*, 227 (1970) 680.
11 M. B. Wilson and P. K. Nakane, in W. Knapp, K. Holubar and G. Wick (Editors), *Immunofluorescence and Related Staining Techniques*, Elsevier/North Holland Biomedical Press, Amsterdam, 1978, p. 215.
12 R. S. Matson and C. J. Siebert, *Prep. Chromatogr.*, 1 (1988) 67.
13 L. R. Snyder and J. J. Kirkland, *Introduction to Modern Liquid Chromatography*, Wiley, New York, 1979, pp. 483–540.
14 G. Vanecek and F. E. Regnier, *Anal. Biochem.*, 121 (1982) 156.
15 K. K. Unger, R. Janzen and G. Jilge, *Chromatographia*, 24 (1987) 144.
16 I. Axelsson, *J. Chromatogr.*, 152 (1978) 21.

Journal of Chromatography, 590 (1992) 93–100
Elsevier Science Publishers B.V., Amsterdam

CHROMSYMP. 2378

Importance of intraparticle convection in the performance of chromatographic processes

Alírio E. Rodrigues*, J. C. Lopes, Z. P. Lu, J. M. Loureiro and M. M. Dias

Laboratory of Separation and Reaction Engineering, School of Engineering, University of Porto, 4099 Porto Codex (Portugal)

ABSTRACT

Large-pore materials are used in separation engineering as high-performance liquid chromatographic packings and adsorbents; however, they find also many applications in reaction engineering as catalyst supports and ceramic membrane reactors and in biotechnology as supports for mammalian cell cultures or biomass growth. In these large-pore materials, mass transport by intraparticle forced convection should be considered in process analysis. A brief historical survey of research work concerned with intraparticle forced convection is given, showing that the concept to be retained is that of effective diffusivity augmented by convection. The behaviour of the height equivalent to a theoretical plate as a function of bed superficial velocity is explained on the basis of the above concept. Analogies between slab and spherical particle geometries are discussed.

INTRODUCTION

Large-pore materials (*i.e.*, with pores larger than 1000 Å, as shown in Fig. 1) are used in several chemical engineering areas, namely as catalyst supports for selective oxidations [1,2], steam reforming, ammonia synthesis [3,4], etc., as adsorbents for the removal of carbonyl disulphide from propylene [5] or chromatographic supports, as high-performance liquid chromatographic (HPLC) packings based on alumina [6], polystyrene [7,8] or silica gel [9] for protein separations, as ceramic membranes [10], as supports for mammalian cell culture [11,12] and biomass growth [13] and in gel permeation chromatography [14].

The importance of intraparticle forced convection flow in large-pore or "gigaporous" materials (following Horváth's nomenclature [15]) was first discussed, as far as we could trace back, by Wheeler [16] in his landmark paper on "reaction rates and selectivity in catalyst pores". He concluded that intraparticle convective flow "is negligible except in the case of high-pressure reactions on catalysts with very large pores". He also wrote the mass balance equation for a species in a pore when diffusion, convection and reaction compete at the steady state. The parameter relating intraparticle convective flow and diffusive flow (although not in dimensionless form) was denoted b. However, he did not solve the model equation and so he missed the point, later

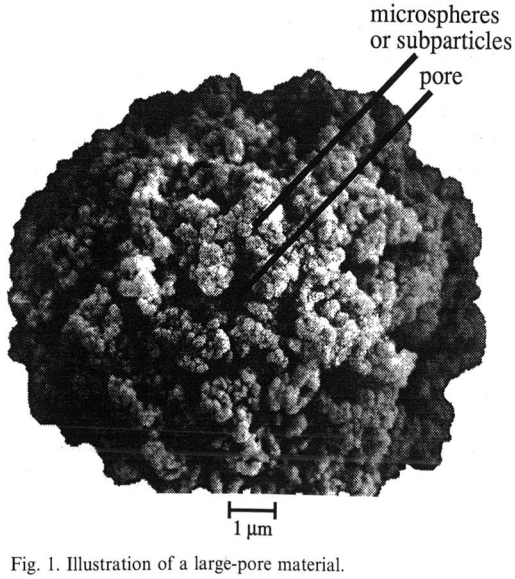

Fig. 1. Illustration of a large-pore material.

0021-9673/92/$05.00

recognized by Nir and Pismen [17], that in the intermediate range of Thiele modulus the catalyst effectiveness factor was enhanced by intraparticle convection.

The need for large pores in catalyst preparation was recognized by Nielsen *et al.* [3] and Harbord [4], among others. Nielsen *et al.* claimed that "it would be appropriate if ... the catalyst in addition to the said micropores would have a system of coarse pores adapted to serve as ways of admission to the micropores".

In recent years, the use of large-pore supports in HPLC provided an extended area of application of the concept which is responsible for the enhanced performance observed with such supports. The concept can be presented as diffusivity augmented by convection, as shown in 1982 by Rodrigues *et al.* [2].

This paper has the following objectives: (i) to provide a historical survey of the use of large-pore supports in chemical engineering; (ii) to show that the concept behind the observed improvement in the performance of chromatographic processes is the diffusivity augmented by convection in large-pore supports; (iii) to draw analogies between slab and spherical geometries; and (iv) to discuss the behaviour of the height equivalent to a theoretical plate (HETP) as a function of superficial velocity.

CONCEPT OF DIFFUSIVITY AUGMENTED BY CONVECTION INSIDE PORES

Intraparticle mass transport includes, in general, flux contributions due to diffusion (Knudsen and continuum or ordinary diffusion), N_i^d, intraparticle forced convection (viscous or Poiseuille flow), N_i^v, and surface diffusion, N_i^s [18], as shown in Fig. 2. The total flux of species i is then

$$N_{i,\text{total}} = N_i^d + N_i^v + N_i^s \tag{1}$$

In the following we shall restrict the analysis to diffusive and viscous flow inside large-pore materials.

Let us consider mass transport of an inert or passive species inside a large-pore particle with slab geometry. The transient mass balance for species i is

$$D_e \cdot \frac{\partial^2 c_i'}{\partial z'^2} - v_0 \cdot \frac{\partial c_i'}{\partial z'} = \varepsilon_p \cdot \frac{\partial c_i'}{\partial t} \tag{2}$$

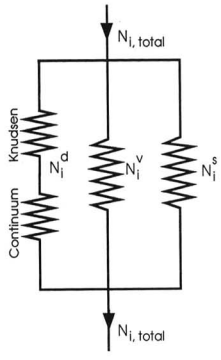

Fig. 2. Flux contributions of diffusion, convection and surface diffusion to the total flux.

where c_i' is the concentration of species i in the fluid phase inside the pores, z' is the particle space coordinate, t is the time variable, ε_p is the intraparticle porosity (pore volume/particle volume), v_0 is the intraparticle convective velocity and D_e is the effective diffusivity.

Introducing the dimensionless space variable $x = z'/l$ (l = half-thickness of the slab) and time constants for diffusion $\tau_d = \varepsilon_p l^2/D_e$ and convection $\tau_c = \varepsilon_p l/v_0$, we obtain

$$\frac{\partial^2 c_i'}{\partial x^2} - \frac{\tau_d}{\tau_c} \cdot \frac{\partial c_i'}{\partial x} = \tau_d \cdot \frac{\partial c_i'}{\partial t} \tag{2a}$$

The important parameter relating intraparticle convective flow and diffusive flow is the intraparticle Peclet number:

$$\lambda = \frac{\tau_d}{\tau_c} = \frac{v_0 l}{D_e} \tag{3}$$

introduced by Nir and Pismen [17] and closely related to the parameter b of Wheeler [16].

The transfer function of the particle system relating the Laplace transforms of the average tracer concentration inside the particle and the surface concentration is

$$g_p(s) = \frac{(e^{2r_2} - 1)(e^{2r_1} - 1)}{e^{2r_2} - e^{2r_1}} \frac{\sqrt{\lambda^2/4 + \tau_d s}}{\tau_d s} \tag{4}$$

where $r_1, r_2 = \lambda/2 \pm \sqrt{\lambda^2/4 + \tau_d s}$.

The classic analysis which considers only an "apparent" effective diffusivity, $\tilde{D}_e$, combines diffu-

sion and convection of the inert tracer; therefore, the unsteady-state mass balance equation is

$$\tilde{D}_e \cdot \frac{\partial^2 c_i'}{\partial z'^2} = \varepsilon_p \cdot \frac{\partial c_i'}{\partial t} \tag{5}$$

or

$$\frac{\partial^2 c_i'}{\partial x^2} = \tilde{\tau}_d \cdot \frac{\partial c_i'}{\partial t} \tag{5a}$$

with $\tilde{\tau}_d = \varepsilon_p l^2/\tilde{D}_e$. The transfer function is now

$$\tilde{g}_p(s) = \frac{\tanh \sqrt{\tilde{\tau}_d s}}{\sqrt{\tilde{\tau}_d s}} \tag{6}$$

Model equivalence between moments of eqns. 4 and 6 leads to

$$\tilde{\tau}_d = \tau_d f(\lambda) \tag{7}$$

or

$$\tilde{D}_e = \frac{D_e}{f(\lambda)} \tag{8}$$

where $\tilde{D}_e$ is the "apparent" or "augmented" effective diffusivity due to convection and

$$f(\lambda) = \frac{3}{\lambda}\left(\frac{1}{\tanh \lambda} - \frac{1}{\lambda}\right)$$

The enhancement of the effective diffusivity, D_e by convection is

$$\frac{1}{f(\lambda)} = \frac{1}{\frac{3}{\lambda}\left(\frac{1}{\tanh \lambda} - \frac{1}{\lambda}\right)} \tag{9}$$

as shown in Fig. 3.

Eqn. 8 provides a tool for calculating the augmented effective diffusivity for any set of operating conditions. When intraparticle convective flow is negligible ($\lambda \ll 1$), $\tilde{D}_e = D_e$; at high λ, however, the enhancement of the effective diffusivity is $\tilde{D}_e/D_e = \lambda/3$ and so $\tilde{D}_e = v_0 l/3$.

This result should be compared with those in other works. Van Kreveld and Van den Hoed [19] suggested that intraparticle convection could be important and used an augmented diffusivity containing a term proportional to the bed superficial velocity u_0, *i.e.*, $\tilde{D}_e = D + u_0 D'$. In the limit of strong convection $\tilde{D}_e = u_0 D'$. Later, Afeyan *et al.* [7], following this idea, used $\tilde{D}_e \approx v_0 d_p/2$ "based on the assumption that the concentration terms governing

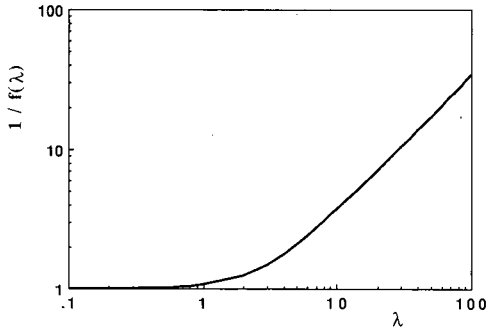

Fig. 3. Enhancement of effective diffusivity by convection $1/f(\lambda)$ as a function of the intraparticle Peclet number λ.

diffusion and convection can be treated as approximately equal". If we try to make an analogy with slab geometry where $\tilde{D}_e \approx v_0 l/3$, we shall obtain $l = 3\ d_p/2$, which does not make sense. This calls for a closer examination of the analogy between slab and spherical geometries.

ANALOGY BETWEEN SLAB AND SPHERICAL GEOMETRIES

In catalytic reaction engineering, analogies between various particle shapes can be made by introducing a characteristic dimension V_p/A_p (ratio of particle volume and external area). For slabs this dimension is the half-thickness l, for spheres it is $R_p/3$, where R_p is the particle radius, and for infinite cylinders it is $R_p/2$.

The equivalence for steady-state reaction/diffusion problems between slab and spherical catalysts is then based on

$$l_{slab} = R_{p,sphere}/3 \tag{10a}$$

However, for transient diffusion the equivalence should be based on the equality of the diffusion time constants for slabs and spheres, *i.e.*, [20]

$$\tau_{d,slab} = \frac{\varepsilon_p l^2}{D_e} \quad \text{and} \quad \tau_{d,sphere} = \frac{\varepsilon_p R_p^2}{5\ D_e}$$

where the diffusion time constant for sphere results from the linear driving force approximation. The result is

$$l_{slab} = R_{p,sphere}/\sqrt{5} \quad \text{(transient diffusion)} \tag{10b}$$

Similarly for fully convective flow ($\lambda \gg 1$), the equivalence between slab and sphere should be based on the equality of the time constants for intraparticle convection, *i.e.*,

$$\tau_{c,slab} = 2\, l/v_0 \quad \text{and} \quad \tau_{c,sphere} = \langle l_c \rangle / v_0$$

It can be shown [21] that the average convective path for a sphere is $\langle l_c \rangle = 4\, R_p/3$. Hence the equivalence leads to

$$l_{slab} = R_{p,sphere}/1.5 \quad \text{(transient convection)} \quad (10c)$$

INTRAPARTICLE CONVECTIVE VELOCITY, v_0

The intraparticle convective velocity, v_0, is calculated from Darcy's law:

$$v_0 = -\frac{B_p}{\mu} \cdot \frac{\Delta p}{2l} \quad (11)$$

where

$$B_p = \frac{\varepsilon_p^3}{150(1-\varepsilon_p)^2} \cdot d_m^2 = \frac{a\varepsilon_p^3}{150(1-\varepsilon_p)^2} \cdot d_{pore}^2$$

is the particle permeability, d_m is the diameter of the microspheres inside the particle, d_{pore} is the pore diameter, $a = d_m^2/d_{pore}^2$ is a constant ($a = 4$ for POROS according to Afeyan *et al.* [7]), ε_p is the intraparticle porosity, μ is the fluid viscosity and $\Delta p/2l$ is the pressure drop across a particle with thickness $2l$.

Komiyama and Inoue [22], in a pioneer (and also forgotten) paper, and later Rodrigues *et al.* [2] used, as a first approximation for calculating the intraparticle convective velocity v_0, the equality between $\Delta p/2l$ and the pressure drop along the bed of length L, $\Delta P/L$, given by Ergun's law, *i.e.*,

$$\frac{\Delta p}{2l} = \frac{\Delta P}{L} \quad (12)$$

After correction to refer fluxes to the same area, we obtain a relationship between v_0 and the bed superficial velocity u_0. Generally the relationship is $v_0 = a_1 u_0 + a_2 u_0^2$. In the case of laminar flow through the bed, the relationship is simply $v_0 = a_1 u_0$, where

$$a_1 = \frac{B_p}{B_b} \cdot \frac{1-\varepsilon_b}{\varepsilon_p} \quad (13)$$

$$B_b = \frac{\varepsilon_b^3}{150(1-\varepsilon_b)^2} \cdot d_p^2$$

is the bed permeability, ε_b is the interparticle bed porosity and d_p is the particle diameter.

An order of magnitude analysis carried out by Afeyan *et al.* [7] showed that the intraparticle Peclet number in HPLC operations can be as high as 60.

EFFECT OF INTRAPARTICLE CONVECTION ON HETP

HETP is often used as a measure of the performance of chromatographic processes. The Van Deemter equation [23] describes how the HETP changes with the bed superficial velocity u_0. For a fixed-bed chromatographic process including axial dispersion, intraparticle diffusion and convection and based on linear adsorption equilibrium between mobile and stationary phases $q_i^* = m\, c_i'$, the model equations are as follows.

The mass balance for species i in the fluid phase is

$$\varepsilon_b D_{ax} \cdot \frac{\partial^2 c_i}{\partial z^2} - u_0 \cdot \frac{\partial c_i}{\partial z} - \left[\varepsilon_b \cdot \frac{\partial c_i}{\partial t} + b\varepsilon_p(1-\varepsilon_b) \frac{\partial \langle c_i' \rangle}{\partial t} \right] = 0 \quad (14)$$

where c_i is the concentration of species i in the fluid phase outside the particles, z is the bed axial coordinate, u_0 is the bed superficial velocity (flowrate/bed cross-sectional area $= U/A$), $\langle c_i' \rangle$ is the average concentration of species i in the fluid phase inside the particles and

$$b = 1 + \frac{1-\varepsilon_p}{\varepsilon_p} m = 1 + k^*$$

(k^* is the capacity ratio for the particle). In dimensionless form, the mass balance is

$$\frac{1}{Pe} \cdot \frac{\partial^2 c_i}{\partial \zeta^2} - \frac{\partial c_i}{\partial \zeta} - \left[\varepsilon_b \cdot \frac{\partial c_i}{\partial \theta} + b\varepsilon_p(1-\varepsilon_b) \frac{\partial \langle c_i' \rangle}{\partial \theta} \right] = 0 \quad (14a)$$

where $Pe = u_0 L/(\varepsilon_b D_{ax})$ is the Peclet number, $\zeta = z/L$ is the dimensionless bed axial coordinate, $\theta = t/\tau = t\, u_0/L$ is the dimensionless time and L is the bed length.

Boundary and initial conditions for eqn. 14a are $\zeta = 0$, $c_i = M\, \delta(\theta)$; $\zeta \to \infty$, c_i limited and $\theta = 0$, $c_i = 0$, $\forall \zeta$.

The mass balance for species i inside the particle in dimensionless form is

$$\frac{\partial^2 c_i'}{\partial x^2} - \lambda \cdot \frac{\partial c_i'}{\partial x} = b\alpha \cdot \frac{\partial c_i'}{\partial \theta} \tag{15}$$

where $\alpha = \tau_d/\tau$, with boundary and initial conditions $x = 0$ and $x = 2$, $c_i' = c_{is}'$ and at $\theta = 0$, $c_i' = 0$, $\forall x$.

The transfer function of the system relating the outlet concentration and the inlet concentration in the Laplace domain is

$$G(s) = \exp\left[\frac{Pe}{2} - \sqrt{\frac{Pe^2}{4} + PeN(s)}\right] \tag{16}$$

with

$$N(s) = \varepsilon_b s + b\varepsilon_p(1 - \varepsilon_b)s g_p(s) \tag{16a}$$

where $g_p(s)$ is given by eqn. 4 after replacing $\tau_d s$ by $b\alpha s$, to account for the Laplace transform relative to the reduced time θ instead of the real time t and for the linear adsorption of species i inside the particle.

The moments of the impulse response are

$$\mu_1 = \varepsilon_b + \varepsilon_p(1 - \varepsilon_b)b \tag{17a}$$

$$\mu_2 = \frac{2}{3}\varepsilon_p(1 - \varepsilon_b)b^2\alpha f(\lambda) + \left(1 + \frac{2}{Pe}\right)[\varepsilon_b + \varepsilon_p(1 - \varepsilon_b)b]^2 \tag{17b}$$

and so the variance is

$$\sigma^2 = \frac{2}{Pe} \cdot \mu_1^2 + \frac{2}{3}\varepsilon_p(1 - \varepsilon_b)b^2\alpha f(\lambda) \tag{17c}$$

The HETP defined as $\sigma^2 L/\mu_1^2$ is then

$$\text{HETP} = \frac{2L}{Pe} + \frac{2}{3} \cdot \frac{\varepsilon_p(1 - \varepsilon_b)b^2\alpha L}{[\varepsilon_b + \varepsilon_p(1 - \varepsilon_b)b]^2} \cdot f(\lambda) \tag{18}$$

or

$$\text{HETP} = A + \frac{B}{u_0} + Cu_0 \tag{19}$$

In the classical analysis by Van Deemter *et al.* [23], where intraparticle forced convection is not considered, $f(\lambda) = 1$ and so

$$C = \frac{2}{3} \cdot \frac{\varepsilon_p(1 - \varepsilon_b)b^2}{[\varepsilon_b + \varepsilon_p(1 - \varepsilon_b)b]^2} \cdot \overline{|\tau_d|} \tag{20}$$

Here this coefficient is modified to account for the augmented effective diffusivity [24], *i.e.*, τ_d is replaced by $\tau_d f(\lambda)$ as shown in eqn. 7, *i.e.*,

$$C = \frac{2}{3} \cdot \frac{\varepsilon_p(1 - \varepsilon_b)b^2}{[\varepsilon_b + \varepsilon_p(1 - \varepsilon_b)b]^2} \cdot \overline{|\tau_d f(\lambda)|} \tag{21}$$

At high λ ($\lambda \gg 1$), we have $\tau_d f(\lambda) = 3\, l\, \varepsilon_p/v_0$ and so the limiting value of the HETP, neglecting the contribution of dispersion, is given by

$$\text{HETP} \approx \frac{2\varepsilon_p^2(1 - \varepsilon_b)b^2}{[\varepsilon_b + \varepsilon_p(1 - \varepsilon_b)b]^2} \cdot \frac{l}{v_0} \cdot u_0 \tag{22}$$

As $v_0 = a_1 u_0$ with a_1 given by eqn. 13, we obtain

$$\text{HETP} \approx \frac{2\varepsilon_p^2(1 - \varepsilon_b)b^2 l}{a_1[\varepsilon_b + \varepsilon_p(1 - \varepsilon_b)b]^2} \tag{22a}$$

For highly adsorbed solutes, $b \gg 1$, we have

$$\text{HETP} \approx \frac{2l}{(1 - \varepsilon_b)a_1} \tag{23}$$

Fig. 4 shows HETP as a function of the bed superficial velocity for conventional supports and large-pore supports. Using the data of Afeyan *et al.* [7], $d_p = 10\ \mu m$, $d_{pore} = 7000$ Å, $\varepsilon_p = 0.5$, $\varepsilon_b = 0.35$, we obtain $B_b = \varepsilon_b^3 d_p^2/[150\ (1 - \varepsilon_b)^2] \approx 6.8 \cdot 10^{-10}$ cm^2, $B_p = 4\varepsilon_p^3 d_{pore}^2/[150\ (1 - \varepsilon_p)^2] \approx 6.5 \cdot 10^{-11}$ cm^2 and $a_1 = B_p(1 - \varepsilon_b)/(B_b\varepsilon_p) \approx 0.126$, which means that the intraparticle convective velocity is around 4.5% of the bed interstitial velocity, and so for highly adsorbed solutes HETP $\approx 8\ d_p$ according to eqn. 23. For non-retained species $b = 1$ and from eqn. 22a we obtain HETP $\approx 2\ d_p$.

Fig. 5 shows the upper limit of the reduced HETP,

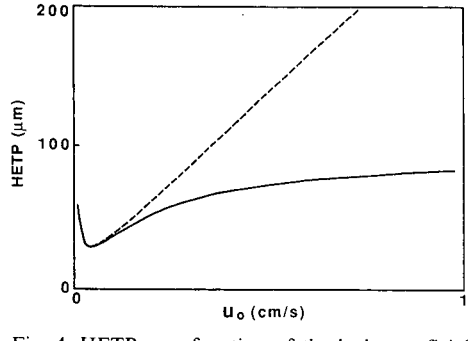

Fig. 4. HETP as a function of the bed superficial velocity u_0. Dashed line, Van Deemter equation for conventional supports; solid line, extension of Van Deemter equation to large-pore supports.

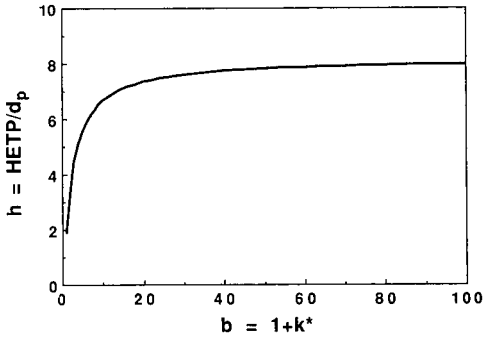

Fig. 5. Reduced HETP (h = HETP/d_p) as a function of the parameter $b = 1 + k^*$.

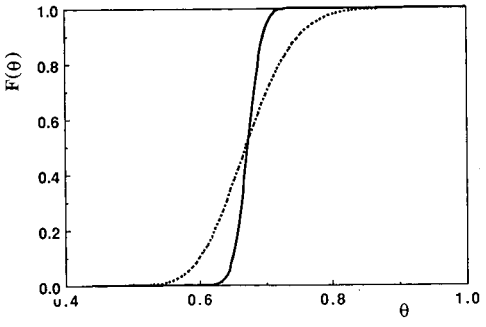

Fig. 7. Breakthrough curves $F(\theta) = c_{out}/c_{feed}$ as a function of reduced time. Dashed line, $u_0 = 0.282$ cm/s, no convection ($\lambda = 0$); solid line, with intraparticle convection, $u_0 = 0.282$, 0.576 and 0.963 cm/s.

h (= HETP/d_p), for high λ as a function of the parameter $b = 1 + k^*$.

The response of the chromatographic column to an impulse of inert tracer can be obtained by inversion of the bed transfer function, eqn. 16, *i.e.*, $E(\theta) = \mathscr{L}^{-1}[G(s)]$. Fig. 6 shows $E(\theta)$ as a function of the reduced time θ for conventional supports ($\lambda = 0$) and for a large-pore support ($\lambda = 35.5$). It can be seen that intraparticle convection sharpens the peak and so leads to a lower HETP.

Fig. 7 shows the breakthrough curves, *i.e.*, bed responses to step changes in feed concentration, $F(\theta) = c_{out}/c_{feed}$, for conventional supports ($\lambda = 0$) and large-pore supports, where intraparticle convection is important. In this instance the curves were calculated at three different superficial velocities and were identical, showing that velocity has no influence on the breakthrough curves. This is equivalent to the plateau in HETP *versus* u_0 curve shown in Fig. 4.

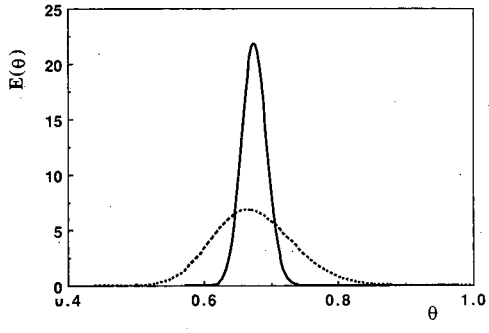

Fig. 6. Impulse response of the HPLC column to an inert tracer as a function of reduced time ($u_0 = 0.282$ cm/s; $\alpha = 0.0157$). Dashed line, no intraparticle forced convection ($\lambda = 0$); solid line, $\lambda = 35.5$.

CONCLUSIONS

The improvement of the performance of chromatographic processes using large-pore supports is due to the effective diffusivity augmented by convection. A complete relationship between the augmented diffusivity and the intraparticle Peclet number is available for slab geometry. Analogies between slab and sphere can be drawn in limiting cases.

It is interesting that some large-pore catalysts compete with shell-type catalysts, *e.g.*, in ethylene oxidation; in HPLC there is also a choice between pellicular and flow-through particles.

In HPLC, increasing the bed superficial velocity will lead to a limiting value of HETP which is proportional to the particle diameter and depends on the bed and particle permeabilities. The performance of a chromatographic column containing a large-pore packing is better than that with conventional supports, as the HETP is lower; moreover, increasing u_0 does not lead to a significant decrease in column efficiency and so one can speed up the separation. Along HETP *versus* u_0 curves the intraparticle Peclet number is changing. However, in gas–solid chromatography the relationship between the intraparticle convective velocity v_0 and the bed superficial velocity u_0 is $v_0 = a_1 u_0 + a_2 u_0^2$ (assuming Ergun's law for the bed pressure drop); as a consequence, HETP will pass through a maximum

before it reaches a plateau at a high bed superficial velocity [24].

In this work the kinetics of adsorption/desorption on the stationary phase were assumed to be infinitely fast, so the results presented here correspond to the more favourable situation; nevertheless, they are supported by experimental observations [7,8,15,20]. This assumption is not always valid. Slow kinetics will contribute with an extra term for HETP in the Van Deemter equation, proportional to u_0, *i.e.*, $D\,u_0$. However, the HETP for large-pore packings will be always lower than the corresponding HETP obtained with conventional supports [25].

ACKNOWLEDGEMENTS

Financial support from JNICT, INIC and Fundação Oriente is gratefully acknowledged.

SYMBOLS

b parameter ($= k^* + 1$)
B_b bed permeability, m^2
B_p particle permeability, m^2
c_i species concentration in the external fluid phase, kmol/m^3
c_i' species concentration in the fluid phase inside the particle, kmol/m^3
d_m diameter of microspheres inside the particle, m
d_p particle diameter, m
d_{pore} pore diameter, m
D_e effective diffusivity, m^2/s
$\tilde{D}_e$ augmented effective diffusivity, m^2/s
$E(\theta)$ impulse response of the bed
$F(\theta)$ response of the bed to a step input of concentration
h reduced HETP ($=$ HETP/d_p)
HETP height equivalent to a theoretical plate, m
k^* particle capacity factor
l half thickness of the slab, m
L bed length, m
m slope of the adsorption equilibrium isotherm
Pe Peclet number
Δp pressure drop across the particle, Pa
ΔP bed pressure drop, Pa
q_i^* adsorbed phase concentration in equilibrium with c_i', kmol/m^3 of solid
R_p particle radius, m
s Laplace variable
t time, s
u_0 bed superficial velocity, m/s
v_0 intraparticle convective velocity, m/s
x reduced space coordinate for the particle ($= z'/l$)
z axial coordinate for the bed, m
z' axial coordinate for the particle, m

Greek symbols

α ratio of time constant for diffusion and space time ($= \tau_d/\tau$)
ε_b bed porosity (interparticle volume/bed volume)
ε_p intraparticle porosity (pore volume/particle volume)
λ intraparticle Peclet number
μ fluid viscosity, kg/m · s
μ_i moments of ith order of the impulse response
θ reduced time ($= t/\tau$)
σ^2 variance
τ space time ($= L/u_0$), s
τ_c time constant for intraparticle convection, s
τ_d time constant for intraparticle diffusion, s
$\tilde{\tau}_d$ "apparent" time constant for intraparticle diffusion, s
ζ reduced axial coordinate for the bed ($= z/L$)

REFERENCES

1 D. Cresswell, *Appl. Catal.*, 15 (1985) 103.
2 A. E. Rodrigues, B. Ahn and A. Zoulalian, *AIChE J.*, 28 (1982) 541.
3 A. Nielsen, S. Bergd and B. Troberg, *US Pat.*, 3 243 386 (1966).
4 N. Harbord, *Br. Pat.*, 1 484 864 (1977).
5 P. T. K. Liu, presented at *AIChE Meeting, New Orleans, 1988.*
6 *Unisphere, Technical Information*, Biotage, Charlottesville, USA, 1990.
7 N. Afeyan, N. Gordon, I. Mazsaroff, L. Varady, S. Fulton, Y. Yang and F. Regnier, *J. Chromatogr.*, 519 (1990) 1.
8 L. Lloyd and F. Warner, *J. Chromatogr.*, 512 (1990) 365.
9 *Daisogel SP2705, Technical Information*, Daiso, Osaka, 1991.
10 M. Chaara and R. Noble, *Sep. Sci. Technol.*, 24 (1989) 893.
11 J. Vournakis and P. Ronstadler, *Bio/Technology*, 7 (1989) 143.
12 M. Young and R. Dean, *Bio/Technology*, 5 (1987) 835.
13 K. Breitenbucher, K. Siegel, A. Knupper and M. Radke, *Water Sci. Technol.*, 22 (1990) 25.
14 J. Watson, in P. Williams and M. Hudson (Editors), *Recent Developments in Ion-Exchange 2*, Elsevier, Amsterdam, 1990, pp. 277–286.

15 Cs. Horváth, presented at the *NATO ASI Meeting on Chromatographic and Membrane Processes in Biotechnology, Azores, 1990.*
16 A. Wheeler, *Adv. Catal.*, 3 (1951) 250.
17 A. Nir and L. Pismen, *Chem. Eng. Sci.*, 32 (1977) 35.
18 E. Mason and A. Malinauskas, *Gas Transport in Porous Media: the Dusty Gas Model*, Elsevier, Amsterdam, 1983.
19 M. van Kreveld and N. van den Hoed, *J. Chromatogr.*, 199 (1978) 71.
20 G. Carta, University of Virginia, personal communication, 1988.
21 A. E. Rodrigues, J. C. Lopes, M. M. Dias and G. Carta, *AIChE J.*, submitted for publication.
22 H. Komiyama and H. Inoue, *J. Chem. Eng. Jpn.*, 7 (1974) 281.
23 J. van Deemter, F. Zuiderweg and A. Klinkenberg, *Chem. Eng. Sci.*, 5 (1956) 271.
24 A. E. Rodrigues, Z. P. Lu and J. M. Loureiro, *Chem. Eng. Sci.*, 46 (1991) 2765.
25 A. E. Rodrigues, Z. P. Lu, A. Ramos, J. M. Loureiro and M. Diaz, *Chem. Eng. Sci.*, submitted for publication.

Journal of Chromatography, 590 (1992) 101–112
Elsevier Science Publishers B.V., Amsterdam

CHROMSYMP. 2469

Adsorption kinetics of albumin on a cross-linked cellulose chromatographic ion exchanger

G. Leaver[☆], J. A. Howell[☆☆] and J. R. Conder*

Chemical Engineering Department, University of Wales, Swansea SA2 8PP (UK)

ABSTRACT

Cross-linked, regenerated cellulose offers faster separation of proteins than softer gels can achieve. The kinetics of adsorption of bovine serum albumin have been studied on a Vistec granular DEAE-cellulose. A differential bed technique has been applied to proteins for the first time and allows results to be obtained more rapidly than with a larger bed. The dependence of the adsorption rate on the superficial flow velocity, salt concentration and protein concentration is examined. Although salt and protein compete strongly for adsorption sites the initial rate of adsorption is insensitive to salt concentration but sensitive to protein concentration. The rate-determining step in adsorption appears to be predominantly diffusion within the pores of the particles. Two single-step models of the kinetics have been developed: a pore diffusion model predicts the breakthrough curves better than a lumped mass transfer model, but a two-step model is likely to give better predictive accuracy than either. Some guiding principles are derived for optimising protein throughput.

INTRODUCTION

The largest part of the production costs of new biotechnology products usually arises in downstream processing. Processing sequences increasingly use chromatographic separation stages. Two important processes in which chromatographic stages have recently been introduced are the separation of blood proteins from animal and human blood.

Large quantities of valuable protein, in the form of animal blood from abattoirs and poultry processing, are currently wasted as process effluent [1]. The protein in blood can be separated from non-proteins by ion-exchange adsorption and desorption [2,3]; a protein powder produced in this way is now on the market for use in food mixes. The value of blood proteins, however, can be greatly increased if they are fractionated into specific proteins such as albumin [4]. This protein accounts for half the protein content of blood and its recovery is a potentially high tonnage process.

For fractionation of human blood proteins the classical alcohol precipitation techniques of Cohn and co-workers [5,6] are still dominant. In recent years, one of the most significant modifications to the Cohn process has been the incorporation of ion-exchange separation stages. New separation protocols have been devised based on ion-exchange, affinity or size-exclusion chromatography [7–14]. Production chromatography of proteins [15] and the relative merits of different forms of the technique [16] have been reviewed. Much of the literature is concerned with qualitative descriptions of the process; there is little information on the effect of process variables on performance for affinity chromatography [17–20] and even less for ion-exchange chromatography [21,22].

In order to design a chromatographic process to purify proteins, it is important to be able to predict the performance as a function of the operating conditions. We have recently studied the effect of operating conditions on the separation of albumin from bovine serum on a Vistec diethylaminoethyl (DEAE) cellulose ion exchanger [16]. The Vistec

☆ Present address: Warren Spring Laboratory, Gunnels Wood Road, Stevenage, Herts. SG1 2BX, UK.
☆☆ Present address: Chemical Engineering Department, University of Bath, Claverton Down, Bath BA2 7AY, UK.

0021-9673/92/$05.00

medium is a cross-linked, regenerated cellulose which provides an improved adsorbent matrix for the chromatographic separation of proteins [23]. Optimal operation was shown to require trade-offs between the major operating variables such as feed band width, feed dilution, eluent velocity, column length and packing rigidity [16]. A better understanding of the way in which the process variables determine performance can be gained by studying their influence on the process equilibria and adsorption kinetics directly. We have recently reported an investigation of the equilibria of adsorption of bovine serum albumin (BSA) on the Vistec ion-exchanger [23]. Here we describe a study of the adsorption kinetics of the same process. The first part of this study concerns the effect of process variables on the kinetics. In the final part a simplified kinetic model is developed and validated to permit prediction of breakthrough curves.

EXPERIMENTAL METHOD

Adsorption kinetics are often studied by using a stirred vessel but this method has only limited applicability: if there is significant extra-particle resistance to mass transfer the kinetics depend on the mixing pattern and differ from those in a packed bed. A packed bed technique is better suited to obtaining kinetic data that are to be used in designing packed columns. (A further advantage of the packed bed approach is described below.) We have adopted a variant of the packed bed technique that uses a very short "differential" bed. The technique was originally devised by Tien and Thodos [24] to study the adsorption of oxalic acid and allows results to be obtained more rapidly than with a longer bed.

The packed column was 15 mm high × 76 mm in diameter, giving an empty column volume (ECV) of 68 ml. With such a short bed it is important to achieve a uniform flow distribution over the cross-section. The column was constructed from QVF glass tubing and Corning flange pieces. Polypropylene end-plates with a central tapped hole for the liquid inlet or outlet (and, in the case of the inlet plate, a second tapped hole for a pressure gauge) were separated by a shallow (*ca.* 2 mm) chamber from an 8-hole flow distributor, in turn separated from a coarse (*ca.* 80 μm) mesh and 10 mm thick stainless-steel sinter retaining the packing. This arrangement produced a good distribution of liquid flow over the cross-section. The direction of flow was downward.

The materials were as previously described [23]. The D2 grade of Vistec DEAE-cellulose medium was used throughout. The particle size was determined to be 192 $\pm$ 36 μm by 242 $\pm$ 78 μm. BSA was made up in Tris buffer with sodium chloride added to the desired ionic concentration [23].

At the start of each run water was passed through the bed. When the conductivity was about $20 \cdot 10^{-6}$ S the feed was switched to albumin solution of the desired concentration and ionic strength. Conductivity and pH were continuously monitored at the outlet of the bed. The protein breakthrough curve was monitored with a Pye UV20 continuous detector at a wavelength of 280 nm. This detector, however, was insensitive to concentration change at high protein concentrations. Samples were therefore taken from the detector exit and analysed on a Pye SP6UV spectrophotometer at 280 nm to measure the concentration at specific points on the breakthrough curve. When the run was complete the bed was regenerated in accord with the manufacturer's literature, by switching the feed to water, then 0.2 *M* salt solution to desorb the protein, and finally water again. Subsequent measurements showed that a minimum salt concentration of 0.26 *M* would be required to desorb protein completely [23]. All protein concentrations reported in this paper (including simulations, which use experimental data) are therefore nominal and must be increased by 0.12 kg/kg dry medium to give true concentrations.

The adsorption kinetics were studied by following the progress of the breakthrough curve, which is a plot of the protein concentration c_o in the liquid eluting from the column outlet against time elapsed after a concentration step change from $c = 0$ to $c = c_f$ is introduced at the inlet. The mean concentration q of protein adsorbed on the solid at any point P on the breakthrough curve is obtained by a mass balance, *i.e.*, by subtracting the sum of (i) the mass of protein eluted from the column up to point P and (ii) the mass of protein in the liquid holdup (in the bed, column end pieces and connecting tubing) from the mass fed to the column and dividing by the dry mass W of the ion exchanger. Thus,

$$q = \frac{F}{W}\left[\int_0^t (c_f - c_o)\,dt - c_f t_M\right] \quad (1)$$

where F is the volumetric flow-rate and t_M is the liquid holdup time in the bed. t_M was determined by switching the feed stream to water, which does not desorb protein.

EXPERIMENTAL RESULTS AND DISCUSSION

Establishing the differential bed method

The mean protein concentration in the solid phase q is shown as a function of ECVs passed in Fig. 1. The breakthrough curves from which these plots are derived started together at 1.8 ± 0.2 ECV, which barely exceeds the liquid holdup (1.65 ECV). This is good evidence that the bed is acting as a true differential bed. Confirmation comes from the shape of the breakthrough curve. The present adsorption system has an isotherm with Langmuir-type curvature, concave towards the mobile phase concentration axis [23]. A bed long enough to contain several theoretical plates would therefore give a breakthrough curve which would start at a time later than t_M and develop rapidly through a steep, sigmoid form to early completion, *i.e.*, the migrating frontal boundary would be of the constant-pattern self-sharpening type [25]. The fact that the progress of breakthrough here occupies many column volumes confirms that the bed is of "differential" length.

Effect of superficial velocity

A comparison of Fig. 1 and the adsorption isotherms [23] for corresponding operating conditions shows that equilibrium is not established within the several minutes of the transient study. For example, at an ionic concentration of 5 kg/m^3, a liquid phase protein concentration of 5 kg/m^3 would produce an equilibrium solid concentration of 0.52 kg/kg but nominal values of only 0.11–0.19 kg/kg, corresponding to a true 0.23–0.31 kg/kg, are reached in Fig. 1. Part of this difference is due to the use of virgin medium for each equilibrium isotherm point as against bed regeneration in the kinetic studies. Even so, complete attainment of equilibrium appears to require times of the order of a few hours rather than a few minutes. The influence of slow adsorption kinetics is confirmed by the evidence in Fig. 1 that, in terms of column volumes passed, breakthrough develops more slowly at higher velocities.

Fig. 2 shows the same data as Fig. 1 replotted with time instead of ECV as abscissa. The order of the curves for different velocities is reversed. This is as expected for a differential bed if the adsorption rate is controlled more by the kinetics of mass transfer

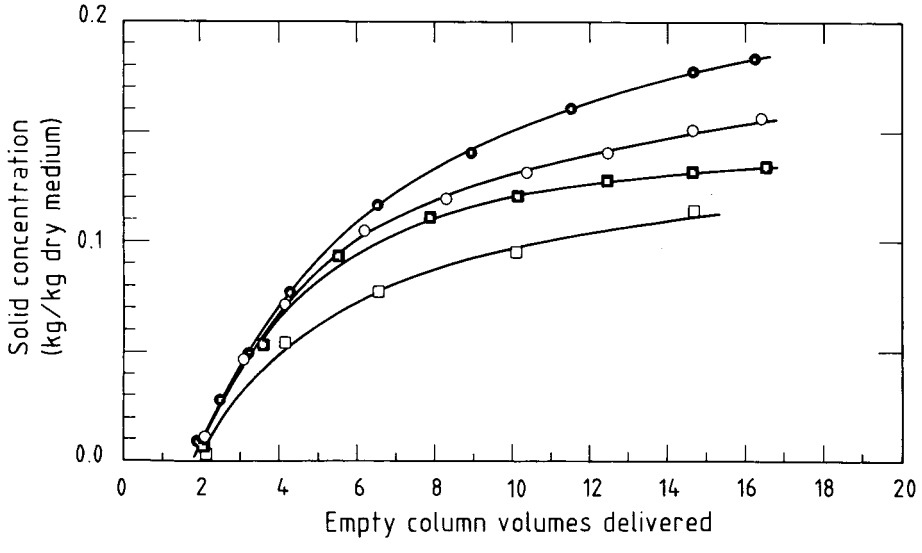

Fig. 1. Effect of superficial velocity u on protein breakthrough curve for ionic concentration (NaCl) 5 kg/m^3, pH 7.5, c_f = 5 kg/m^3. u: ● = 0.06 mm/s; ○ = 0.13 mm/s; ■ = 0.28 mm/s; □ = 0.86 mm/s.

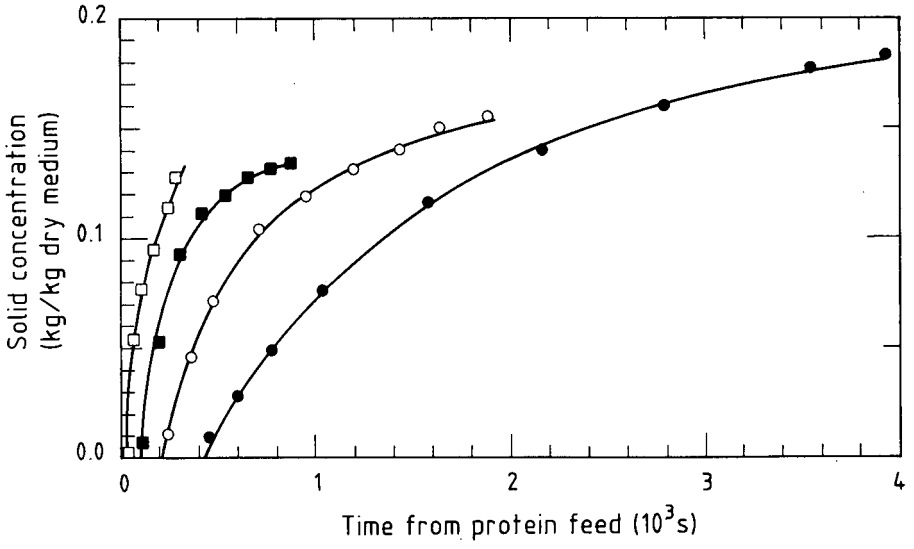

Fig. 2. As Fig. 1 but with abscissa expressed as time from step change in protein feed concentration to c_f at column inlet. Symbols as in Fig. 1.

within the particles (*e.g.*, by pore diffusion) than that through the liquid "film" outside the particles.

From a practical point of view, a low velocity has the advantage of achieving a given adsorbed concentration with least wastage of protein in the effluent (Fig. 1). On the other hand, it is seen from Fig. 2 that, where cycle time is more important than wastage, a high velocity gives a faster increase in the amount of protein adsorbed.

Effect of ionic concentration

Fig. 3 shows the effect of ionic concentration on

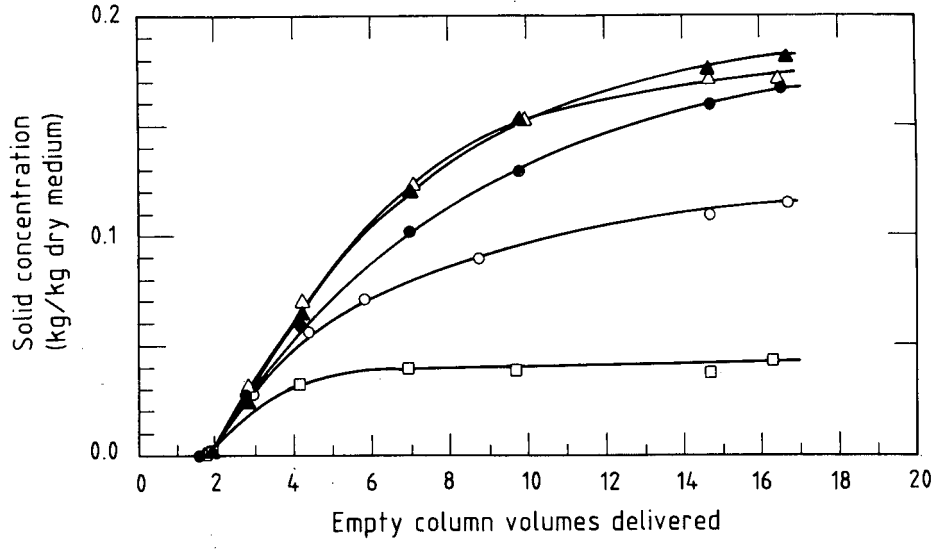

Fig. 3. Effect of ionic concentration I (kg NaCl/m^3) on breakthrough curve at pH 7.5, c_f = 5 kg/m^3, superficial velocity 0.37 mm/s. I: ▲ = 0 kg/m^3; △ = 1 kg/m^3; ● = 3 kg/m^3; ○ = 5 kg/m^3; □ = 10 kg/m^3.

the progress of adsorption. Initially, the rate of adsorption is not very sensitive to the ionic concentration. As equilibrium is approached, however, the adsorption rate becomes more sensitive to ionic concentration; this behaviour reflects the pattern of the adsorption isotherms previously reported [23] in that the adsorbed concentration at equilibrium decreases as the ionic concentration in the feed increases. The change in sensitivity to ionic concentration probably reflects a change from transport-limited to thermodynamic-limited control of the kinetics. The initial adsorption rate is controlled by mass transfer through the liquid film and internal pores. Subsequently the important factor becomes competition with other ions for sites on the ion exchanger surface.

There are two other notable differences between equilibrium and transient behaviour. First, reduction of the ionic concentration within the range 0–5 kg/m^3 significantly improves the rate of adsorption seen in Fig. 3, but has no beneficial effect on the equilibrium uptake of protein previously reported [23]. The equilibrium uptake increases with decreasing ionic concentrations down to 5 kg/m^3 but varies little at lower ionic concentrations (so long as the ratio of salt to protein concentrations is maintained above 20).

Secondly, in the batch (equilibrium) studies it is necessary to use high initial concentrations of protein in the liquid phase to achieve a given final uptake. At low ionic concentrations this creates a risk of agglomeration of the protein molecules. The problem does not arise in the continuous flow process: the protein feed concentration is the same at the beginning and end of the process. Even at zero concentration of added salt, sufficient salts are present in the buffer solution of the feed to maintain the protein/salt concentration below its critical value [23] of 20 and the protein remains unagglomerated.

Effect of protein feed concentration

Fig. 4 shows the effect of varying the protein feed concentration c_f at a constant ionic concentration of 3 kg/m^3. The non-linear relationship between protein uptake and feed concentration for a given volume of eluate passed is as expected from the isotherm, which is of the Langmuir type [23]. Because the relationship is non-linear, higher protein uptake is achieved only at the cost of a greater proportional loss of protein in the eluent stream.

The initial rate of adsorption is more sensitive than the later rate to protein feed concentration, *i.e.*, the proportion of the equilibrium solid concentration achieved at any given time less than infinite time

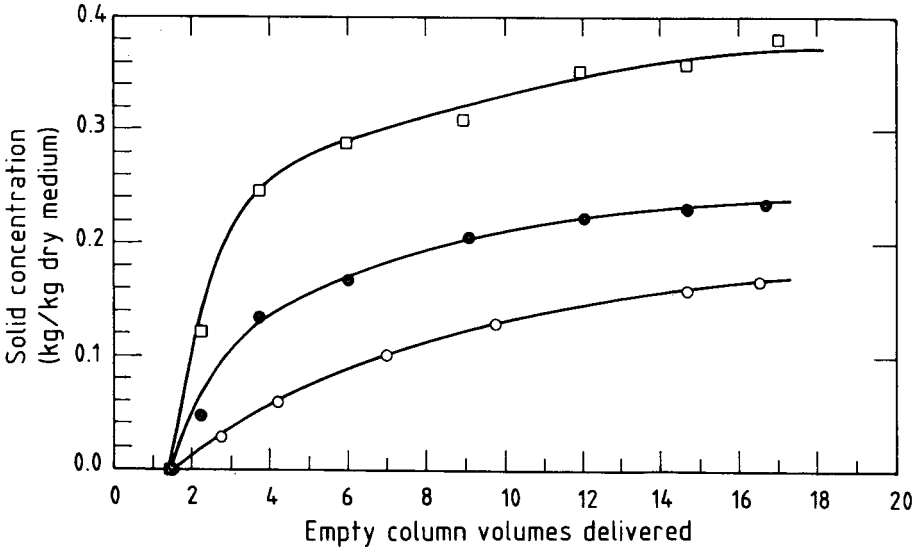

Fig. 4. Effect of protein feed concentration c_f on breakthrough curve at pH 7.5, ionic concentration (NaCl) 5 kg/m^3, superficial velocity 0.37 mm/s. c_f: □ = 25 kg/m^3; ● = 10 kg/m^3; ○ = 5 kg/m^3.

is higher for higher protein feed concentrations. This finding is important for optimising the performance of the chromatographic separation of proteins because it implies that the protein feed should be introduced at as high a concentration as possible. For example, passing 20 ECVs of feed of concentration 5 kg/m^3 would produce an adsorbed concentration of about 0.17 kg/kg. The same mass of protein fed at a concentration of 10 kg/m^3 in a feed band of 10 ECVs would raise the adsorbed concentration to 0.21 kg/kg. The faster adsorption achieved by doubling the protein concentration outweighs the halving of available contact time. This conclusion applies only if the salt concentration exceeds 5 kg/m^3 and if the volume of feed is concentrated without change in the salt concentration. In practice, simple concentration or dilution of feed will change the concentration, not only of protein but also of salt.

Dilution: combined effects of ionic and protein concentrations

Fig. 5 demonstrates the effect of combining two different protein concentrations with two ionic concentrations.

As expected, there are two regimes of behaviour depending on contact time. The initial adsorption rate (low contact times, solid concentration much less than equilibrium value) is largely unaffected by ionic concentration but is more sensitive than the later rate to protein feed concentration. The later adsorption rate, corresponding to high contact times where the solid concentration is a substantial fraction of the equilibrium value, is affected by both ionic and protein concentrations.

The effect of feed dilution is seen by comparing curves 2 and 3. Curve 3 was obtained by diluting, to a five times greater volume, a protein feed similar to that of curve 2. Despite the lower protein concentration in diluted feed, the combined effects of lower ionic concentration and greater adsorption time (in the sense of a greater volume of more dilute feed delivered) give a three times greater uptake of protein on completion of delivery. In the earliest stages of delivery, however, the undiluted feed gives the greater uptake. Thus, the effective capacity of the ion exchanger for protein generally increases with dilution unless contact times are short. This is consonant with the chromatographic findings [16].

MODELLING THE ADSORPTION KINETICS

Models of protein adsorption in packed beds

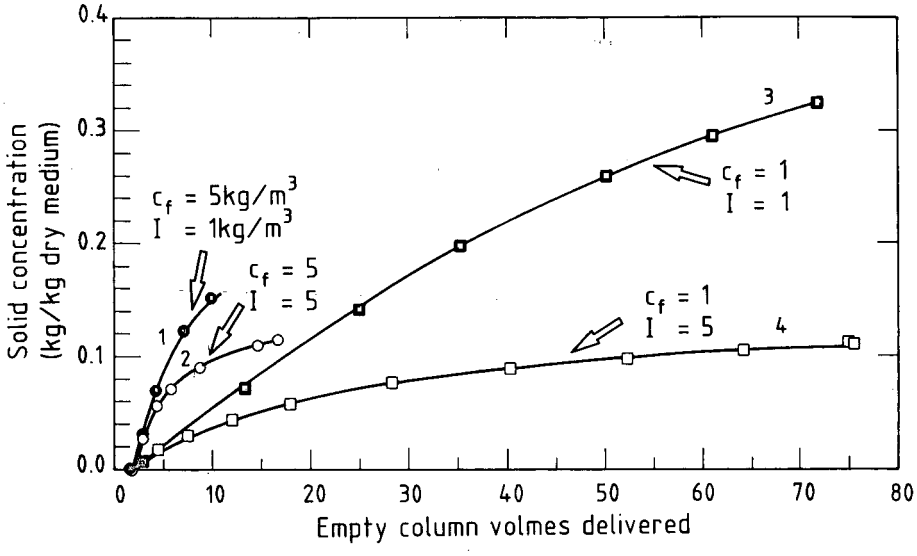

Fig. 5. Effect of protein concentration c_f and ionic concentration I at pH 7.5, superficial velocity 0.37 mm/s.

[17,20–22,26–28] differ from each other in two main characteristics: the type of equilibrium isotherm, and the nature of the mass transfer resistance to the sorption process.

Protein adsorption isotherms are usually found to be favourable, *i.e.*, concave to the liquid concentration axis. The Langmuir isotherm, which is of this type, can be theoretically justified for proteins [23]. It relates q and c, the concentrations in the solid and liquid phases, respectively, at equilibrium:

$$q = \frac{K_m q_m c}{1 + K_m c} \tag{2}$$

q_m is the adsorbent capacity and K_m (the ratio of the adsorption and desorption rate constants) determines the curvature of the isotherm. Previous models of protein adsorption have sometimes been based on a linear or rectangular ("irreversible") isotherm [20,27]. These can be regarded as extreme cases of a Langmuir isotherm, with K_m equal to 0 or ∞, respectively. Since the isotherm has a major effect on the model breakthrough curve we have instead adopted the normal (finite K_m) Langmuir isotherm which fits BSA adsorption on Vistec well [23].

Adsorption into porous particles is assumed to proceed in a series of steps: (i) diffusion through the liquid film external to the particle, (ii) diffusion through liquid held in pores of the particle, and (iii) the surface reaction at the liquid-solid interface. Surface diffusion in parallel with pore diffusion [29] is not likely to be significant for proteins. It is assumed that step (iii), surface reaction, is not rate-limiting. This agrees with a recent affinity adsorption study [26]. The simplest modelling approach is to lump the steps together and describe the adsorption rate by a single term involving a lumped mass transfer coefficient. Such a model can also encompass the case where transfer across the liquid film is rate-limiting since the rate expressions have the same mathematical form. The alternative limiting case is that pore diffusion, rather than the liquid film, is rate-limiting. The experimental evidence so far described indicates that both pore diffusion and the liquid film may determine the rate of adsorption, but that pore diffusion may be dominant. A model based on one of these processes alone is simpler and makes less demands on computer time and storage. We have therefore sought to compare two versions of the model, one based on a lumped mass transfer resistance and the other on pore diffusion. An analytical solution exists for the lumped mass transfer model [30] but we have developed a numerical solution in parallel with the pore diffusion model for comparability.

In both models it is additionally assumed that (i) axial dispersion is negligible in the packed bed, (ii) the particles are spherical and of uniform size, density and porosity, and (iii) ion-exchange groups are uniformly distributed throughout each particle. There is evidence that assumptions (ii) and (iii) are reasonably well satisfied for the D2 grade of Vistec used here [23]. In addition, since protein concentrations are small, volume changes in the liquid and diffusion-induced convection in particle pores are neglected.

Model development

The basis of a packed bed adsorption model is a mass balance for the adsorbate in the fluid phase in the voids external to the particle. Two approaches are available. The mass balance may be based either on an element of the packed bed [31] or on an element of the moving liquid. We have adopted the second approach.

The column is divided up lengthwise into a number n_c of sections short enough for the protein concentrations to be regarded as uniform within each section. At zero time the protein concentration in the inter-particle liquid in the first section is raised from zero to c_f and thereafter maintained at that value. During the time that the first elemental volume of protein solution remains in the first section it loses some protein by adsorption into the packing. The depleted liquid then passes into the second column section and is further depleted of protein. In general, when an elemental volume of liquid $\varepsilon \Delta v$ passes from section l to section $(l + 1)$, it is depleted of protein according to the mass balance equation

$$c_{l+1} = c_l - \frac{R \Delta t}{\varepsilon \Delta v} \tag{3}$$

where R is the rate of transfer of protein into the adsorbent particles in section l, calculated from the appropriate rate equation given below, and Δt is the time increment

$$\Delta t = \frac{\varepsilon \Delta v}{F} \tag{4}$$

(Symbols are defined at the end of the paper.) The value of c_{l+1} so calculated is the protein concentration in the liquid phase presented to the next column section as the elemental volume of liquid progresses along the column.

The scheme is to start at zero time at the column inlet and calculate c_2 from c_1 ($= c_f$). l is incremented to scan the progress of the first liquid element from inlet to outlet of the column. After each scan, time is incremented at the column inlet by Δt and the scan is repeated. The data-pair t and c_l at the column outlet where $l = n_c + 1$ are recorded at regular time intervals to give the breakthrough curve.

Rate equation for lumped mass transfer resistance

The increment in the mean concentration of protein in the solid phase of the adsorbent in column section l in time Δt can be expressed as

$$\Delta q = k(c_l - c^*)\Delta t \tag{5}$$

where c^*, the liquid concentration in the intra-particle pores in equilibrium with q, is calculated from the current value of q via the Langmuir isotherm eqn. 2. The new value of q is calculated by adding Δq to the current value and the new c^* is derived. The desired rate term is then given by

$$R\Delta t = \Delta v(\phi \Delta c^* + G\Delta q) \tag{6}$$

Rate equation for pore diffusion resistance

Consider a spherical surface of radius r within a spherical, porous particle. The fraction of the spherical surface occupied by pores is taken to be the same as the fraction of particle volume occupied by pores, *i.e.*, $\phi/(1 - \varepsilon)$ [31]. A mass balance on protein diffusing through the pore-occupied fraction of the spherical surface leads to the equation

$$\frac{\mathscr{D}}{r^2}\frac{\partial}{\partial r}\left(r^2\frac{\partial c}{\partial r}\right) = \frac{\partial c}{\partial t} + \frac{G}{\phi}\frac{\partial q}{\partial t} \tag{7}$$

Substituting for $\partial q/\partial c$ from eqn. 2, we obtain

$$\frac{\partial c}{\partial t} = \frac{\mathscr{D}}{1 + \dfrac{G}{\phi}\cdot\dfrac{q_m K_m}{(1 + K_m c)^2}}\left[\frac{\partial^2 c}{\partial r^2} + \frac{2}{r}\cdot\frac{\partial c}{\partial r}\right] \tag{8}$$

The partial differential equation is solved numerically with an explicit form of computational molecule. Using a first order forward difference formula for $\partial c/\partial t$ and $\partial c/\partial r$ and a second order central difference formula for $\partial^2 c/\partial r^2$, we obtain

$$c_i^{j+1} = c_i^j + \frac{\mathscr{D}\Delta t}{1 + \dfrac{G}{\phi}\cdot\dfrac{q_m K_m}{(1 + K_m c)^2}}\cdot \left[\frac{c_{i+1}^j - 2c_i^j + c_{i-1}^j}{(\Delta y)^2} - \frac{2(c_{i+1}^j - c_i^j)}{\Delta y\left(\dfrac{d_p}{2} - y\right)}\right] \tag{9}$$

where i is the distance counter along the pore and j is the time counter.

The boundary conditions are

$$\begin{aligned} &c_1^j = c_l, \quad j \geqslant 1 \\ &c_i^1 = 0, \quad i = 2 \text{ to } n \\ &\partial c/\partial y = 0, \quad y = d_p/2 \end{aligned} \tag{10}$$

Eqn. 9 permits the new concentration profile of protein along a pore (*i.e.*, a set of c_i for $i = 1$ to n) after a time increment Δt to be calculated from the previous pore profile by repeated application of eqn. 9. The mass transfer rate R is then obtained from the concentration gradient at the mouth of the pore by the equation

$$R = \frac{\mathscr{D}s}{\Delta y}(c_l - c_2^j) \tag{11}$$

where s, the total area of pore mouth in an elemental section Δv of the column, is given by

$$s = 6\phi\Delta v/d_p \tag{12}$$

RESULTS OF THE SIMULATION

Breakthrough curves have been simulated using both the lumped mass transfer and pore diffusion versions of the model and compared with experimental data. The simulations were performed with the 15 mm long differential bed divided into 15 elemental sections and with parameter values $G = 154$ kg/m^3, $G/\phi = 380$ kg/m^3, $d_p = 200$ μm, $u = 3.65 \cdot 10^{-4}$ m/s, $c_f = 5$ kg/m^3, $I = 5$ kg/m^3, pH 7.5, and $q_m = 0.42$. For the pore diffusion model the pore length, $d_p/2$, was divided into $n = 20$ sections, the minimum number below which the breakthrough curve became dependent on n. The numerical computation schemes showed no sign of instability over the range of variables used.

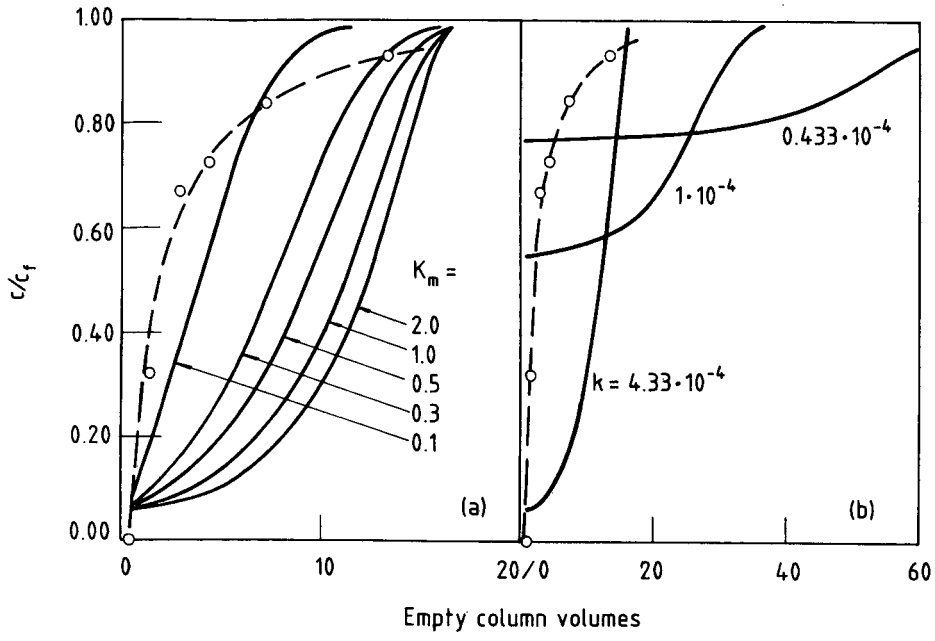

Fig. 6. Simulated breakthrough curves using lumped mass transfer model. (a) Effect of Langmuir constant $K_m/m^3\ kg^{-1}$ with $k = 4.33 \cdot 10^{-4}\ m^3/(kg\ s)$. (b) Effect of mass transfer coefficient $k/m^3\ (kg\ s)^{-1}$ with $K_m = 2\ m^3/kg$. The broken curves are experimental.

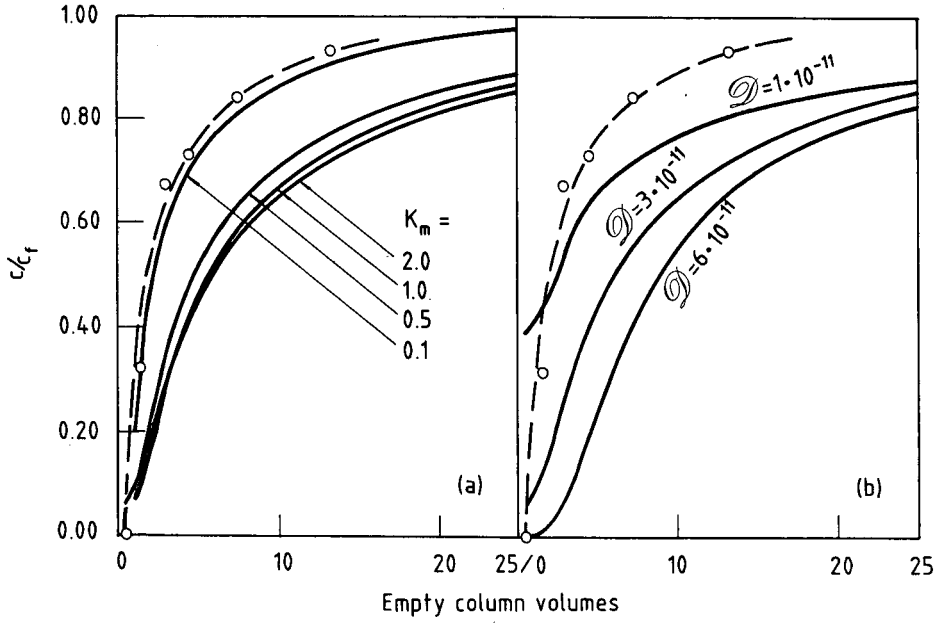

Fig. 7. Simulated breakthrough curves using pore diffusion model. (a) Effect of Langmuir constant K_m with $\mathscr{D} = 3 \cdot 10^{-11}\ m^2\ s^{-1}$. (b) Effect of diffusivity $\mathscr{D}/m^3\ s^{-1}$ with $K_m = 2\ m^3/kg$. The broken curves are experimental.

The sensitivity of the two models to the Langmuir isotherm's non-linearity parameter K_m is shown in Figs. 6a and 7a. The sensitivity increases rapidly as K_m falls, as anticipated from eqn. 2. It is evident that models based on the simplifying assumption of a linear ($K_m \to 0$) or rectangular ($K_m \to \infty$) isotherm will give very different results and are unlikely to be satisfactory. Particularly noteworthy is the way the lumped mass transfer breakthrough curves change shape as K_m varies and tend to converge at high degrees of breakthrough.

Figs. 6b and 7b show that at low values of their respective rate parameter (k or $\mathscr{D}$) both models predict breakthrough curves starting at high values of protein concentration. The rate at which the curves develop subsequently, however, is more sensitive to the lumped mass transfer coefficient than to pore diffusivity. The curves in Fig. 7b cross above 30 ECV.

An experimental breakthrough plot is shown in Figs. 6 and 7 for the same conditions as the simulated curves. The Langmuir parameter K_m to be associated with the experimental plot lies between 0.5 and 2.0 m^3/kg. The range reflects irreproducibility in the regenerated medium but is not as wide as it seems since both the Langmuir isotherm and the simulated breakthrough curves are insensitive to K_m at these (large) values of K_m. Only one parameter, k or $\mathscr{D}$, is to be obtained by fitting the simulated curves to the experimental data. It is evident from Figs. 6 and 7 that neither model provides a very good fit. However, the exponentially shaped breakthrough curves of the pore diffusion model accord better with the experimental shape than do the generally sigmoid-shaped curves of the lumped mass transfer model. This is consistent with the earlier conclusion that pore diffusion offers a larger resistance than external film transport. Examination of Figs. 6 and 7 indicates that a two-step model in which a pore diffusion resistance is combined with an external resistance would be likely to bring the curves into closer alignment with experiment, as has been found for an affinity adsorption system [26].

Fig. 7 suggests that the effective pore diffusion coefficient is about $3 \cdot 10^{-11}$ m^2/s. This is half the value of $6.0 \cdot 10^{-11}$ m^2/s predicted by the correlation of Young *et al.* [32] for BSA at 293 K in free solution. The high value of 1/2 in comparison with literature values of 1/20–1/100 [21,22] is probably due mainly to the large pore size of the Vistec medium, which has been estimated at 50–100 nm [33].

CONCLUSIONS

The purpose of studying the adsorption kinetics is to provide a basis for optimising the design and operating conditions of the chromatographic separation. Several guiding principles can be deduced from this study.

Amongst the variables that determine the throughput (processing rate) of protein, those that relate to the adsorption kinetics include superficial velocity, feed volume (band width), protein feed concentration and ionic concentration. Optimisation will involve trade-offs between these variables.

If the feed is dialysed before it is chromatographed, the protein concentration and ionic concentration can be controlled independently to maximise adsorption. This benefit is offset by the extra cost, and possibly time, consumed by the extra unit operation of dialysis. If the feed is not dialysed, the two concentrations are coupled. Dilution may then be a beneficial tactic. It increases the effective adsorption capacity unless the feed band width, and hence contact time, is abnormally small. With a normal column of, say, 0.3 m length, as opposed to a differential bed, even 0.03 ECV of bovine plasma is in the range where the effective capacity improves with dilution [16]. The overall effect on the protein throughput, however, also depends on how much the overall cycle time has to be raised to process the larger volume of diluted feed.

As the liquid velocity is increased, the bed contact time available for protein adsorption decreases. This is partly counteracted by an increase in the adsorption rate to an extent depending on the nature of the controlling mass transfer resistance. The net result is some fall in the effective adsorption capacity of the bed. The fall is found to be small for the BSA + Vistec system under chromatographic process conditions [16]. Liquid velocity then controls protein throughput more through the cycle time than through the effective capacity, and the throughput increases almost linearly with velocity.

Since the mass transfer kinetics are largely controlled by pore diffusion, the use of smaller particles will increase the rates of adsorption and desorption. With a compressible medium, however, reduced

particle size can be achieved only at the expense of reduced velocity and the throughput will not necessarily benefit from use of smaller particles.

In choosing a model to analyse performance it is not satisfactory to simplify the adsorption isotherm to a linear or rectangular form. Of single-step kinetic models, a pore diffusion model represents the BSA + DEAE-Vistec system better than a lumped mass transfer model. A two-step model, however, is likely to perform better still since pore diffusion is not completely rate-limiting.

SYMBOLS

c protein concentration in liquid, kg/m^3
c_f protein feed concentration in liquid, kg/m^3
c_l^j protein concentration in ith section of a pore at jth time increment, kg/m^3
c_l protein concentration in liquid between particles in lth section of column, kg/m^3
c^* protein concentration in pore (intra-particle) liquid in equilibrium with q, kg/m^3
c_o protein concentration in the liquid eluting from the column oulet, kg/m^3
$\mathscr{D}$ effective diffusivity of protein in pores, m^2/s
d_p particle diameter, m
F volumetric flow-rate of liquid through column, m^3/s
G pseudo-density of solid phase of adsorbent (dry weight per swollen bulk volume), kg/m^3
I ionic (added NaCl) concentration, kg/m^3
K_m Langmuir constant (ratio of adsorption and desorption rate constants), m^3/kg
k overall mass transfer coefficient, m^3/(kg s)
l column section
n number of elemental sections in a pore = $d_p/(2\Delta y)$
n_c number of elemental sections in column
q mass of protein per unit mass of dry adsorbent, kg/kg
q_m Langmuir constant (adsorption capacity), kg/kg
R rate of transfer of protein from extra-particle liquid to adsorbent in column section l, kg/s
r distance from centre of particle, m
s total area of pore mouth in an elemental section Δv of the column, m^2
t time, s
Δt time increment defined by eqn. 4, s
t_M liquid holdup time in the bed, s
u superficial velocity of liquid, m/s
Δv volume of elemental section of column, m^3
W dry mass of the ion exchanger, kg
y distance into pore from mouth, m
Δy length of elemental section of pore, m
ε void fraction of bed (extra-particle voidage/bulk volume)
ϕ pore fraction of bed (intra-particle pore volume/bulk volume)

REFERENCES

1 M. D. Rankin, in R. A. Grant (Editor), *Applied Protein Chemistry*, Applied Science Publishers, Essex, 1980, Ch. 6, pp. 169–180.
2 D. T. Jones, *Process Biochem.*, 9, No. 19 (1974) 17.
3 D. T. Jones, in G. G. Birch, K. J. Parker and J. F. Morgan (Editors), *Food from Waste*, Applied Science Publishers, 1976, Ch. 17. p. 242.
4 D. Halliday, *Process Biochem.*, 10, No. 4 (1975) 11.
5 E. J. Cohn, L. E. Strong, W. L. Hughes, D. J. Mulford, J. N. Ashworth, M. Merlin and H. L. Taylor, *J. Am. Chem. Soc.*, 68 (1946) 459.
6 E. J. Cohn, W. L. Hughes and J. H. Weare, *J. Am. Chem. Soc.*, 69 (1947) 1753.
7 J. M. Curling, L. O. Lindquist and S. Erikson, *Process Biochem.*, 12 (1977) 22.
8 J. M. Curling, J. Berglof, L. O. Lindquist and S. Erikson, *Vox Sang.*, 33 (1977) 97.
9 J. M. Curling, in R. Epton (Editor), *Chromatography of Synthetic and Biological Polymers*, Ellis Horwood, Chichester, 1978, Ch. 6.
10 J. M. Curling, in J. M. Curling (Editor), *Methods of Plasma Protein Chromatography*, Academic, London, 1980, pp. 77–91.
11 J. Saint-Blanchard, J. M. Kirzin, P. Riberon, F. Petit, J. Fourcart, P. Girot and C. Boscetti, in T. C. J. Gribnau, J. Visser and R. J. F. Nivard (Editors), *Affinity Chromatography and Related Techniques*, Elsevier, Amsterdam, 1982, p. 305.
12 J. Travis, J. Bowen, D. Tewkesbury, D. Johnson and R. Pannell, *J. Biochem.*, 157 (1976) 301.
13 R. Hanford, W. d'A. Maycock and L. Vallet, in R. Epton (Editor), *Chromatography of Synthetic and Biological Polymers*, Ellis Horwood, Chichester, 1978, Ch. 23.
14 J. L. Tayot, M. Tardy, P. Gattel, R. Plan and M. Roumiantzeff, in R. Epton (Editor), *Chromatography of Synthetic and Biological Polymers*, Ellis Horwood, Chichester, 1978, Ch. 8.
15 J. C. Janson and P. Hedman, *Adv. Biochem. Eng.*, 25 (1982) 43.
16 G. Leaver, J. R. Conder and J. A. Howell, *Sep. Sci. Technol.*, 22 (1987) 2037.
17 H. A. Chase, *J. Chromatogr.*, 297 (1984) 179.
18 P. D. G. Dean, W. S. Johnson and F. A. Middle, *Affinity Chromatography*, IRL Press, Oxford, 1985, Ch. 4.
19 J. P. Hamman and G. J. Calton, (*ACS Symposium Series*,

No. 271), American Chemical Society, Washington, DC, 1985, p. 105.
20 F. H. Arnold, J. J. Chalmers, M. S. Saunders, M. S. Croughan, H. W. Blanch and C. R. Wilke, (*ACS Symposium Series*, No. 271), American Chemical Society, Washington, DC, 1985, p. 113.
21 E. E. Graham and C. F. Fook, *AIChE J.*, 28 (1982) 245.
22 H. S. Tsou and E. E. Graham, *AIChE J.*, 31 (1985) 1959.
23 J. R. Conder, G. Leaver and J. A. Howell, *Inst. Chem. Eng. Symp. Ser.*, No. 118 (1990) 1.
24 C. Tien and G. Thodos, *Chem. Eng. Sci.*, 13 (1960) 120.
25 J. R. Conder and J. H. Purnell, *Trans. Faraday Soc.*, 65 (1969) 824.
26 B. J. Horstmann and H. A. Chase, *Chem. Eng. Res. Des.*, 67 (1989) 243.
27 F. H. Arnold, H. W. Blanch and C. R. Wilke, *Chem. Eng. J.*, 30 (1985) B25.
28 J. P. van der Wiel and J. A. Wesselingh, in A. E. Rodrigues, M. D. Levan and D. Tondeur (Editors), *Adsorption, Science and Technology*, Kluwer, Dordrecht, 1989.
29 T. W. Weber and R. K. Chakravorti, *AIChE J.*, 20 (1974) 228.
30 N. K. Hiester and T. Vermeulen, *Chem. Eng. Prog.*, 48 (1952) 505.
31 R. G. Lee and T. W. Weber, *Can. J. Chem. Eng.*, 47 (1969) 54.
32 M. E. Young, P. A. Carroed and R. L. Ball, *Biotech. Bioeng.*, 22 (1980) 947.
33 R. V. Dove, personal communication, 1982.

Journal of Chromatography, 590 (1992) 113–117
Elsevier Science Publishers B.V., Amsterdam

CHROMSYMP. 2396

Optical resolution by simulated moving-bed adsorption technology

Masakazu Negawa* and Fumihiko Shoji

Process Technology Centre, Daicel Chemical Industries, Ltd., 1239 Shinzaike, Aboshi-ku, Himeji Hyogo, 671 12 (Japan)

ABSTRACT

The application of the simulated moving bed adsorption (SMBA) technique to optical resolution using eight columns packed with chiral stationary phases was studied. The SMBA system was compared with the conventional batch system, and it was concluded that the former is better from the point of productivity and solvent recovery. In addition, it was shown that an optimum particle size of the chiral phase to attain the maximum productivity exists if a certain upper limit of the pressure drop is assumed.

INTRODUCTION

Recently, in the fields of pharmacy and agrochemicals, a racemic material tends to be substituted by an optically active material more active than the antipode. Considering the growing demand for optically active materials, we decided to develop a new technique that is more productive than a conventional batch system. The simulated moving bed adsorption (SMBA) technique is a useful means of separating large amounts of compounds as it is a continuous separation process. We therefore started this study to apply SMBA technology to the production of optically active materials. This technique was originally developed by Universal Oil Products to separate *n*-hexane and cyclohexane from their mixture [1], and recently it was applied to the separation of water-soluble materials (*e.g.*, a glucose–fructose mixture) [2]. In these instances theoretically the resolution was easy as the feed concentrations were as high as about 40% and the adsorption isotherms were linear. In contrast, our application was difficult as the solubility of the material in the mobile phase (an organic solvent) was very low and the adsorption isotherms were non-linear [3]. We are now developing computer software to simulate an SMBA system with non-linear adsorption isotherms and the results will be reported elsewhere. In this paper, we report the first separation of optical isomers by an SMBA process and demonstrate that the process has a much higher productivity than a conventional batch process.

EXPERIMENTAL

SMBA system

Fig. 1. illustrates the concept of the SMBA system for optical resolution. The umbrellas symbolize optical isomers, the conveyor belt the stationary phase and the wind the mobile phase. The open umbrellas, which are the enantiomers retained more weakly, and the closed umbrellas, which are the enantiomers retained more strongly, are on the conveyor belt. Hence we can obtain enantiomers continuously.

Fig. 2. is a schematic diagram of the experimental apparatus used. The eight adsorption columns packed with a Chiralcel OD-type packing material were connected to rotary valves. The packing materials were prepared by coating cellulose tris(3,5-dimethylphenyl carbamate) on silica gels of 20, 75 and 100 μm diameter. Each column was 15 cm × 2 cm I.D. All the adsorption column were kept at 25°C by circulating thermostated water through the jackets. The positions of the feed, raffinate, extract and desorbent were fixed, but the lines connected to the rotary valves were controlled with the system controller [Japan Spectroscopic (Jasco) Model 802-

0021-9673/92/$05.00

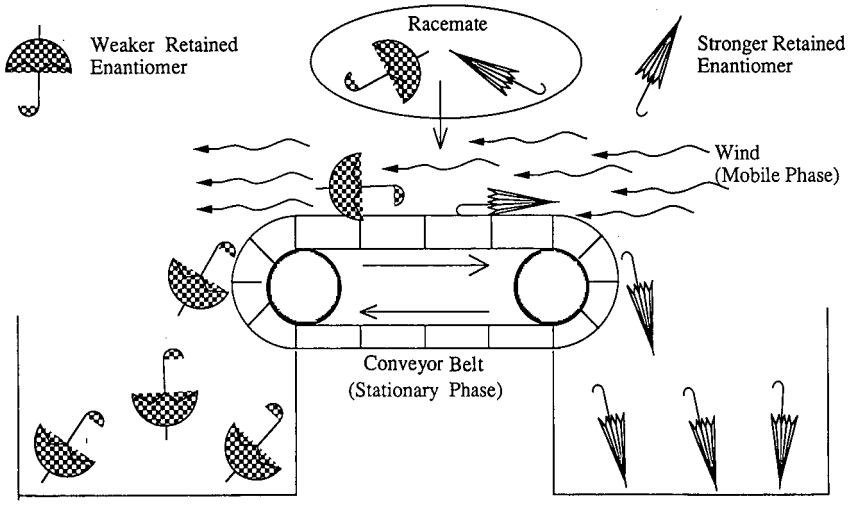

Fig. 1. Concept of the simulated moving-bed adsorber (SMBA) system for optical resolution.

SC system controller]. The feed and drainage pumps were used as the pumps for the high-performance liquid chromatographic (HPLC) system (Jasco 887-PU). The intermittent rotation of the rotary valves produced counter-current movements of the adsorbent phase to the liquid stream in the system. In Fig. 1 the stationary phase is moving, but in the real equipment the feed line, desorbent feed line, raffinate line and extract lines are moving intermittently. The desorbent was a *n*-hexane–isopropanol (9:1). The racemate used was 1-phenylethanol. The raffinate and extract were collected at certain in-

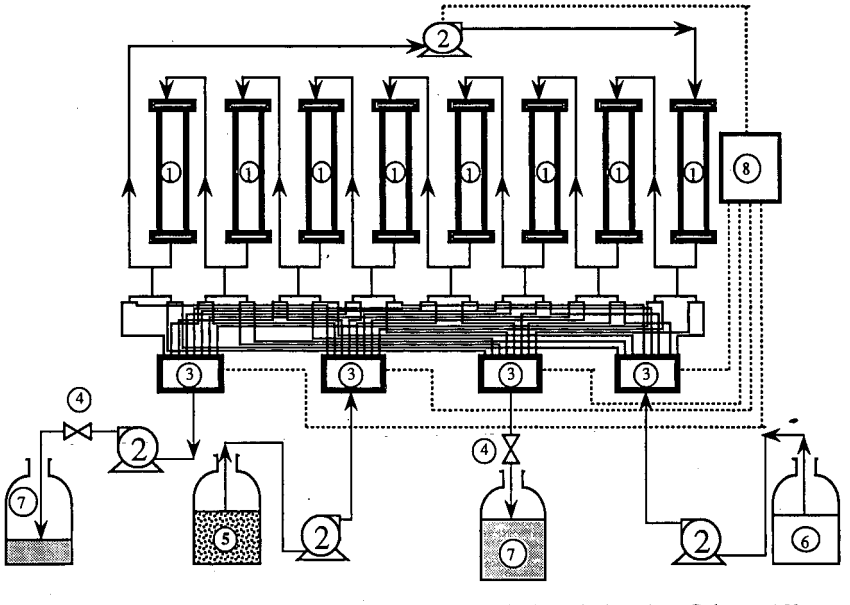

Fig. 2. Schematic flow diagram of SMBA system for optical resolution. 1 = Column, 150 mm × 20 mm (I.D.), packed with Chiralcel OD (20 μm, 75 μm, 100 μm); 2 = HPLC pump; 3 = rotary valve (8-port type); 4 = back-pressure valve; 5 = feed (racemate) reservoir; 6 = desorbent reservoir; 7 = extract and raffinate collector; 8 = system controller.

tervals (*e.g.*, 1 h) and their optical purities were measured by HPLC. A Shimadzu LC-6A HPLC system equipped with a Chiralcel OD column (25 cm × 0.46 cm I.D.) (Daicel) and a Model SPD-6AV detector was employed. The eluent *n*-hexane–isopropanol (9:1) at a flow-rate of 1.0 ml/min. 1-Phenylethanol was detected of 260 nm and determined by the external standard method.

Conventional batch system

The column size was 50 cm × 1 cm I.D., the column temperature was 25°C, the eluent was *n*-hexane–isopropanol (9:1) at a flow-rate of 4.7 ml/min and a 50-μl aliquot of the sample solution (2%, w/w, in the above-mentioned mixture) was injected every 8 min.

RESULTS AND DISCUSSION

Measurement of the basic physical properties

In the SMBA system eight columns were connected in series, so the pressure drop becomes very high. We therefore chose packing materials with some larger particle sizes (20,75 and 100 μm) and compared their performances and the pressure drops in the SMBA systems. Table I shows the number of theoretical plates of a single column (25 cm × 1 cm I.D.).

Results of SMBA experiments

The results of the SMBA experiments are shown in Figs. 3–6. As shown in Fig. 3, we divided eight columns into four zones. Zones 1 and 4 have one column each, zones 2 have four columns and zone 3 has two columns. In ordinary set-ups each zone has two columns, but in our case the above arragement

TABLE I

NUMBER OF THEORETICAL PLATES

Experimental conditions: column, 25 cm × 1 cm I.D.; mobile phase, *n*-hexane–isopropanol (9:1, v/v); flow-rate, 4.7 ml/min; temperature, 25°C; sample, *trans*-stilbene oxide, 5000 ppm; sample loading, 20 μl.

Particle size (μm)	No. of theoretical plates
20	1673
75	262
100	120

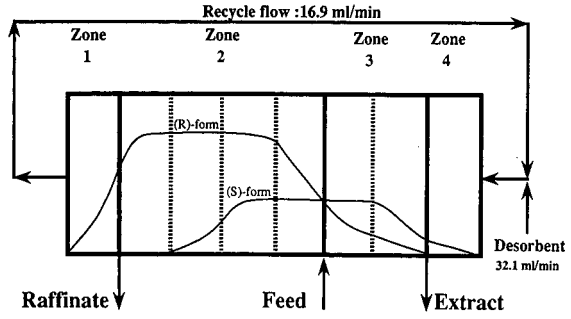

Fig. 3. Experimental results of optical resolution with the SMBA system. Conditions: packing, Chiralcel OD, particle diameter 20 μm; column 150 m × 20 mm I.D. (× 8); sample, 1-phenylethanol; mobile phase, *n*-hexane–isopropanol (9:1, v/v); cycle time; 2.9 min; temperature; 25°C. The distribution of the two enantiomers is shown conceptually. Feed: racemic 1-phenylethanol, 0.5 ml/min, 39 100 ppm (racemate); raffinate: (*R*)-(+)-1-phenylethanol, 5.4 ml/min, 1728 ppm (99% e.e.); extract: (*S*)-(−)-1-phenylethanol, 27.2 ml/min, 360 ppm (92% e.e.).

gave better results. This means that the role of zones 2 and 3, which was the separation of the racemate, was more important than the role of zones 1 and 4, which was washing the column. The feed concentration was very low compared with the above-mentioned water-soluble compounds as the solubility of the racemate in the mobile phase was low. In spite of these unfavourable conditions, we could eliminate the racemate with a high efficiency [99% enantiomer excess (e.e.)].

Fig. 4. shows the effect of the flow-rate of the extract on the purity of the product enantiomers.

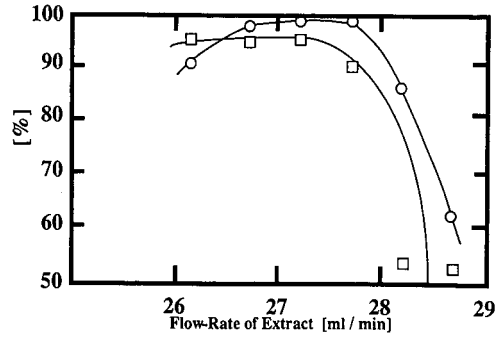

Fig. 4. Effect of the flow-rate of the extract on the purity of the product enantiomers. Experimental conditions as in Fig. 3 except for the flow-rate of the raffinate and extract. □ = (*S*)-(−)-phenylethanol in extract (%); ○ = (*R*)-(+)-phenylethanol in raffinate (%).

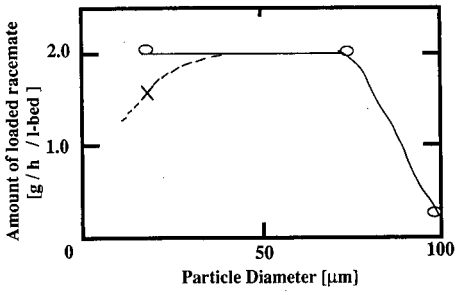

Fig. 5. Relationship between particle diameter and sample loading.

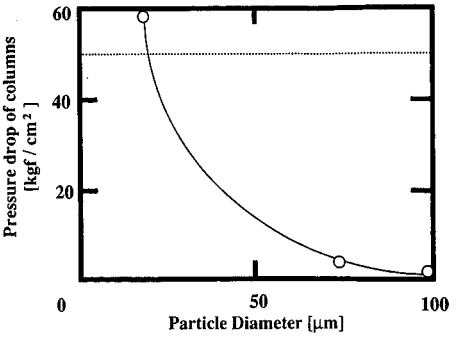

Fig. 6. Relationship between particle diameter and the pressure drop of the columns.

The conditions of the experiments except the flow-rates of the raffinate and the extract were the same as those in Fig. 3. A satisfactory optical purity of the raffinate (98% e.e.) could be obtained only in a limited range of the flow-rate ratio of the raffinate and the extract. This severe limitation may be rationalized as follows. When the extract flow-rate was too low, the flow-rate in zone 2 became too large, causing the elution of the *S*-form in the raffinate; when the extract flow-rate was too high, the flow-rate in zone 2 became too large, causing too much *S*-form to remain in zone 4, which was incompletely washed out to contaminate the raffinate. Both factors seem to be the outcome of the low resolution of the enantiomers on the columns.

Fig. 5. shows the relationship between the particle size and the load calculated from the maximum feed concentration, which kept the purity of the raffinate higher than 98% e.e. Fig. 6 shows the relationship between the particle size and the total pressure drop of all columns. Fig. 5 clearly shows that the amount of the loaded racemate decreased when the particle size was larger than 75 μm. On the other hand, the total pressure drop sharply increased when the particle size decreased. If the upper limit of the total pressure drop of the system is assumed to be 50 kgf/cm^2, the amount of loaded racemate should follow the broken line in Fig. 5 and the presence of the optimum particle size is predicted. To determine the optimum particle size, a more de-

TABLE II

COMPARISON OF THE CHARACTERISTICS OF THE SMBA SYSTEM WITH A CONVENTIONAL BATCH SYSTEM IN THE OPTICAL RESOLUTION OF 1-PHENYLETHANOL BY CHIRALCEL OD (20 μm)

Parameter	Conventional batch operation	SMBA system	SMBA/Batch
Loading of racemate (g/h · l bed)	0.13	2.05	16:1
Productivity of (*R*)-(+)-enantiomer (g/h · l bed)	0.016	0.981	61:1
Amount of used solvent [l/g (*R*)-(+)-enantiomer]	463.4	5.3	1:87
Concentration of refined (*R*)-(+)-solution (p.p.m.)	8.7	1728.4	200:1
Enantiomer excess of the product (% e.e.)	99.0	98.7	1:1
Yield of (*R*-(+)-1-phenylethyl alcohol (%)	24.6	95.5	4:1

tailed study must be conducted with particle sizes between 20 and 75 μm. If the upper limit is 100 kgf/cm^2, the amount follows the solid line in Fig. 5.

We compared the SMBA system and a conventional batch system and the results are given in Table II. The SMBA system was apparently superior to the conventional batch system in the following two respects: the productivity per unit amount of the packing material was 61 times larger, and the amount of solvent used was on 87th and the concentration of the raffinate was 200 times higher. Hence the cost of solvent recovery is much lower with the SMBA system.

REFERENCES

1 D. B. Broughton, *US Pat.*, 2 985 589 (1961).
2 K. Hashimoto, S. Adachi and H. Noujima, *J. Chem. Eng. Jpn*, 16 (1983) 400.
3 K. Hashimoto, M. Yamada and Y. Shirai, *J. Chem. Eng. Jpn*, 20 (1987) 405.

Journal of Chromatography, 590 (1992) 119–126
Elsevier Science Publishers B.V., Amsterdam

CHROMSYMP. 2416

Experimental study of the production rate of pure enantiomers from racemic mixtures

Stephen C. Jacobson and Georges Guiochon*

**Department of Chemistry, University of Tennessee, Knoxville, TN 37996-1501, and Division of Analytical Chemistry, Oak Ridge National Laboratory, Oak Ridge, TN 37831-6120 (USA)*

ABSTRACT

Elution band profiles were determined experimentally for the racemic mixture of D- and L-mandelic acid on a bovine serum albumin chemically bonded phase. The results show significantly different profiles for a given amount of either isomer, whether pure or in the racemic mixture. The production rate at 99% purity is more than one order of magnitude higher under overlapping band than under touching band conditions. In the former instance, the recovery yield and production rate are always higher for the less retained enantiomer.

INTRODUCTION

The separation and purification of compounds by preparative liquid chromatography has been an area of increasingly intense interest over the past decade [1]. Important progress has been made in the understanding of the processes that control the migration, broadening and separation of the high-concentration bands injected into chromatographic columns, and also the interactions between the bands of the different components of feedstock mixtures [2–11]. Excellent agreement has been achieved between the experimental band profiles and those which can be calculated by applying the theory of non-linear chromatography [12–16].

The optimization of the experimental conditions for a preparative separation by chromatography has been extensively studied [2,3,17–24]. Several general approaches toward optimization have been undertaken: (1) purely empirical methods [3,17]; (2) semi-empirical methods based on oversimplifying assumptions, such as a non-competitive behavior of the mixture components [2,21,24]; and (3) more complex methods based on the theoretically sound assumption of competitive behavior between the mixture components, but also on the simplifying assumption of a Langmuir isotherm model [18–20, 22,23]. Controversies have arisen regarding the comparative advantages and drawbacks of the touching and the overlapping band approaches [18–24], and even regarding the need to use a competitive isotherm in order to simulate accurately the band profiles [23–25]. On the other hand, the practical usefulness of the displacement effect has been established beyond doubt [3,26].

More practically, debates have also arisen between theorists and experimentalists regarding the selection of the parameters that should be optimized. These parameters should include the efficiency parameters [19] (*e.g.*, the column length, the particle size of the stationary phase [3,20] and the reduced velocity) and the loading factor [19,22]. In some instances, however, the optimization is limited to the sample size [10,27], *i.e.*, to the concentration and/or the volume of the feedstock sample injected. In practice, many chromatographers are limited by the equipment and/or by the available supplies and can only optimize the sample size, especially with wide-bore columns that cannot be operated under high pressure and, for this reason, should be operated at the maximum possible pressure. Another source of argument concerns the acceptable values of the recovery yield and the extent of compromise that is affordable between a high yield and a high

0021-9673/92/$05.00

production rate. This is strictly case dependent. Essentially, two options are available, and all intermediates are hybrids of these two primary choices. If the compound to be purified is expensive compared with the cost of the chromatography, then a touching bands situation [2,23] is desirable in order to ensure the highest yield. If the compound to be purified is inexpensive compared with the cost of the chromatography, then a highly overloaded injection is desirable in order to maximize the production rate [18]. For intermediate cases, a trade-off strategy is available [22].

One of the fundamental reasons why such controversies arise and linger is the lack of relevant experimental data. The acquisition of such data is simple but the choice of separation problems of relevant importance is critical if we really want to clarify some of the current issues. It is necessary to validate the theory of non-linear chromatography as it has been derived [18–20]. If the retention mechanism can be elucidated and the equilibrium isotherms of the main components of the feedstock can be measured in a relatively broad concentration range, then the band profiles can be simulated using the proper algorithm [4–9,11] and the optimum conditions under which to perform the experiment can be determined easily [10,18–20,22,23]. This curtails the number of experiments needed for an empirical determination of these conditions. It was the primary aim of this study to provide such data illustrating the fundamental importance of a sound theoretical approach for a satisfactory optimization of experimental conditions.

Chiral separations [28,29] have become increasingly important and commonplace over the past decade, and the advent of a variety of stationary phases has widened the range of enantiomers that can be analyzed. Bovine serum albumin (BSA) bonded covalently to porous silica [30] or adsorbed on silica [31] has been used for chiral separations, and the two types of columns have recently been compared [32]. Previously, DL-mandelic acid has been separated under linear chromatographic conditions [32], and N-benzoylated amino acid derivatives have been investigated under overloaded conditions [15] and found to have a bi-Langmuir isotherm on this stationary phase.

The production of either pure enantiomer from a racemic mixture is a problem which is simple and can be stated clearly enough to be easily studied and solved from theoretical standpoint. However, it is a relevant problem in the pharmceutical industry. This justifies our choice of system for this study. In this paper, we present experimental results that demonstrate again the displacement and the tag-along effects and permit the measurement of the sample size dependence of the production rates and recovery yields of the two enantiomers for a specified purity on the sample size. A comparison between the performance of touching and overlapping bands is possible.

DEFINITIONS

For the sake of clarity and continuity [18–20,33], we have found it useful to summarize here the definitions of the main optimization parameters as stated previously [18]. These definitions are those used in this paper.

Purity

The purity, Pu, of a component i in the presence of a component j is

$$Pu_i = n_i/(n_i + n_j) \tag{1}$$

where n_i and n_j are the amounts of components i and j in the collected fraction, respectively.

Recovery yield

The recovery yield, R_i, of a component i is

$$R_i = n_i/n_{i,\text{tot}} \tag{2}$$

where n_i is the amount of a component i collected in the purified fraction and $n_{i,\text{tot}}$ is the total amount of this component i injected with the sample. It is assumed that all the solute injected is eluted. Detector calibration proved that this is true within the accuracy of the determination of peak areas. This accuracy, in turn, is limited by the influence of the signal noise on the end-time of the integration of the tail of the second-component peak.

Cycle time

The cycle time, t_c, is the time which separates two consecutive injections. It is usually arbitrarily defined, either as the corrected analytical retention time of the second component, $t_{R,0} - t_0$ [18–20], or as the difference between the time when the first

component concentration exceeds a certain threshold and the time when the second component concentration decreases below the threshold value [10,13,27,33].

Production rate

The production rate, *Pr*, is the amount of a component *i* collected in the fraction at the specified purity per unit time:

$$Pr_i = n_i/t_c \quad (3)$$

Relative production rate

The relative production rate is the production rate of one component relative to its production rate in the case of touching bands.

EXPERIMENTAL

Equipment

A modular chromatograph was assembled, consisting of a Waters (Milford, MA, USA) Model 510 pump, a Waters Gradient Controller, a Scientific Systems (State College, PA, USA), LP-21 pulse damper, a Valco Electric (Houston, TX, USA) injector with a 50-μl injection loop, a Spectroflow Model 757 UV detector (Kratos Analytical, Ramsey, NJ, USA) and a Spectra-Physics (San Jose, CA, USA) integrator with a Labnet Data Acquisition Card hooked up to an IBM (Boca Raton, FL, USA) AT computer. The fractions in the mixed bands region were collected with a Gilson (Middleton, WI, USA) Model 203 fraction collector and analyzed on an HP 1090 liquid chromatograph (Hewlett-Packard, Palo Alto, CA, USA) equipped with a diode-array UV–VIS detector and a computer data acquisition system.

Materials

Column. The column dimensions were 150 mm × 4.6 mm I.D. The capacity factors under linear conditions were $k'_L = 3.42$ and $k'_D = 4.75$, giving a selectivity $\alpha = 1.39$. At a flow rate of 1 ml/min, the void time was 1.86 min, and the column efficiency was 1000 plates for both enantiomers.

Stationary phase. A quaternary ammonium anion-exchange stationary phase (301TPB-10; Vydac, Hesperia, CA) with an average particle size of 10 μm and an average pore size of 30 nm was used.

Chemicals. DL-Mandelic acid, D-mandelic acid, L-mandelic acid, and bovine serum albumin (BSA) (No. A-7638) were purchased from Sigma (St. Louis, MO, USA) and used without further purification.

Mobile phase. For the elution profiles, the mobile phase was 50 m*M* aqueous sodium phosphate buffer (pH 6.3) and for the pumping of BSA onto the column the mobile phase was a 10 m*M* aqueous phosphate buffer (pH 6.8).

Procedures

The BSA was affixed in the column by pumping a 1 mg/ml BSA solution in 10 m*M* phosphate buffer (pH 6.8) onto the column until the BSA breakthrough was detected. The amount of BSA loaded in the column was calculated from the breakthrough curve and was 176 mg. Before the enantiomeric separations were undertaken, the column was equilibrated with 50 m*M* phosphate buffer (pH 6.3) for 75 column volumes. Elution of BSA at this pH was negligible.

Two sets of elution profiles were determined. First, samples of increasing amounts of the racemic mixture (sample size 1.6–25.6 μg, increasing in proportions 1, 2, 4, 8 and 16) were injected in order to investigate the effects of the competitive behavior of the enantiomers. The profiles obtained are shown in Figs. 1–3. Second, the pure isomers were injected separately, each in the same amount as before, in order to compare the band profiles obtained under non-competitive with competitive conditions. The elution profiles of the racemic mixtures and the pure enantiomers were converted by direct calibration of the detector response to concentration profiles. At the wavelength used, 250 nm, the calibration graphs were linear and the regressions were carried out using a standard procedure.

For the higher concentration injections (Figs. 1c, 2 and 3), the chromatograms exhibit overlapping bands. In order to determine accurately the individual band profiles, fractions in the mixed bands region were collected and reinjected under linear conditions for quantitative analysis. This procedure permits the exact determination of the concentration of each enantiomer. The interval for collection was one fraction every 6 s, *i.e.*, the limit frequency of the model fraction collector employed. The mixed zone was 7.65–8.15 min for Figure 1c (six fractions),

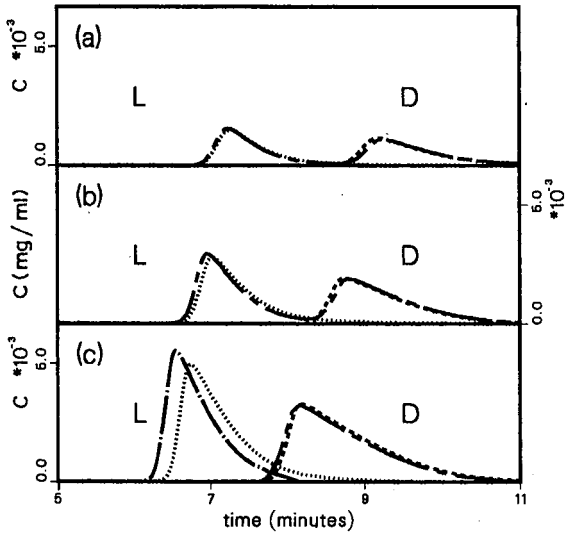

Fig. 1. Comparison between the elution profiles of the enantiomers of DL-mandelic acid with competition, (1) L-isomer (– · – · –) and (2) D-isomer (————); and without competition, (3) L-isomer (.....) and (4) D-isomer (--------). (a)Experimental conditions: stationary phase, BSA ionically immobilized on anion exchanger; mobile phase, 50 m*M* phosphate buffer (pH 6.3); flow-rate, 1 ml/min; sample size, (1) 0.80, (2) 0.80, (3) 0.80 and (4) 0.80 μg. (b) Same conditions as for (a) except twice the sample size: (1) 1.6, (2) 1.6, (3) 1.6 and (4) 1.6 μg. (c) Same conditions as for (a), except four times the sample size: (1) 3.2, (2) 3.2, (3) 3.2 and (4) 3.2 μg.

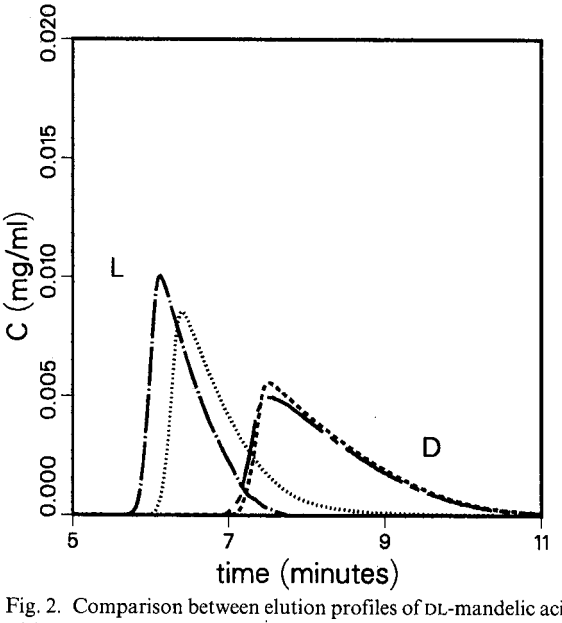

Fig. 2. Comparison between elution profiles of DL-mandelic acid with competition. Same experimental conditions as for Fig. 1a, except eight times the sample size: (1) 6.3, (2) 6.3, (3) 6.4 and (4) 6.4 μg.

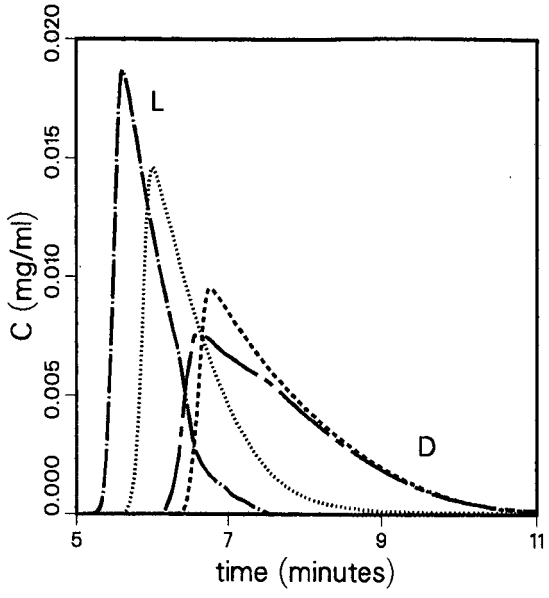

Fig. 3. Comparison between elution profiles of DL-mandelic acid with competition. Same experimental conditions as for Fig. 1a, except sixteen times the sample size: (1) 12.7, (2) 12.7, (3) 12.8 and (4) 12.9 μg.

6.95–7.75 min for Fig. 2 (nine fractions) and 6.15–7.55 min for Fig. 3 (fifteen fractions). In Fig. 1b, the mixed zone was too dilute to collect fractions and analyze them. In Fig. 1a, no mixed zone existed because of the touching bands condition. In order to integrate accurately the area underneath the band profiles to determine the cut points for specified purities, points between collected fractions were linearly interpolated at 1-s intervals.

RESULTS AND DISCUSSION

If an organic synthesis produces a racemate which later must be separated, the ratio of the enantiomers is 1:1. Although stereoselective synthesis may produce mixtures considerably enriched in one of the enantiomers, the racemic mixture remains the most important one to study.

Band profiles

In Figs. 1–3, a series of chromatograms of DL-mandelic acid are illustrated, demonstrating both the displacement and the tag-along effects [7,15,34] by overlaying the elution profiles obtained from the racemic mixture, *i.e.*, under competitive conditions

(solid lines), and the elution profiles obtained from the pure enantiomers (dashed lines), *i.e.*, under non-competitive conditions. The series of chromatograms differ only in the amounts injected (more precisely, in the sample concentrations). In Fig. 1a, the touching bands situation occurs, and the agreement between the chromatogram of the racemate and the chromatograms of the pure enantiomers is very good, *i.e.*, within experimental error, much as in analytical chromatography. From Figs. 1–3, the sample sizes increase in the proportions 1, 2, 4, 8 and 16. As the amount increases, the non-linear effects intensify, in addition to the consequences of the competition for adsorption between molecules of the enantiomers. In such a mixture, however, the displacement effect is more visible than the tag-along effect, although both are present (*e.g.*, Fig. 3).

Given a defined system, the degree to which the tag-along and displacement effects contribute to the distortion of the band profiles of the racemic mixture depends solely on the sample concentration. The higher this concentration the greater is the band overlap observed. For the displacement effect, the sharp front and diffuse rear of the less retained component, the L-isomer, elutes before what is predicted by the elution profile of injection of pure L-mandelic acid. Also, a slight enrichment of the peak maxima is observed. Both effects are seen as early as in Fig. 1b, where the degree of band interference of the elution chromatogram is insignificant. Of course, this observation translates the fact that the bands have severely interfered during part of their migration along the column. Thus, in Fig. 1b and c, although the bands appear to be fairly well resolved with nearly a baseline separation, the memory effects of the displacement are still present. For the tag-along effect, the front of the more retained component, the D-isomer, elutes prior to the time predicted by the injection of the pure D-mandelic acid, and the maximum of the peak is lower and flatter than expected. These consequences of the tag-along effect are seen only in Figs. 2 and 3. As predicted [34], the diffuse rear of the profile of the D-isomer under competition coincides exactly with that of the non-competitive, pure injection of the D-isomer.

The band profiles of the pure enantiomers exhibit quasi-Langmuirian behavior which allows the assumption that the mixed band region follows similar behavior under competitive conditions. Fraction collection has been shown to be a viable means for determining the concentrations of the two enantiomers in the mixed zone of the chromatogram [15]. Following fraction collection and analysis, the mixed zones for Figs. 3–5 are calculated and behave as expected. Consequently, the method of Knox and Pyper [2] and the method of Golshan-Shirazi and Guiochon [18,19,22,23] are implemented as guidelines. The former method employs no competition for adsorption between components and is useful only in the touching bands case (Fig. 1a), whereas the latter includes competition and is useful in all cases, whether the bands are resolved or overlap (Figs. 1b, 1c, 2 and 3).

Production rate and recovery yield

The data associated with Figs. 1–3 concerning the recovery yields (Fig. 4) and the relative production rates (Fig. 5) are listed in Table I. The relative production rate was calculated rather than an absolute quantity as the experimental conditions can fluctuate. The cycle time, usually arbitrarily set, is constant for the five injections and therefore does not have to be established exactly because of the calculation of a relative production rate. The relative production rates are calculated by discarding any intermediate fractions, *i.e.*, the fraction collected between cut times in Figs. 1c, 2 and 3 is not recycled.

The cut times are the starting and stopping points for the collection of fractions of purified components of the L- and D-isomers, respectively. For the first component, the L-isomer, the fraction is collect-

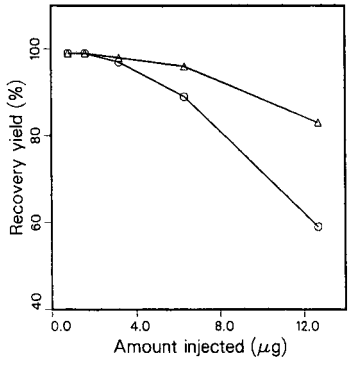

Fig. 4. Variation of the recovery yield with the amount injected for (△) the L-isomer and (○) the D-isomer. See Table I for calculated values.

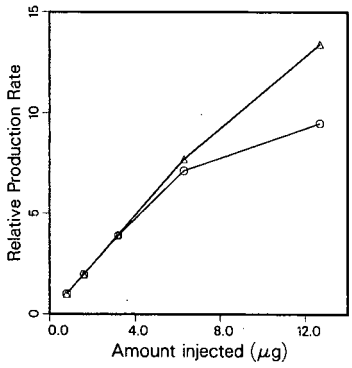

Fig. 5. Variation of the relative production rate with the amount injected for (△) the L-isomer and (○) the D-isomer. See Table I for calculated values.

ed from the start of the elution profile up to the cut time, and for the second component, the D-isomer, the fraction is collected from the second cut time to the end of the elution profile. In Fig. 1a and b, only one cut is necessary to achieve the desired purity and a 100% recovery yield is achieved. Also, although recovery yields and production rates for lower product purities could be calculated easily, only a purity of 99% has been applied to all five instances, for the sake of simplicity in the comparison.

Fig. 4 shows that the recovery yield remains constant and is unity until past the conditions corresponding to touching bands (conditions of Fig. 1c). As long as the purity of each fraction is within specifications, the yield is unity. The recovery yields for the L-isomer (the first eluted) are always better than those for the D-isomer. The yields of the two components remain acceptable up to the conditions corresponding to Fig. 2 (89 and 96%). As long as the recovery yields are high, the production rate increases in proportion to the sample amount (Fig. 5), then it tends to level off. It is important to observe that even under the conditions of Fig. 3, where the two bands are not resolved and an analyst would conclude that there is an excessive degree of overload (rightly so for analytical purposes, wrongly for preparative purposes), the production rate for the L-isomer is far from its maximum.

Comparing Figs. 4 and 5 or the corresponding columns in Table I, one can see that a point of diminishing return is reached when the recovery yield drops below *ca.* 90%. This is clearer with the second-component data, because the phenomenon takes place at lower sample amounts for the second than for the first component. When the recovery yield drops from 99 to 89%, the production rate of the second component increases sevenfold. When the yield decreases further, from 89 to 59%, the production rate increases by only 33%. In practice, the conditions in Fig. 2 are close to the optimum for the production of the second component and those in Fig. 3 for the production of the first component.

These results confirm that the choice of the optimum production rate depends on the recovery yield that is deemed satisfactory. If the starting product (feedstock) is plentiful and can be wasted, then low recovery yields are acceptable, allowing higher production rates (conditions in Fig. 3 or even higher loading). On the other hand, expensive pharmaceuticals may require nearly 100% recovery yields, resulting in lower production rates (conditions in Fig. 1c or 2). The recovery yields (Fig. 4) and relative production rates (Fig. 5) for the L-isomer (first eluted) are better than those for the D-isomer. For the purpose of highest recovery yields and production rates, the displacement effect on the first component is highly desirable while the tag-along effect on the second component is detrimental. The choice of the chiral phase used must be made according to the enantiomer of preference.

One drawback of a stationary phase involving the immobilization of a protein is the poor efficiency exhibited by the column. The reduced plate height of

TABLE I

RELATIVE PRODUCTION RATES AND RECOVERY YIELDS FOR 99% PURE ENANTIOMER FRACTIONS

Fig.	Enantiomer	Cut time (min)	Recovery yield (%)	Relative production rate
1a	L	8.60	99+	1.00
	D	8.60	99+	1.00
1b	L	8.27	99	1.97
	D	8.27	99	1.97
1c	L	7.80	98	3.94
	D	7.90	97	3.89
2	L	7.18	96	7.70
	D	7.47	89	7.12
3	L	6.31	83	13.4
	D	7.23	59	9.47

15 is high and the low column efficiency limits the range of sample amounts that can usefully be investigated. However, the separation factor is large (α = 1.4) and the column efficiency (*ca.* 1000 theoretical plates) exceeds the value that would correspond to the optimum for maximum production rate [19,22,33].

CONCLUSIONS

The experimental results reported here are in qualitative agreement with the theoretical conclusions published previously [18,19]. The following conclusions are of practical importance. The recovery yield and the production rate achieved with the less retained enantiomer are higher than with the more retained enantiomer. Depending on which isomer is most strongly needed, a chiral selective stationary phase or its antipode should be selected, whenever possible. In order to perform a preparative separation and purification of a two-component mixture, *e.g.*, a racemic mixture, a decision as to what are acceptable losses in order to achieve the greatest amount of the pure compound(s) desired must be made. If some losses and interfering bands are permitted, the cut points must be established from the competitive, not the non-competitive chromatogram, otherwise, undesirable results are obtained. Overlapping conditions, with apparently total loss of resolution (in the analytical sense) permit a dramatic increase in the production rate (up to tenfold or more, Fig. 5), provided a moderate recovery yield is acceptable.

As this order of magnitude increase in the production rate is achieved by merely increasing the sample amount, all the cost components remain constant. Therefore, the cost of the extraction or purification is divided by the same amount. Major economic losses are thus incurred by those who persist in ignoring the basic results of non-linear chromatography.

ACKNOWLEDGEMENTS

The gift of the anion-exchange stationary phase by Vydac is gratefully appreciated. This work was supported in part by grant CHE-8901382 from the National Science Foundation and by the cooperative agreement between the University of Tennessee and the Oak Ridge National Laboratory. We acknowledge the continuing support of our computational effort by the University of Tennessee Computing Center.

REFERENCES

1 M. Verzele and C. Dewaele, *Preparative High Performance Liquid Chromatography*, TEC, Ghent, 1986.
2 J. H. Knox and H. M. Pyper, *J. Chromatogr.*, 363 (1986) 1.
3 J. Newburger, L. Liebes, H. Colin and G. Guiochon, *Sep. Sci. Technol.*, 22 (1987) 1933.
4 M. W. Phillips, G. Subramanian and S. M. Cramer, *J. Chromatogr.*, 454 (1988) 1.
5 A. J. Howard, G. Carta and C. H. Byers, *Ind. Eng. Chem. Res.*, 27 (1988) 1873.
6 G. Guiochon, S. Golshan-Shirazi and A. Jaulmes, *Anal. Chem.*, 60 (1988) 1856.
7 G. Guiochon and S. Ghodbane, *J. Phys. Chem.*, 92 (1988) 3682.
8 S. Golshan-Shirazi, B. C. Lin and G. Guiochon, *J. Phys. Chem.*, 93 (1989) 6871.
9 Q. Yu and N.-H. L. Wang, *Comput. Chem. Eng.*, 13 (1989) 915.
10 A. Katti and G. Guiochon, *Anal. Chem.*, 61 (1989) 982.
11 M. Czok and G. Guiochon, *Anal. Chem.*, 62 (1990) 189.
12 S. Golshan-Shirazi and G. Guiochon, *Anal. Chem.*, 60 (1988) 2634.
13 A. M. Katti and G. Guiochon, *J. Chromatogr.*, 499 (1990) 21.
14 A. M. Katti, Z. Ma and G. Guiochon, *AICh J.*, 36 (1990) 1722.
15 S. Jacobson, S. Golshan-Shirazi and G. Guiochon, *J. Am. Chem. Soc.*, 112 (1990) 6492.
16 M. Z. El Fallah and G. Guiochon, *Anal. Chem.*, 63 (1991) 859.
17 L. R. Snyder, G. B. Cox and P. E. Antle, *Chromatographia*, 24 (1987) 82.
18 S. Golshan-Shirazi and G. Guiochon, *Anal. Chem.*, 61 (1989) 1276.
19 S. Golshan-Shirazi and G. Guiochon, *Anal. Chem.*, 61 (1989) 1368.
20 S. Golshan-Shirazi and G. Guiochon, *Am. Biol. Lab.*, 8, No. 8 (1990) 26.
21 L. R. Snyder, J. Dolan and G. B. Cox, *J. Chromatogr.*, 484 (1989).
22 S. Golshan-Shirazi and G. Guiochon, *J. Chromatogr.*, 536 (1991) 57.
23 S. Golshan-Shirazi and G. Guiochon, *J. Chromatogr.*, 523 (1990) 1.
24 L. R. Snyder, J. Dolan and G. B. Cox, *J. Chromatogr.*, 523 (1990) 11.
25 L. R. Snyder, J. Dolan and G. B. Cox, *J. Chromatogr.*, 484 (1989).
26 J. Newburger and G. Guiochon, *J. Chromatogr.*, 523 (1990) 63.
27 S. Ghodbane and G. Guiochon, *J. Chromatogr.*, 444 (1988) 275.
28 D. W. Armstrong and S. M. Han, *CRC Crit. Rev. Anal. Chem.*, 19 (1988) 175.
29 W. H. Pirkle and T. C. Pochapsky, *Chem. Rev.*, 89 (1989) 347.

30 S. Allenmark, B. Bomgren and H. Boren, *J. Chromatogr.*, 237 (1982) 473.
31 P. Erlandsson, L. Hansson and R. Isaksson, *J. Chromatogr.*, 370 (1986) 475.
32 S. Andersson, S. Allenmark, P. Erlandsson and S. Nilsson, *J. Chromatogr.*, 498 (1990) 81.
33 A. M. Katti, E. Dose and G. Guiochon, *J. Chromatogr.*, 540 (1991) 1.
34 S. Golshan-Shirazi and G. Guiochon, *J. Phys. Chem.*, 94 (1989) 4143.

Journal of Chromatography, 590 (1992) 127–132
Elsevier Science Publishers B.V., Amsterdam

CHROMSYMP. 2445

Application of preparative liquid chromatography to the isolation of enantiomers of a benzodiazepinone derivative

Anita Katti*,☆, Per Erlandsson☆☆ and Richard Däppen

Central Analytical Department, Ciba-Geigy Ltd, CH-4002 Basle (Switzerland)

ABSTRACT

The isolation of milligram amounts of the enantiomers of a benzodiazepinone derivative was performed on an analytical cellulose tribenzoate-based column by multiple repetitive injections. An enantiomeric purity greater than 98% was required. First, an analytical method was developed to maximize the resolution by adjusting the mobile phase composition, flow-rate and most importantly the column temperature. Then the preparative separation was optimized by adjusting the sample size and detecting the sample where its UV absorbance was low. The locations of the cut points were determined by use of detector response levels. The method development, preparative separations and analytical assays of the fractions obtained were all performed on analytical columns.

INTRODUCTION

There are added complications in the preparative chromatography of chiral compounds compared with other small molecules because of the higher cost of the packing material, the large number of chiral packing materials, the low loadability of chiral columns [1], the strong temperature dependences [2,3] and often the limited choice of compatible mobile phases. Low loadability is typically due to limited ligand-binding capacities. Temperature increases can accelerate the kinetics of mass transfer but, depending on the combined effect of chiral selectivity and chromatographic efficiency, the resolution may increase or decrease [4].

There are three primary approaches to isolating milligram amounts of substances in elution chromatography: (1) employ an analytical column, typically 25 cm × 4.6 mm I.D. packed with 5- or 10-μm material, and perform hundreds of repetitive injections to isolate the compounds of interest [5]; (2) employ a large column, typically 25 cm × 2 cm I.D. packed with 10–20-μm particles, and make only a few injections to isolate the desired amount [6,7]; or (3) employ medium-pressure technology using columns packed with 40–60-μm materials and in one or two runs to isolate the desired amount of substance at the desired purity [8,9]. For each of these approaches there is a trade-off between the cost of the packing material, the cost of the preparative chromatograph, the time to perform the separation and in some instances the time required to make large amounts of stationary phase together with packing and testing columns. For approaches (2) and (3) a method is also required to determine the purity of the collected fractions. The first approach will consume the smallest amount of solute during method development and will minimize the loss of solute due to unforseen effects such as irreversible adsorption. In this work, the first approach was used in view of the availability of automated analytical equipment, good stability of the column packing material, the high cost of large columns and the amount of solute available.

Theoretical models have been used to predict overloaded elution profiles for several chiral systems with extremely high accuracy [10]. Several op-

* Present address: Mallinckrodt Specialty Chemicals, St. Louis, MO 63147, USA.
** Present address: Svensk Oljeextraktion AB, P.O. Box 3, S-374 21 Karlshamn, Sweden.

0021-9673/92/$05.00

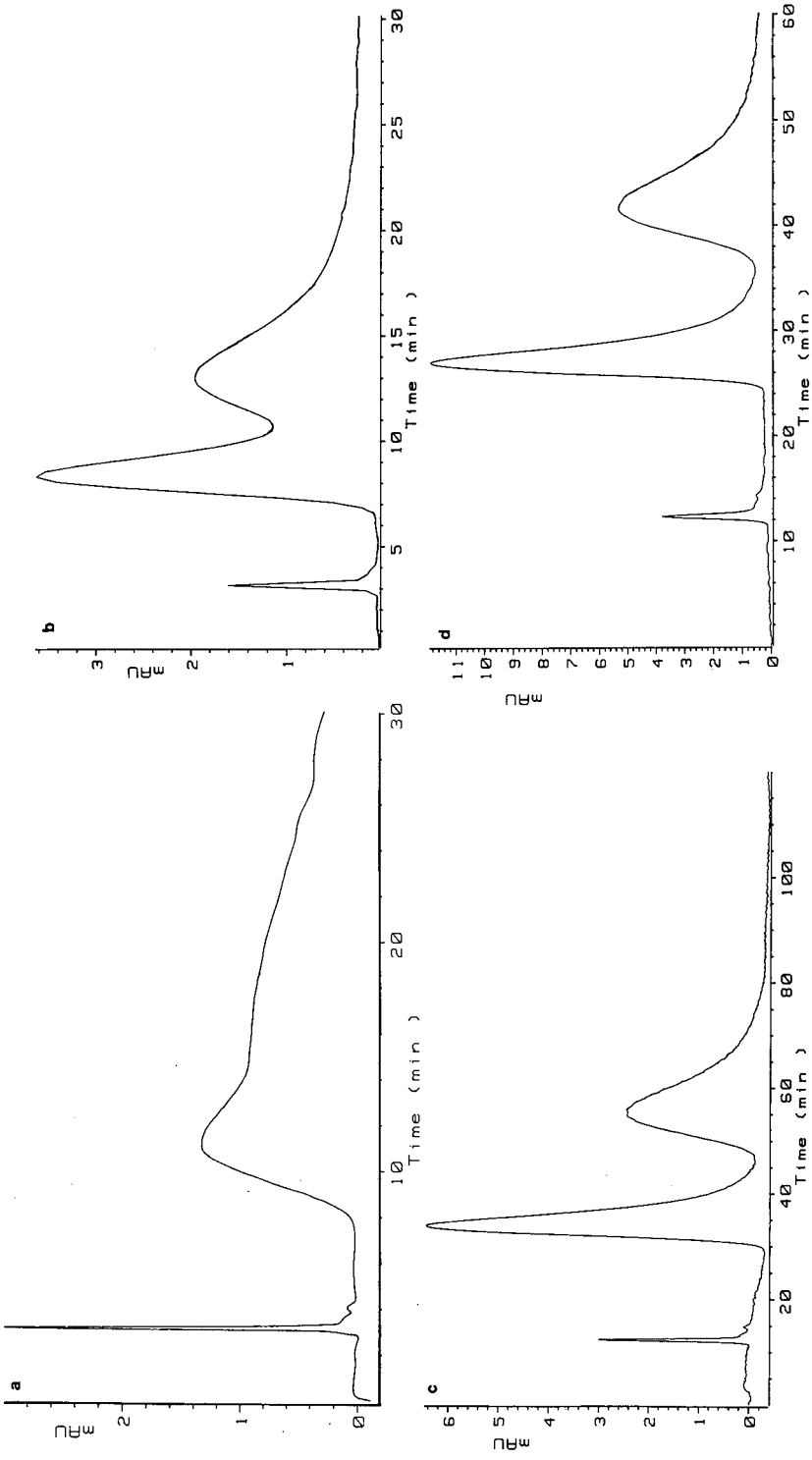

Fig. 1. Optimization of the analytical method, 1.0 μg of the solute in 10 μl of *n*-hexane–2-propanol (50:50, v/v) was injected on to the column in the Hewlett-Packard LC system. UV detection at 230 nm. (a) Flow-rate 1.0 ml/min, 22°C, *n*-hexane–2-propanol (50:50, v/v); (b) flow-rate 1.0 ml/min, 40°C, *n*-hexane–2-propanol (50:50, v/v); (c) flow-rate 0.25 ml/min, 40°C, *n*-hexane–2-propanol (50:50, v/v); (d) flow-rate 0.25 ml/min, 45°C, *n*-hexane–2-propanol (40:60, v/v).

timization theories have been presented with different assumptions [11–13]. The application of some of these concepts is considered in this paper.

This paper illustrates a practical example of the optimization of the experimental conditions for the isolation of a pair of enantiomers. First an analytical method was developed in order to improve the resolution by adjusting the eluent composition, the flow-rate and the temperature. Then the production rate was increased and optimized by increasing the sample size.

EXPERIMENTAL

Analytical system

Both analytical and preparative separations were performed on a Chiralcel OB 250 × 4.6 mm I.D. column obtained from Daicel Chemical Industries (Tokyo, Japan). This chiral column contains cellulose tribenzoate coated on 10-μm silica. Two 250 × 4.6 mm I.D. Chiracel OB columns were employed, one for the preparative purification and one for the analytical work. The chromatographic set-up for analytical method development consisted of a Hewlett-Packard (Waldbronn, Germany) Model 1090 M liquid chromatograph equipped with a ternary solvent delivery system and a diode-array detector, all controlled by a Hewlett-Packard ChemStation. Some analytical experiments were also performed on the preparative Kontron system (see below) which was replumbed for analytical purposes.

Preparative system

A Kontron (Zürich, Switzerland) MT2 data acquisition system was employed to control a Kontron Model 420 high-performance liquid chromatographic (HPLC) pump and a Model 425 low-pressure gradient former. The outlet of the pump was connected to a Valco (Houston, TX, USA) six-port pneumatic valve, then to the Chiracel OB column placed in a column thermostat from Hengeler Analytik-Instrumente (Riehen, Switzerland) maintained at 40°C. The column outlet was connected to a Kratos (Ramsey, NJ, USA) Spectroflow 783 UV detector and then to the second six-port valve on the Gilson (Villier Le Bel, France) Model 232/401 sample processor [14]. Repetitive large-volume injections for the preparative isolations were made by sending a sequence of ASCII codes [15] from the Kontron data system to a Hamilton (Bonaduz, Switzerland) Microlab M dispenser which aspirated and dispensed the sample into the loop of the Valco valve. The position of the Valco valve was controlled by contact closures.

The equipment used is specified in the figure captions as either Hewlett-Packard LC or Kontron LC. The collected fractions were evaporated to dryness in a Büchi (Flawil, Switzerland) Rotavapor RE. Resolutions (R_s), separation factors (α) and capacity factors (k') were calculated as described previously [16]. Reduced plate heights (h) were calculated using the peak width at the baseline. The column void volume was determined by injecting 20 μg of 1,3,5-tri-*tert.*-butylbenzene in 20 μl of *n*-hexane–2-propanol (95:5, v/v) using *n*-hexane–2-propanol (90:10, v/v) as the mobile phase at flow-rate of 1.0 ml/min at *ca.* 22°C.

Chemicals

1,3,5-Tri-*tert.*-butylbenzene was purchased from Aldrich-Chemie (Steinheim, Germany) and HPLC-grade *n*-hexane and 2-propanol from Fluka (Buchs, Switzerland) and used as received. The racemic benzodiazepinone derivative was obtained as a research sample from Ciba-Geigy (Basle, Switzerland).

RESULTS AND DISCUSSION

There are a large number of chiral stationary phases prepared by adsorption of cellulose derivatives on macroporous silica supports [17]. These phases shows good peak symmetry and efficiency; additionally, relative high loading capacities have been reported [18]. Therefore, the commercial columns selected for this work were those packed with cellulose tribenzoate coated on macroporous silica.

The selection of eluents was limited as only *n*-hexane modified with 2-propanol or ethanol was recommended. Moreover, relatively small changes, such as changing the eluent modifier from 2-propanol to ethanol or methanol, cause irreversible changes in the retention characteristic of the column. The mobile phase composition was optimized by testing eluents of increasing concentration of 2-propanol. The retention of the solute was observed to decrease with increasing amount of 2-propanol in the mobile phase.

The flow-rate and temperature were optimized

TABLE I

SUMMARY OF CHROMATOGRAPHIC DATA

1.0 mg of the solute in 10 ml of *n*-hexane–2-propanol (50:50, v/v) was injected on to the column in the Hewlett-Packard LC system. UV detection at 230 nm.

n-Hexane–2-propanol (v/v)	Flow-rate (ml/min)	Temperature (°C)	k'_1	a	R_s	h_1	h_2	Fig.
50:50	1.0	22	2.8	1.8	<0.4	>1000	>2000	1a
50:50	1.0	40	1.9	1.9	0.7	320	950	1b
50:50	0.5	40	1.8	1.9	1.2	140	340	
50:50	0.25	40	1.9	2.0	1.5	98	210	1c
40:60	0.25	40	1.5	2.0	1.5	87	180	
40:60	0.25	45	1.3	2.0	1.6	57	140	1d

consecutively. Fig. 1 illustrates selective chromatograms obtained during the optimization of these two parameters. Fig. 1a shows the separation of the racemic mixture under analytical conditions, 1.0 μg of sample in 10 μl of *n*-hexane–2-propanol (50:50, v/v) at room temperature (*ca.* 22°C) at a flow-rate of 1 ml/min. On increasing the temperature to 40°C, holding all other parameters constant, the selectivity was hardly affected and the apparent column efficiency increased (Fig. 1b). In order to increase further the column efficiency and thus the resolution, the flow-rate was reduced to 0.25 ml/min. Lastly, the conditions which resulted in the highest resolution (1.6) were *n*-hexane–2-propanol (40:60, v/v) at a flow-rate of 0.25 ml/min and 45°C (Fig. 1d). The chromatographic data describing these analytical results are summarized in Table I.

According to the manufacturer, the maximum operating temperature was 40°C; therefore, in order to minimize degradation of the column under conditions of large sample sizes, all the preparative operations were run at 40°C. The analytical separation factor under these conditions was 1.9–2.0. In order to increase the production rate, the sample size was increased by increasing the injection volume at a constant sample concentration of 0.5 mg/ml. Fig. 2 illustrates the chromatograms obtained at sample sizes of 0.5, 0.75 and 1 mg; however, in order to prevent detector saturation, the wavelengths monitored were 230, 295 and 300 nm, respectively. In view of the high purity requirements and in an effort to complete the isolation without recycling or reprocessing the collected fractions, the sample size chosen was 0.75 mg per injection.

The fraction cuts were made on the basis of the detector response levels, rather than time. Therefore, if degradation of the separation or shifts in retention time occurred, the purity of the fractions could be maintained. Fig. 3 illustrates the cut points. The solid vertical lines indicate the location of hard cuts, made on a time basis at 17 and 79 min. The horizontal line indicates the detector response cut-off level, which was made at 900 mV. Between 17 and 79 min when the detector response increased above 900 mV or dropped below 900 mV, a contact closure signal was sent to the sample processor,

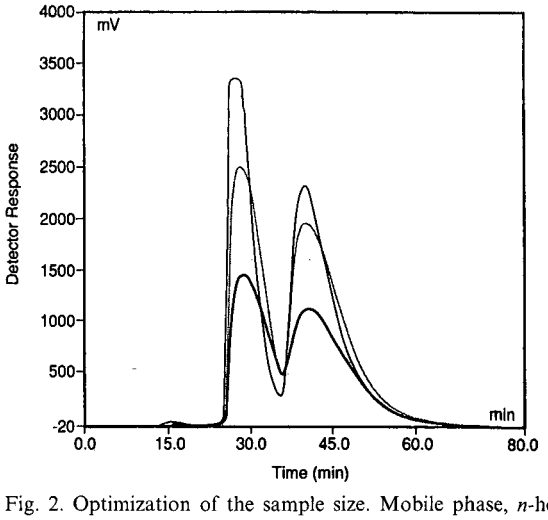

Fig. 2. Optimization of the sample size. Mobile phase, *n*-hexane–2-propanol (40:60, v/v); flow-rate, 0.25 ml/min; solute concentration, 0.5 mg/ml; Kontron LC system. Injection volume: thin solid line, 1.0 ml; dotted line, 1.5 ml; thick solid line, 2.0 ml. Detection wavelength: thin solid line, 230 nm; dotted line, 295 nm; thick solid line, 300 nm.

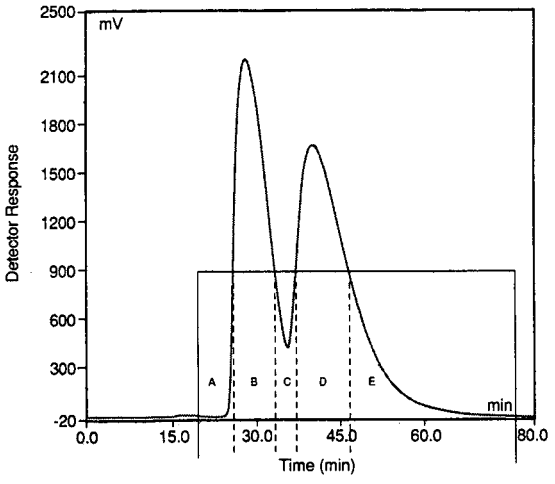

Fig. 3. Preparative chromatogram with cut points. Flow-rate, 0.25 ml/min; mobile phase, *n*-hexane–2-propanol (40:60, v/v); temperature, 40°C; UV detection at 295 nm; injection volume 1.5 ml; solute concentration, 0.5 mg/ml; Kontron LC system.

causing the fraction to be collected in the next free vessel. The dashed vertical lines indicate the expected location of the cuts taking into account the dead volume the solvent traverses between the detector outlet and the free vessel.

Reproducibility of the preparative chromatograms over a 2-day period including a change of sample solution is shown in Fig. 4. Excellent reproducibility was observed. Despite covering the sample, slight increases in the amount injected were observed owing to evaporation of the sample solvent over time.

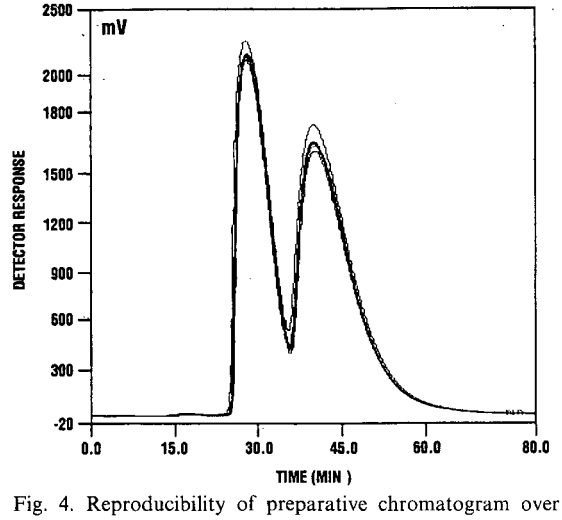

Fig. 4. Reproducibility of preparative chromatogram over 2 days. Experimental conditions as Fig. 3.

Analysis of the fractions gave the following results. Fraction A contained a negligible amount of the early-eluting enantiomer. Fraction B was collected at >99% enantiomeric purity. Fraction C was a mixture of both enantiomers. Fraction D contained about 7% and fraction E 5% of the early-eluting enantiomer. Fig. 5 shows the chromatogram of fraction B (dashed line) overlayed with the chromatogram of fraction D (solid line).

After 7 days of continuous operation, 17 mg of the first-eluting enantiomer were obtained at the purity required. However, in order to increase the purity of the later eluting enantiomers, fractions D and E were mixed, concentrated and reprocessed. This second preparative step was performed under the same experimental conditions as the first step. Fig. 6 shows a preparative chromatogram where 0.75 mg of total sample per run was injected. Similarly, cuts were made on the basis of detector response levels, 800 mV. The inset in Fig. 6 shows the analysis after fractions B2 and C2 had been mixed. The enantiomeric purity of the later eluting enantiomer was 98% and 19 mg were obtained. The second chromatographic step needed about 100 h of continuous operation.

When the analysis of the fractions were performed on a second chromatograph simultaneously with the preparative separations, the whole project, including method development, preparative chromatography and assay of fractions, was accomplished in 3 weeks.

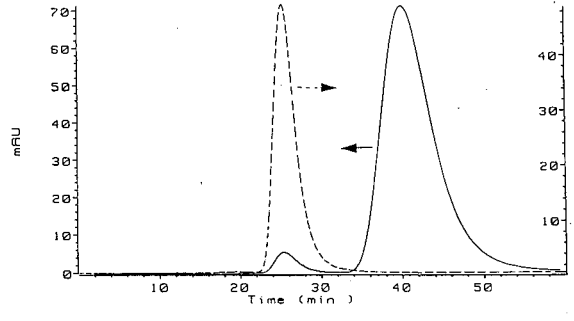

Fig. 5. Test of enantiomeric purity by analysis of the fractions. Mobile phase, *n*-hexane–2-propanol (40:60, v/v); flow-rate, 0.25 ml/min; temperature, 45°C; UV-detection at 230 nm; Hewlett-Packard LC system. Dashed line, fraction B; solid line, fraction D.

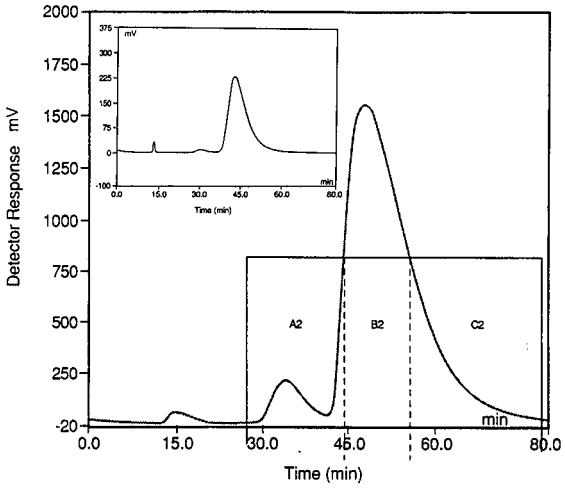

Fig. 6. Preparative chromatogram, second step. Experimental conditions as Fig. 3. Inset: test of enantiomeric purity for the second pass, fraction B2 + C2. Experimental conditions as Fig. 5, except temperature 40°C, but on the Kontron analytical system.

To achieve the isolation with a single preparative injection, assuming the same linear velocity, column length, particle size and chromatographic efficiency, we would have needed a 3.8 cm diameter column.

REFERENCES

1 P. Erlandsson, L. Hansson and R. Isaksson, *J. Chromatogr.*, 370 (1986) 475.
2 F. Antia and Cs. Horváth, *J. Chromatogr.*, 435 (1988) 1.
3 S. Allenmark, *Chromatographic Enantioseparation: Methods and Applications*, Ellis Horwood, Chichester, 1988, Ch. 5, pp. 70–72.
4 R. Isaksson, P. Erlandsson, L. Hansson, A. Holmberg and S. Berner, *J. Chromatogr.*, 498 (1990) 257.
5 A. Katti, *Chromatographia*, 25 (1992) in press.
6 J. Newburger and G. Guiochon, *J. Chromatogr.*, 523 (1990) 63.
7 E. P. Kroeff, R. A. Owens, E. L. Cambell, R. D. Johnson and H. I. Marks, *J. Chromatogr.*, 461 (1989) 45.
8 G. K. Sofer and L. E. Nystrom, *Process Chromatography, a Practical Guide*, Wiley, New York, 1984.
9 W. H. Pirkle and R. W. Anderson, *J. Org. Chem.*, 39 (1974) 3901.
10 S. Jacobson, S. Golshan-Shirazi and G. Guiochon, *J. Am. Chem. Soc.*, 112 (1990) 6493.
11 S. Golshan-Shirazi and G. Guichon, *J. Chromatogr.*, 517 (1990) 229.
12 L. R. Snyder and G. B. Cox, *J. Chromatogr.*, 483 (1989) 85.
13 J. H. Knox and M. Pyper, *J. Chromatogr.*, 363 (1986) 1.
14 A. M. Katti and G. Guiochon, *Am. Lab.*, October (1989) 17.
15 A. Doppler, Kontron, Basle, personal communication.
16 L. R. Snyder and J. J. Kirkland, *Introduction to Modern Liquid Chromatography*, Wiley, New York, 1979, 2nd ed., Ch. 2, pp. 22–37.
17 Okamoto, M. Kawashima and K. Hatada, *J. Am. Chem. Soc.*, 106 (1984) 5357.
18 Y. Okamoto, M. Kawashima, R. Aburatani, K. Hatada, T. Nishiyama and M. Masuda, *Chem. Lett.*, (1986) 1237.

Journal of Chromatography, 590 (1992) 133–138
Elsevier Science Publishers B.V., Amsterdam

CHROMSYMP. 2467

Separation of *cis* and *trans* isomers from a mosquito repellent, CIC-4, via semi-preparative high-performance liquid chromatography and the repellent effect of each☆

J. David Warthen, Jr.*, Albert B. Demilo and Barbara A. Leonhardt

Insect Chemical Ecology Laboratory, Plant Sciences Institute, Agricultural Research Service, United States Department of Agriculture, 10 300 Baltimore Avenue, Beltsville, MD 20705-2350 (USA)

William R. Lusby

Insect Neurobiology and Hormone Laboratory, Plant Sciences Institute, Agricultural Research Service, United States Department of Agriculture, Beltsville, MD 20705 (USA)

E. David Devilbiss

Insect Chemical Ecology Laboratory, Plant Sciences Institute, Agricultural Research Service, United States Department of Agriculture, Beltsville, MD 20705 (USA)

Carl E. Schreck

Mosquito and Fly Research, Agricultural Research Service, United States Department of Agriculture, 1700 SW 23rd Drive, P.O. Box 14565, Gainesville, FL 32604 (USA)

ABSTRACT

CIC-4 (1,1,4,5,6,7,8,8*a*-octahydro-3H-2-benzopyran-3-one) is a fused bicyclic lactone which acts as a non-contact insect repellent for *Aedes aegypti* at 1% concentration in 95% aqueous ethanol when applied topically to rhesus monkeys. Chromatographic and spectroscopic analyses of a synthetic sample indicated the presence of *cis*- and *trans*-fused isomers. To supply each isomer for the assessment of mosquito repellent efficacy on humans, we developed a semi-preparative high-performance liquid chromatographic separation technique for the isomer separation. A column of 5-μm silica was used for isolating milligram quantities of each isomer. By this method, each isomer was obtained in >95% gas–liquid chromatographic (GLC)-purity for biological evaluation. Supporting GLC and electron impact and chemical ionization gas chromatography–mass spectrometric data are also presented for each isomer. Biological evaluation on the human arm using *Anopheles quadrimaculatus*, *Aedes aegypti*, and *Anopheles albimanus* as the test species was effective in determining relative repellency to the standard N,N-diethyl-3-methyl-benzamide.

INTRODUCTION

In 1959, Korte *et al.* [1] reported the synthesis of DL-iridomyrmecin [2] (Fig. 1), a natural insecticide isolated from the Argentine ant, *Iridomyrmex humilis* (Mayr). He also reported methods for synthesizing a variety of related bicyclic γ- and δ-lactones, some of which exhibited insecticidal properties. It was not until 1982, however, that the insecticidal properties of iridomyrmecin and some of the other bicyclic lactones were studied in more detail [3]. At that time, it was also found that this class of com-

☆ Mention of a commercial or proprietary product in this paper does not constitute a recommendation or endorsement of the product by the US Department of Agriculture.

0021-9673/92/$05.00

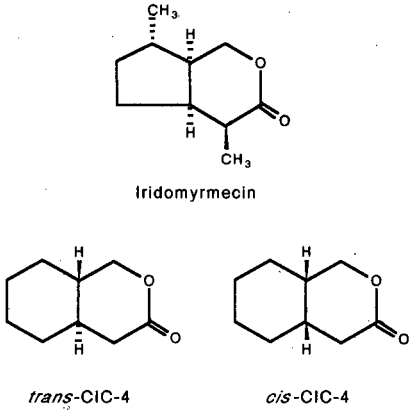

Fig. 1. Structures of iridomyrmecin, *trans*-CIC-4, and *cis*-CIC-4.

pounds demonstrated a non-contact insect repellent effect. Relatively long-lasting repellent compounds, having essentially no toxic effects on humans are in demand to prevent insect bites and disease transmission.

CIC-4 (1,1,4,5,6,7,8,8*a*-octahydro-3H-2-benzopyran-3-one) (Fig. 1) is one of these fused bicyclic δ-lactones which acts as a non-contact insect repellent. It proved effective against *Aedes aegypti* (L.) at 1% concentration in 95% aqueous ethanol when applied topically to rhesus monkeys; and was active at the same concentration against fire ants, fleas, and flies. The insect repellent properties of CIC-4 and iridomyrmecin are comparable in certain tests [3].

Since the synthesis of CIC-4 generates two geometric isomers (Fig. 1), and previous repellency data were reported for the CIC-4 mixture on monkeys [3], we felt it necessary to separate the isomers and evaluate each for efficacy on humans. We therefore report both the semi-preparative high-performance liquid chromatographic (HPLC) method for separating the geometric isomers and the repellent effects of the isomers for three species of mosquitoes: *Anopheles quadrimaculatus* Say, *Aedes aegypti*, and *Anopheles albimanus* Wiedemann.

EXPERIMENTAL

Materials and reagents

N,N-Diethyl-3-methylbenzamide (deet) was obtained from Virginia Chemicals (Portsmouth, VA, USA), and two lots of the CIC-4 mixture [containing about 1:1 isomers by gas–liquid chromatography (GLC)] were provided by Coulston (Alamagordo, NM, USA). UV-grade *n*-hexane was obtained from Baxter Burdick & Jackson (Muskegon, WI, USA), and reagent-grade anhydrous diethyl ether was obtained from Fisher Scientific (Fair Lawn, NJ, USA).

HPLC

An ALC-100 liquid chromatograph (equipped with two Model 6000A pumps and a U6K injector) was used for analytical HPLC; and a Delta Prep 3000 liquid chromatograph, both from Waters (Milford, MA, USA), was used for semi-preparative HPLC. Both instruments were controlled by an 840 data and chromatography control station (a Digital Professional 380 computer connected via two Systems Interface Modules). A Waters Model 440 absorbance detector with an extended wavelength module and a Waters Lambda-Max Model 481 LC Spectrophotometer, were used at 214 nm for UV absorbance detection for analytical and semi-preparative HPLC runs, respectively; fractions were collected manually. A 5-μm Hypersil, Shandon Southern Products (Chesshire, UK), stainless-steel column (23 × 0.43 cm I.D.) and a 5-μm silica, YMC (Morris Plains, NJ, USA), stainless-steel column (25 × 2.0 cm I.D.) were used for analytical and semi-preparative separations, respectively.

Samples for analytical HPLC were 5.0 mg of neat CIC-4, and samples for semi-preparative HPLC were 50 mg of CIC-4 in sufficient diethyl ether–*n*-hexane (15:85) to make 1.0 ml of solution.

Analytical HPLC required a flow-rate of 2.0 ml/min, and semi-preparative HPLC required a flow-rate of 30.0 ml/min; the eluent was diethyl ether–*n*-hexane (15:85, v/v).

GLC

Hewlett-Packard (Baltimore, MD, USA) 5880A and 5830A, and a Shimadzu GC-9A (Columbia, MD, USA) gas chromatograph, each equipped with a capillary injector system and a flame ionization detector, were used for GLC analyses. A Hewlett-Packard 5730A gas chromatograph, equipped with a flame ionization detector, was also used for GLC analyses. A Hewlett-Packard dimethyl silicone fused-silica capillary column (12 m × 0.2 mm I.D.)

was used on the 5880A; an Analabs (Norwalk, CT, USA) 3% butanediol adipate on Gas Chrom Q (100–120 mesh) packed column (12 ft. × 1/8 in. O.D.) was used on the 5730A; a Restek Corp. (Bellefonte, PA, USA) Stabilwax (15 m × 0.53 mm I.D.) was used on the 5830A; and Supelco, (Bellefonte, PA, USA) Supelcowax 10 (60 m × 0.25 mm I.D., 0.25 mm film thickness) and Supelco SPB 1701 (30 m × 0.25 mm I.D.) fused-silica capillary columns were used on the GC-9A gas chromatograph.

GC-mass spectrometry (MS)

Electron impact (EI)-MS were recorded on a Finnigan (San Jose, CA, USA) GC–MS INCOS 50 quadrupole mass spectrometer. The GC component was equipped with a J&W Scientific (Deerfield, IL, USA) DB-1 fused-silica capillary column (60 m × 0.25 mm I.D.). The DB-1 column was held at 100°C for 1 min, then programmed at 20°C/min to 280°C, and held at 280°C until peak elution. In the EI-mode, 70 eV was used.

Chemical ionization (CI)-MS were recorded on a Finnigan Model 4510 mass spectrometer equipped with an INCOS data system. The GC component was equipped with a J&W Scientific DB-1 fused-silica capillary column (30 m × 0.32 mm I.D., 0.25 μm film thickness). The DB-1 column was held at 70°C for 2 min, then programmed at 10°C/min to 260°C, and held at 260°C until peak elution (helium carrier pressure, 13 p.s.i.). An ammonia pressure of 0.6 torr was used with the source at 60°C.

IR analyses

A Perkin-Elmer (Norwalk, CT, USA) IR Spectrophotometer Model 882 was used for IR analyses.

Mosquito repellent bioassay on humans

Anopheles quadrimaculatus, Aedes aegypti, and *Anopheles albimanus* mosquitoes were each used in the repellent bioassay on human volunteers.

Each test substance was dissolved in acetone, and the resulting solution was used to impregnate a cotton muslin bandage cloth (5 × 10 cm) at the rate of 1.0 mg/cm^2. The treated cloth was stapled over a 4 × 9 cm rectangular opening which had been cut in a 12.7 × 20.3 cm file card. The cloth was allowed to dry for 15 min before testing.

The cards and attached cloths were taped over a nylon stocking-covered forearm so that only the treated cloth allowed the mosquitoes access to the skin. The hand and wrist were protected with a rubber glove and tape. The arm was exposed for 1 min in a stock cage (37 × 38 × 46 cm), which contained approximately 1500 5- and 7-day-old female mosquitoes. Failure of the repellent candidate was indicated by >3 bites through the treated cloth.

The minimum effective dose (MED) was determined on chemicals that were effective at the 1.0 mg/cm^2 dosage. The method of testing was the same, except that the treatment dose was reduced by half until >3 bites/min were received at the lowest dose. The MEDs were determined on the fresh treatments (air-dried for 15 min) and after 24 h.

The repellent, deet, was used as a standard of comparison for mosquito repellency in the bioassay.

RESULTS AND DISCUSSION

The elution order of the CIC-4 isomers for GLC and HPLC (Fig. 2) columns was *trans* followed by *cis*. (The actual assignment of isomer configuration was accomplished via NMR analyses [4].) The HPLC peaks preceeding the *trans* and *cis* isomers were strong UV absorbers since the weight of the HPLC-recovered CIC-4 isomers was equal to that of the CIC-4 mixture being injected. In this study, milligram quantities approaching 1.0 g of each isomer of CIC-4 were obtained semi-preparatively on 5-μm silica for mosquito repellency tests. The retention times of the two isomers were 33 min (*trans*-CIC-4) and 41 min (*cis*-CIC-4) (Fig. 2).

Preliminary GLC data revealed that the CIC-4 mixture contained two substances in a 1:1 ratio. The isomers were analyzed by GLC on a dimethyl silicone capillary column (Table I) as they were separated and then analyzed on 3% butanediol adipate, Stabilwax, Supelcowax 10, and Supelco SPB 1701 columns for confirmation. The best GLC separation of the isomers was afforded by Supelcowax 10 with *trans* at 26.5 and *cis* at 28.5 min. The GLC purity of the separated geometric isomers was >95%.

IR analysis of the CIC-4 mixture showed an ester carbonyl absorption at 1735 cm^{-1}; the range for an acyclic δ-saturated lactone is 1735–1750 cm^{-1} [5]. Lack of a hydroxy absorption in both the alcohol and carboxylic acid areas of the spectrum indicated

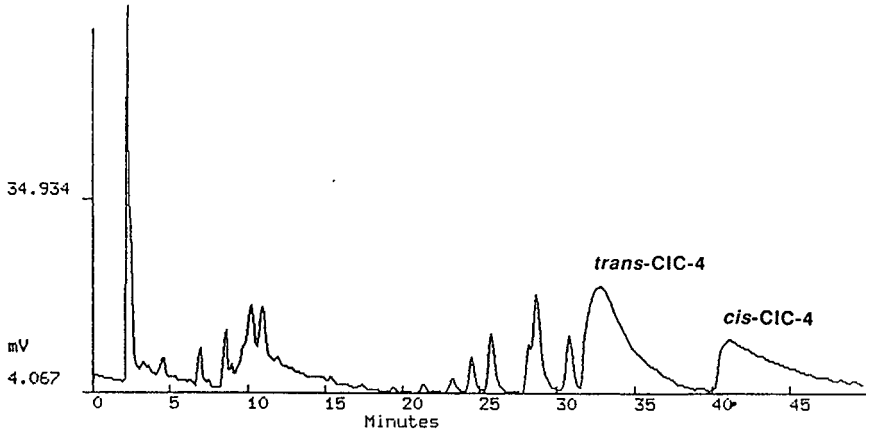

Fig. 2. Separation of *trans*-CIC-4 and *cis*-CIC-4 on 5-μm silica (25 × 2.0 cm I.D.). Eluent, diethyl ether–*n*-hexane (15:85, v/v), flow-rate, 30 ml/min; detector, 214 nm.

that the lactone ring was intact and that no hydrolytic cleavage had occurred.

EI-GC–MS fragmentation patterns were similar for the two isomers (1:1 ratio) (Table II) except that *trans*-CIC-4 had a base peak of *m/e* 87 and *cis*-CIC-4 had a base peak of *m/e* 67. Also, the *cis* isomer showed an appreciable amount of *m/e* 136 $(M\text{-}18)^+$ while the *trans* isomer showed only a trace of this ion. Although this is an uncommon fragmentation for esters, the *cis* isomer seems to be more susceptible than the *trans* to form this fragment. An MS library search identified isoiridomyrmecin and isomyrmecin as compounds with similar fragmentation patterns.

CI-GC–MS analysis with NH_3 (Table II) of CIC-4 (1:1 isomer ratio) established the molecular weight of each resolved isomer as 154. Analysis of each isomer with N^2H_3 revealed identical data that confirmed the absence of exchangeable protons, thus supporting the cyclic lactone structure.

In the bioassay against *Anopheles quadrimaculatus* (Table III), CIC-4 mixture (lots 1 and 2), the isomers, and deet were equally effective for 5 days at 1.0 mg/cm^2. The 24-hr post-treatment MED test revealed that all the samples and deet were equally repellent at 0.125 mg/cm^2, while the 15-min test revealed that CIC-4 mixture (lots 1 and 2) and the isomers were effective at 0.008 mg/cm^2 (deet was effective at 0.004 mg/cm^2).

TABLE I

GAS–LIQUID CHROMATOGRAPHIC ANALYSES OF CIC-4

Column	Parameters	Sample	Retention (min)	% Purity (isomer ratio)
3% Butanediol adipate	90°C for 2 min, 4°C/min to 210°C, 30 ml He/min	CIC-4	21.2, 22.2	(50:50)
Stabilwax	60–220°C at 10°C/min, 7 ml He/min	CIC-4	13.3, 13.8	99.1[a]
Supelcowax 10	100°C for 1 min, 10°C/min to 220°C, 1 ml He/min	CIC-4	26.5, 28.5	99.0[a] (51.2:48.8)
Dimethylsilicone	50°C for 5 min, 20°C/min to 105°C, held 7.25 min,	CIC-4	9.7, 10.2	(50.8:49.0)
	10°C/min to 125°C, held 13 min, 2.0 ml He/min	*trans*-CIC-4	9.7	95.7
		cis-CIC-4	10.2	100.0
Supelco SPB 1701	70–200°C at 15°C/min, held 30 min, He at 2.0 kg/cm^2	CIC-4	27.6, 28.7	(50.9:48.0)
		trans-CIC-4	27.6	94.2
		cis-CIC-4	28.7	98.8

[a] Total isomer (*trans* and *cis*) content in sample.

TABLE II

GAS–LIQUID CHROMATOGRAPHIC–MASS SPECTROMETRIC ANALYSES OF CIC-4

MS mode	*trans*-CIC-4 (*m/e*)	*cis*-CIC-4 (*m/e*)
Electron impact	41, 57, 67, 87 (100), 95, 124, trace 136 $[M-18]^+$	41, 57,67 (100), 87, 95, 124, 136 (28) $[M-18]^+$
Chemical ionization (NH_3)	172 $[M+NH_4]^+$ 189 $[M+(NH_3)_2H]^+$ 206 $[M+(NH_3)_3H]^+$ 326 $[2M+NH_4]^+$	172 $[M+NH_4]^+$ 189 $[M+(NH_3)_2H]^+$ 206 $[M+(NH_3)_3H]^+$ 326 $[2M+NH_4]^+$
Chemical ionization (N^2H_3)	176 $[M+N^2H_4]^+$ 196 $[M+(N^2H_3)_2{}^2H]^+$ 216 $[M+(N^2H_3)_3{}^2H]^+$ 330 $[2M+N^2H_4]^+$	176 $[M+N^2H_4]^+$ 196 $[M+(N^2H_3)_2]^+$ 216 $[M+(N^2H_3)_3{}^2H]^+$ 330 $[2M+N^2H_4]^+$

TABLE III

REPELLENT EFFECTIVENESS ON CLOTH OF CIC-4 MIXTURE, *trans*-CIC-4, AND *cis*-CIC-4 ON THREE SPECIES OF MOSQUITOES

Chemical	No. of days effective[a] on cloth at 1.0 mg/cm²	MED[b] (mg/cm²) on cloth at post-treatment time	
		15 min	24 hr
Anopheles quadrimaculatus			
CIC-4, lot 1	6	0.008	0.125
CIC-4, lot 2	6	0.008	0.125
trans-CIC-4	5	0.008	0.125
cis-CIC-4	6	0.008	0.125
Deet standard	6	0.004	0.125
Aedes aegypti			
CIC-4, lot 1	1	0.125	1.0
CIC-4, lot 2	1	0.125	1.0
trans-CIC-4	1	0.125	1.0
cis-CIC-4	1	0.125	1.0
Deet standard	5	0.032	0.5
Anopheles albimanus			
CIC-4, lot 1	1	0.5	1.0
CIC-4, lot 2	1	0.5	1.0
trans-CIC-4	1	0.125	1.0
cis-CIC-4	1	0.5	1.0
Deet standard	5	0.5	0.5

[a] All treatments tested until >3 bites were received during a 1-min exposure.

[b] Minimum effective dose.

In tests of CIC-4 (lots 1 and 2), *trans*-CIC-4, and *cis*-CIC-4 at the 1.0 mg/cm² against *Aedes aegypti*, each substance was as effective as deet for 1 day; deet repelled for 5 days. The MED 15-min post-treatment test revealed that CIC-4 mixture (lots 1 and 2) and the isomers were effective at 0.125 mg/cm², whereas deet was effective at 0.032 mg/cm². The 24-h MED for CIC-4 mixture (lots 1 and 2) and the isomers was 1.0 mg/cm²; the MED of deet was 0.5 mg/cm².

At 1.0 mg/cm² against *Anopheles albimanus*, CIC-4 mixture (lots 1 and 2) and its separated isomers were as effective as deet for 1 day, but deet repelled for 5 days. The 15-min post-treatment MED tests revealed that CIC-4 (lots 1 and 2), *cis*-CIC-4, and deet were equal in repellency at 0.5 mg/cm²; whereas, *trans*-CIC-4 was effective at 0.125 mg/cm². After 24 h, CIC-4 mixture (lots 1 and 2) and the isomers were effective at 1.0 mg/cm²; deet was effective at 0.5 mg/cm².

Thus the MED on cloth against *Anopheles albimanus* revealed a difference in the repellency of the *trans*- and *cis*-CIC-4 isomers, but no differences were found with the other mosquitoes.

CONCLUSIONS

Milligram quantities approaching 1.0 g of *cis* and *trans* isomers of CIC-4 (1,1,4,5,6,7,8,8*a*-octahydro-3H-2-benzopyran-3-one) were obtained from a 1:1 mixture by a semi-preparative HPLC separation technique. By this method, each isomer was >95% GLC-pure and each was evaluated for its efficacy in mosquito repellency tests. GLC, EI- and CI-GC–MS data supported the fact that the CIC-4 mixture contained configurational isomers and that these were present in approximately a 1:1 ratio.

The cloth bioassay on the human arm using *Anopheles quadrimaculatus*, *Aedes aegypti*, and *Anopheles albimanus* as the test species indicated that there were no differences in repellency between lots 1 and 2 of CIC-4, and there were no appreciable differences in rellency between *trans*-CIC-4, *cis*-CIC-4, and the CIC-4 mixture. Moreover, the deet standard was more effective than CIC-4 or its separated isomers in both MED and duration of effectiveness, except with *Anopheles quadrimaculatus* where there was equivalent duration of effectiveness for CIC-4 (lots 1 and 2), the separated isomers, and deet for 5 days.

ACKNOWLEDGEMENTS

The authors acknowledge the kind help of Mr. Samuel Spencer and Mr. Victor Levi in the HPLC separation and the GLC analyses of the geometric isomers.

The authors are also appreciative of the personal communication (1990) provided by Dr. F. Coulston claiming that new collaborative research with Dr. F. Korte (Technical University of Munich, Germany) produced simular results; *i.e.*, in mosquito tests (*Aedes aegypti* and *Anopheles quadrimaculatus*), the CIC-4 isomers showed no difference in repellent effects and that the isomers were as effective as the CIC-4 mixture.

REFERENCES

1 F. Korte, J. Falbe and A. Zschocke, *Tetrahedron*, 6 (1959) 201.
2 S. Budavari, M. J. O'Neil, A. Smith and P. E. Heckelman (Editors), *The Merck Index*, 11th Ed., 1989, p. 804, abstract 4972.
3 F. Coulston and F. Korte, *U.S. Pat. 4 663 346* (May 5, 1987).
4 A. B. DeMilo, J. D. Warthen, R. M. Waters and W. F. Schmidt, *Presented at the 25th Middle Atlantic Regional Meeting, Delaware Section ACS*, University of Delaware, May 21–23, 1991.
5 K. Nakanishi, *Infrared Absorption Spectroscopy*, Holden-Day, San Francisco, CA, 1964, p. 44.

Journal of Chromatography, 590 (1992) 139–145
Elsevier Science Publishers B.V., Amsterdam

CHROMSYMP. 2401

Purification of erucic acid by preparative high-performance liquid chromatography and crystallization

Prabha Painuly* and Charles M. Grill

Separations Technology, Division of EM Industries, Inc., P.O. Box 352, Wakefield, RI 02880-0352 (USA)

ABSTRACT

Erucic acid (C22:1 fatty acid) has been found to be useful in the treatment of adrenoleukodystrophy (ALD). It appears to work by reducing the blood levels of very-long-chain fatty acids (VLCFAs) which destroy the myelin sheaths of the nerves. Erucic acid was purified by reversed-phase high-performance liquid chromatography (HPLC) on columns packed with YMC C_{18} (10–20 μm, 120 Å). Using ethanol–water as the mobile phase, the recovery of erucic acid was 69% and the purity was more than 97% as measured by gas chromatography. The amount of saturated VLCFAs was found to be within the limits specified for ALD treatment. The production rate (yield per 8 h shift) was low, however. Using methanol–water instead of ethanol–water as the mobile phase, a ninefold increase in the production rate was achieved. The recovery of erucic acid was 65% and the purity of erucic acid was 98%. All other purity specifications were met. By performing a low-temperature crystallization after the preparative HPLC step, the production rate was increased a further 142%. This represents a 22-fold increase in production rate over the ethanol–water method. The crystalline erucic acid was found to be 99% pure. All other purity requirements were met. The yield for the combined process (HPLC plus crystallization) decreased to 55%, however.

INTRODUCTION

Adrenoleukodystrophy (ALD) is an inherited disease characterized by unusual accumulations of very-long-chain saturated fatty acid (VLCFA) molecules, found in small amounts in the diet and also synthesized in the body. These fats destroy the myelin sheath that insulates and protects the nerves. The symptoms of ALD are memory loss, involuntary motion and death within a few years.

Oral feeding of the monounsaturated fatty acid erucic acid ($\Delta^{13:14}$-docosenoic acid, C22:1) was found to reduce the blood levels of these VLCFAs. A single enzyme was found to be responsible for elongating both long-chain monounsaturated fatty acids and saturated acids whose accumulation is associated with ALD. It was concluded that long-chain monounsaturated fatty acids may work by monopolizing the enzyme, keeping it busy making the apparently harmless unsaturated fatty acids so that the production of the saturated VLCFAs is suppressed [1].

At the request of the United Leukodystrophy Foundation, we undertook to develop a method of purifying erucic acid with the following specifications: (1) the C22:1 content should be $96 \pm 2\%$ in the final product; (2) the C20:1 content should be $\leqslant 2\%$; (3) the saturated C22:0 fatty acid and VLCFA contents should be $< 0.1\%$; and (4) the purified product in the free fatty acid form are preferred to the esters.

In our initial efforts to develop a method which met the above specifications, we used ethanol–water as the mobile phase [2]. Although all purity specifications were met using this solvent system, our efforts in this direction were abandoned when the production rate (defined as the amount of purified erucic acid collected per 8-h shift) proved to be too low.

We found that with methanol–water as the mobile phase, the production rate of erucic acid was greatly increased relative to the method using ethanol–water. This paper reports our efforts to optimize the purification of erucic acid using methanol–water as the mobile phase.

0021-9673/92/$05.00

EXPERIMENTAL

Crude mixtures of fatty acids containing *ca.* 90% [by gas chromatography (GC)] or erucic acid C22:1 (rapeseed oil) was supplied by POS Pilot Plant (Saskatoon, Canada).

For high-performance liquid chromatography (HPLC) for development of the purification methods, the system consisted of a Varian Vista 5500 HPLC, a Rheodyne Model 7125 injector and a Knauer UV detector. The chromatograph used for the larger scale preparative runs was a NovaPrep 5000 from Separations Technology (Wakefield, RI, USA). The data were recorded on a Spectra-Physics integrator and transferred to a personal computer. Fatty acids were detected by UV measurement at 214 nm and by refractive index (RI) detection.

Separations were performed on columns packed at Separations Technology with YMC C_{18} (10–20 μm, 120 Å). For method development a column with dimensions 20 × 0.46 cm I.D. was used. For the initial scale-up, a 20 cm × 1.93 cm I.D. column was used. For the larger scale runs, a 20 cm × 7.5 cm I.D. annular expansion column from Separations Technology was used.

The solvents used were methanol and water (both HPLC grade, Fisher) and were filtered through a 5-μm filter. For the method development and initial scale-up runs performed on the Varian instrument, the solvents were sparged with helium. This was not required for the larger scale runs as the NovaPrep 5000 system uses high-pressure gradient generation. For all injections, 50% (w/v) solutions of the crude fatty acid mixture in methanol–water (95:5) was used.

GC was used to measure the purity of the fractions collected. To facilitate GC analyses, the fatty acids collected were converted into their volatile methyl esters using boron trifluoride–methanol according to the method of Pelick and Mahadevan [3]. The methyl esters were determined by GC on a capillary column. A 50% solution of the methyl ester in hexane (2–4 μl) was used for injection onto the GC column.

Fig. 1 shows the GC trace of a standard solution of fatty acid methyl esters (FAMEs). Note that all the FAMEs are well resolved. Hence GC is a valid method for determining the purity of the collected HPLC fractions.

RESULTS AND DISCUSSION

Two methods were developed to purify erucic acid using methanol–water as the HPLC mobile phase. In the first method reversed-phase HPLC alone was used and in the second reversed-phase HPLC was followed by low-temperature crystallization (LTC).

HPLC-only method

The initial methods development and loading studies were carried out on the 20 cm × 0.46 cm I.D. column. Methanol–water (95:5) was found to be the most suitable composition for this purification. The total run time was 66 min; after 55 min, the column was washed with methanol for 5 min and then re-equilibrated with methanol–water (95:5) for 6 min. After extensive loading studies the maximum load that would give the desired purity was found to be 100 mg. The flow-rate was 0.6 ml/min.

A representative chromatogram is shown in Fig. 2. The erucic acid was collected from 34 to 40 min as shown by the dashed lines. The yield was 65% and the purity by GC was 99%.

The initial scale-up was performed on the 20 cm × 1.93 cm I.D. column. The same mobile phase

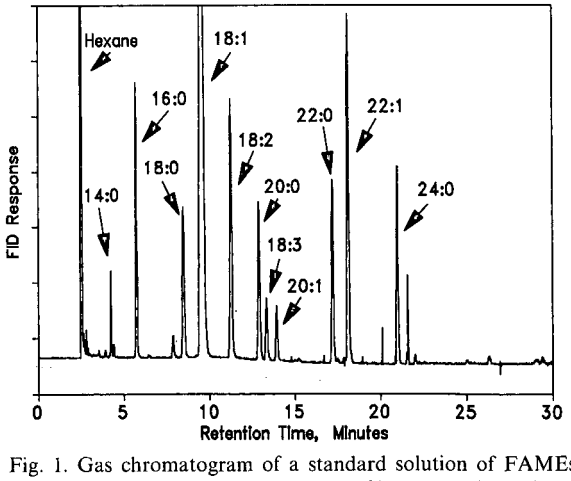

Fig. 1. Gas chromatogram of a standard solution of FAMEs showing that GC resolves the FAMEs of interest and can therefore be used to measure the purity of the collected fractions. Hewlett-Packard Model HP5890 gas chromatograph; column, Supelco SP 2300 fused silica, 30 m × 0.32 mm I.D.; column temperature programmed from 170 to 220°C at 4°C/min; carrier gas, helium. FID = Flame ionization detection.

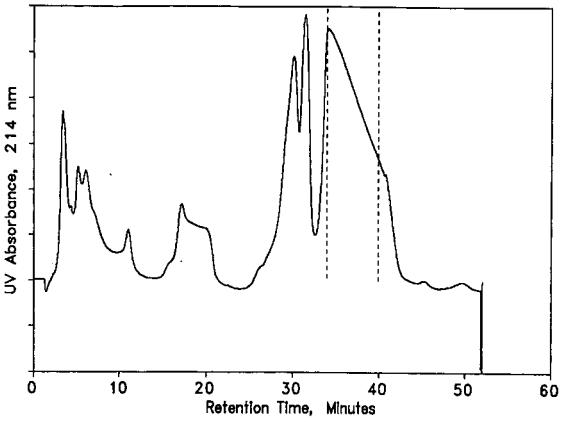

Fig. 2. Method development chromatogram using methanol–water as the mobile phase. Flow-rate, 0.6 ml/min; load, 100 mg; initial mobile phase, methanol–water (95:5); step gradient to 100% methanol at 55 min.

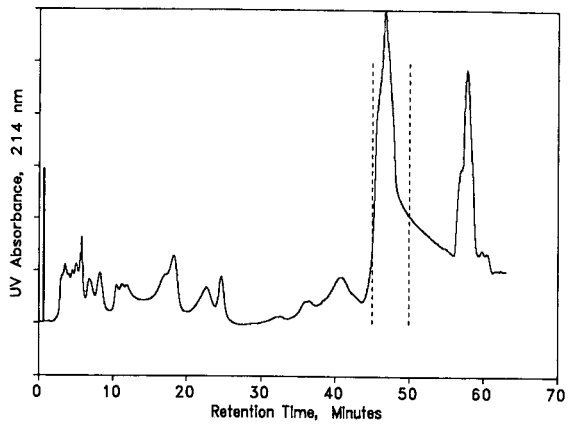

Fig. 3. Initial scale-up on the 20 cm × 1.93 cm I.D. column. Flow-rate, 10.6 ml/min; load, 1.76 g; initial mobile phase, methanol–water (95:5); step gradient to 100% methanol at 55 min.

[methanol–water (95:5)] and methanol were used. In calculating the scale-up parameters for larger columns, the linear velocity is kept constant for each column in order to maintain column efficiency. In such a scale-up, the volumetric flow-rate scales as the square of the column radius, the crude loading scales as the entire volume of the column and the run time and back-pressure scale as the length of the column. The predicted loading, recovery, mobile phase flow-rate and solvent usage for this larger column were calculated using the method development data and are shown in Table I. As seen, the calculated load was 1.76 g and the calculated flow-rate was 10.6 ml/min. To obtain the production rate (grams of erucic collected per 8-h shift) given in Table I, note that each run takes 66 min (1.1 h). Therefore, seven runs can be made in a shift. The production rate is then obtained by multiplying the yield per run in Table I by seven.

Fig. 3 shows a representative chromatogram of the direct scale-up to the 1.93 cm I.D. column using the data in Table I. The erucic acid is in the large peak that elutes near 48 min. A comparison of Figs. 2 and 3 will show that the retention time for the erucic acid peak is longer on the 1.93 cm I.D. column than on the 0.46 cm I.D. column, *i.e.*, the 1.93 cm I.D. column is more efficient. We were able, therefore, to increase the load above that calculated in Table I from the method development data. We therefore increased the load from 1.76 to 2 g. As this amount of overloading causes a decrease in retention time, it was possible to decrease the flow-rate (thereby further increasing the efficiency) without decreasing the production rate. Hence the flow-rate was reduced from 10.6 to 6.0 ml/min, and the gradient conditions were changed to those in Table II. A representative chromatogram is shown in Fig. 4.

In an early experiment, fifteen fractions were collected. Each fraction was dried by rotary evaporation and converted to the methyl ester for GC analysis. The GC analysis showed that fractions 9, 10, 11 and 12 collected between retention times of 25

TABLE I

CALCULATED SCALE-UP PARAMETERS FOR THE 20 cm × 1.93 cm I.D. COLUMN

Column length × I.D. (cm)	Load (g per run)	Yield (g per run)	Yield (%)	Production rate yield (g per shift)	Flow-rate (ml/min)
20 × 0.46	0.100	0.065	65%	0.46	0.6
20 × 1.93	1.76	1.14	65%	7.98	10.6

TABLE II

GRADIENT CONDITIONS FOR FIGS. 4 AND 6

Mobile phase flow-rate, 6.0 ml/min.

Time (min)	A[a] (%)	B[a] (%)
0	100	0
50	100	0
51	0	100
60	0	100
61	100	0
66	100	0

[a] A = methanol–water (95:5, v/v); B = methanol.

and 36 min each contained 97–99% of erucic acid and met the other purity specifications of the project. Fraction 13, collected between 36 and 40 min, contained 92.2% of erucic acid, but it also contained more than 1% of saturated C24:0 fatty acid. All the fractions collected after 36 minutes contained an increasing amount of long chain saturated fatty acid, especially C24:0 saturated fatty acid. We therefore performed a run in which one fraction was collected between 25 and 36 min, shown by the dashed lines in Fig. 4. This fraction gave a yield of 65% and 1.3 g of erucic acid were recovered. GC analysis of the methyl ester showed it to be 98% pure erucic acid. All other purity specifications were also met.

Note that two types of traces are shown in Fig. 4, obtained by RI and UV detection. The size of an RI peak is about proportional to the concentration of the compounds in the peak. Thus, in Fig. 4, the RI trace shows that most of the erucic acid lies between retention times of 25 and 40 min. The intensities of the UV peak are determined by electronic transitions within the molecules responsible for the peaks. The relative intensities of two peaks, therefore, are not necessarily related to the relative concentrations of the compounds in the peaks. Thus the UV trace in Fig. 5 shows that there is a compound with a retention time near 20 min, and the RI trace shows that this compound is in low concentration.

In an effort to increase the production rate, we switched to methanol as mobile phase at 36 min, as the collection of erucic acid is completed at this point. This method was chosen as the optimum HPLC-only method. The chromatographic conditions are given in Table III and the chromatogram is shown in Fig. 5. Unfortunately, the peak near 50 min retention time tailed to such an extent that the length of the run was not decreased significantly. Thus switching to methanol at 36 min decreased the total run time by only 1 min.

Further work showed that when the load was increased to more than 2.0 g for this column, the purified erucic acid contained long-chain fatty acids, especially the C24:0 which elutes after erucic acid, due to the tag-along effect [4–6]. In order to main-

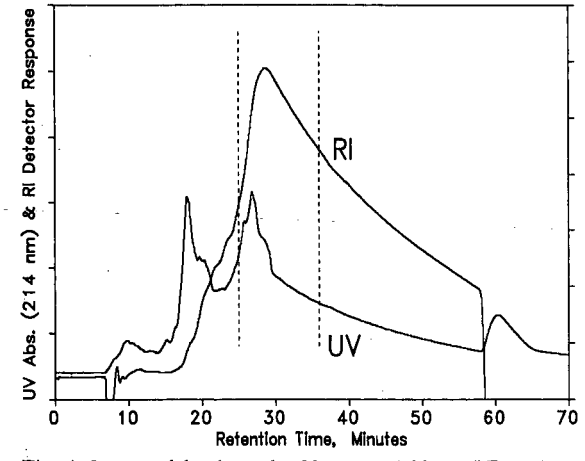

Fig. 4. Increased load on the 20 cm × 1.93 cm I.D. column. Flow-rate, 6.0 ml/min; load, 2.0 g; step gradient to 100% methanol at 50 min. Other conditions as in Table II.

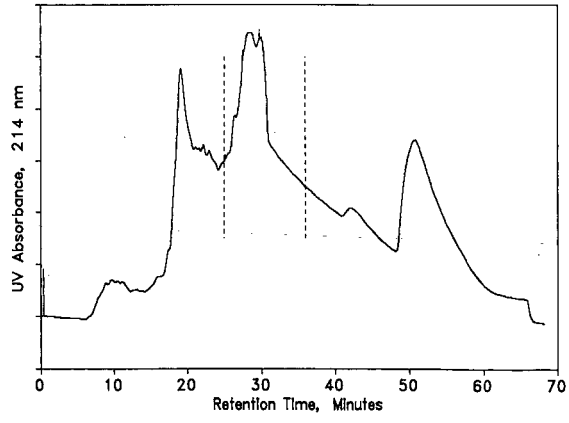

Fig. 5. Optimized chromatogram of HPLC-only method on the 20 cm × 1.93 cm I.D. column. Flow-rate, 6.0 ml/min; load, 2.0 g; step gradient to 100% methanol at 35 min. Other conditions as in Table III.

TABLE III

GRADIENT CONDITIONS FOR THE OPTIMIZED HPLC-ONLY METHOD (FIG. 5)

Column dimensions, 20 cm × 1.93 cm I.D.; load, 2 g; mobile phase flow-rate, 6.0 ml/min.

Time (min)	A[a] (%)	B[a] (%)
0	100	0
35	100	0
36	0	100
55	0	100
56	100	0
65	100	0

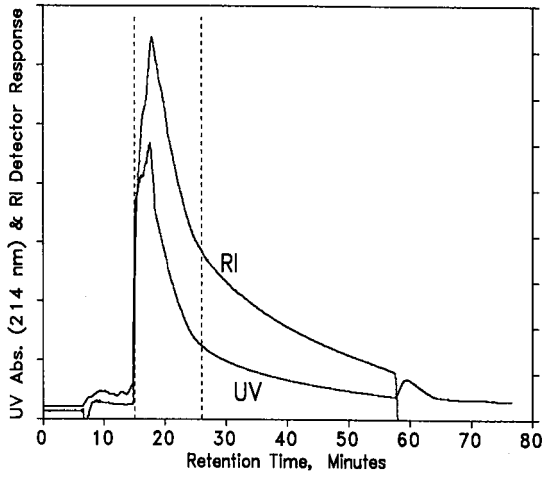

Fig. 6. Initial chromatogram of HPLC–LTC method on the 20 cm × 1.93 cm I.D. column. Flow-rate, 6.0 ml/min; load, 4.0 g; step gradient to 100% methanol at 50 min. Other conditions as in Table II.

tain the desired purity, a narrower fraction would have to be collected. Thus the production rate would be lowered.

HPLC followed by low-temperature crystallization (HPLC–LTC method)

Low-temperature crystallization was investigated as a purification technique for the fatty acids. Several crystallizations were performed on the crude products and on the fractions obtained from the HPLC runs. The crystals and the mother liquors were converted into the methyl esters and analyzed by GC for their fatty acid composition.

At the temperatures used in the crystallization (5–7°C), the fatty acids with chain lengths shorter than erucic acid remained in solution and were thus easily separated by filtering. However, erucic acid and the VLCFAs, because of their higher melting points, crystallized together.

The crystallization results prompted us to attempt the purification by combining HPLC and LTC. We hypothesized that the loading could be substantially increased if the HPLC run were followed by the crystallization step. The HPLC run should remove the later eluting VLCFAs, and the crystallization should remove the earlier eluting, shorter chain fatty acids.

To test this hypothesis, the load was increased to 4 g. The gradient conditions were the same as used in Fig. 4 and are given in Table II. Fig. 6 shows the HPLC run. A comparison with Fig. 4 shows a reduction in retention time and a loss of resolution. After several experiments it was determined that the fraction between 15 and 26 min, shown by the dashed lines in Fig. 6, would yield acceptable purity results. This fraction was collected and kept at 5–7°C in an ice-bath. The crystalline product obtained was filtered under suction in a Buchner funnel using a glass-fiber filter. The crystals were analyzed by GC for their fatty acid composition and purity. The purity of the erucic acid was found to be greater than 99%, and the method met all the other purity specifications. However, the overall yield of erucic acid from the HPLC–LTC procedure was only 55%.

For the final HPLC–LTC method, we switched to methanol as mobile phase at 26 min, since the collection was completed at this point. This decreased the run time significantly from 66 to 46 min, thus increasing the production rate. The chromatographic conditions for the optimized HPLC–LTC method are given in Table IV and the chromatogram is shown in Fig. 7. Again the erucic acid peak was collected from 15 to 26 min, as shown by the dashed lines.

Summary of the 20 × 1.93 cm column results

Table V gives a summary of the results obtained on the 20 cm × 1.93 cm I.D. column. The run times include the time necessary to equilibrate the column between runs. Note that as the run time for the

TABLE IV

GRADIENT CONDITIONS FOR THE OPTIMIZED HPLC–LTC METHOD (FIG. 7)

Column dimensions, 20 × 1.93 cm I.D.; load, 4 g; flow-rate, 6.0 ml/min.

Time (min)	A[a] (%)	B[a] (%)
0	100	0
26	100	0
27	0	100
40	0	100
41	100	0
46	100	0

[a] A = methanol–water (95:5, v/v); B = methanol.

HPLC-only method is slightly longer than 1 h, seven HPLC-only runs could be made in an 8-h shift. Thus 9.1 g of erucic acid could be produced in an 8-h shift (1.3 g × 7 runs). This represents a ninefold increase in the production rate (grams collected per shift) compared with the method with ethanol–water as the mobile phase.

The run time for the HPLC–LTC method is 0.77 h; hence ten of these runs could be made in an 8-h shift. This leads to a production rate of 22 g of erucic acid collected per 8-h shift (2.2 g × 10 runs). This represents a 22-fold increase in the production rate relative to the ethanol–water method. The time needed for the crystallization step was less than 30 min. Hence at this scale, the production rate is controlled by the HPLC step. That is, since the crystallization step can be carried out simultaneously with the next HPLC run, and since the HPLC run takes a longer time (0.77 h, Table V), the average time for the entire HPLC–LTC procedure will be 0.77 h once a steady production stream is established.

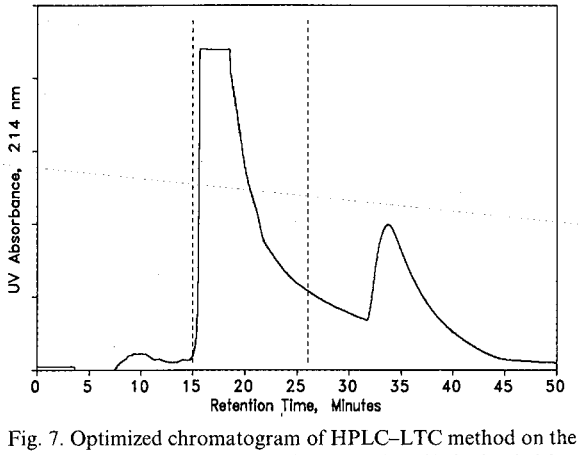

Fig. 7. Optimized chromatogram of HPLC–LTC method on the 20 cm × 1.93 cm I.D. column. Flow-rate, 6.0 ml/min; load, 4.0 g; step gradient to 100% methanol at 26 min.

TABLE V

SUMMARY OF OPTIMIZED HPLC METHODS ON THE 20 cm × 1.93 cm I.D. COLUMN USING METHANOL–WATER

Parameter	Method	
	HPLC-only	HPLC/LTC
Run time (h)	1.08	0.77
Methanol usage (l per run)	0.377	0.265
Methanol usage (l per shift)	2.64	2.65
Load (g per run)	2.0	4.0
Load (g per shift)	14	40
Yield (g per run)	1.3	2.2
Yield (g per shift)	9.1	22
Yield (%)	65	55
Erucic acid purity (%)	98	>99
C24:1 content (%)	0.01	0.02
C20:1 content (%)	0.04	0.03
C16:0–C20:0 content (%)	0.04	0.06
C22:0 and longer saturated VLCFA content (%)	0.045	0.041

Note also that even though more runs are made per shift with the HPLC–LTC method, the methanol consumption per shift is about the same as for the HPLC-only method. Thus, in determining whether the method is acceptable, one should consider production rate, yield and methanol consumption per gram of purified erucic acid.

Scale-up to 20 cm × 7.5 mm I.D. annular expansion column

We scaled up the HPLC–LTC method, which we consider to be the better of the two methods, to the 20 cm × 7.5 cm I.D. annular expansion column. The calculated scale-up parameters are given in Table VI and the chromatogram is shown in Fig. 8. The gradient conditions were the same as those given in Table V. The erucic acid fraction was collected from 7 to 26 min as shown by the dashed lines in Fig. 8. After low-temperature crystallization, the purity of this fraction was found by GC to be

TABLE VI

CALCULATED SCALE-UP PARAMETERS FOR THE HPLC–LTC METHOD ON THE 20 cm × 7.5 cm I.D. ANNULAR EXPANSION COLUMN

Parameter	Value	Parameter	Value
Run time (h)	0.77	Yield (g per shift)	332
Load (g per run)	60.6	Flow-rate (ml/min)	90.6
Load (g per shift)	604	Methanol usage (l per shift)	32.9

98.8% and the yield was 59%. The levels of the other fatty acids were below those specified in the Introduction.

In comparison with the HPLC–LTC run on the 20 cm × 1.93 cm I.D. column (Fig. 7), both peaks have shifted to shorter retention times on the 20 cm × 7.5 cm I.D. column (Fig. 8). This indicates that the larger column is more overloaded than the 20 cm × 1.93 cm I.D. column. Hence the run time is slightly shorter than predicted in Table VI. With this reduction in run time, it appears that one or two more runs could be made in an 8-h shift, thus further increasing the production rate.

CONCLUSIONS

We have shown that preparative HPLC can be used to purify erucic acid from rapeseed oil to a level that could be used in clinical trials to treat adrenoleukodystrophy. Using ethanol–water as the mobile phase, the production rate was too low to be of practical significance. With methanol–water as the mobile phase, the production rate is much higher. When low-temperature crystallization is combined with HPLC, the production rate is more than doubled in comparison with HPLC alone. It appears that the HPLC–LTC method, on scale-up to larger systems, could be used to produce enough erucic acid for clinical trials. However, further engineering is needed (in such areas as solvent recycling) to make the method economically feasible.

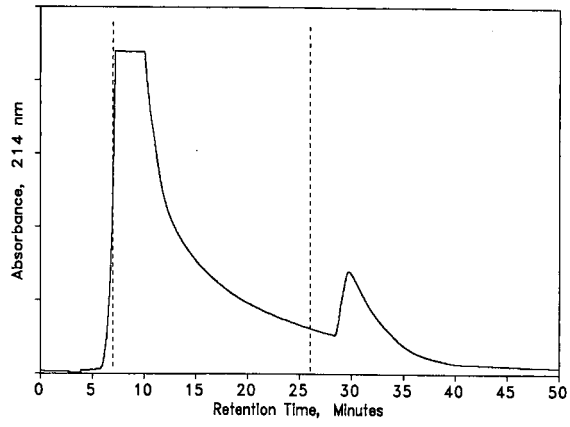

Fig. 8. Chromatogram of HPLC–LTC method scaled-up to the 20 cm × 7.5 cm I.D. annular expansion column. Flow-rate, 90.6 ml/min; load, 60.4 g.

ACKNOWLEDGEMENTS

A large part of this work was funded (under contract) by the United Leukodystrophy Foundation and Tradcom, Inc. (both of Dekalb, IL, USA). Thanks are also due to POS Pilot Plant (Saskatoon, Canada) for providing the crude fatty acid samples.

REFERENCES

1 J. Adler and M. Hager, *Newsweek*, November 16 (1987) 98.
2 P. Painuly and C. M. Grill, *Purification of C22:1 Fatty Acid (Erucic Acid) by Preparative HPLC*, Technical Report, Separations Technology, Wakefield, RI, 1990 (a copy of this report can be obtained from the authors.)
3 N. Pelick and V. Mahadevan, in E. G. Perkins (Editor), *Analysis of Lipids and Lipoproteins*, American Oil Chemists Society, Champaign, IL, 1975, pp. 23–35.
4 S. Golshan-Shirazi and G. Guiochon, *Am. Biotech. Lab.*, 8 No. 8 (1990) 26.
5 G. Guiochon and S. Ghodbane, *J. Phys. Chem.*, 92 (1989) 3682.
6 G. Guiochon, S. Ghodbane, S. Golshan-Shirazi, J. Huang, A. Katti, B. Lin and A. Ma, *Talanta*, 36 (1989) 19.

Journal of Chromatography, 590 (1992) 147–151
Elsevier Science Publishers B.V., Amsterdam

CHROMSYMP. 2418

Glucose–fructose equilibria on Dowex Monosphere 99 CA resin under overloaded conditions

M. Saska*, S. J. Clarke, Mei Di Wu and K. Iqbal

Audubon Sugar Institute/Sugar Station, Louisiana State University Agricultural Center, Baton Rouge, LA 70803 (USA)

ABSTRACT

Matching of the numerical simulation of the band propagation with experimental elution profiles of glucose and fructose was used to obtain the adsorption isotherms of glucose and fructose at 70°C on Dowex Monosphere 99 CA resin (Dow Chemical), an adsorbent widely used in the high-fructose corn syrup (HFCS) industry. The respective distribution coefficients, $K_G = 0.245 + 0.0051c_G + 0.003c_F$ and $K_F = 0.47 + 0.007c_G + 0.0049c_F$, are non-linear and dependent on the concentrations of both sugars. Contrary to some previous reports, the height equivalent to a theoretical plate of glucose (2.7 cm) was less than that of fructose (3.5 cm). The ideal chromatographic model with the band spreading originating in an implicit way from the numerical integration of the appropriate partial differential equation was found suitable to fit the coupled, non-linear behavior of glucose–fructose mixtures and can be a useful tool for modelling and optimization of the industrial simulated moving bed HFCS process.

INTRODUCTION

The continuous simulated moving bed (SMB) fructose-selective adsorption separation of glucose–fructose mixtures has been a standard process in high-fructose corn syrup (HFCS) production for a decade. In the last 2 years, using the potassium form of sulphonated polystyrene resins, the technology has been applied on an industrial scale to the desugarization of sugarbeet molasses (ion-exclusion) and, pending resolution of problems with pretreatment of the more impure sugarcane solutions, it also promises new possibilities in the sugarcane industry.

For reliable modeling and design of a large-scale SMB operation, it is crucial to understand the properties of the adsorbent, *viz.*, adsorption equilibria (partition coefficients) and mass transfer rates. These should be determined preferably by pulse testing [1] on the SMB system itself or a scalable pilot plant to account correctly not only for the properties of the adsorbent but also for the band broadening from column connections and valves and column packing characteristics. Care should be taken that the loading, flow-rates and range of concentrations in the tests are comparable to the conditions prevailing in the SMB process. It was shown recently [2] that the frequently made assumption of linear and uncoupled isotherms of glucose and fructose on Ca^{2+} polystyrene resins may not be valid at high concentrations (see Table I) and that it affects considerably the predicted steady-state profile within an SMB system. This in turn leads to operational parameters (switching time and flow-rates) that, if based on the model, result in less than optimum separation.

In this paper we report results of measuring the adsorptive properties of a Dowex Monosphere 99 CA resin (Ca^{2+} form; Dow Chemical, Midland, MI, USA) for glucose and fructose under conditions of high concentrations. The isotherms obtained were used to model the SMB separation of glucose–fructose mixtures.

EXPERIMENTAL

The SMB pilot plant at Audubon Sugar Institute consists of eight identical jacketed glass columns (210 cm × 6 cm I.D., column volume 5940 ml) connected with a series of either computer- or manually operated solenoid valves and sampling ports. The pulse tests were done on either six or seven in-series connected columns, packed with

0021-9673/92/$05.00

Dowex Monosphere 99 CA resin (particle size 0.32 mm, 6% cross-linked) and kept at 70°C, by first feeding the top of the first column with predetermined amounts (±1 g) of fructose–glucose solutions of various compositions and then eluting the components with hot deionized water (*ca.* 75°C) at flow-rates between 120 and 160 ml/min (±0.1 ml/min). The direction of the flow was downwards in all columns to eliminate problems with fluidizing the resin bed [7]. The elution time was measured from the moment of switching the water pump on. The samples were then taken periodically and their concentration (refractive index) determined off-line. High-performance liquid chromatographic (HPLC) analysis (Aminex HPX-87N column, Bio-Rad Labs.) was used with two-component feeds. In the high-load tests (*e.g.*, runs 5, 6, 11 and 12 in Fig. 2), columns one (runs 5 and 12) and one and two in series (runs 6 and 12) were used as feed reservoirs by feeding these columns with the feed until the outlet reached the inlet composition. Then a connection was made with the remainder of the columns and the feed eluted as before.

The response signals were integrated numerically to give the mean and variance of the elution peaks:

$$t' = \int ct\,dt / \int c\,dt \tag{1}$$

$$\sigma^2 = \int c(t - t')^2 dt / \int c\,dt \tag{2}$$

The chromatographic height equivalent to a theoretical plate (HETP) was calculated as $L'(\sigma/t')^2$, where the total column length L was corrected for the length of the feed "plug" L_f as

$$L' = L - \tfrac{1}{2}L_f = L - \tfrac{1}{2}m_f/(\rho\varepsilon A)$$

where ρ is the feed density and A the column cross-sectional area. In high-load tests, L_f was taken as L or $2L$ (L = column length, 210 cm) depending on whether one or two columns were equilibrated initially with the feed. Thus, in the HFCS experiments, the load with respect to fructose was higher (by the excess in the solid phase) than would correspond to the HFCS composition.

The assumed form of the distribution coefficients was as before (Table I):

$$K_G \equiv q_G/c_G = K_{G0} + A_1 c_G + B_1 c_F \tag{3}$$

$$K_F \equiv q_F/c_F = K_{F0} + A_2 c_G + B_2 c_F \tag{4}$$

where c is the liquid concentration (g per 100 ml) and q the concentration in the resin (g per 100 ml of resin), and the coefficients were obtained by matching the experimental profiles with those calculated from a local equilibrium model:

$$\partial c/\partial t + [(1 - \varepsilon)/\varepsilon]\partial q/\partial t + v(\partial c/\partial z) = 0 \tag{5}$$

The time and space partial derivatives were replaced as usual with finite differences of the forward and backward types, respectively, and solved on a Model 386-based PC. The non-linearities stemming from the form of the distribution coefficients were accommodated with an internal iteration procedure. The time and length integration steps, 0.8 min and 10 cm, of the discretized eqn. 5 were chosen such as to match the profiles of low-concentration pulse responses (Fig. 1) and thus substitute for the lack of explicit axial dispersion terms (axial mixing and mass transfer) in the master equation. The slight underestimation of the peak heights of glucose (see also Fig. 3) indicates that the band broadening (and HETP) is less than that of fructose and therefore slightly different integration steps should be used for the two sugars.

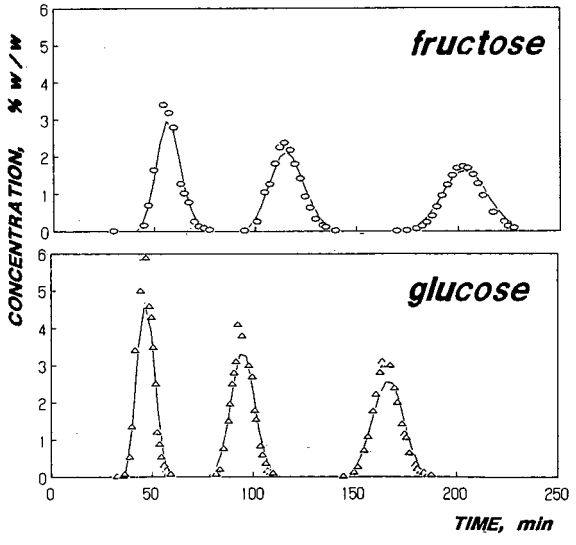

Fig. 1. Experimental (symbols) and calculated (solid lines) elution profiles of (○) fructose and (△) glucose (single-component feeds). A total of six in-series columns were used, with sampling after two, four and six columns. Fructose experiment: c_f = 19.8%, q = 146.5 ml/min. Glucose experiment: c_f = 23.6%, q = 150.2 ml/min. K_{G0} = 0.245; A_1 = 0.0051; K_F^0 = 0.47; B_2 = 0.0049.

K_{G0} and K_{F0} were obtained by matching the low-concentration feed profiles (single-component feeds) with those calculated while neglecting the concentrationn dependent terms of the distribution coefficients ($A_1 = A_2 = B_1 = B_2 = 0$). A_1 and B_2 were obtained from single-component runs with feed concentrations from 15 to 60 wt.% (with $A_2 = B_1 = 0$), and the cross-coefficients, A_2 and B_1 were obtained from runs where the feed was an HFCS syrup diluted to between 10 and 60% (w/w). The system void fraction, $\varepsilon = 0.47$, which includes the column connections, valves, etc., was found from pulse tests with a high-molecular-weight dextran.

RESULTS AND DISCUSSION

The HETP evaluated from runs 1–4 and 7–10 is 2.7 ($\sigma = 0.5$, $N = 4$) and 3.5 cm ($\sigma = 0.2$, $N = 4$) for glucose and fructose, respectively, about one third of those found by Ching and Ruthven [4] on smaller columns.

The retention time (empty column bed volumes eluted at the peak maxima) generally increases (Fig. 2) with increasing column load (proportional to the feed volume and concentration), although the volume-averaged concentrations of the bands as they move through the column should prove a more meaningful parameter in correlating the retention times.

The average values of the parameters determined here fall within the ranges found previously for similar resins (Table I):

$$K_G = 0.245 + 0.0051c_G + 0.003c_F \quad (6)$$

$$K_F = 0.47 + 0.007c_G + 0.0049c_F \quad (7)$$

The separation on the Dowex Monosphere 99 CA resins, judged by the K_{F0}/K_{G0} ratio of 1.92 at 70°C, appears to be superior to that on Duolite resins at the same temperature (Table I).

The upward curvature of the isotherms causes the characteristic "sharpening" of the fructose band (Fig. 3): while the tail ($c_G = 0$) is made steeper because $B_2 > 0$ (a low-concentration element of the solutions trqvels faster that a high-concentration element, *i.e.*, the peak of the band), the broadening of the front (that would be expected in a single component band) is countered by the effect of glucose, *i.e.*, the front of the fructose band is slowed

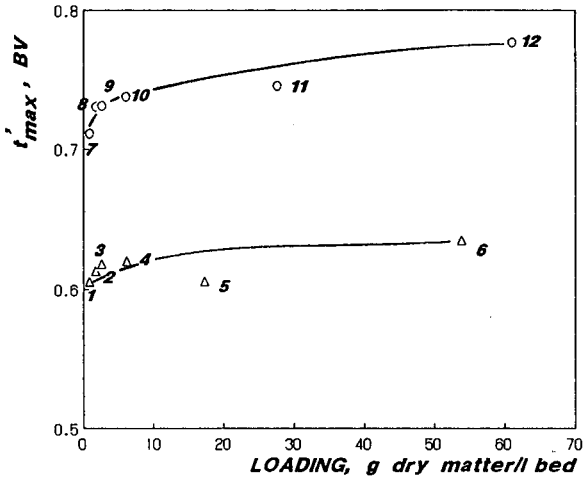

Fig. 2. Retention times ($qt'_{max}/L'A$) in bed volumes at the peak maxima at different column loadings. Single-component feeds. The run parameters for experiments 1–12 were as follows [experiment No. (c_f, % dry matter; dry matter fed, g; L_f, cm)]: 1 (11.0; 33; 11); 2 (20.5; 62.5; 11); 3 (30.4; 96.7; 11); 4 (60.5; 219; 11); 5 (16.8; 668; 210); 6 (20; 1603; 420); 7 (10; 30; 11); 8 (20.4; 62.6; 11); 9 (29.7; 95.0; 11); 10 (59.7; 217.9; 11); 11 (20.0; 905; 210); 12 (20.0; 1814; 240).

on account of glucose relative to the velocity of the maximum of the fructose band.

The non-linearity and dependence of the isotherms can be qualitatively understood by considering the limited accessibility of the internal surface of the resin to the sugar molecules. The volume-weighted median pore size (diameter) of the resin is *ca.* 10 Å (manufacturer's information), *i.e.*, half of the total volume of the pores is composed of pores smaller than 10 Å and half of pores larger than 10 Å. Therefore, a large fraction of the pores have diameters rougly equal to the diameter of the hydrated sugar molecules. Penetration into these micropores then involves displacing the hydration layers of the counter ions and also, perhaps, those of the diffusing sugar molecules, a process favoured by the increasing sugar concentration in the liquid and by the diminishing concentration of the water molecules at high sugar concentrations. The degree of hydration and the diameter of the hydrated sugar clusters are known to be less at high sugar concentrations. The contraction of the resin at high sugar concentrations (Fig. 4) may also be expected, however, to contribute at least partially to the non-linearities. Whereas the pore volume and mean pore size are likely to

TABLE I

PARTITION COEFFICIENT OF GLUCOSE (K_G) AND FRUCTOSE (K_F) ON SEVERAL SULPHONATED POLYSTYRENE RESINS IN THE Ca^{2+} FORM

$K_G = K_{G0} + A_1c_G + B_1c_F$; $K_F = K_{F0} + A_2c_G + B_2c_F$. A zero indicates that this parameter was not determined (a linear model was assumed *a priori*) rather than that is was determined to be zero.

Sorbent	Ref.	T (°C)	K_{G0}	A_1	B_1	K_{F0}	A_2	B_2	K_{F0}/K_{G0}
Dowex 50W-X8	3	30	0.30	0	0	0.80	0	0	2.7
Zerolit 225 SRC 14	4	20	0.20	0	0	0.78	0	0	3.9
		30	0.20	0	0	0.67	0	0	3.4
		48	0.20	0	0	0.56	0	0	2.8
		60	0.20	0	0	0.49	0	0	2.5
Duolite C204	5	29	0.5	0	0	0.88	0	0	1.8
		52.5	0.5	0	0	0.75	0	0	1.5
		70	0.5	0	0	0.67	0	0	1.3
Korela VO7C	6		0.215	0	0	0.472	0	0	2.2
Duolite C204	7	25	0.51	0	0	0.88	0	0	1.7
Zerolit SRC14	8, 9	25	0.126	0.0039	0.0042	0.38	0.0065	0.00075	3.0
Duolite C204	2	55	0.36	0.001	0.0015	0.465	0.0015	0.0025	1.3
Duolite C204F	10	60	0.374	0	0	0.468	0	0	1.3
Dowex Monosphere 99 CA	This work	70	0.245	0.0051	0.003	0.47	0.007	0.0049	1.9

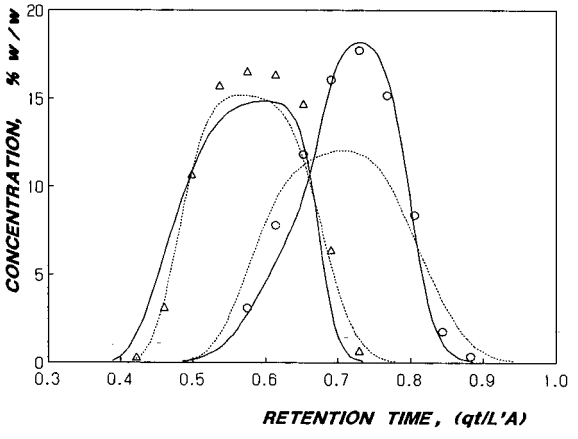

Fig. 3. Measured elution profiles [(△) glucose; (○) fructose] and thise calculated from the non-linear model (solid lines): K_{G0} = 0.245; A_1 = 0.0051; B_1 = 0.001; K_{F0} = 0.47; A_2 = 0.01; B_2 = 0.0049. Dotted lines represent a "best" linear model: K_{G0} = 0.35; K_{F0} = 0.60; $A_1 = A_2 = B_1 = B_2 = 0$. q = 135 ml/min; feed, 30% (w/w) HFCS.

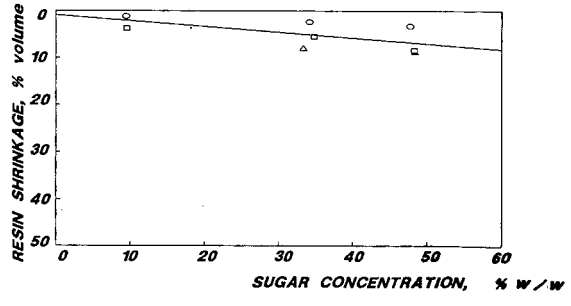

Fig. 4. Shrinkage of the resin beads at 25°C and various sugar concentrations (△ = glucose; ○ = fructose; □ = sucrose; two experimental points for glucose, at concentrations 9.5 and 48.5%, are obscured by other points). Dowex Monosphere 99 CA resin. Determination by direct measurement of the beads diameters at high magnifications [11]. The solid line is the least-squares fit of all points.

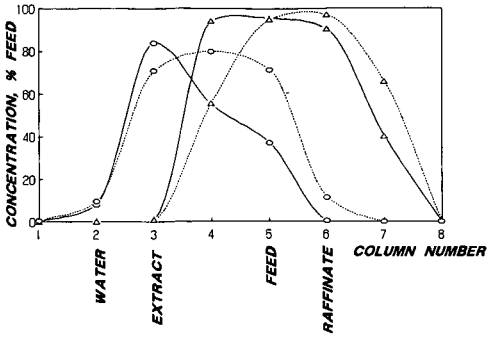

Fig. 5. Simulated steady-state SMB profiles (△ = glucose; ○ = fructose) for linear (dotted lines) and non-linear (solid lines) isotherms. Parameters as listed in Fig. 3. Feed, 30% HFCS; flow-rates, feed 23.3 ml/min (0.029 BV/h (BV = bed volume)), water 46.6 (0.059), extract (fructose product) 28.3 (0.036), raffinate (glucose product) 41.7 (0.053), recycle 100 (0.126); switching time, linear 30.4 min, non-linear 28.8 min; total bed volume, 47.52 l. System configuration: water, in column 2; extract, out of column 3; feed, in column 5; raffinate, out of column 6.

decrease as a result of bead contraction and thus contribute to a Langmuir-type behaviour, the bed void fraction may not be a constant as assumed in the above partial differential equation but rather an increasing function of concentration. This would then be expected to contribute to the upward curvature of the isotherms.

As expected, the simulated steady-state SMB profiles differ significantly depending on the assumed adsorption characteristics of the components (Fig. 5). If known accurately under the conditions prevailing in the SMB process, they can in turn be used to optimize the SMB separation. The simulation can be handled with a fast personal computer [12] and thus provide an accessible tool for efficient operation.

REFERENCES

1 A. deRosset, R. W. Neuzil and D. J. Korous, *Ind. Eng. Chem., Process Des. Dev.*, 15 (1976) 261.
2 C. B. Ching, C. Ho, K. Hidajat and D. M. Ruthven, *Chem. Eng. Sci.*, 42 (1987) 2547.
3 Y. S. Ghim and H. N. Chang, *Ind. Eng. Chem., Fundam.*, 21 (1982) 369.
4 C. B. Ching and D. M. Ruthven, *Can. J. Chem. Eng.*, 62 (1984) 398.
5 C. B. Ching and D. M. Ruthven, *Chem. Eng. Sci.*, 41 (1986) 3063.
6 P. E. Barker and G. Ganetsos, *J. Chem. Tech. Biotechnol.*, 35 (1985) 217.
7 C. B. Ching and D. M. Ruthven, *Chem. Eng. Sci.*, 40 (1985) 877.
8 P. E. Barker and S. Thawait, *J. Chromatogr.*, 295 (1984) 479.
9 D. M. Ruthven, *J. Chromatogr.*, 351 (1986) 337.
10 V. Viard and M. L. Lameloise, *Récents Progrès en Génie des Procédés*, Vol. 8a, Lavoisier, Paris, 1989, p. 233.
11 M. Mrini, *M.S. Thesis*, Louisiana State University, Baton Rouge, LA, in progress.
12 M. Saska, unpublished results.

Journal of Chromatography, 590 (1992) 153–161
Elsevier Science Publishers B.V., Amsterdam

CHROMSYMP. 2395

Isolation of experimental anti-AIDS glycerophospholipids by micro-preparative reversed-phase high-performance liquid chromatography

J. V. Amari and P. R. Brown*

Department of Chemistry, University of Rhode Island, Kingston, RI 02881 (USA)

P. E. Pivarnik, R. K. Sehgal and J. G. Turcotte*

Department of Medicinal Chemistry, University of Rhode Island, Kingston, RI 02881 (USA)

ABSTRACT

The experimental anti-AIDS glycerophosphatidic acid: nucleoside (*sn*-1/*sn*-2 diacylglycerol:dideoxynucleotide) drugs 3′-azido-3′-deoxythymidine monophosphate diglyceride (AZT-MP-DG) and 2′,3′-dideoxycytidine monophosphate diglyceride (ddC-MP-DG) were isolated and purified by reversed-phase high-performance liquid chromatography (HPLC). The chromatographic separation was based on the glycerophospholipid moiety of the drugs and detection of the nucleoside component. The separations were optimized on method development columns packed with the stationary phase to be used in the micro-preparative column and monitored by a UV detector. Fractions were collected and analyzed for purity by analytical-scale HPLC and by thin-layer chromatography (TLC). The purity of the recovered drugs based on UV and light-scattering detection and on TLC was greater than 99%. The purified compounds were isolated for studies on structure confirmation, physical, biophysical and formulation properties and anti-HIV efficacy in culture.

INTRODUCTION

In the treatment of acquired immunodeficiency syndrome (AIDS), AIDS-related complex (ARC) and early human immunodeficiency virus (HIV) infection, chemotherapeutic agents are designed to attack one or more stages of the replicative cycle of the HIV [1–4]. An anti-retroviral analogue of thymidine, 3′-azido-2′,3′-dideoxythymidine (azidothymidine, AZT), which inhibits reverse transcription (polymerase), is currently the only drug approved by the US Food and Drug administration (FDA) for the treatment of AIDS/ARC and early asymptomatic HIV infection [5]. However, AZT and other dideoxynucleosides (*e.g.*, ddC and ddI) exhibit dose-limiting toxicity and have relatively short circulating lifetimes [6,7]. In an effort to increase serum half-lives and decreased toxicity and consequently to increase efficacy, a new group of experimental liponucleotide anti-AIDS drugs, originating from earlier work on anti-cancer liponucleotides [8–11], have recently been synthesized [12,13]. These drugs include 16:0/18:1ω9 (*sn*-1/*sn*-2) phosphatidic acid:dideoxynucleoside or diacylglycerol:dideoxynucleotide conjugates, AZT monophosphate diglyceride, (AZT-MP-DG) and dideoxycytidine monophosphate diglyceride (ddC-MP-DG) (Fig. 1) [12,13]. To isolate and purify enough material for molecular confirmation, biophysical and anti-HIV (in culture) studies, a micro-preparative reversed-phase high-performance liquid chromatographic (RP-HPLC) separation was developed.

Chromatographic purification techniques of naturally occurring liponucleotides have been accomplished by thin-layer chromatography (TLC), normal-phase column chromatography on a silica support and ion-exchange column chromatography on silica modified with diethylaminoethyl (DEAE) moieties [14–16]. Synthetic liponucleotides have been purified by TLC and adsorption chromatogra-

0021-9673/92/$05.00

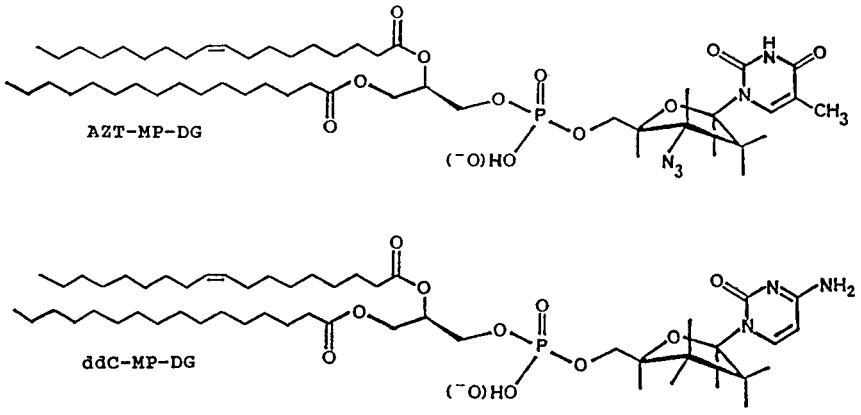

Fig. 1. Structures of AZT-MP-DG and ddC-MP-DG.

phy [17–19] and DEAE chromatography [18,19].

Solvents used to elute the liponucleotides usually contain large amounts of chloroform. As this halogenated solvent is a carcinogen, it is preferable not to use it for the preparative isolation and purification of a drug. In addition, chloroform precludes monitoring by ultraviolet (UV) detection at wavelengths less than 240 nm. As phosphatic acid and other possible contaminants of the synthetic mixture absorb at wavelengths below 210 nm, UV-transparent solvents must be used. To eliminate the use of chloroform, which is often used with silica columns to purify compounds, an RP-HPLC method was developed utilizing a UV-transparent solvent system. The solutes were monitored in the wavelength range 260–280 nm and in the low end of the UV range. In addition, an analytical HPLC method with UV spectral characterization was applied to determine the purity of the fractions [20].

EXPERIMENTAL

Sample preparation

AZT-MP-DG. AZT-MP-DG in the synthetic reaction mixture was first separated from the bulk of starting materials and side-products by silica gel column chromatography. A solution containing *ca.* 50 μg/μl of AZT-MP-DG was prepared in chloroform–methanol (8:2) with 10 μl of 0.01% butylated hydroxytoluene (BHT) in methanol added as an antioxidant.

ddC-MP-DG. The gross impurities were separated from ddC-MP-DG in the synthetic reaction mixtures by adsorption HPLC [18]. The fractions were collected and pooled. The pooled fractions were taken to dryness with a stream of nitrogen, leaving *ca.* 100 mg of a clear, waxy solid. To dissolve the solid, 2 ml of chloroform–methanol (3:2) were used together with 10 μl of 0.01% BHT in methanol. The concentration of the working solution was *ca.* 50 μg/μl.

Materials

All solvents and reagents (Fisher Scientific, Pittsburgh, PA, USA) for the method development, micro-preparative separations and analysis were of HPLC grade. Water was doubly distilled and deionized. Each solvent was filtered through a 0.45-μm nylon-66 filter (AllTech, Deerfield, IL, USA). The mobile phases contained 1–1.4 m*M* KH_2PO_4 adjusted to pH 2.4 with phosphoric acid.

Method development

The chromatographic system used for the method development studies consisted of a Model M6000A pump (Waters–Millipore, Milford, MA, USA), a Rheodyne (Berkeley, CA, USA) Model 7125 injector with a 100 μl loop and a Knauer variable-wavelength UV detector (Sonntek, Woodclift Lake, NJ, USA). Method development columns were 25 × 0.46 cm I.D., packed with YMC Prep-10 C_{18} (10-μm) silica (Yamamura Chemical, Kyoto, Japan). The columns were packed using a Haskel (Burbank, CA, USA) Pump. The separa-

tions were optimized on a small scale, thus reducing solvent and sample consumption.

The wavelengths used to monitor the separations were 267 nm for AZT-MP-DG and 280 nm for ddC-MP-DG. Absorption at these wavelengths was due to the pyrimidine moieties.

The mobile phase consisted of methanol–1.4 m*M* KH_2PO_4 (93:7, v/v) at pH 2.4 for AZT-MP-DG and methanol–1 m*M* KH_2PO_4 (95:5, v/v) at pH 2.4 for ddC-MP-DG. After elution of the liponucleotides, the columns were flushed with 100% methanol to elute any strongly retained impurities. After the highly retained solutes had been washed off with methanol, the column was re-equilibrated with the mobile phase. The optimum method development flow-rate was 2.8 ml/min for AZT-MP-DG and 3.5 ml/min for ddC-MP-DG. All separations were achieved at room temperature. The chromatograms were recorded on an HP 3394A integrator (Hewlett-Packard, Avondale, PA, USA) at 0.2 cm/min and an Omniscribe recorder (Houston Instruments, Austin, TX, USA) at 0.25 cm/min.

Micro-preparative HPLC

Micro-preparative separations were carried out on a 25 × 1.0 cm I.D. column packed with YMC Prep-10 C_{18} (10-μm) silica (Yamamura Chemical, Japan). The HPLC system was a SepTech (Wakefield, RI, USA) NovaPrep 5000 operated at a flow-rate of 10 ml/min for AZT-MP-DG and 15 ml/min for ddC-MP-DG. The system was operated under computer control, utilizing TurboPrep software (SepTech). The variable-wavelength detector was set at 267 nm with a sensitivity of 0.64 a.u.f.s. to monitor AZT-MP-DG and at 280 nm for ddC-MP-DG. The working solution was injected manually with a syringe. The NovaPrep contains two pumps: pump A delivered methanol–KH_2PO_4 and pump B methanol.

Analytical HPLC

The fractions collected during method development and micro-preparative separations were analyzed for purity. The analytical system consisted of a Waters Model M6000 pump, a Rheodyne 10-μl injector, a Schoeffel Spectro Flow Monitor SF 770 variable-wavelength detector (Kratos, Westwood, NJ, USA), a rapid-scanning UV detector (Barspec, Rehovot, Israel) and an evaporative light-scattering detector (Varex, Burtonsville, MD, USA).

For the AZT-MP-DG analysis a 25 × 0.40 cm I.D. LiChrospher 100 C_{18} (5-μm) column (EM Science, Gibbstown, NJ, USA) with methanol–1 m*M* KH_2PO_4 (pH 2.4) (95:5) as the mobile phase at a flow-rate of 1.5 ml/min was used. A sensitivity of 0.02 a.u.f.s. and wavelengths of 267 and 208 nm [the two absorbance maxima of AZT-MP-DG (Fig. 2a)] were used to monitor the solute. The low wavelength was useful to detect impurities lacking strong UV chromophores such as phosphatidic acid or glycerol.

The ddC-MP-DG was analyzed on a 25 × 0.46 cm I.D. C_{18} (5-μm) column (HPLC-Systeme, Berlin, Germany) with methanol–1 m*M* KH_2PO_4 (pH 2.4) (95:5) as the mobile phase at a flow-rate of 2 ml/min. To monitor the solute, wavelengths of 280 and 208 nm were used [the two absorbance maxima of ddC-MP-DG (Fig. 2b)].

For the liponucleotides the light-scattering detector was used under the following conditions: nitrogen pressure, 85 mmHg; exhaust temperature, 92.5°C; and heater temperature, 150.0°C. The mobile phase was methanol–1 mM ammonia solution (pH 2.4) (95:5) at a flow-rate of 1.2 ml/min.

Collected and pooled fractions were also analyzed by TLC on silica gel plates (Fisher Scientific). The mobile phase was chloroform–methanol–2-propanol–water–triethylamine (30:9:25:7:25) [21]. For detection, molybdenum blue, which is specific for phosphorus in the glycerophospholipids, and sulfuric acid, which is a general reagent for all organic compounds, were used.

RESULTS AND DISCUSSION

Liponucleotides are analogues of glycerophospholipids. Like naturally occurring glycerophospholipids, they are composed of a polar head group and two non-polar fatty acid chains esterified to the diglyceride moiety. The polar head groups of the experimental drugs AZT-MP-DG and ddC-MP-DG consist of the anti-viral nucleosides (AZT and ddC) coupled to 16:0/18:1ω9 (*sn*-1/*sn*-2) phosphatidic acid (PA) [12,13]. The physical properties of the liponucleotides resemble those of natural glycerophospholipids. Thus separations have been based on glycerophospholipids which are generally separated using the normal-phase mode. However, normal-phase separations for glycerophospholipids

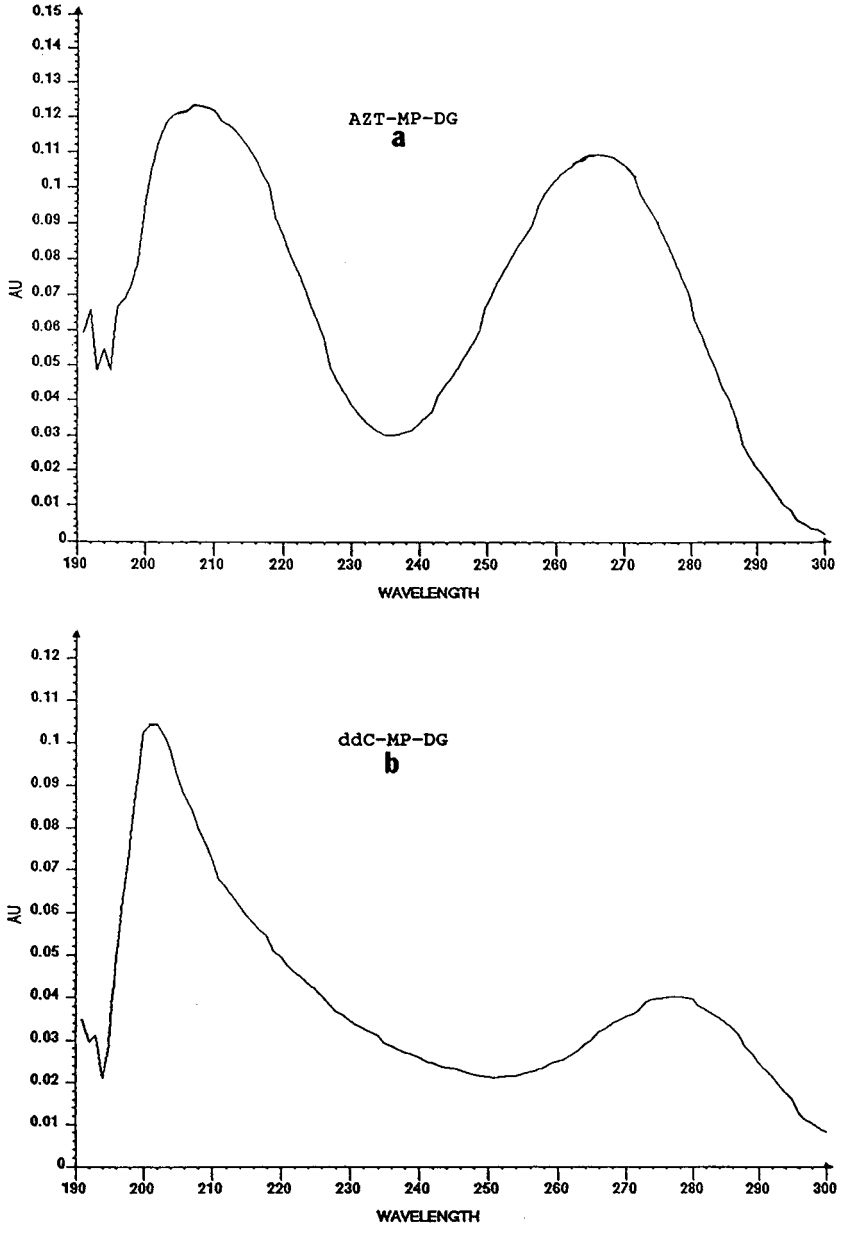

Fig. 2. (a) UV spectrum of purified AZT-MP-DG obtained with the rapid-scanning detector. Scan rate, ten spectra per second. Absorbance maxima: 208 and 267 nm. Analytical chromatographic conditions: mobile phase, methanol–1 m*M* KH_2PO_4 (pH 2.4) (95:5); flow-rate, 1.5 ml/min. (b) UV spectrum of purified ddC-MP-DG obtained with the rapid-scanning detector. Scan rate, ten spectra per second. Absorbance maxima: 208 and 280 nm. Analytical chromatographic conditions: mobile phase, as in (a); flow-rate, 2 ml/min.

require ternary mobile phases and/or gradient elution whereas with RP-HPLC a binary mobile phase with isocratic elution can be used, which is preferable for preparative separations. Mobile phase compositions for the reversed-phase separation of natural glycerophospholipids typically contain 90–95% methanol and 1–2 m*M* KH_2PO_4 [22,23]. In addition to KH_2PO_4, ammonium acetate can be

used as the salt in the mobile phase [24]. Ammonium acetate 1 m*M* gave the same *k'* values as those obtained with 1 m*M* KH_2PO_4.

For purity analysis, aliquots of the collected fractions were injected onto the analytical columns. As commercial standards were not available for either compound, the liponucleotide peaks were characterized with UV detection using absorbance ratios and peak-purity measurements [25]. In addition to UV and TLC analysis, a light-scattering detector was used.

AZT-MP-DG

The optimum mobile phase composition for AZT-MP-DG was methanol–1.4 m*M* KH_2PO_4 (pH 2.4) (93:7). The AZT-MP-DG solution was injected onto the analytical 5-μm column to determine the number of components present (Fig. 3). Impurities eluted near the solvent front and after the AZT-MP-DG peak.

Using the method development column, a loading study was performed to determine the highest load injectable while maintaining a purity level of 99%. Various volumes of the AZT-MP-DG solution were injected and fractions collected. Each fraction was concentrated with a stream of nitrogen to *ca.* 2 ml and analyzed by HPLC. An aliquot of 100 μl of the 50 μg/μl (5 mg) solution was the optimum load.

The separation was scaled up to the micro-preparative column. For the micro-preparative separation a flow-rate of 10 ml/min provided adequate retention and resolution. A 400-μl (20-mg) aliquot was injected (Fig. 4), which produced a split peak. Eighteen 5-ml fractions were collected across the split peak and each was concentrated by rotary vacuum distillation to *ca.* 2 ml. Each fraction was analyzed for purity by analytical HPLC. The *k'* values of the AZT-MP-DG fractions across the split peak were identical (3.5). Hence the peak splitting may be attributed to the solvent effect due to the chloroform used as the sample diluent. Peak splitting has also been reported at the analytical level for the AZT-MP-DG [20]. Fractions 1 and 2 were discarded because of early-eluting impurities. Fractions 3–17, containing AZT-MP-DG of 99% purity, were

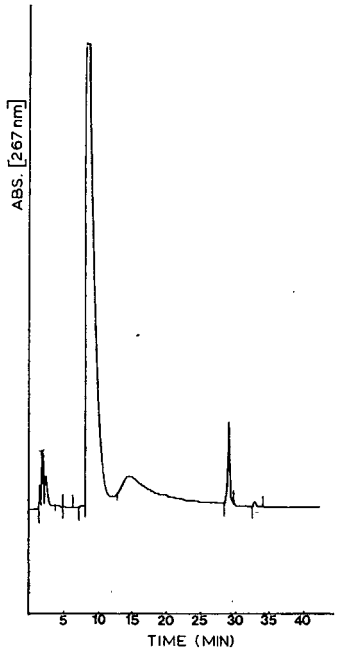

Fig. 3. Analytical HPLC of crude AZT-MP-DG, 5 μl of 50 μg/μl solution (a.u.f.s. 0.04). For chromatographic conditions, see Experimental.

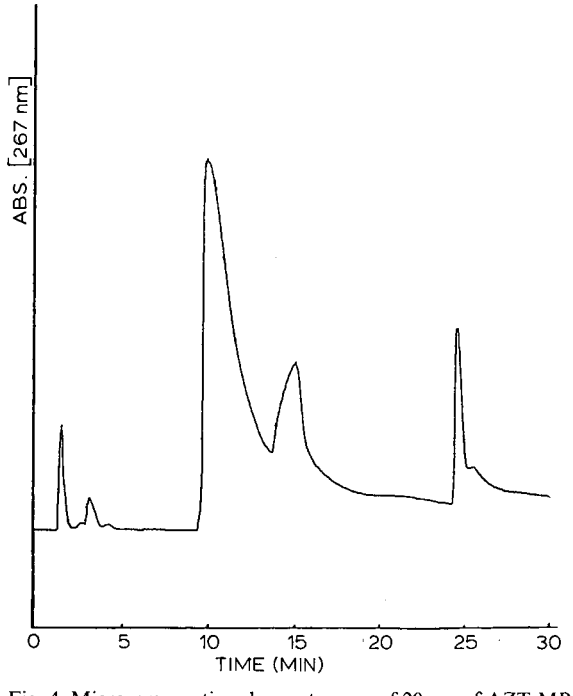

Fig. 4. Micro-preparative chromatogram of 20 mg of AZT-MP-DG. Mobile phase, methanol–1.4 m*M* KH_2PO_4 (pH 2.4) (93:7); flow-rate, 10 ml/min; 267 nm; 0.64 a.u.f.s. Fraction were collected between 9 and 20 min.

pooled. Fraction 18 contained a very minor amount of the product and an impurity after the product, so it was not added to the pool. The pooled fractions were concentrated to *ca.* 2 ml with rotary vacuum distillation. Fig. 5a illustrates the chromatogram of the pooled fractions. Based on UV detection at 267 nm, the purity of the AZT-MP-DG was 99.8%. The pooled fractions were also monitored at 208 nm to detect any impurities that did not absorb at 267 nm (Fig. 5b). However, no additional impurities were detected at 208 nm. Peak splitting was not observed for the pooled fractions, because the AZT-MP-DG recovered was in a solvent mixture similar to the mobile phase used for the analytical HPLC.

The rapid-scanning UV detector was used to obtain absorbance ratios and peak-purity values. Three wavelengths (267, 220 and 208 nm) were used to determine the ratios. The ratios at 267/220, 267/208 and 220/208 nm were compared to ratios obtained on previously purified AZT-MP-DG. For multiple determinations the absorbance ratios were consistent, as shown in Table I. Peak-purity values were determined by normalizing the UV spectra along three points of the chromatographic peak of interest. Peak-purity values indicate if an impurity is co-eluting with the solute of interest. Low peak-purity values (<1.000) indicate with high confidence that no other component(s) was co-eluted with the solute of interest [26]. A peak-purity value of 0.225 was determined for AZT-MP-DG, which compared favorably with a value of 0.215 determined for a batch of AZT-MP-DG synthesized previously. To determine the mass of AZT-MP-DG recovered, the pooled fractions were evaporated to dryness with a stream of nitrogen and then extracted (three times) with chloroform–methanol (8:2). The extraction solvent was evaporated with nitrogen, leaving 18 mg of purified AZT-MP-DG.

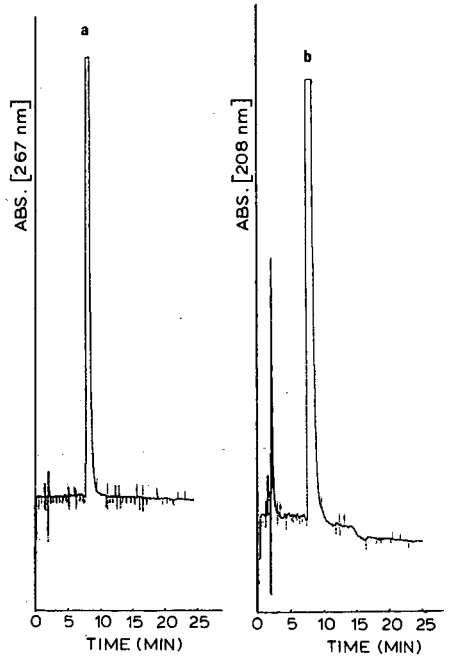

Fig. 5. Analytical HPLC of pooled AZT-MP-DG fractions at (a) 267 and (b) 208 nm (0.02 a.u.f.s.). For chromatographic conditions, see Experimental.

ddC-MP-DG

The ddC-MP-DG mixture was first chromatographed on an analytical column (Fig. 6). In comparison with AZT-MP-DG, more impurities were found. On the method development column an aliquot of 100 μl of the working solution (5 mg) provided the optimum load. During the loading study, the column displayed overload when the k' values decreased with increasing mass injected. The flow-rate was directly scaled to 15 ml/min and 25 mg was the mass injected onto the micro-preparative column. The chromatogram was similar to that in the method development separation (Fig. 7). Nine fractions were collected across the ddC-MP-DG peak. Each fraction was concentrated by rotary vacuum distillation for HPLC analysis.

TABLE I

POOLED AZT-MP-DG FRACTIONS FROM MICRO-PREPARATIVE SEPARATION

	Wavelength ratio		
	267/220 nm	267/208 nm	220/208 nm
	1.22	0.92	0.75
	1.29	0.90	0.70
	1.24	0.86	0.69
Mean:	1.25	0.89	0.71
S.D.:	0.0360	0.03	0.033
R.S.D. (%)[a]:	2.88	3.30	4.58

[a] Relative standard deviation.

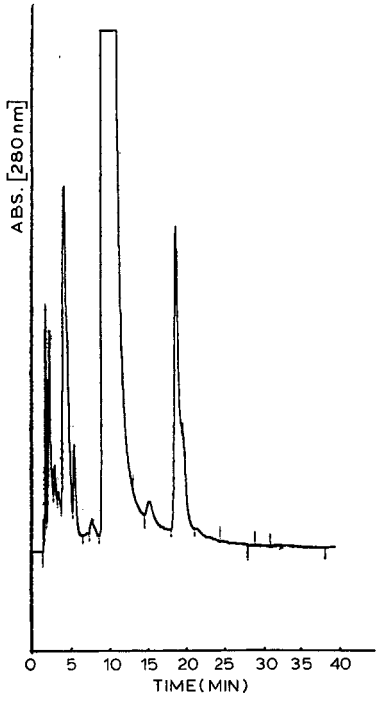

Fig. 6. Analytical HPLC of crude ddC-MP-DG, 5 μl of 50 μg/μl solution (a.u.f.s. 0.04). For chromatographic conditions, see Experimental.

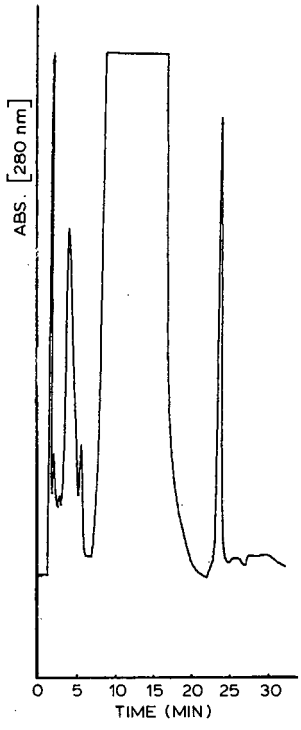

Fig. 7. Micro-preparative chromatogram of 25 mg of ddC-MP-DG. Mobile phase methanol–1 mM KH_2PO_4 (pH 2.4) (95:5); flow-rate, 15 ml/min; 280 nm; 0.64 a.u.f.s. Fractions were collected between 7 and 20 min.

The ddC-MP-DG fractions were monitored at 280 and 208 nm and fractions 4–8 were pooled. Fractions 1–3 were not pooled because an impurity eluted prior to the ddC-MP-DG and in fraction 9 an impurity that eluted after ddC-MP-DG was present. As with AZT-MP-DG, monitoring the ddC-MP-DG at 208 nm did not reveal any additional impurities. Representative chromatograms of the pooled fractions at 280 and 208 nm are shown in Fig. 8a and b, respectively. Based on UV absorption, the purity of the pooled ddC-MP-DG was 99.8%. The pooled fractions were also monitored with the rapid-scanning UV detector. Absorbance ratios, listed in Table II, at 280, 220 and 208 nm were determined. The ratios were consistent for multiple injections. A peak purity of 0.326 was obtained for the pooled fractions, indicating that a single component, ddC-MP-DG, was present. To determine the mass of ddC-MP-DG recovered, the pooled fractions were evaporated to dryness with a stream of nitrogen and then extracted (three times) with chloroform–methanol (3:2). The extraction solvent was evaporated with nitrogen, leaving 13.4 mg of purified ddC-MP-DG.

Impurities

Impurities such as phosphatidic acid are difficult to detect with UV detectors even at low wavelengths. Therefore, an evaporative light-scattering detector was used for monitoring compounds that do not possess UV-absorbing chromophores. Pooled fractions of AZT-MP-DG were analyzed with an evaporative light-scattering detector to confirm the purity (Fig. 9) Based on the light-scattering chromatogram, the purity of AZT-MP-DG was greater than 99%.

TLC is very valuable for determining phosphorus-containing compounds selectively by using a molybdenum blue reagent. Universally all carbon-containing compounds were monitored by charring with sulfuric acid. With silica gel thin-layer plates and detection with these two reagents, no impurities

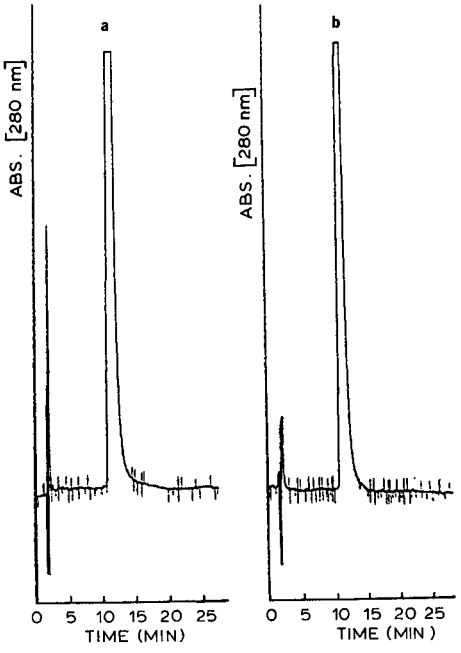

Fig. 8. Analytical HPLC of pooled ddC-MP-DG fractions at (a) 280 and (b) 208 nm (0.02 a.u.f.s.). For chromatographic conditions, see Experimental.

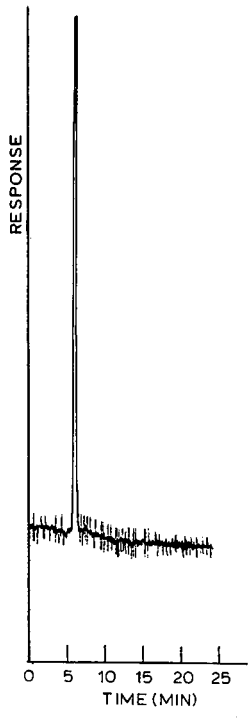

Fig. 9. Evaporative light-scattering chromatogram of pooled AZT-MP-DG fractions. Chromatogrpahic conditions: mobile phase, methanol–1 m*M* ammonia solution (pH 2.4) (95:5); flow-rate, 1.2 ml/min; detector range (sensitivity), 5; heater and exhaust temperatures, 150.0 and 92.5°C, respectively.

were detected in fractions 3–17 of AZT-MP-DG, in fractions 4–8 of ddC-MP-DG or in the pooled fractions of both compounds.

In conclusion, a micro-preparative separation has been developed for the isolation and purification of new experimental anti-HIV glycerophospholipids. The conditions were based on separations of naturally occurring glycerophospholipids on reversed-phase supports and detection based on the nucleotide moiety. The eluent allows for low-UV monitoring to detect impurities that lack strong UV chromophores. AZT-MP-DG and ddC-MP-DG were obtained in purities greater than 99%. The purities were also confirmed using an evaporative light-scattering detector and TLC. The optimized conditions for the micro-preparative column can be adopted with larger preparative columns when greater amounts of the liponucleotides are to be purified.

TABLE II

POOLED ddC-MP-DG FRACTIONS FROM MICRO-PREPARATIVE SEPARATION

	Wavelength ratio		
	280/220 nm	280/208 nm	220/208 nm
	0.62	0.92	0.68
	0.59	0.89	0.66
	0.59	0.89	0.66
Mean:	0.60	0.90	0.67
S.D.	0.016	0.014	0.0072
R.S.D. (%):	2.70	1.58	1.08

ACKNOWLEDGEMENTS

The authors thank SepTech, a Division of EM Industries for the method development columns and YMC for donating the stationary phase and the micro-preparative column. They also thank Varey Corp. for the use of the evaporative light-scattering detector, Barspec Corp. for the rapid-scanning UV detector and Dr. Fred Rabel of EM Science and I.

Molnar of HPLC-Systeme (Berlin, Germany) for the analytical columns. This research was supported in part by a grant from the US National Institute of Allergy and Infectious Diseases (AI 25690) and the National Cooperative Drug Discovery Group for the Treatment fo AIDS (NCDDG/HIV).

REFERENCES

1 D. D. Ho, R. J. Pomerantz and J. C. Kaplan, *N. Engl. J. Med.*, 317 (1987) 278.
2 W. C. Greene, *N. Engl. J. Med.*, 324 (1991) 308.
3 H. Mitsuya, R. Yarchoan and S. Border, *Science (Washington, D.C.)* 249 (1990) 1533.
4 E. DeClercq, *Trends Pharmacol. Sci.*, 11 (1990) 198.
5 P. A. Volberding, S. W. Lagakos, M. A. Koch, C. Pettinelli, M. W. Myers, D. K. Booth, H. H. Balfour, R. C. Reichman, J. A. Bartlett, M. S. Hirsch, R. L. Murphy, W. D. Hardy, R. Soeiro, M. A. Fischl, J. G. Bartlett, T. C. Merigan, N. E. Hyslop, D. D. Richman, F. T. Valentine, L. Corey and the AIDS Clinical Trials Group of the National Institute of Allergy and Infectious Diseases. *N. Engl. J. Med.*, 322 (1990) 941.
6 D. D. Richman, M. A. Fiscl, M. H. Grieco, M. S. Gottlieb, P. A. Volberding, O. L. Laskin, J. M. Leedom, J. E. Groopman, D. Mildvan, M. S. Hirsch, G. C. Jackson, D. T. Durack, D. Phil, S. Nusinoff-Lehram and the AZT Collaborative Working Group. *N. Engl. J. Med.*, 317 (1987) 192.
7 R. Yarchoan, H. Mitsuya, C. E. Myers and S. Border, *N. Engl. J. Med.*, 321 (1989) 726.
8 C. H. R. Raetz, M. Y. Chu, S. P. Srivastava and J. G. Turcotte, *Science (Washington, D.C.)* 196 (1977) 303.
9 J. G. Turcotte, S. P. Srivastava, W. A. Meresak, B. H. Rizkalla and T. P. Wunz, *Biochim. Biophys. Acta*, 619 (1980) 604.
10 J. G. Turcotte, S. P. Srivastava, J. M. Steim, P. Calabresi, L. M. Tibbetts and M. Y. Chu, *Biochim. Biophys. Acta*, 619 (1980) 619.
11 V. C. M. Yang, J. G. Turcotte and J. M. Steim, *Biochim. Biophys. Acta*, 689 (1982) 37577.
12 J. M. Steim, C. C. Neto, P. S. Sarin, D. K. Sun, R. K. Sehgal and J. G. Turcotte, *Biochem. Biophys. Res. Commun.*, 171 (1990) 458.
13 J. G. Turcotte, R. K. Sehgal, C. C. Neto, P. S. Sarin and J. M. Steim, unpublished data.
14 C. R. H. Raetz and E. P. Kennedy, *J. Biol. Chem.*, 248 (1973) 1098.
15 G. Hauser and J. Eichberg, *J. Biol. Chem.*, 250 (1975) 105.
16 W. Thompson and G. MacDonald, *J. Biol. Chem.*, 250 (1975) 6779.
17 K. Y. Hostetler, L. M. Stuhmiller, H. B. M. Lenting, H. van den Bosch, and D. D. Richman, *J. Biol. Chem.*, 265 (1990) 6112.
18 P. E. Pivarnik, R. K. Seghal, J. G. Turcotte, J. V. Amari and P. R. Brown, in preparation.
19 R. R. Ritacco and J. G. Turcotte, unpublished data.
20 J. V. Amari, P. R. Brown, P. E. Pivarnik, R. K. Sehgal and J. G. Turcotte, *J. Pharm. Biomed. Anal.*, in press.
21 J. C. Touchstone, J. C. Chen and K. M. Beavere, *Lipids*, 15 (1980) 61.
22 S. J. Robins and G. M. Patton, *J. Lipid Res.*, 27 (1986) 131.
23 S. Cantafora, M. Cardelli and R. Masella, *J. Chromatogr.*, 507 (1990) 339.
24 J. V. Amari and P. R. Brown, unpublished results.
25 J. V. Amari, P. R. Brown and J. G. Turcotte, in preparation.
26 *Chrom-A-Scope Users' Manual*, Barspec, Rehovot, 1987.

Journal of Chromatography, 590 (1992) 163–168
Elsevier Science Publishers B.V., Amsterdam

CHROMSYMP. 2382

Preparative high-performance liquid chromatographic separation and isolation of bacitracin components and their relationship to microbiological activity

Robert G. Bell*

A.L. Laboratories, Inc., 400 State Street, Chicago Heights, IL 60411 (USA)

ABSTRACT

Bacitracin, a polypeptide antibiotic, is one of the most commonly used antibiotics in the world. The approved method of analysis for bacitracin is microbial. To correlate the microbiological method with a high-performance liquid chromatographic (HPLC) method, bacitracin was chromatographed using HPLC with ultraviolet detection and a YMC basic column. Adequate separation of the isomers was obtained to scale up this procedure to preparative HPLC using a Prep HPLC system and a 250 × 21 mm YMC basic column. The various fractions were separated, isolated and examined for microbial activity. The individual fractions could be precipitated by adding zinc or methylene disalicylic acid and lowering the pH. The crude fractions were recycled to ensure chromatographic purity. The chromatograms can accurately predict (in minutes) the microbiologically determined potency which usually takes 16–24 h to develop. The chromatographic procedure also provides information on the amounts of isomers and degradation products present in the sample, whereas the microbiological assay only provides activities or potencies of the antibiotic. The reported HPLC method also possesses some advantages over some other published HPLC methods in terms of accuracy and time of analysis.

INTRODUCTION

Bacitracin, a polypeptide antibiotic produced by strains of *Bacillus licheniformis* and *B. subtilus*, is one of the most commonly used antibiotics in the world, especially as an animal feed additive [1,2]. Actually, the various products generally referred to as "bacitracin" are mixtures of similar polypeptides which may differ by only one amino acid. These similar polypeptides have been given the designations A, A_1, B, B_1, B_2, C, D, E, F_1, F_2, F_3, G and X [3–8]. Bacitracin A is of primary importance and is highly biologically active (Fig. 1). Bacitracin B differs from A by the replacement of isoleucine with valine, although the exact position of the replacement is not clear. Bacitracins C, D and E are active, but less so than A or B. Bacitracin F (Fig. 1) is the oxidative deaminated compound containing a ketothiazole instead of an aminothiazoline moiety [9,10].

Traditionally, microbiological methods [6,11,12] have been used for the qualitative and quantitative determination of bacitracin, although counter-current distribution [13,14] and column chromatography have also been used [15,16]. Tsuji *et al.* [8] initially developed a high-performance liquid chromatographic (HPLC) method using gradient elution for the separation of bacitracin. By comparing the microbial and HPLC values for bacitracin A and B, the HPLC method was further improved by Tsuji and Robertson [4]. Gallagher *et al.* [17] have developed an isocratic method which has also been accepted by the AOAC as an official procedure for bacitracin [18]. Recently Pavli and co-workers [19–21] and Oka *et al.* [22] have described isocratic methods for the separation and quantitation of bacitracin components utilizing silica-based or polymer reversed-phase columns.

The above methods provide a great advantage over the microbial method of analysis for bacitracin

* Present address: Barre-National Inc., 7205 Windsor Boulevard, Baltimore, MD 21207, USA.

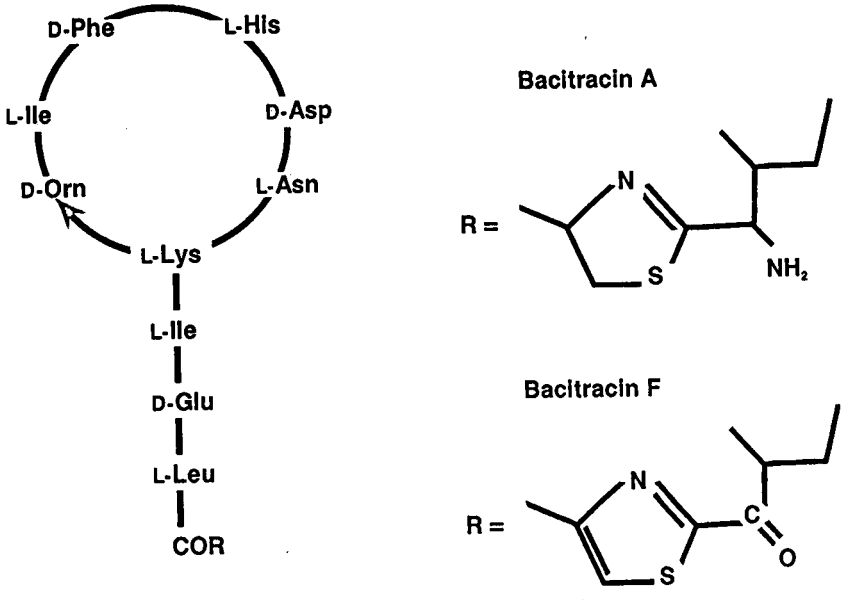

Fig. 1. Structures of bacitracins A and F.

in terms of time of analysis and specificity. The approved microbial method requires 16–24 to develop and is not able to identify and/or quantitate the degradative bacitracin F components. The above HPLC methods only use the bacitracin A and B fractions to quantitate the total microbial activity of bacitracin neglecting the minor components, which, depending on the source and starting materials of the fermentation process, may contribute significantly to microbial activity. The feed industry produces thousands of pounds of bacitracin daily. Determining the potency of bacitracin by HPLC allows constant monitoring of the fermentation process, as well as aiding in blending and quality control of bagging. This allows production to produce the antibiotic on a continual basis, assured that the previous lots were in specification and in good agreement with the pending microbiological assay. In order to provide a rapid, reliable and reproducible HPLC method that will successfully predict, within 2%, the microbiologically determined potency of bacitracin, the components of bacitracin need to be separated analytically, scaled up to the preparative mode for isolation and subsequent microbial potency determination of the isolates. These crude fractions are recycled to ensure chromatographic purity. This information is entered into the integration scheme and, with mobile phase adjustment, a rapid and reproducible analytical HPLC method can be developed that will successfully determine the microbial activity of bacitracin.

EXPERIMENTAL

Apparatus

The HPLC system consisted of a modified Shimadzu chromatographic SCL-6B system controller, LC-6A analytical pumps, LC-8A preparatory pumps, SIL-6B injector capable of delivering accurately 1 μl to 2 ml, a SPD-6AV detector with analytical and preparative flow cells and a SIL-601 integrator.

Stainless-steel columns (250 × 4.6 mm I.D. and 250 × 21 mm I.D.) prepacked with YMC basic (C_8, 200 Å, 5 μm); YMC, Morris Plains, NJ, USA) were used for the analytical and preparative separations, respectively.

The mobile phase for the isocratic separation consisted of HPLC-grade methanol–50 m*M* potassium dihydrogenphosphate buffer (pH 6.5) (59:41), made with distilled, deionized water.

The mobile phase for gradient elution consisted of HPLC-grade methanol (pump A) and 50 m*M* potassium dihydrogenphosphate (pH 6.5) (pump

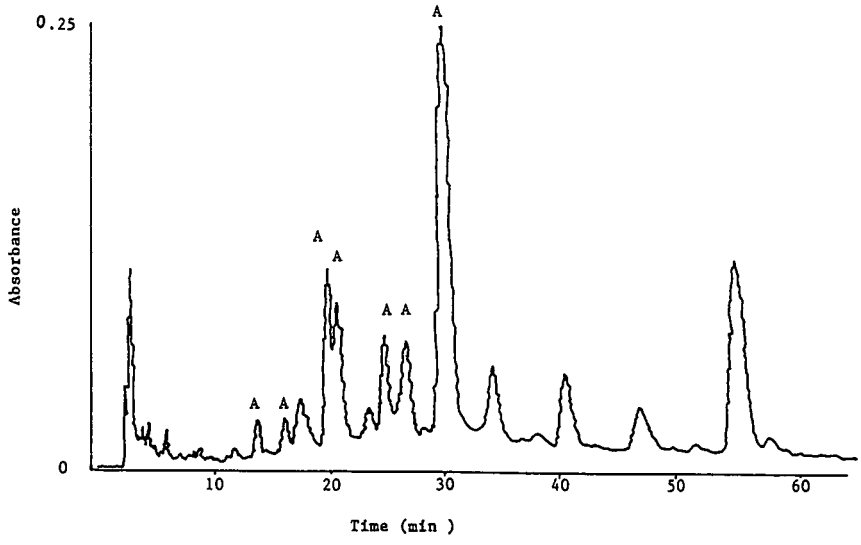

Fig. 2. HPLC profile of the separation of the isomers of bacitracin. A YMC basic column (250 × 4.6 mm I.D.) was used with a linear gradient from 57 to 63% methanol (pump A) and 43 to 37% 50 m*M* phosphate buffer (pH = 6.5) (pump B). Flow-rate, 1 ml/min. An "A" designates microbial activity.

B), made with distilled, deionized water. A linear gradient was programmed (57% A initial, 63% A final) for 1 h.

Preparation of bacitracin standards and samples

Approximately 1 g of zinc bacitracin USP reference standard (U.S.P.C., Rockville, MD, USA) was dissolved in 100 ml of acidic methanol solution (20 m*M* hydrochloric acid in 80% methanol). The solution was mixed, vortexed, centrifuged and filtered (0.45 μm). Samples of bacitracin were prepared in the same manner.

Chromatographic conditions

The column temperature was 25°C. Injection volumes were 100 μl and 2 ml for the analytical and preparative procedures, respectively. The flow-rates were 1 ml/min for the analytical procedure and 20 ml/min for the preparative procedure. The detector used both analytical and preparative flow cells that were monitored at 215 nm.

Microbiological conditions

Bacitracin potency was determined microbiologically following the USP XXII <81> procedure [12]. The cylinder plate assay was used utilizing *Micrococcus luteus* as the test organism. After incubation, the plates were analyzed using a computerized zone reader which consisted of a video imager that, in conjunction with a computer, will construct a linear curve for five standards and calculate the concentration of the unknown by imaging the zone of inhibition and comparing it to the standard curve.

RESULTS AND DISCUSSION

The chromatographic profile of bacitracin using gradient elution is shown in Fig. 2. Good separation exists for the isomer using these conditions. Heart cuts of each of these peaks on a preparative scale provide crude preparations of the bacitracin fractions. These crude fractions were recycled to improve their chromatographic purity. The methanol–phosphate mobile phase used for the chromatographic separations is ideally suited for microbiological plating without further modification. The crude fractions can be precipitated by adding zinc chloride or methylene disalicyclic acid and adjusting the pH accordingly. The gradient procedure is not ideally suited for routine analysis. Time of analysis and reequilibration hamper this procedure. An isocratic mobile phase consisting of methanol–phosphate buffer (59:41) was developed. Adequate separation of the isomers exists for scale up to pre-

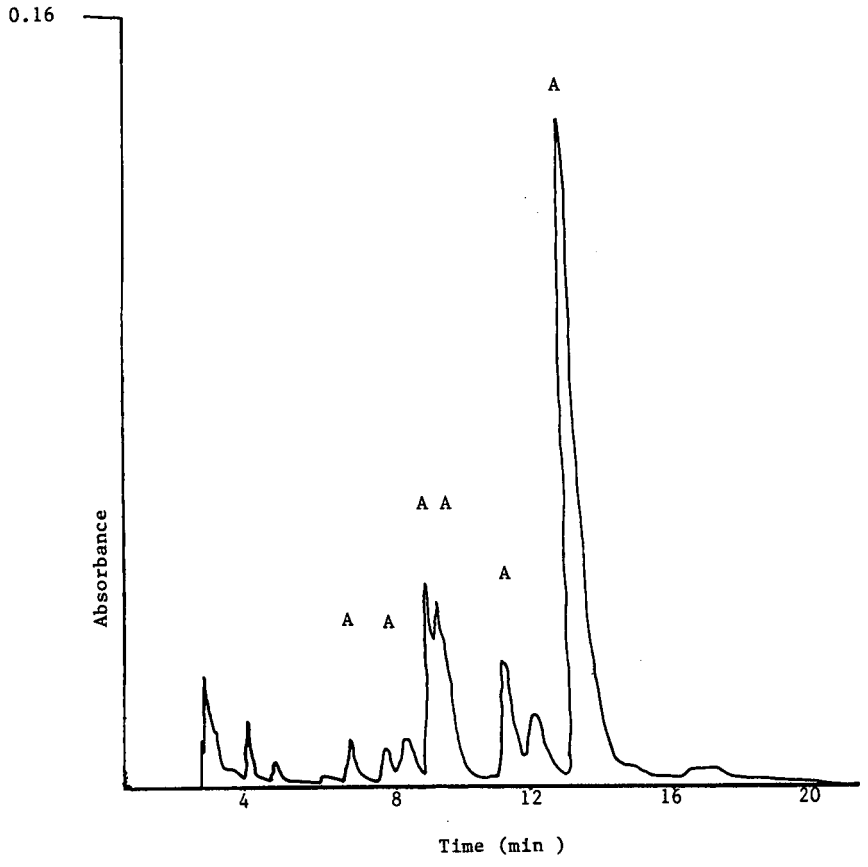

Fig. 3. Prep HPLC profile of the separation of bacitracin isomers. A YMC column (250 × 21 mm I.D.) was used with a methanol–50 m*M* phosphate buffer (pH 6.5) (59:41). Flow-rate 20 ml/min. An "A" designates microbial activity.

parative HPLC that allows all of the isomers to elute within 22 min. Scale up considerations for the flow-rate and sample load were as follows:

$$\text{flow-rate} = \text{flow-rate}_{\text{anal}} \cdot \frac{(D_{\text{prep}})^2}{(D_{\text{anal}})^2}$$

$$\text{sample load} = \text{load}_{\text{anal}} \cdot \frac{(D_{\text{prep}})^2 L_{\text{prep}}}{(D_{\text{anal}})^2 L_{\text{anal}}}$$

where D and L are the diameter and length, respectively. The conversion from analytical to preparative chromatography in this situaton involved approximately a twenty-fold scale factor. The linear range for this assay is 10–2000 I.U. (68.9 I.U./mg).

Fig. 3 illustrates the preparative chromatogram of bacitracin. There is excellent scale up between the analytical and the preparative procedure. This is due in part to the identical lots of packing material used for both the analytical and preparative columns, thus reducing the chances of lot-to-lot variability. The collected fractions were immediately plated to determine their microbiological potency. (An "A" indicates microbial activity as shown in Figs. 2 and 3.) Accurate assessment of the identities of the individual peak were not possible except for the A and F fractions. A corrected activity was calculated for the active peaks by determining their individual potencies, chromatographic area and amount injected [activity (U)/area/weight]. A response factor was then calculated relative to bacitracin A. The corrected responses were approximately equal, which allows the peak areas of the active peaks to approximate bacitracin potency.

TABLE I

COMPARISON OF 50 g/lb BACITRACIN POTENCIES AS DETERMINED MICROBIOLOGICALLY AND BY HPLC

Method	Concentration (g/lb)		R.S.D. (%)	*n*
	Range	Mean		
Microbial	49.8–51.4	50.6	1.23	509
HPLC	48.8–50.8	50.0	0.94	509

Previous studies [4,17,21] only use bacitracins A, B and B_2 to estimate the potency of bacitracin. These peaks usually account for approximately 80–95% of the total area of active components. Comparison of their HPLC potencies range from 1 to 15% of the microbiologically determined potencies. Pavli and Sokolic [21] reported a range of 2–16% average difference between the HPLC and the microbial-determined bacitracin potency. The HPLC-determined potency was consistently lower than the microbial-determined potency. Tsuji *et al.* [8] reported a range of 2–7% average difference for the HPLC- and microbial-determined potencies. The HPLC-determined potencies tended to be higher than the microbial-determined potencies. Both studies involved a small number of samples and indicated that the HPLC-determined potency compared statistically to the microbial-determined potency. Table I shows the comparisons of HPLC-determined potencies for 509 different lots of bacitracin (50 g/lb) *versus* the microbiologically determined potencies. There is excellent agreement between the means of the two methods for a large number of samples. This agreement can be attributed to several factors. This chromtographic method takes into account all of the active peaks, not only bacitracin A_1, B_1 and B_2. The microbiological assay employs automated media preparation of the plating media and analyte, and a computerized zone reader utilizing linear regression analysis of the zones of inhibition, thus reducing some of the variability [manual reading involves technician reading errors, scale reading errors (± 1 mm) etc.] associated with microbial assays.

It is important to note that different producers of bacitracin will have unique profiles with differing microbial activities. For this system, to accurately assess the microbial potencies, the manufactured product as well as the USP bacitracin potencies of the individual active peaks must be examined.

The time of analysis can be shortened by adjusting the organic composition and the pH. Increasing the organic modifier or reducing the pH will result in shorter run times without compromising the accuracy of the assay. This affords the producer accurate determination of the potency of bacitracin in minutes, instead of 16–24 h that are needed for incubation and development of the microbial assay. It also provides information on the degradation products of bacitracin that can be caused by production. The microbiological assay cannot. This procedure provides a more complete chromatographic profile than the other existing HPLC procedures, and shortening the column length to 150 mm and increasing the organic modifier by 2% will reduce the time of analysis to approximately 12 min this making this isocratic procedure quicker than the existing chromatographic procedures published to date. Time of analysis has been further shortened by the use of 50-mm columns packed with 3-μm particles, while still maintaining the resolution of the isomers.

CONCLUSIONS

This chromatographic procedure possesses several advantages over the existing HPLC procedures for bacitracin. All of the microbiologically active peaks are considered for potency determination, not only the A and B peaks. The time of analysis is considerably shorter than those of the other HPLC procedures. This HPLC-determined potency of bacitracin has better agreement with the microbiologically determined potency than the other HPLC procedures for bacitracin. This HPLC procedure and the other existing HPLC procedures provide information on the amounts of the individual components of bacitracin as well as information on the degradation and non-active components present in the sample. The HPLC procedures can accurately estimate bacitracin potency in minutes *versus* the 16–24 h needed for the microbiologically determined potency.

ACKNOWLEDGEMENTS

The author wishes to acknowledge A. L. Laboratories, Inc., Dr. A. Hirsch, P. Arvia-Stonerock,

K. Newman, L. Panozzo, M. K. Peterson and C. Reithel.

REFERENCES

1 D. J. Hanson, *Chem. Eng. News*, 63 (1985) 7.
2 T. Yagasaki, *J. Food Hyg. Soc. Jpn.*, 27 (1986) 451.
3 G. G. F. Newton and E. P. Abraham, *Biochem. J.*, 53 (1953) 597–664.
4 K. Tsuji and J. H. Robertson, *J. Chromatogr.*, 112 (1975) 663–672.
5 O. Froyshov, in E. J. Vandamme (Editor), *Biotechnology of Industrial Antibiotics*, Marchel Dekker, New York, 1983, pp. 665–694.
6 G. A. Brewer, in K. Florey (Editor), *Analytical Profiles of Drug Substances*, Vol. 9, Academic Press, New York, London, 1980; pp. 1–69.
7 L. C. Craig and W. Konigsberg, *J. Org. Chem.*, 22 (1957) 1345–1353.
8 K. Tsuji, J. H. Robertson and J. A. Bach, *J. Chromatogr.*, 99 (1974) 597–608.
9 E. Manekata, T. Shiba and T. Kaneko, *Bull. Chem. Soc. Jpn.*, 46 (1973) 3835.
10 G. G. F. Newton, E. P. Abraham, H. W. Florey and N. Smith, *Br. J. Pharmacol.*, 6 (1951) 417.
11 *The British Pharmacopoeia 1980*, Vols. I and II, Department of Health and Social Security, London, 1980; pp. 42–43.
12 *The United States Pharmacopeia XXII*, National Formulary United States Pharmacopeial Convention, Rockville, MD 1989, pp. 1488–1493.
13 L. C. Craig, J. R. Weisiger, W. Hausmann and E. J. Harfenist, *J. Biol. Chem.*, 199 (1952) 259.
14 L. C. Craig, W. F. Phillips and M. Burachik, *Biochemistry*, 8 (1969) 2348.
15 W. Konigsberg and L. C. Craig, *J. Am. Chem. Soc.*, 81 (1959) 3452.
16 D. R. Storm and J. L. Strominger, *J. Biol. Chem.*, 248 (1973) 3940.
17 J. B. Gallagher P. W. Love and L. L. Knots, *J. Assoc. Off. Anal. Chem.*, 65 (1982) 1178–1185.
18 W. Horwitz (Editor), *Official Methods of Analysis-AOAC*, 2004, The Association of Official Analytical Chemists, Washington, DC, 1982, pp. 491–493.
19 V. Pavli and J. Mohorič and R. Dobrovoljc, *8th Yugoslav Pharmaceutists Symposium, Bled, 1980*, Abstract, pp. 84–85.
20 V. Pavli and A. Krbavcic, *Sci. Pharm.*, 549 (1986) 293–294.
21 V. Pavli and M. Sokolic, *J. Liq. Chromatogr.*, 13 (1990) 303–318.
22 H. Oka, Y. Ikai N. Kawamura, M. Yamada, K. Harada, Y. Yamazaki and M. Suzuki, *J. Chromatogr.*, 462 (1989) 315–322.

Journal of Chromatography, 590 (1992) 169–173
Elsevier Science Publishers B.V., Amsterdam

CHROMSYMP. 2376

Preparative isolation of vitamin D_2 from previtamin D_2 by recycle high-performance liquid chromatography

William Steven Letter

VAREX Corporation, 4000 Blackburn Lane, Burtonsville, MD 20866 (USA)

ABSTRACT

A preparative high-performance liquid chromatographic method, based on recycle chromatography, to separate vitamin D_2 (ergocalciferol) from previtamin D is described. The method provides efficient separation by means of a mixture of methanol, acetonitrile and hexane as eluent on a reversed-phase C_{18} column. Scale-up to a 2-in. diameter column resulted in the collection of 100% pure fractions based on UV detection at 265 nm. The total throughput and the economics of the purification were also optimized.

INTRODUCTION

The use of high-performance liquid chromatography (HPLC) to separate vitamin D_2 (ergocalciferol) from its precursors is well documented [1–8]. Reversed-phase chromatography of vitamin D_2 from tachysterol and vitamin D_3 (cholecalciferol) have been reviewed [5–8], but the resolution of the peaks was either partial or only one of the peaks could be isolated. A method for resolving these components in a crude vitamin D resin or crude extract is of value in the preparative isolation of one or more of these components.

Recycle chromatography allows a sample to be passed over a column several times without the need for re-injection of the sample or a long column. This results in the use of less solvent while still attaining high resolution and efficiency throughout the separation. In preparative chromatography this has an additional and very important advantage of maintaining a reasonable back-pressure as the column used need not be longer to allow for the added efficiency desired.

Recycle chromatography coupled to a more selective method of separating the vitamin D_2 and D_3 and tachysterol components would allow for high-purity fractions of these components to be collected for research or production use with minimum solvent use and better than average yield. The vitamin D_2 fraction was of particular interest in this work and a method for the recovery of 100% pure fractions of this vitamin from a crude vitamin D resin is described in this paper.

EXPERIMENTAL

Materials

Vitamin D resin was obtained from Vitamins, Inc. (Chicago, IL, USA). Vitamin D_2 and D_3 standards were obtained from Sigma (St. Louis, MO, USA). All of the solvents used for the separations were of HPLC grade from Burdick & Jackson (Muskegon, MI, USA).

Instrumentation

The preparative HPLC system used consisted of a VERSA Prep from VAREX (Burtonsville, MD, USA) complete with a variable-wavelength Linear Model 200 UV–VIS detector equipped with a 4.6-μl, 3-mm path-length flow cell. A 2.0-ml sample loop was fitted to the unit's Rheodyne Model 7125 injection valve. Also part of the VERSA Prep System was an IBM AT Type computer data acquisition, control and analysis system, a sixteen-port fraction collection system and recycle capability.

The analytical system used for fraction purity assessment was an HP 1050 Q HPLC System from Hewlett-Packard (Avondale, PA, USA), complete

0021-9673/92/$05.00

with their MS-DOS ChemStation Data acquisition, control and analysis system. An LDC/Milton Roy (Rochester, NY, USA) Spectromonitor D variable-wavelength detector was also used.

Chromatographic conditions

To avoid premature degradation of the pure vitamin standards, all samples and fractions were kept at less than 4°C, in the absence of oxygen and away from any light sources whenever possible. Fractions were analyzed as soon as collected to minimize errors in purity assessment.

All analytical separations were conducted using a 25 cm × 4.6 mm I.D. Zorbax PRO-10, C_{18} columns from DuPont (Wilmington, DE, USA). The flow-rate was set at 1.00 ml/min. A Rheodyne Model 7125 valve with a 20-μl loop was always overfilled 2.5 times for each injection. The UV detector was set at 265 nm except where noted otherwise.

The preparative separations were completed on the same type of material used in the analytical column above except that either a 25 cm × 1 or 2 in. I.D. column was used as needed. All of the preparative columns were packed in our laboratory. The flow-rate through the 1 in. I.D. column was preset at 25.0 ml/min and that through the 2 in. I.D. column at 90.0 ml/min. The 2.0-ml loop was always overfilled with sample 2.5 times prior to injection. UV detection at 300 nm, rather than 265 nm, was used to reduce peak saturation at the higher loads.

All chromatography was performed using a mobile phase consisting of methanol–acetonitrile–hexane (95:3:2, v/v/v). The solvents were premixed in advance and fully sparged with helium before use.

The vitamin D_2 standards were weighed and diluted into vials containing the mobile phase to cover a range of concentrations from 25 to 2500 ng/μl (or 200–20000 USP units, where $4 \cdot 10^6$ USP units = 1 g of vitamin D_2). All collected fractions and standards were diluted as needed and analyzed on the analytical system to determine their total peak area and purity. Linear regression performed on the calibration graph allowed quantification to be performed on the collected fractions.

RESULTS AND DISCUSSION

A modified reversed-phase method for separating a variety of fat-soluble vitamins was developed. The method provided for an almost baseline separation of vitamins D_2 and D_3. Because of the reproducibility and good resolution of the vitamin D_2 and D_3 peaks, this method was chosen for the preparative chromatography which follows.

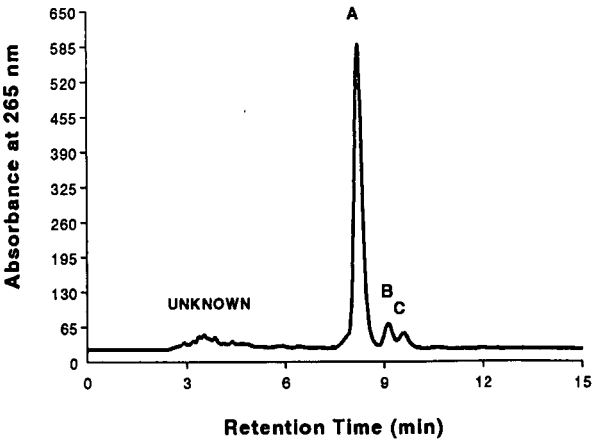

Fig. 1. Chromatogram of crude vitamin D resin at 265 nm obtained by using the system described. Components identified include (A) vitamin D_2 (ergocalciferol), (B) vitamin D_3 (cholecalciferol) and (C) tachysterol.

Seven pure vitamin D_2 solutions containing amounts between 25 and 2500 ng/μl were chromatographed on the analytical system to determine the equation of the calibration line. Table I gives the equation of the calculated line and the concentration *vs.* area responses obtained. Once determined, all subsequent fractions collected were analyzed in a similar fashion to determined their purity and total

TABLE I

RESULTS OF THE ANALYSIS OF VITAMIN D_2 STANDARDS

Linear regression ($r^2 = 0.999$); $y = 0.0401x - 202$.

Vitamin D_2 (ng/μl)	USP Units[a]	Peak-area units
25	200	416
50	400	755
100	800	1570
250	2000	3855
500	4000	7638
1250	10 000	18 984
2500	20 000	40 334

[a] $4 \cdot 10^6$ USP units = 1 g of vitamin D_2.

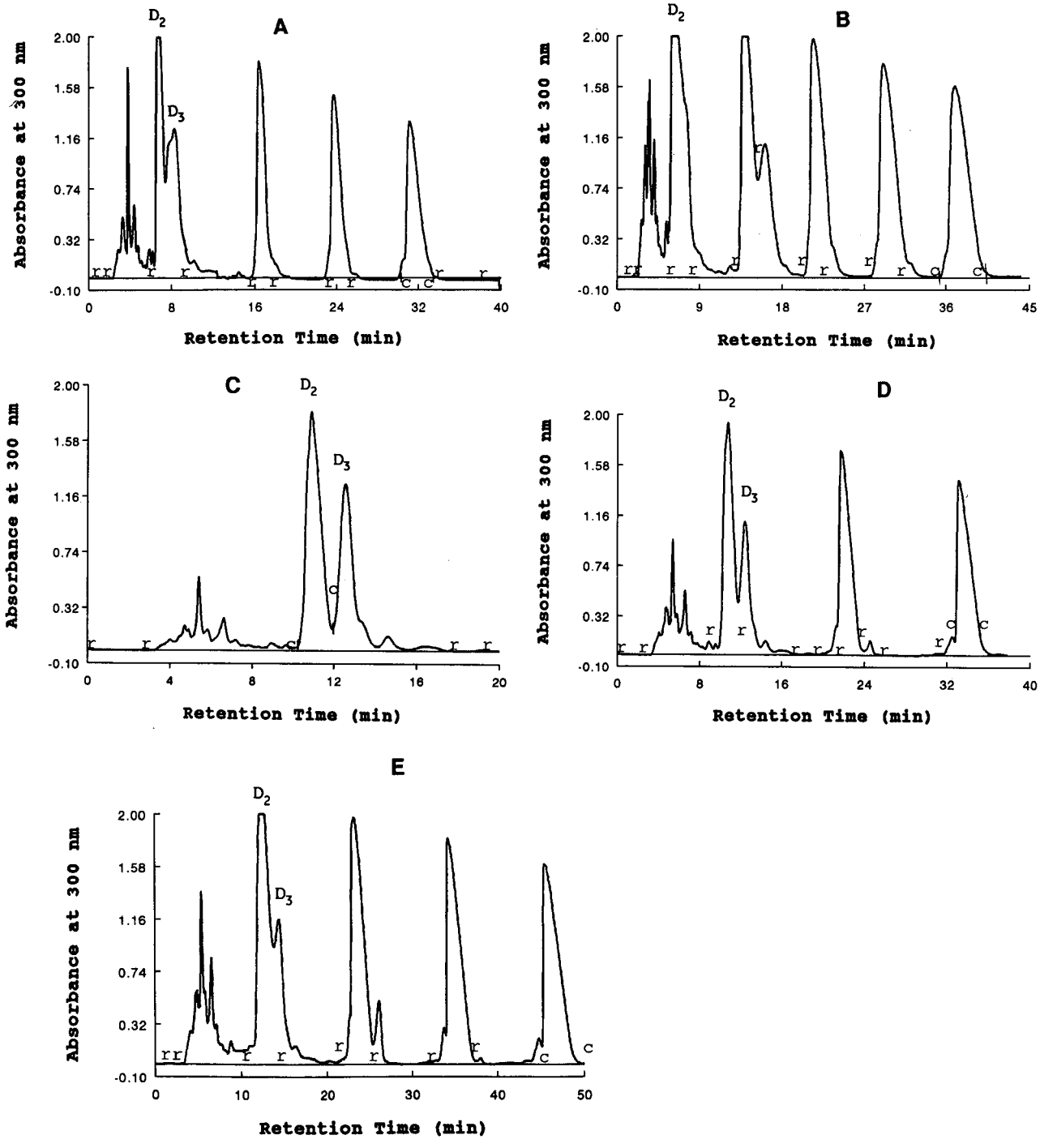

Fig. 2. Preparative chromatograms of vitamin D resin obtained on a Zorbax PRO-10 C_{18} column using methanol–acetonitrile–hexane as eluent. UV absorbance detection at 300 nm. (A) 1 in. I.D. column and 200-mg load; (B) same column as (A) but 400-mg load; (C) 2 in. I.D. column and 500-mg load; (D) same column as (C) but 1-g load; (E) same column as (C) but 2-g load. Letters r denote points at which recycle mode was started; c denotes point of collection.

area. All analytical determinations were performed at 265 nm.

A sample of the crude resin was analyzed using the same technique and found to contain 70% pure vitamin D_2 by percentage peak-area calculations. The chromatogram of the crude resin is shown in Fig. 1.

Crude resin dissolved in 2.00 ml of mobile phase containing either 200 or 400 mg of resin was injected onto the 25 cm × 1 in. I.D. column at a flow-rate of 25.0 ml/min. The UV–VIS detector was set at 300 nm. The resulting chromatograms are shown in Fig. 2A and B. These chromatograms show the crude resin being recycled and purified as the sample passes over the same column.

The use of recycle chromatography allowed the non-vitamin D_2-containing resin to exit to waste while the peak of interest was allowed to cycle back onto the column for further separation. The peak of interest was then collected when the chromatogram showed sufficient resolution for the peak to be collected at 100% purity.

The above procedure was repeated with larger sample loads on the 25 cm × 2 in. I.D. column. The vitamin D_2 was selectively recycled until a 100% pure peak could be fractioned out of the resulting material. The 2 in. I.D. column was run at a higher flow-rate of 90.0 ml/min and at a detection wavelength of 300 nm to reduce peak saturation. The resulting chromatograms are shown in Fig. 2C–E.

The fractions from all of the preparative runs were collected, measured for total volume and analyzed after appropriate dilutions on the analytical HPCL system. The total recovery of vitamin D_2 was between 60 and 100% on the two preparative columns. An example chromatogram of the analysis of the resulting pure preparative vitamin D_2 fraction collected is shown in Fig. 3 and confirms a 100% pure vitamin D_2 fraction.

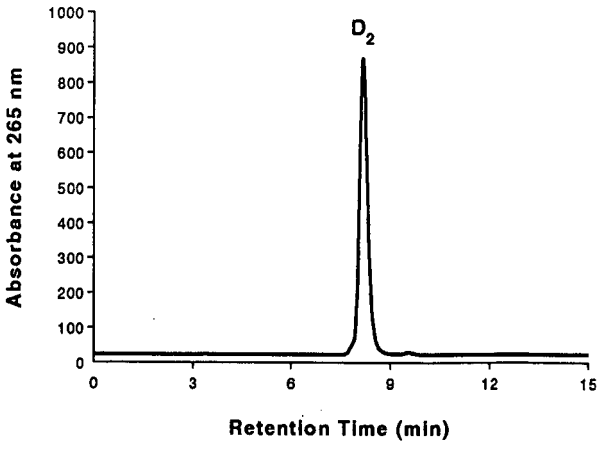

Fig. 3. Analytical chromatogram of vitamin D_2 on a Zorbax PRO-10 C_{18} column using methanol–acetonitrile–hexane as eluent. UV absorbance detection at 265 nm.

The recovery and throughput using recycle chromatography are listed in Table II and show peak throughputs of 6.6 mg/min of vitamin D_2 on the 1 in. I.D. column and 16.4 mg/min using the 2 in. I.D. column. These rates reflect the savings in solvent achieved by using the recycle technique.

CONCLUSIONS

The method described demonstrates the use and advantages of recycle chromatography in a preparative mode. The savings in solvent and in the other-

TABLE II

PREPARATIVE THROUGHPUT AND YIELD OF VITAMIN D_2 BY RECYCLE CHROMATOGRAPHY

Column I.D. (in.)	Raw resin injected (mg)	Vitamin D_2 collected (total) (mg)	Potential vitamin D_2 possible (mg)	Recovery (%)	Throughput (mg/min)
1	200	119	140	85	6.6
1	400	251	280	90	6.6
2	500	(356)	350	> 100	8.9
2	1000	515	700	74	11.7
2	2000	834	1400	60	16.4

wise use of a longer, higher back-pressure column are obvious. The gain in efficiency from recycling the peak is equivalent to using a much longer column. Recycling the peak and not the other resin components allowed an easy recovery of the vitamin D_2 by simply collecting it once it was very pure. All of this was done on a column which normally would not have the efficiency alone to separate the peak on the first pass without a loss of either material or purity.

This method proved useful in the separation and purification of vitamin D_2 from its pre-vitamin components. This same technique could be used to separate other fat-soluble vitamins in a similar manner.

REFERENCES

1 K. A. Tartivita, J. P. Sciarello and B. C. Rudy, *J. Pharm. Sci.*, 65 (1976) 1024–1027.
2 E. Egaas and G. Lambertsen, *Int. J. Vitam. Nutr. Res.*, 49 (1979) 35–42.
3 C. Mackay, J. Tillman and D. T. Burns, *Analyst (London)*, 104 (1979) 626–636.
4 G. A. Walker, B. E. Carpenter and D. L. Tuescher, *J. Pharm. Sci.*, 69 (1980) 846–849.
5 G. Jones, *Clin. Chem.*, 24 (1978) 287–298.
6 R. M. Shepard, R. L. Horst, A. J. Hamstra and H. F. DeLuca, *Biochem. J.*, 182 (1979) 55–69.
7 M. Osadca and M. Araujo, *J. Assoc. Off. Anal. Chem.*, 60 (1977) 993–997.
8 N. A. Parris, *J. Chromatogr.*, 157 (1978) 161–170.

END OF SPECIAL ISSUE

Stationary Phases in Gas Chromatography

by **H. Rotzsche**, *VEB Chemiewerk, Nünchritz, Radebeul, Germany*

Journal of Chromatography Library Volume 48

The primary aim of this volume is to make the chemist familiar with the numerous stationary phases and column types, with their advantages and disadvantages, to help in the selection of the most suitable phase for the type of analytes under study. The book also provides detailed information on the chemical structure, physicochemical behaviour, experimental applicability, physical data of liquid and solid stationary phases and solid supports. Such data were previously scattered throughout the literature. To understand the processes occurring in the separation column and to offer a manual both to the beginner and to the experienced chromatographer, one chapter is devoted to the basic theoretical aspects. Further, as the effectiveness of the stationary phase can only be considered in relation to the column type, a chapter on different column types and the arrangement of the stationary phase within the column is included.

The secondary aim of this book is to stimulate the development of new and improved standardized stationary phases and columns, in order to improve the reproducibility of separations, as well as the range of applications.

Contents: **1. Introduction. 2. Basic Concepts.** Basic components of a gas chromatographic system. Raw data measured from the chromatogram. Derived basic chromatographic parameters. Flow of gases in a gas chromatographic column and formation of bands. Thermodynamic bases of gas chromatography. The quality of chromatographic separation. The time of analysis. Definition of symbols used and list of essential relationships. **3. The Chromatographic Column.** Packed columns. Micro-packed columns. Open-tubular columns. Properties and comparison of the main column types. **4. Characterization of Stationary Phases.** Intermolecular forces. Quantities for the description of interactions. **5. Solid Stationary Phases.** Classification of adsorbents. Carbon adsorbents. Boron nitride and molybdenum disulphide. Adsorbents with hydroxylated and dehydroxylated surfaces. Porous organic polymers. Substances forming inclusion compounds. Modified adsorbents. **6. Chemically Bonded Stationary Phases.** Adsorbents for bonding reactions. Bonding reactions. Properties and characterization of chemically bonded phases. Outlook and prospects for chemically bonded phases. **7. The Solid Support.** The particle size and shape. The surface area. Activity of the original and of the coated solid support. Diatomite supports. Synthetic silica-based supports (Volaspher and quartz). Silica gel. Micro glass beads and porous layer beads. Fluorocarbon supports. Other support materials. **8. Liquid Stationary Phases.** General properties of liquid stationary phases. Hydrocarbons. Silicones. Alcohols, ethers and carbohydrates. Esters. Nitriles and nitrile ethers. Nitro compounds. Amines. Amides. Heterocyclics. Sulphur compounds. Fluorine compounds. Fatty acids and their salts. Salts. Chiral stationary phases. Liquid crystals. Mixed stationary phases. **9. Selection of Stationary Phases.** General recommendations for choosing a suitable stationary phase. Choosing stationary phases for special separation problems with regard to the desired selectivity. Preferred stationary phases. Approaches to stationary phase selection. **Literature. Indexes.**

1991 xiv + 410 pages
Price: US $ 166.50 / Dfl. 325.00
ISBN 0-444-98733-9
Co-edition with Akademische Verlagsgesellschaft Geest & Portig K.-G., Leipzig, Germany

Elsevier Science Publishers
P.O. Box 211, 1000 AE Amsterdam, The Netherlands
P.O. Box 882, Madison Square Station, New York, NY 10159, USA

PUBLICATION SCHEDULE FOR 1992

Journal of Chromatography and *Journal of Chromatography, Biomedical Applications*

MONTH	O 1991	N 1991	D 1991	J	F	M	
Journal of Chromatography	585/1	585/2 586/1 586/2 587/1	587/2 588/1+2	589/1+2 590/1 590/2	591/1+2 592/1+2 593/1+2	594/1+2 595/1	The publication schedule for further issues will be published later
Cumulative Indexes, Vols. 551–600							
Bibliography Section						610/1	
Biomedical Applications				573/1 573/2 574/1	574/2	575/1 575/2	

INFORMATION FOR AUTHORS

(Detailed *Instructions to Authors* were published in Vol. 558, pp. 469–472. A free reprint can be obtained by application to the publisher, Elsevier Science Publishers B.V., P.O. Box 330, 1000 AH Amsterdam, The Netherlands.)

Types of Contributions. The following types of papers are published in the *Journal of Chromatography* and the section on *Biomedical Applications:* Regular research papers (Full-length papers), Review articles and Short Communications. Short Communications are usually descriptions of short investigations, or they can report minor technical improvements of previously published procedures; they reflect the same quality of research as Full-length papers, but should preferably not exceed five printed pages. For Review articles, see inside front cover under Submission of Papers.

Submission. Every paper must be accompanied by a letter from the senior author, stating that he/she is submitting the paper for publication in the *Journal of Chromatography*.

Manuscripts. Manuscripts should be typed in double spacing on consecutively numbered pages of uniform size. The manuscript should be preceded by a sheet of manuscript paper carrying the title of the paper and the name and full postal address of the person to whom the proofs are to be sent. As a rule, papers should be divided into sections, headed by a caption (*e.g.*, Abstract, Introduction, Experimental, Results, Discussion, etc.). All illustrations, photographs, tables, etc., should be on separate sheets.

Introduction. Every paper must have a concise introduction mentioning what has been done before on the topic described, and stating clearly what is new in the paper now submitted.

Abstract. All articles should have an abstract of 50–100 words which clearly and briefly indicates what is new, different and significant.

Illustrations. The figures should be submitted in a form suitable for reproduction, drawn in Indian ink on drawing or tracing paper. Each illustration should have a legend, all the *legends* being typed (with double spacing) together on a *separate sheet*. If structures are given in the text, the original drawings should be supplied. Coloured illustrations are reproduced at the author's expense, the cost being determined by the number of pages and by the number of colours needed. The written permission of the author and publisher must be obtained for the use of any figure already published. Its source must be indicated in the legend.

References. References should be numbered in the order in which they are cited in the text, and listed in numerical sequence on a separate sheet at the end of the article. Please check a recent issue for the layout of the reference list. Abbreviations for the titles of journals should follow the system used by *Chemical Abstracts*. Articles not yet published should be given as "in press" (journal should be specified), "submitted for publication" (journal should be specified), "in preparation" or "personal communication".

Dispatch. Before sending the manuscript to the Editor please check that the envelope contains four copies of the paper complete with references, legends and figures. One of the sets of figures must be the originals suitable for direct reproduction. Please also ensure that permission to publish has been obtained from your institute.

Proofs. One set of proofs will be sent to the author to be carefully checked for printer's errors. Corrections must be restricted to instances in which the proof is at variance with the manuscript. "Extra corrections" will be inserted at the author's expense.

Reprints. Fifty reprints of Full-length papers and Short Communications will be supplied free of charge. Additional reprints can be ordered by the authors. An order form containing price quotations will be sent to the authors together with the proofs of their article.

Advertisements. The Editors of the journal accept no responsibility for the contents of the advertisements. Advertisement rates are available on request. Advertising orders and enquiries can be sent to the Advertising Manager, Elsevier Science Publishers B.V., Advertising Department, P.O. Box 211, 1000 AE Amsterdam, Netherlands; courier shipments to: Van de Sande Bakhuyzenstraat 4, 1061 AG Amsterdam, Netherlands; Tel. (+31-20) 515 3220/515 3222, Telefax (+31-20) 6833 041, Telex 16479 els vi nl. *UK*: T. G. Scott & Son Ltd., Tim Blake, Portland House, 21 Narborough Road, Cosby, Leics. LE9 5TA, UK; Tel. (+44-533) 753 333, Telefax (+44-533) 750 522. *USA and Canada*: Weston Media Associates, Daniel S. Lipner, P.O. Box 1110, Greens Farms, CT 06436-1110, USA; Tel. (+1-203) 261 2500, Telefax (+1-203) 261 0101.

Laboratory information management

new!

An International Journal
Section of Chemometrics and Intelligent Laboratory Systems

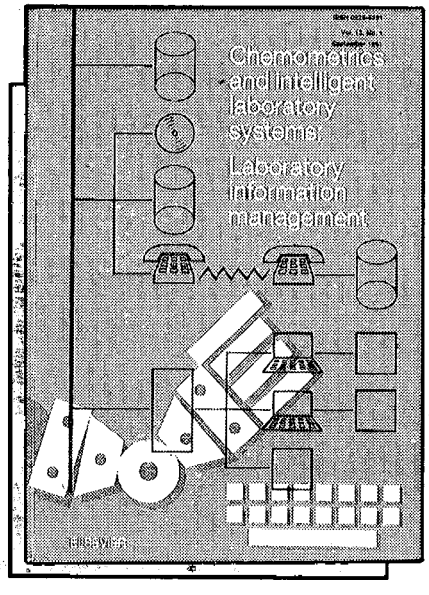

Editor:
R.D. McDowall, Beckenham, Kent, UK
Editor for North America:
R.R. Mahaffey, Eastman Chemicals Division, Kingsport, TN, USA

The journal covers all aspects of information management in a laboratory environment, such as information technology, storage, processing and flow of data. The following topics are covered:

- **Laboratory Information Management Systems (LIMS)**
- **Means of integrating and merging laboratory information**
- **Networks**
- **Regulatory Aspects**
- **Electronic Laboratory Notebooks**
- **Human aspects of laboratory automation**

Subscription Information:
1992: Vol. 17 (3 issues)
Dfl. 406.00 / US$ 201.00
(including postage)
ISSN 0925-5281

A Free Sample Copy is Available on Request

Elsevier Science Publishers
P.O. Box 330
1000 AH Amsterdam
The Netherlands
Tel: (31-20) 5862 873
Fax: (31-20) 5862 845

in the USA and Canada
P.O. Box 882
Madison Square Station
New York, NY 10159, USA
Tel: (212) 633 3750
Fax: (212) 633 3764

ELSEVIER SCIENCE PUBLISHERS